Normalized Mechanical Properties of Resedimented Gulf of Mexico Clay from Integrated Ocean Drilling Program Expedition Leg 308

by

David P. C. Mazzei

BSCE, Northeastern University
Boston, Massachusetts
(2007)

Submitted to the Department of Civil and Environmental Engineering
in partial fulfillment of the requirements for the degree of

MASTER OF ENGINEERING
in Civil and Environmental Engineering

at the

MASSACHUSETTS INSTITUTE OF TECHNOLOGY

June 2008

Signature of Author: _____
Department of Civil and Environmental Engineering
May 9, 2008

Certified by: _____
John T. Germaine
Senior Research Associate of Civil and Environmental Engineering
Thesis Supervisor

Accepted by:_____
Daniele Veneziano
Chairman, Departmental Committee for Graduate Students

Normalized Mechanical Properties of Resedimented Gulf of Mexico Clay from Integrated Ocean Drilling Program Expedition Leg 308

by

David P. C. Mazzei

Submitted to the Department of Civil and Environmental Engineering on May 9, 2008 in partial fulfillment of the requirements for the Degree of Master of Engineering in Civil and Environmental Engineering.

Abstract

During Integrated Ocean Drilling Program (IODP) Expedition Leg 308, many Whole Core Samples were recovered from the Ursa Basin in the Gulf of Mexico. Post-cruise geotechnical testing found these samples to be highly disturbed due to the sampling process. This research will determine mechanical properties of laboratory Resedimented samples created using recovered Leg 308 sediment. A seven triaxial compression tests, K_o consolidated, were performed to ascertain these mechanical properties as a function of consolidation stress. Consolidation stress for these specimen ranges from 150 kPa up to 1,200 kPa. Axial strain induced on the soil during laboratory consolidation was approximately 60%. Results show that with an increase in K_o values there is a decrease in undrained shear strength, which is in accord with research completed on resedimented Boston Blue clay (RBBC) at MIT and also intact material that was recovered from this expedition. Undrained shear strength of the material is between 0.24 and 0.27, which is weaker than what is expected, according to SHANSEP. Friction angle of the material ranges from approximately 22° to 26°. There is not any apparent relationship between K_o and modulus, friction angle or consolidation stress. Reaching end of primary proved to be a difficult task, concluding that it is reached after approximately five days. CRS data was used to corroborate values such as C_v, (0.0004 cm^2/sec) and to more clearly map compression behavior. The results will provide a data base perform analysis and design of offshore structures and calibrate soil models.

Thesis Supervisor: John T. Germaine
Title: Senior Research Associate of Civil and Environmental Engineering

TABLE OF CONTENTS

LIST OF FIGURES

LIST OF TABLES

ACKNOWLEDGEMENTS

To my parents,

John and Patricia

I am the wisest man alive, for I know one thing, and that is that I know nothing.

Socrates

LIST OF SYMBOLS

Notes:
(1)   Prefix Δ indicates a change.
(2)   Suffix $_f$ indicates a final or failure condition.
(3)   A superscript prime on stress indicates an effective stress.
(4)   A superscript prime on a property indicates a value in terms of effective stress.

SYMBOL	DEFINITION
A/D	Analog to Digital
BBC	Boston Blue Clay
CK_oUC	K_o Consolidated Undrained Compression Test
CRS	Constant Rate of Strain Test
DC	Direct Current
GMC	Gulf of Mexico Clay
LIR	Load Increment Ratio
LVDT	Linear Variable Differential Transformer
IODP	Integrated Ocean Drilling Program
MIT	Massachusetts Institute of Technology
NC	Normally Consolidated
OC	Overconsolidated
OCR	Overconsolidation Ratio
RBBC	Resedimented Boston Blue Clay
RGMC	Resedimented Gulf of Mexico Clay
UUC	Unconsolidated Undrained Compression Test
SHANSEP	Stress History and Normalized Soil Engineering Properties
A (A_f)	Skempton's pore pressure parameter (at failure)
B	Skempton's pore pressure parameter
C_v	Coefficient of consolidation
e	Void ratio
e_i	Initial void ratio
E_u	Secant modulus
H_d	Drainage path length
k	Permeability
m	Slope of OCR vs. Shear Stress, $d\log(Su/\sigma'_{vc})/d\log OCR$
p'	Mean effective stress, $(\sigma_1 + \sigma_3)/2$
q	Shear stress, $(\sigma_1 - \sigma_3)/2$
S	Undrained strength ratio
S_i	Initial saturation
S_u	Undrained shear strength
TX	Triaxial
t_p	Time to end of primary
Δu	Excess pore pressure
Δu_s	Shear-induced pore pressure
w	Water content

ε_a	Axial strain
ε_{ai}	Axial strain before K_o consolidation
ε_{vol}	Volumetric strain
σ_1	Major principle stress
σ_3	Minor principle stress
σ_c	Cell pressure
σ'_i	Sampling effective stress
σ'_{lc}	Laboratory Consolidation Effective Stress
σ'_p	Preconsolidation effective stress
σ'_{vc}	Vertical consolidation effective stress
σ'_{vm}	Vertical maximum effective stress
ϕ'	Effective friction angle

Chapter 1

Introduction

I have not failed. I've just found 10,000 ways that won't work.

Thomas Alva Edison

1.1 Background and Problem Statement

Triaxial testing is certainly a landmark test to determine mechanical properties of geotechnical material. From this experiment, one can learn an extraordinary amount of information regarding the material's mechanical properties. Such information is often used in the design of foundations for offshore structures which are founded on sediments, such as Gulf of Mexico Clay. There is a particular geohazard and geophysical interest in soils in this region of the world, in part, because offshore structures are constructed on this soil, or soils similar to the soil of interest in this thesis.

Gulf of Mexico Clay was created from alluvial deposits settling outside of the Mississippi River Delta in the Gulf of Mexico. This particular sediment is formed when physical and chemical weathering of rocks occurs in the Mississippi River Basin and is transported downstream. As the sediment travels in the water more weathering occurs and thus the grain size of the sediment in the river changes as the soil is abraded. As the river containing the sediments flows into a larger body of water, such as the Gulf of Mexico, the sediment's velocity decreases and sedimentation occurs at the bottom of the ocean. In this particular region, deposition of this material is so rapid that pore pressures do not have time to dissipate before more sediment is lain above, creating more pore pressure. Gulf of Mexico clay has more of a flocculated structure because of the presence of salt water during its deposition (Lambe and Whitman, 1969).

In order to understand the sediments, both geophysically and geotechnically, it is important to retrieve whole core samples of the sediment. However, a common problem that arises during the sampling process of sediments is disturbance. Disturbance occurs

when energy is transferred from a source (i.e., simply shaking a Shelby tube) to the soil, causing displacements within the soil which tend to break down bonds between particles. Disturbance of the bonds generally causes the structure of the material to be weaker than its natural state.
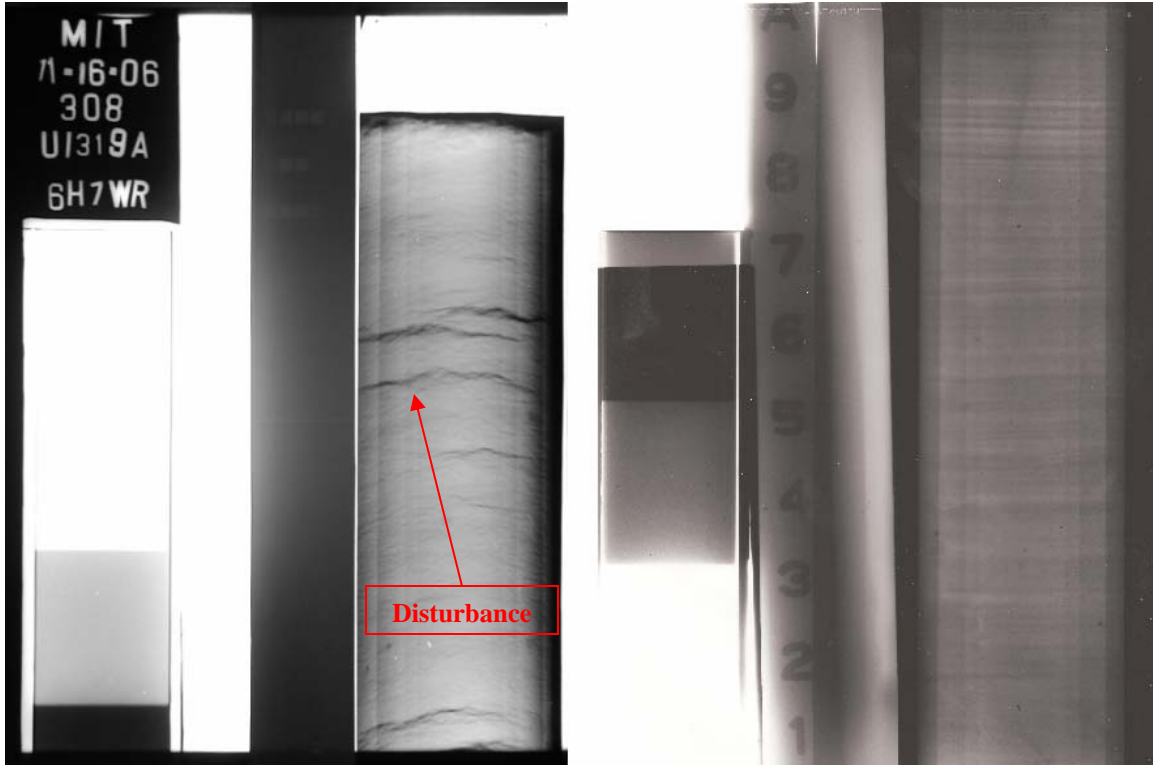
Figure 1.1: Radiographs Showing Disturbed Sample (left) and Undisturbed Sample. Dark lines can easily be seen in the image on the left, signifying disturbance. Lines due to disturbance do not appear on the right figure.

Changing of the soil structure can drastically change mechanical properties. It is desirable to keep the soil structure in its natural condition because its engineering behavior determined in the lab will be more representative of in-situ behavior (Lambe and Whitman 1969). Other effects of disturbance on soil include: decreased permeability and lower strength. There have been many studies regarding this issue on how to reduce the amount of disturbance during sampling, but inevitably, there will always be some disturbance in a soil sample, even with the use of thin walled Shelby tubes. In order to resolve this disturbance issue, techniques have been developed to erase the effects of disturbance in order to ascertain more realistic mechanical properties.

Resedimentation is a process, pioneered at MIT (Wissa 1961), in which the soil's "memory" is erased by grinding down the soil into a powder, adding a certain amount of water to form slurry, and placing the slurry into consolidation tubes. At this point, it is at the scientist's discretion what load to place on the specimen. However, the resedimented soil structure can be quite different than the in-situ soil structure. Even though the soil structure is different, resedimentation allows recreation of an undisturbed specimen with properties fairly similar to in-situ material. More on resedimentation is explained in section 3.5.

To try and avoid disturbance, apparatus, such as the Advanced Piston Corer (APC), is used which employs a piston to push a thin walled Shelby tube into the sediment and uses a vacuum to help secure the sample inside the tube. More detail about the Advanced Piston Corer is discussed in section 2.2.

The effect of disturbance between a tradition rotary coring and APC coring can easily been seen in Figure 2.

Rotary cored   Piston cored
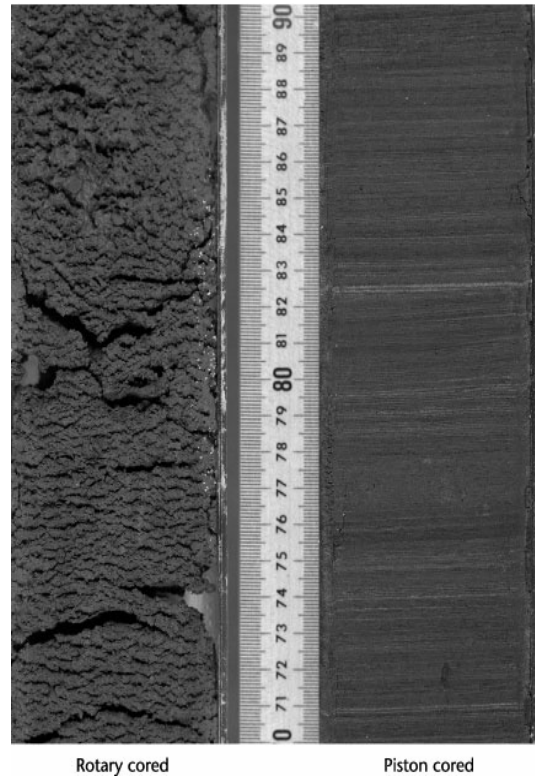
Figure 1.2: Effects of Disturbance (www.iodp.org)

This research avoids the issue of highly disturbed Gulf of Mexico clay soil samples through resedimentation and gains more insight into the soil's normalized mechanical properties after resedimentation. Moreover, it measures the effect of varying consolidation stresses on mechanical properties.

1.2 Objectives of Research

The purpose of this research is three fold: to attain mechanical properties of resedimented soils; to investigate trends of behavior as consolidation stress increases, and to develop a technique to create Resedimented Gulf of Mexico Clay (RGMC).

Mechanical properties, (i.e. friction angle, undrained shear strength, modulus, etc.) will be some of the information that will be obtained from the testing which will ultimately be used in the analysis and design of structures offshore and for calibration of soil models. In addition, constant rate of strain testing (CRS) will be conducted in order to achieve information such as permeability and coefficient of consolidation.

Seven K_o consolidated, undrained, compression, loading (CK_oUC) triaxial tests were conducted at a wide range of consolidation stress levels. Each specimen was consolidated in the laboratory using a dead weight (weights simply placed on a piston atop the specimen) loading system. Three specimens were each consolidated in the laboratory to 98 kPa (1 ksc). The other four specimens were consolidated in the laboratory at 196 kPa (2 ksc), 392 kPa (4 ksc), 588 kPa (6 ksc), and 784 kPa (8 ksc). After the specimen has reached the prescribed load, the specimen was extruded from the consolidation tube and tested in the triaxial machine. The specimen was then K_o consolidated in the triaxial cell to the normally consolidated (NC) range, approximately 1.5 to 2 times past its laboratory consolidation stress. At this point, it is sheared under undrained conditions.

The results of these data will be compared to the results of Resedimented Boston Blue Clay (RBBC) and intact Gulf of Mexico Clay (GMC) and discussion and conclusions will be drawn from these comparisons.

1.3 Thesis Organization

Chapter 2 of this thesis discusses the background of these Gulf of Mexico sediments, its origin and the purpose of the expedition during which the soils were sampled from the Gulf. A discussion of SHANSEP (Stress History and Normalized Soil Engineering Properties) and its application to these Resedimented Gulf of Mexico Clays is provided in this chapter. Discussions of mechanical properties that will be analyzed in this research are presented in this chapter.

Chapter 3 describes the equipment with which the triaxial tests were completed. Procedures regarding how the material was processed in preparation for resedimentation and batch consolidation are also discussed.

Chapter 4 consists of the results of the experimental data set acquired during testing of the seven triaxial tests of the resedimented material, with detailed discussion of Triaxial Test # 815. Moreover, CRS tests and the batch consolidation results will be presented in this chapter.

Chapter 5 will discuss the results of the experimental data set and will also integrate these new results with triaxial test data results from the intact material tested at the MIT geotechnical engineering laboratory.
Additionally, a comparison and discussion of these data to average findings of RBBC will be included. This chapter will discuss the evaluation of these data and its integration with the existing data of intact specimen.

Chapter 6 describes the conclusions of the experimental program and suggests recommendations for future research topics related to this research.

Chapter 2

Background and Normalization of Properties

A person who never made a mistake never tried anything new.

Albert Einstein

2.1 Gulf of Mexico Clay – IODP Expedition Leg 308

From May 30th to July 8th, 2005, Integrated Ocean Drilling Program (IODP) Expedition Leg 308 drilled at six sites, three of which were located in the Ursa Basin in the Gulf of Mexico. These six sites can be broken into two groups: the Brazos-Trinity Region; and the Ursa Basin, shown in Figure 2.1: Exploration of this area is of particular importance
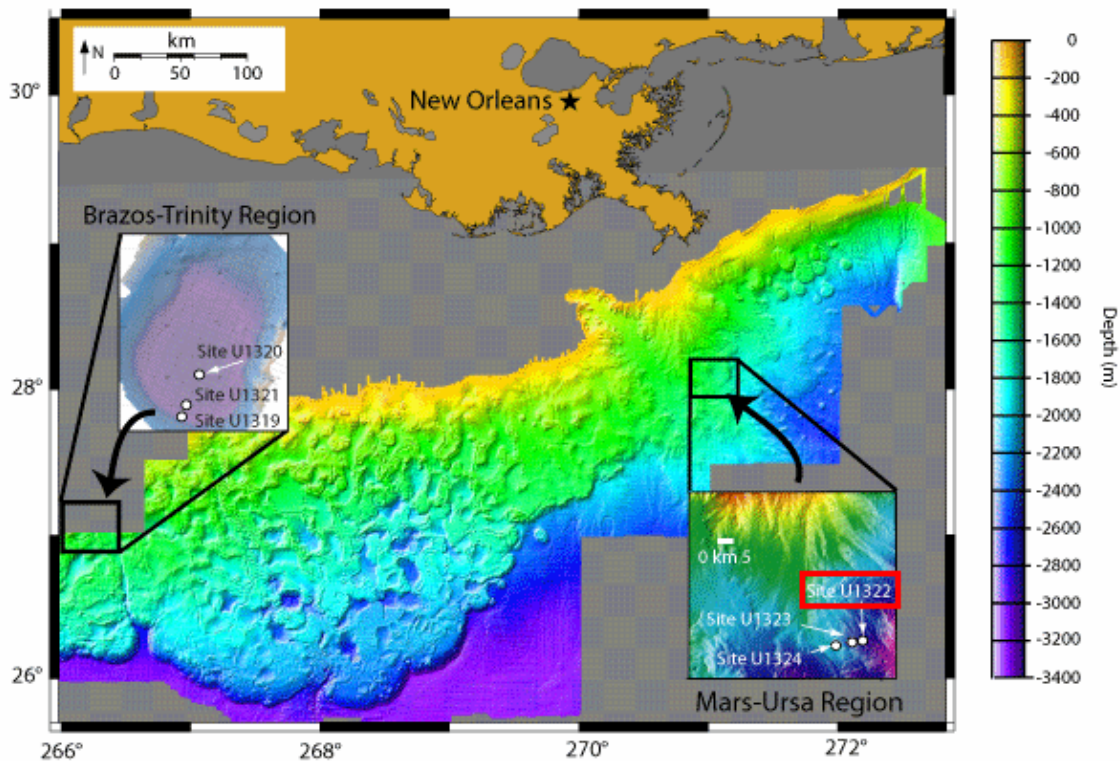
Figure 2.1: Bathymetric image of the continental slope of the Gulf of Mexico. Indicated are the drilling locations at the Brazos-Trinity Basin #4 (Site U1319, U1320, and U1321) and the Mars-Ursa Basin (Site U1322, U1223, and U1324). (www.iodp.org)

for many reasons, including protection of inhabitants of the ring of countries which border the Gulf of Mexico against tsunamis, and also for exploration of essential energy sources.

The Ursa Basin is located approximately 100 miles southeast of New Orleans, Louisiana. This region is of particular interest due to the oilfield which lies approximately two and a half miles below the ocean floor. Site U1322 is the easternmost site drilled in the Ursa Basin during this expedition. The purpose of this boring was to document in-situ temperature and pressure, rock properties, geochemical composition of the pore water, and establish an age model which would help determine sedimentation rates in this area.

Expedition Leg 308 is the first of several excursions that intend to study overpressure and fluid flow on the Gulf of Mexico continental slope. Large sediment deposit rates experienced in this region (greater than 1 mm/year) lead to the overpressurization of the sediments. These pressures tend to flow laterally along layers of soil of high permeability (i.e. sand) and travel to areas of lower overburden pressure. This process could lead to slope instability concerns at the ocean floor, which could trigger larger events like tsunamis. Data gathered from the borings at the six sites manifested an active hydrodynamic environment and gave insight into geological processes that are taking place at the seafloor (Flemings et al., 2006).

One of the key goals for this expedition was to: documentation of physical sediment properties at the location of the smallest overburden in the Ursa Basin, and exploration of fluid flow and fluid pressures in an overpressured basin. At Site U1322 there were four holes bored: A, B, C and D. Site U1322D was drilled specifically to deploy temperature and pressure probes. Core samples were taken explicitly for geotechnical analysis of stress/strain and strength behavior. Geotechnical goals set forth by this expedition include understanding the consolidation process near the seafloor, how overpressuring started in this region, and mechanical properties of these shallow sediments.

The soil used in this research was taken from the Mars-Ursa Region, specifically site U1322D.

Sediments were extracted from the sea bed with the use of an Advanced Piston Corer (APC) seen in Figure 2.2. Intact soil samples are taken using this apparatus. The apparatus is designed for high-resolution climate and paleoceanographic studies. The APC is a hydraulically actuated apparatus which can retrieve a 9.5 meter intact sample with a diameter of 6.2 cm. One can achieve 100% recovery in soft sediments, such as the Gulf of Mexico Clays at this site. The sampler has a rather large, thick structural wall which causes relatively large amounts of disturbance.

Triaxial testing of intact Gulf of Mexico Clay was conducted at MIT, to evaluate its in-situ mechanical properties, based on SHANSEP. In Chapter 5 a comparison of these intact specimen data will be compared to these data of RGMC.
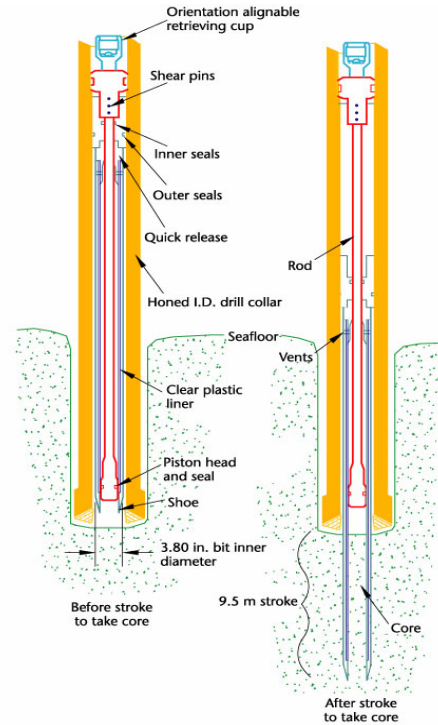
Figure 2.2: Advanced Piston Corer (www.iodp.org)

Total depth to the bottom of Boring U1322D is approximately 1500 meters below sea level. Within the borehole there are alternating layers of muds and clays. Boring U1322D reached to a depth of 240 meters below sea floor (mbsf).

2.2 Normalization of Soil Properties

This section briefly discusses key features of normalized behavior of soils described by the SHANSEP method (Ladd and Foott, 1974; Ladd, 1991). SHANSEP testing was developed at MIT in the 1960's and is a widely used method of quantifying the undrained shear strength of a soil with respect to its overconsolidation ratio (OCR) and consolidation effective stress.

Specimen are consolidated in the triaxial apparatus 1.5 to 2 times the preconsolidation stress, unloaded to the desired OCR and then sheared. Analysis of the data will yield a unique equation which will define the strength of the material at any OCR (Equation 1).

The variables, (S and m), are based on triaxial testing conducted on the material at varying consolidation effective stress and overconsolidation ratios. Once an array of tests has been conducted, S and m parameters can be defined and undrained shear strength can be reasonably predicted, depending on the stresses and OCR observed in the field.

$$S_u / \sigma'_{vc} = S(OCR)^m$$

The undrained strength ratio, S, is simply the ratio of undrained shear strength to consolidation effective stress observed when OCR = 1. It is assumed that S is independent of stress level. The range S for K_o consolidated soils is 0.28 to 0.33 for CK_oUC tests. The exponent m is important when analyzing overconsolidated and is defined as:

$$m = d \log(S_u / \sigma'_{vc}) / d \log OCR$$

Range of m is 0.8 ±0.1. Figure 2.3: displays values of S and m for various tests. There is an extensive series of testing on RBBC. Clay specimens, despite their consolidation stress, and therefore preconsolidation stress, will exhibit similar properties (undrained shear strength, pore pressure parameters, etc.) when normalized with respect to their consolidation stress (Santagata, 1999). A comparison of results is shown in Chapter 5.
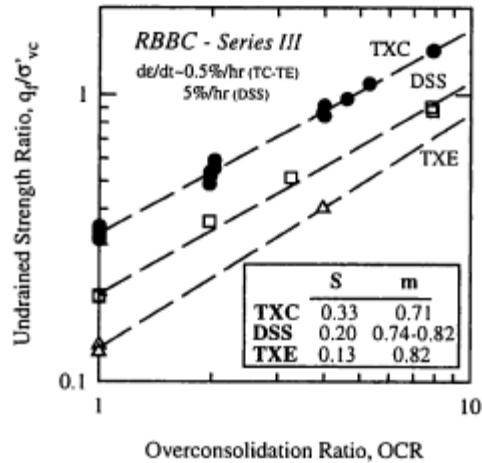
Figure 2.3: Undrained strength ratio versus OCR from CKoU test in triaxial compression (Sinfield 1994, Santagata 1994), extension (Sheahan 1991), and direct simple shear (Ahmed, 1990). Resedimented Boston Blue Clay

2.3 Mechanical Properties

This section defines parameters and/or topics which will be the focus of this research. These mechanical properties are commonly used in geotechnical engineering and must be presented in a clear manner.

Strength

Undrained strength of soil is typically referred to as the shear strength of the soil. Undrained strength is not a unique number. Strength depends on strain rate, type of loading and direction of shearing. In this research, triaxial compression loading undrained shear is measured at a strain rate of 0.5%. This parameter is an extremely important aspect when designing foundations, shallow or deep, on clay. Strength is often overestimated by UUC (unconsolidated-undrained compression test) and other tests, such as the field vane. SHANSEP method of testing is the most widely accepted and accurate method of determining soil's strength for soft and low OCR, non-cemented sediments. One of the outcomes of this research is to compare SHANSEP measurement with resedimented strength measurements.

Strain to Failure

All materials will exhibit some amount of strain during loading. It is important to define soil's deformation behavior so that when structures are built in the field, anticipated strains and deflections can be adequately predicted as best as possible. Strain to failure is important because one must determine when plastic deformations will occur as a function of loading. Chapter 5 discusses strain to failure of Resedimented Gulf of Mexico Clay.

Modulus

Modulus, or stiffness of soil, is another important parameter in designing structures and completing analysis on settlement or analysis of deep foundation systems. Modulus is a relatively complex quantity to determine because the soil yields at very small strains and experiences considerable plastic deformations before failure. Secant Modulus for the material tested is discussed in Chapter 5.

Friction Angle

Friction angle is defined as the angle at which the Mohr-Coloumb failure envelope is oriented on a plot of shear strain versus normal stress for a particular soil. There is quite a wide range of friction angles among clays. The angle is related directly to its strength and is used frequently in the analysis and design of deep and shallow foundation structures.

Chapter 3

Equipment, Materials and Procedures

If we knew what it was we were doing, it would not be called research, would it?

Albert Einstein

3.1 Introduction

The purpose of this chapter is three fold: to describe the equipment (both consolidation and triaxial) used in completing necessary tests; explain which soil was selected in creating specimen for the testing; and to describe the procedure of batching the material into the consolidation tubes.

3.2 Consolidation Equipment

The consolidation cylinder is a clear plastic tube about 30 cm long with an inside diameter of approximately 35 mm, which is the size of the diameter of a typical triaxial specimen. A porous stone topped with 5µm nylon filter fabric lies on a 5 cm tall pedestal which sits at the bottom of the tube. The tube is then placed on a larger porous stone inside a plastic or glass container. Approximately 3 cm of water is added to the jar to keep the specimen saturated during consolidation. Once the slurry fills the tube, another porous stone and

Figure 3.1: Contents of Consolidation Equipment

nylon filter fabric lay on top of the slurry. The top porous stone's edge is beveled away from the soil to allow the stone to slide down without sticking to the tube during consolidation. A 20 cm long plastic piston is placed on top of the top porous stone so that heavier loads can be applied to the soil which induces large deformations without the weight touching the top of the consolidation tube. The entire setup is placed on a ring stand so that clamps can be set up which can help to support the piston so that it stays vertical. The ring stand is also useful for setting up an LVDT which will be placed on top of the weights.

3.3 Triaxial Equipment

MIT's system for computer-controlled triaxial testing was developed in 1991 as part of the FATCAT (Flexible Automation Technology for Computer-Assisted Testing) system and has been continuously improved over the years. The design of the automated stress path cells has combined existing MIT testing equipment with some innovative new components. The triaxial cell is composed of a Wykeham Farrance base from the 1960's with customized features such as linear ball-bearing bushings for alignment and an o-ring seal with an internal load cell to eliminate piston friction, a fixed top cap for testing on clay, top and bottom drainage, ball valves, copper tubing and silicone oil as cell pressure fluid to eliminate the problem of leakage through the membrane. The pore and cell pressure transducers are connected directly to the triaxial base so as to reduce the system compliance. Pressure/volume actuators, equipped with DC electric servo motors, maintain the pore and the cell pressure. These two motors, as well as the motor driving the load frame, are controlled by the MIT designed motor control box. The automated control is performed by a program written in BASIC and running on a personal computer. The program is able to perform all phases of a triaxial test including initial pressure up, back pressure saturation, B-value check, consolidation along any specified stress path or K_o consolidation, and shear in extension or compression. Much of the hardware has been developed in the MIT geotechnical laboratory, including the 22-bit A/D integration card. More recently, the triaxial cells have been modified to accommodate electronics within the pressure chamber. The current systems include internal force transducers to measure

the deviator force applied to the specimen. Cells used for this research are available to test at pressures as high as 2 MPa.

3.4 Tested Material

The material tested comes from one site of the 308 expedition: U1322D. The samples were X-rayed and triaxial tests were completed during a previous project at MIT on intact material directly extruded from the tubes. The material used in this research was resedimented from the trimmings of specimens for those triaxial tests.

Material tested was retrieved at various depths through the profile, but generally all material tested was located in the upper part of the borehole. Table 1 explains the triaxial test number from intact material testing, and resedimented material testing, the site from IODP Leg 308 in which the material was retrieved; the depth at which the material was retrieved, corresponding IODP Leg 308 sample number. Finally, batch number explains the order in which the material was resedimented during this research. Sometimes, multiple batches were resedimented from many bags of trimmings of the same material., resedimented slurry was derived from several bags of trimmings of triaxial test soil from the initial testing. Additional information regarding IODP Leg 308 can be found on the IODP website.

Table 3.1: Triaxial Test Number on Virgin Material, Site of Origin, Interval of Depth (m), Batch Number and Triaxial Test Number on Resedimented Material

Material Used for Resedimentation Slurry					
Intact Material Triaxial Test No.	RGMC Triaxial Test No.	Site	Sample	Depth (mbsf)	Batch No.
TX 734	TX 815, TX 812	U1324B	10H7	89	5,6
TX 778	TX 797	U1322D	1H3	43	1
TX 735	TX 815, TX 812	U1322B	4H3	27	5,6
TX 776	TX 810	U1322D	1H3	43	7
TX 775	TX 801, TX 804, TX807	U1322D	1H3	43	2,3,4
TX 725	TX 801, TX 804, TX807	U1322D	1H2	42	2,3,4
TX 782	TX 801, TX 804, TX807	U1322D	N/A	N/A	2,3,4
TX 779	TX 801, TX 804, TX807	U1322D	1H3	43	2,3,4
TX778, TX779	CRS914,CRS915	U1322D	1H3	43	8

3.5 Resedimentation of Gulf of Mexico Clay

Resedimentation of clays has been a popular technique to "erase" soil's memory of preconsolidation stress and to eliminate any disturbance that the soil has experienced.

The resedimentation process has experienced a number of improvements and modifications over the years. MIT has an extensive set of RBBC data, but none on RGMC.

Resedimentation of Boston Blue Clay (BBC) began with work performed by Bailey, with supervision from Professor Charles C. Ladd, on the effect of salt concentration on the triaxial undrained strength of clay. Over the years, a vast array of data on RBBC, as well as other soils such as Kaolinite, Arctic Soils, Taipei Clay, etc., has been gathered and used to study clay behavior. These experiments have ultimately led to the development of constitutive models at MIT (Whittle 1987, Pestana 1994) and the development of laboratory devices (Dickey 1967, Wissa and Heiberg 1969, Sheahan 1988). For the resedimentation process of BBC, large sources were collected in upwards of 200 kg of soil. The soil is air dried and pulverized to a powder. It is then hydrated, batched, extruded and trimmed for testing.

Since GMC is more difficult to attain than BBC, special care is taken to use every bit of every sample taken from expeditions that collect these soils, such as IODP Leg 308. The resedimentation material is originally taken from the bags of trimmings on previous intact triaxial tests and allowed to air dry for a period of at least 24 hours. Once the soil has desiccated to a point where it is air dry, it is pulverized using a mortar and pestle (crucible) to the point where it will pass through a #100 U.S. sieve. The pulverization of the soil does not affect the grain size distribution because it has a distribution of particles whose size is smaller than that of the #200 U.S. sieve. Once pulverized to this point, distilled water is added to the soil and placed in a covered container in a humid room of at least 90% humidity letting hydration occur for at least 24 hours. After hydration, water and soil is mixed to create a homogeneous slurry using a spatula. No salt is added to the slurry because of the high natural salt content of GMC. The soil and water is mixed to where the slurry is smooth and runny with no lumps. From here, the slurry is placed in a
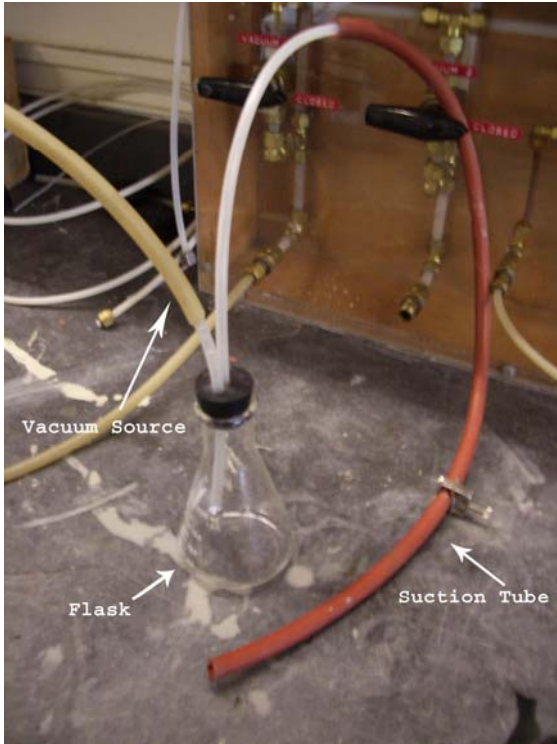
Figure 3.2: Vacuum Apparatus Used to De-air Soil

vacuum apparatus. The apparatus consists of two parts: the vacuum source, and a flask. A rubber stopper with two holes in the top plugs the flask. One hole in the top allows a tube from the vacuum source to be connected to the flask, while the other hole houses a suction tube where soil will be vacuumed in from. The vacuum will be applied through this flask, pulling in slurry to the flask and pulling out air from the slurry as it slides down the inside of the flask. This process de-airs the soil to assure that no air voids are trapped in the soil during casting of the batches.

3.6 Batch Consolidation

After the soil has been prepared as described in Section 3.5, it is ready to be cast in the consolidation tube.

The inside of the tube is coated with silicone oil prior to casting of the soil. This oil will help to maintain little side-wall friction due to shear stress imposed on the specimen as it is consolidated and extruded from the tube.

The de-aired soil is then placed into the setup as using the following technique. A long-necked funnel with a small plastic extension tube is used to place the soil in the consolidation tube. The soil
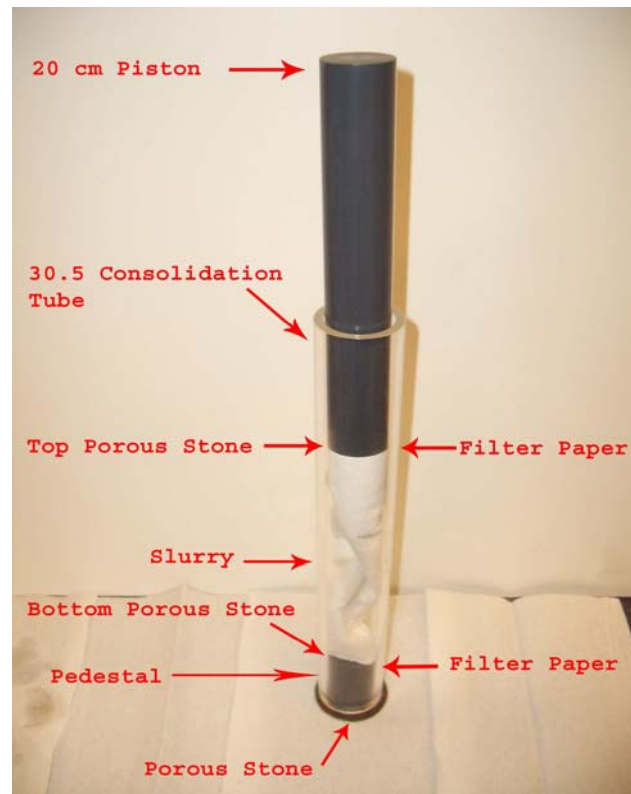
Figure 3.3: Consolidation Equipment

slurry is poured into the funnel and through the tube which is set on the bottom filter paper and porous stone. Slurry is slowly poured and the funnel and tube is rotated constantly as the soil is placed in the consolidation tube. Soil is placed to the top of the consolidation tube and the top filter fabric and porous stone is placed.

3.7 Stress Level

One of the objectives of this research is to determine the effect of stress level on the normalization of properties of the resedimented clay. It is hypothesized that at higher stress levels, normalized behavior of the clay, such as undrained shear strength, will vary. As each specimen was cast, it was consolidated to a unique level of stress. Each specimen was loaded with a load increment ratio (LIR) of 1, and in some cases less. The reason for this was to try and reduce the amount of extrusion of soil between the porous stone and consolidation tube. Even with the LIR = 1 and the filter paper being sized to match the porous stone, there were some instances where a small amount of extrusion occurred in a couple of the batches. All batches would begin with just the top cap as the first load, then 100g
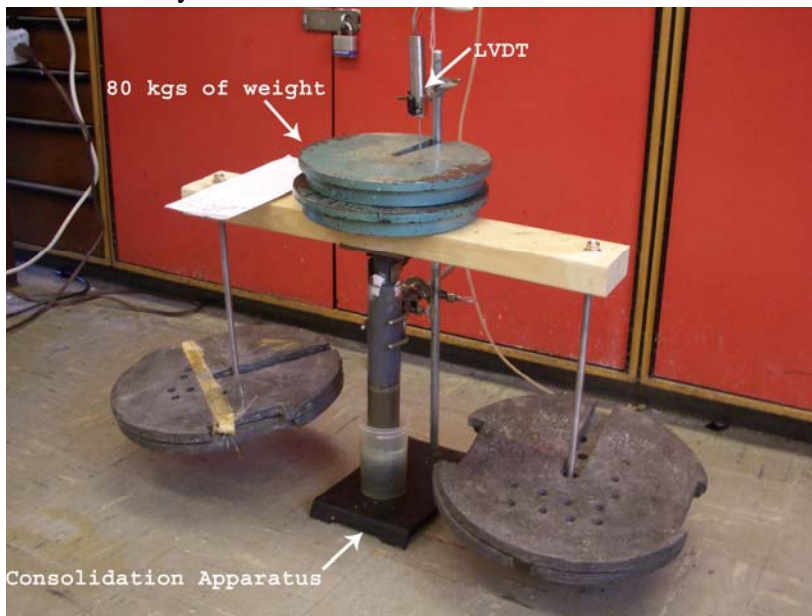
Figure 3.4: Batch 05 Being Loaded to 80kg

would be applied, then 200g, 400g, 800g up until the desired stress level was achieved. After reaching the maximum load desired, the load was kept on the specimen for a certain number of days. One to two days prior to triaxial testing the specimen was unloaded to OCR = 4 to allow to swell. At OCR = 4 the lateral stress ratio is nearly unity. Extruding the soil from the tube under hydrostatic conditions minimizes disturbance due to release of shear stress (Santagata, 1999). Table 3. 2 shows the laboratory consolidation stress, number of days in which each increment was applied, time at maximum load and time at

OCR = 4. Specimens were loaded to different laboratory consolidation stresses with a range from 98 to 784 kPa.

Table 3. 2: Laboratory Preconsolidation Stress of Specimens

Batch No.	Triaxial No.	σ'_p (kPa)	Time per load increment (days)	Time at Maximum Load (days)	Time at OCR=4 (days)
1	TX797	98	1-2	2	1
2	TX801	98	2	3	2
3	TX804	98	3	7	2
4	TX807	196	4	5	2
7	TX810	392	2	5	4
6	TX812	588	2	5	2
5	TX815	784	5	5	2
8	CRS914 CRS915	98	2	6	0

3.8 End of Primary

A relatively difficult aspect of the consolidation phase of this soil was trying to determine the time required to reach the end of primary consolidation. End of primary is defined as the point in time where consolidation has ended and secondary compression, or creep, has begun. This is particularly important because once end of primary has been achieved, it is confirmed that the preconsolidation stress is uniform throughout the specimen.

To establish the time required to reach the end of primary consolidation on Resedimented Gulf of Mexico Clay, an LVDT was placed on the weights on top of the specimen at each load increment during consolidation to track displacement versus time. End of primary readings were tracked on all specimens except Batches 3 and 4. At first (Batches 1 and 2), loads were placed on the specimen at 1 to 2 day increments because it was believed that end of primary would be achieved by then. Results show that end of primary was indeed not achieved. The next specimen, Batch 3, had three day increments; again, end of primary did not occur on these increments. Batch 4 had four day increments, and finally end of primary was reached on Batch 5, which held each weight increment for five days. The final load increment was placed on the soil for at least two days, but usually at least five (See Table 3.2). It is believed that if the final load increment is held for as long as possible, despite how long intermediate increments were held, that end of primary would be achieved. At the end of loading, before specimens were prepared for triaxial testing,

the specimen was allowed to unload for at least two days at OCR = 4, as mentioned in section 3.7.
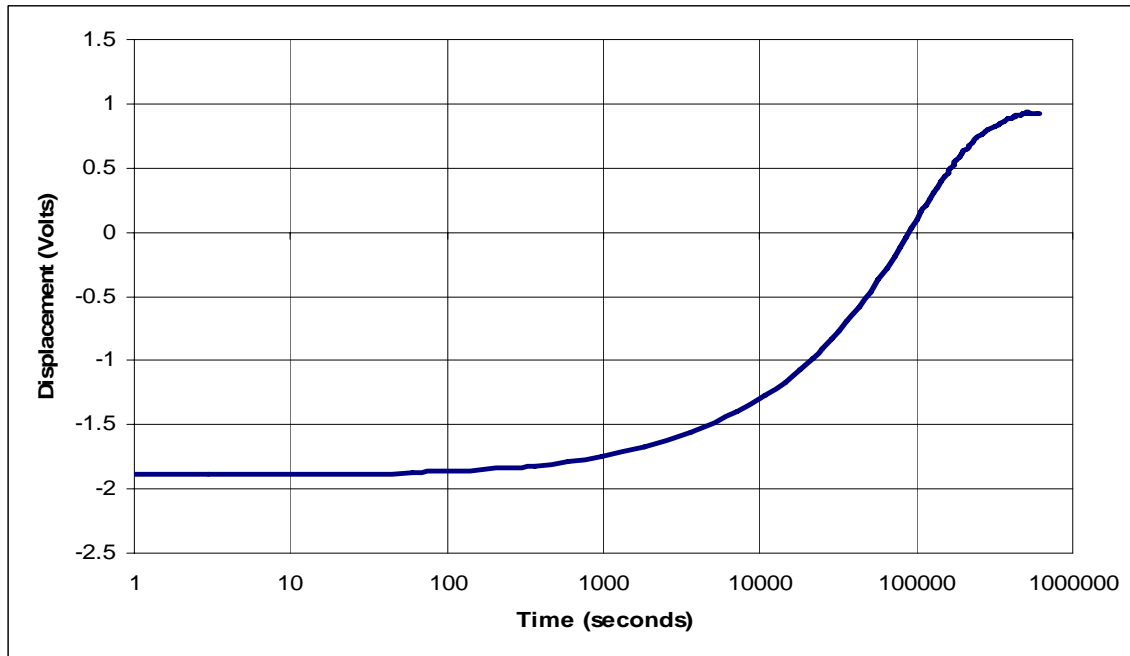
Figure 3.5: Batch 04 Consolidating at 20 kg (final increment). End of Primary occurs in about 3.5 days
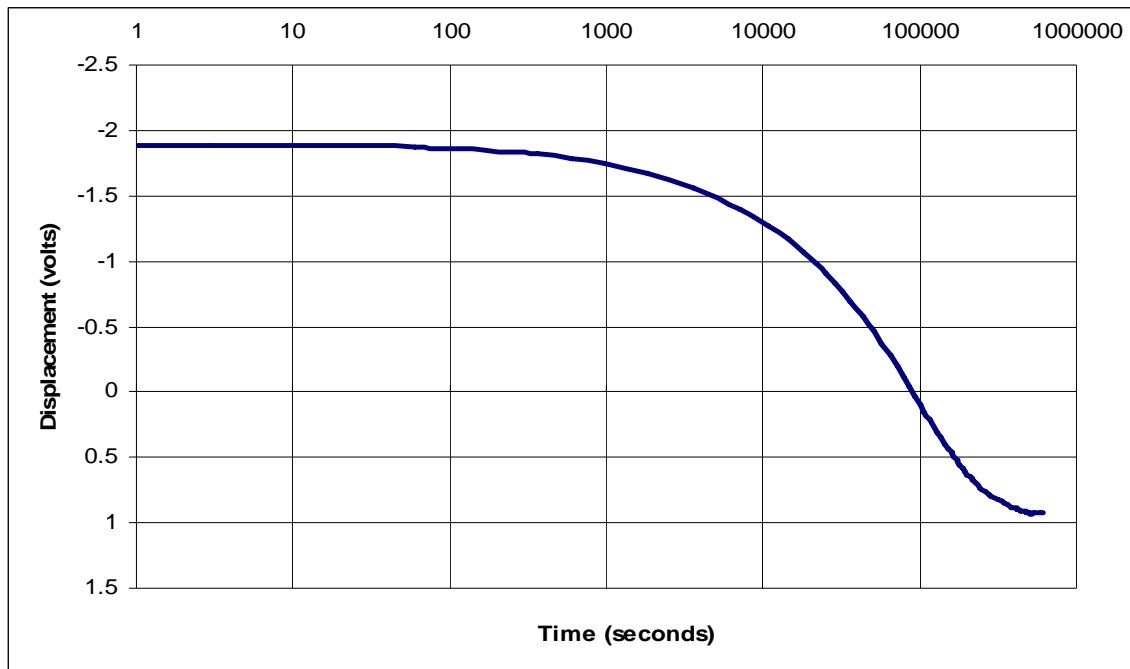
Figure 3.6: Batch 07 at OCR = 4 (20 kgs)

Calculation of C_v from Figure 3.5: $C_v = 0.197 * Hd^2 / t_{50} \Rightarrow approx\ 0.0004cm^2/sec$

Assume: $H_d = 10cm$, $t_{50} = 45,000\,sec$

3.9 Triaxial Procedure

The triaxial test consists of many important steps which assure the validity of a test. Preparation of the specimen, as discussed earlier in this chapter, even before it is tested in the triaxial apparatus, can take weeks, even months to mature.

Setup

After consolidation of the specimen has taken place, as explained in the previous sections of this chapter, the specimen is extruded and prepared for testing. The amount of material extruded often is longer than what is required for the test. Therefore, the specimen must be trimmed on both ends. The diameter of the specimen equals that required for triaxial testing, approximately 35 mm, so trimming the sides is not necessary. The trimmings of the ends are taken for moisture content. Once properly trimmed, the specimen's mass, diameter and height are taken. Three readings of each dimension are taken and the averages are used as the final measurement. After the test, the dry mass is taken and simple calculations are completed to determine the specimen's initial void ratio, saturation and total density.

Before running the test, the apparatus is checked to make sure that it is fully functional. Prior to setup, leakage checks are performed on the system to make sure that there is no escape of pore or cell pressure. If loss of pore or cell pressure occurs during the test, the test is not valid and will provide erroneous data.

It is essential to determine correct "zero values" on all the five transducers (pore pressure, cell pressure, load cell, axial strain LVDT and volumetric strain LVDT) before the test has commenced. These values will be entered into the control computer and real-time calculations of axial pressure, cell pressure, pore pressure, axial and volumetric strain will be recorded by a data logger throughout the test.

Eight, ¼" wide vertical filter strips were placed on the specimen prior to the commencement of the test. The filter strips are evenly placed longitudinally along the specimen's perimeter around the specimen's outside. These strips encourage drainage during the consolidation phase of the test and expedite the test a considerable amount when compared to triaxial tests that do not use filter strips (Bishop and Henkel 1957).

The specimen is covered with two thin membranes which are sealed with three o-rings to the top and bottom of the triaxial's pedestals. After the specimen has been placed in the triaxial cell and the cell is filled with silicone oil, it is desirable to measure the sampling effective stress. This was done by increasing the cell pressure to a prescribed value, typically to one quarter of the laboratory consolidation stress. The specimen is allowed to equilibrate to the increase in cell pressure overnight and the resulting effective stress is taken as the specimen's sampling effective stress. An expected sampling effective stress is one quarter of the preconsolidation stress. However, since the actual preconsolidation stress is not known until after the analysis has been completed, a reasonable sampling effective stress can only be estimated at this point in the test.

Back Pressure Saturation

Backpressure saturation occurs prior to the B-value check. Backpressure saturation is an isotropic loading $(\Delta\sigma_1 = \Delta\sigma_3 = \Delta u)$ of the specimen such that air voids within the specimen and the pore pressure measuring system are essentially compressed to the point where air is driven into solution. At the same time, pore pressure (back pressure) is increased as well while maintaining constant effective stress equal to the sampling effective stress. During backpressure saturation the axial motor is on and the specimen can change in dimension. Backpressure saturation to 196 kPa was performed in the lab. After a B-value check was completed (next section), K_o consolidation takes place occur if the B-value was acceptable. If the B-value is not acceptable, an increase of back pressure of 98 kPa, while maintaining constant effective stress, would be administered and B-value would be checked again.

B-value Check

To assure that the specimen has been fully saturated during backpressure saturation, one must evaluate this by measuring the specimen's B-value. A and B are empirical parameters that were first developed to obtain a clear picture of how the pore pressure responds to the different combinations of applied stress (Skempton, 1954).

$$\Delta u = B\Delta\sigma_3 + A(\Delta\sigma_1 - \Delta\sigma_3)$$

Where A is a parameter that reflects the shear induced pore pressure which is based heavily on OCR and is used to describe the location of undrained shear failure with respect to the initial (p', q) of the shear stress plot. A is dependent on deviator stress, and thus, is important to maintain constant shear stress while measuring the B-value. By eliminating deviator stress increment, the parameter A essentially is negated. Assuming that $A(\Delta\sigma_1 - \Delta\sigma_3) = 0$, we are left with $\Delta u / \Delta\sigma_3 = B$. A B value of unity signifies that an increase in cell pressure (in this particular research the axial stress increment is also the same) yields an increase in pore pressure of the same amount.

During this research, B-value was measured before K_o consolidation. To check the B-value, pore pressure lines are closed so that the specimen can not drain during the B-value check. A cell increment of 25 kPa is applied in one increment and the pore pressure reaction is noted after two minutes. The simple quotient of pore pressure response to cell pressure increase is calculated. Typical values attained for RGMC B-values range from 0.88-0.92. It was not uncommon for B-values calculated to be lower than this range when a backpressure of 196 kPa was applied. In the event that the B-value was relatively low after the first back pressurization, backpressure saturation to an additional 98 kPa was administered on the specimen.

K_o Consolidation

Once a reasonable B-value has been acquired, the specimen then undergoes K_o consolidation. K_o is the coefficient which quantifies lateral earth pressure at rest. It is essential in calculating horizontal in-situ stresses on potential structures. Horizontal effective stress is expressed as:

$$\sigma'_h = K_o * \sigma'_v$$

K_o calculation is defined as the quotient of horizontal effective stress to vertical effective stress when lateral strains is zero.

$$K_o = \sigma'_h / \sigma'_v \text{ when lateral strain} = 0$$

K_o consolidation is performed in the triaxial tests by using a combination of three feedback loops: back pressure is held constant; axial strain at specified rate; and cell pressure is adjusted so that axial strain is held equal to volumetric strain. σ'_1 and σ'_3 are

applied at 0.15% per hour in all tests. The specimen will ultimately be loaded to a maximum effective stress, σ'_{vm} , which is 1.5 to 2 times the laboratory consolidation stress. As consolidation occurs, K_o, which begins at unity, will decrease to a constant value, which is taken as the soil's unique normally consolidated K_o.

Secondary Compression

Once σ'_{vm} has been achieved, the specimen will continue to experience this effective stress for the period of at least 24 hours. During this time, axial strain increases without increased load, which is an effect of secondary compression of the material. From this part of the test, strain versus time can be evaluated which yields C_α, an important property of the creep effects that the soil possesses.

$$C_\alpha = d\varepsilon_a / d \log(t - t_p)$$

Where ε_a is axial strain, t is time, and t_p is time to end of primary in the specimen. Secondary compression reduces the void ratio, expands the yield surface and makes the soil strain.

Shear

During this phase, the soil specimen is brought to failure by a constant rate of axial strain. Before shearing begins, the pore pressure valves on the triaxial are closed such that pore volume within the specimen remains constant. The value of pore pressure should be noted and monitored for 30 minutes before shearing of the specimen to check for leaks in the system. After the leak check is complete, shearing can begin. Cell pressure (σ'_3) is maintained throughout the shearing process while axial strain (σ'_1) increases at a rate of 0.5% per hour. During the shearing process, there is an immediate but gradual increase in the shear stresses in the material. The largest value of q is known as S_u, or maximum undrained shear strength, of the material. The specimen is taken to 10% axial strain in addition to its axial strain after consolidation has ended. After shearing is complete, the specimen is examined for failure planes and failure geometry. The dry mass of the specimen is then measured.

Each test within this research series was performed the same way. Full results of all tests are presented in the subsequent chapters.

Chapter 4

Test Results

Research is what I'm doing when I don't know what I'm doing.

Wernher von Braun

4.1 Presentation of Experimental Test Results: Triaxial Data

All data presented in this chapter was taken with an "in-house" data logger. The data are then taken from the memory of the data logger and reduced using a quick basic version 5.0 program created at MIT. The program uses transducer readings, calibration factors, and normalized zero value readings for all the transducers, initial height and area of the specimen to create output from which plots are created to describe behavior of the soil which are shown in Chapter 5. The reduction program takes into consideration many items, such as: area correction, membrane's resistance, filter strips, etc; and considers them in the calculations of the data. The data are then manipulated to create plots which are analyzed to make conclusions of the soil's engineering properties. The resolution of the transducers is listed in

Table 4.1: Calibration Factor and Resolution of Transducers Used in Data Collection

Transducer	Calibration Factor	Resolution
Pore Pressure	701.62 ksc/v/v	0.00012754
Cell Pressure	-698.1 ksc/v/v	-0.00012690
Load Cell	6714 kg/v/v	0.00122051
Axial DCDT	2.481 cm/v/v	0.00000045
Volumetric DCDT	23.848 cm/v/v	0.00000434

The following chapter discusses in detail the parameters which are investigated during the consolidation and undrained shear phase of each test. Presented are the results of TX815 with a description of the behavior observed.

The consolidation phase yields the following plots of interest: K_o vs. Vertical Effective Stress; and Void Ratio vs. Vertical Effective Stress.

Plots generated during the shear phase of the test include: Undrained Stress Path shown in MIT p'-q space; Secant Modulus vs. Axial Strain; Normalized Shear Strength vs. Axial Strain; Friction Angle vs. Axial Strain; The A Parameter vs. Axial Strain; Excess and Shear-Induced Pore Pressure vs. Axial Strain.

This chapter will discuss how these parameters were extracted from the plots that were produced from the data and significance deviation from expected behavior.

Summary plots displaying results during consolidation and shear phases of all seven triaxial tests are shown at the end of Chapter 5. A summary table following the format of important parameters extracted from both consolidation and shear phases of all seven triaxial tests, and two CRS tests, are shown at the end of Chapter 5. Full plots of results of all seven triaxial tests are located in Appendix A.

Consolidation

The following plots are based on data taken during the consolidation phase of Triaxial Test # 815.

## *Axial Strain as a Function of Vertical Effective Stress*

All tests start with a small positive or negative axial strain, depending on the amount of initial effective stress that was induced prior to back pressure saturation. From these plots, one can notice the preconsolidation stress from the Casagrande Method of analysis (in TX #815, $\sigma'_p \approx 520 kPa$). In most cases the OC and NC regions are not clearly differentiated, making it more difficult to identify σ'_p. All specimens were consolidated to about 1.5 times the laboratory consolidation pressure, in accord with SHANSEP testing recommendations. As mentioned, the final load increment for this specimen was placed for at least five days, and LVDT readings of displacement versus time showed that the specimen has reached end of primary. However, this plot, similar to others, show that preconsolidation stress is lower than that of laboratory consolidation stress.
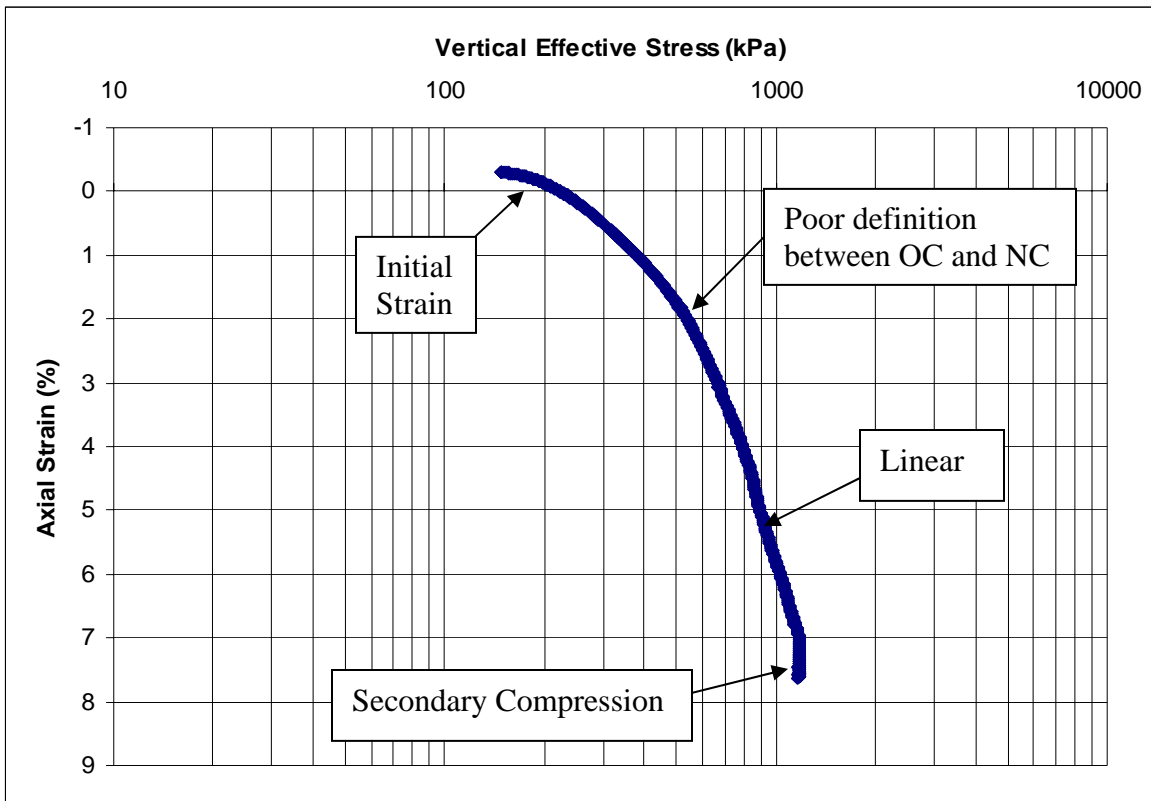
Figure 4.1: Axial Strain vs. Vertical Effective Stress – Triaxial Test #815
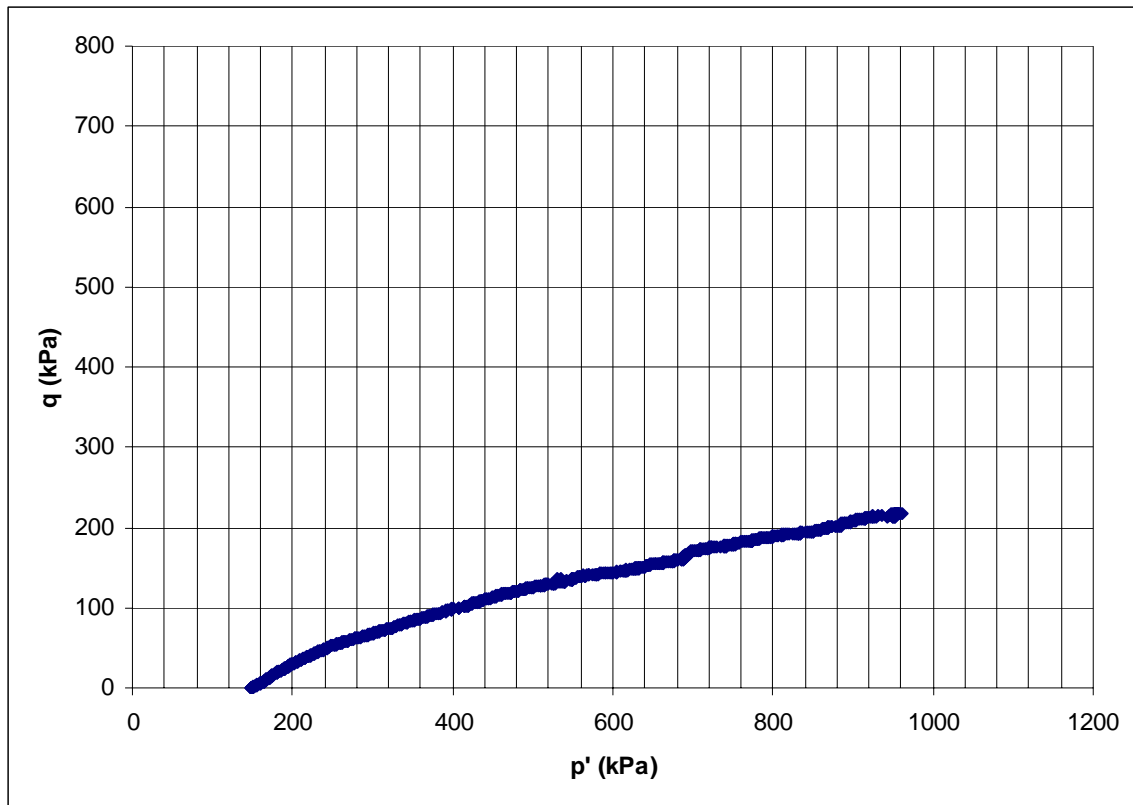
K_o as a Function of Vertical Effective Stress

All tests began with hydrostatic conditions (other than TX810 and TX812, in which case $(\sigma'_1 - \sigma'_3) \neq 0$), and thus K_o begins at unity. As vertical effective stress increases, K_o decreases, and in most cases decreases below its NC steady state value at the end of consolidation. Most tests reach a minimum in K_o as the vertical effective stress reaches the preconsolidation stress. As the specimen reaches its final consolidation stress, K_o more or less reaches a steady state value. K_o is vulnerable to initial strains exhibited on the specimen even before backpressure saturation has begun. Some tests (e.g. TX804 and TX807), experience a higher initial axial strain (-1.74% and -1.46%, respectively) which may lead to a more dramatic decrease in K_o as vertical effective stress increases. During this testing program, NC K_o values ranged from 0.552 – 0.667.
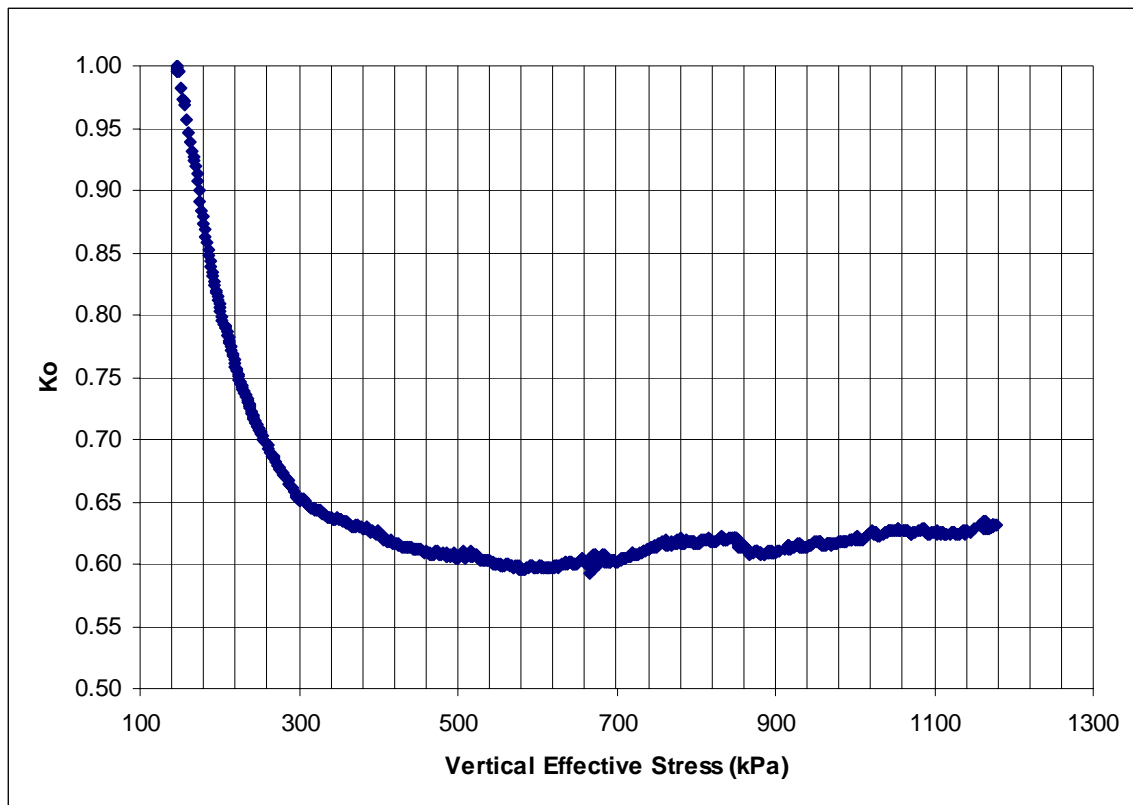
Figure 4.2: K_o versus Vertical Effective Stress – Triaxial Test # 815

## Stress Path During K_o Consolidation

During K_o consolidation, the specimen's pore pressure is held constant as cell and axial pressure is increased with axial strain equal to that of volumetric strain. The valves of the triaxial apparatus remain open as the specimen is allowed to drain at this point in the test. The K_o consolidation line should increase linearly until the desired consolidation stress is reached. During testing, a small fluctuation in the pore pressure caused small changes in the stress path during loading.

Figure 4.3: Stress Path Presented in MIT p'-q space – Triaxial Test # 815

Void Ratio as a Function of Vertical Effective Stress

The following plot compares the void ratio of the specimen with respect to the vertical effective stress. Void ratio versus vertical effective stress presents a straight line, which means that the soil has a linear stiffness over a large region of loading. By converting all test data from strain to void ratio, all test data can be plotted in the same graph and compared directly.
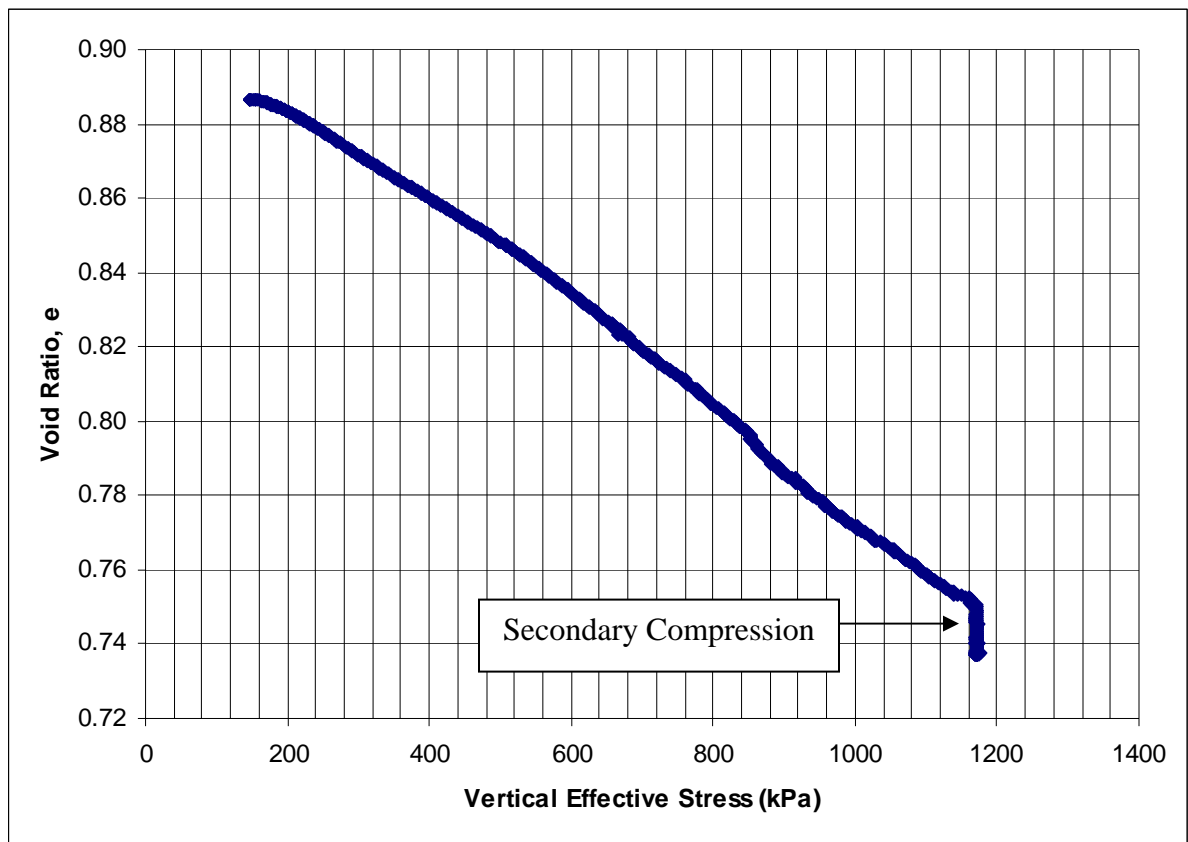
Figure 4.4: Void Ratio vs. Vertical Effective Stress – Triaxial Test # 815

Work Versus Vertical Effective Stress

The main significance of this plot is to confirm the correct preconsolidation stress, and is often a better representation of the actual preconsolidation stress (Becker et al). Axial Strain and Vertical Effective Stress can be used with a number of different methods (e.g. Casagrande, Taylor, etc.) to estimate the preconsolidation stress. This plot can be used to corroborate that data. A line is drawn at the linear portion of the curve and extended down to the Vertical Effective Stress axis. Another line is drawn from the initial slope of the plot. The intercept of the two lines is at the preconsolidation stress ($\sigma'_p = 560 kPa$, best estimate approximately the same as from the Axial Strain vs. Vertical Effective Stress plot).
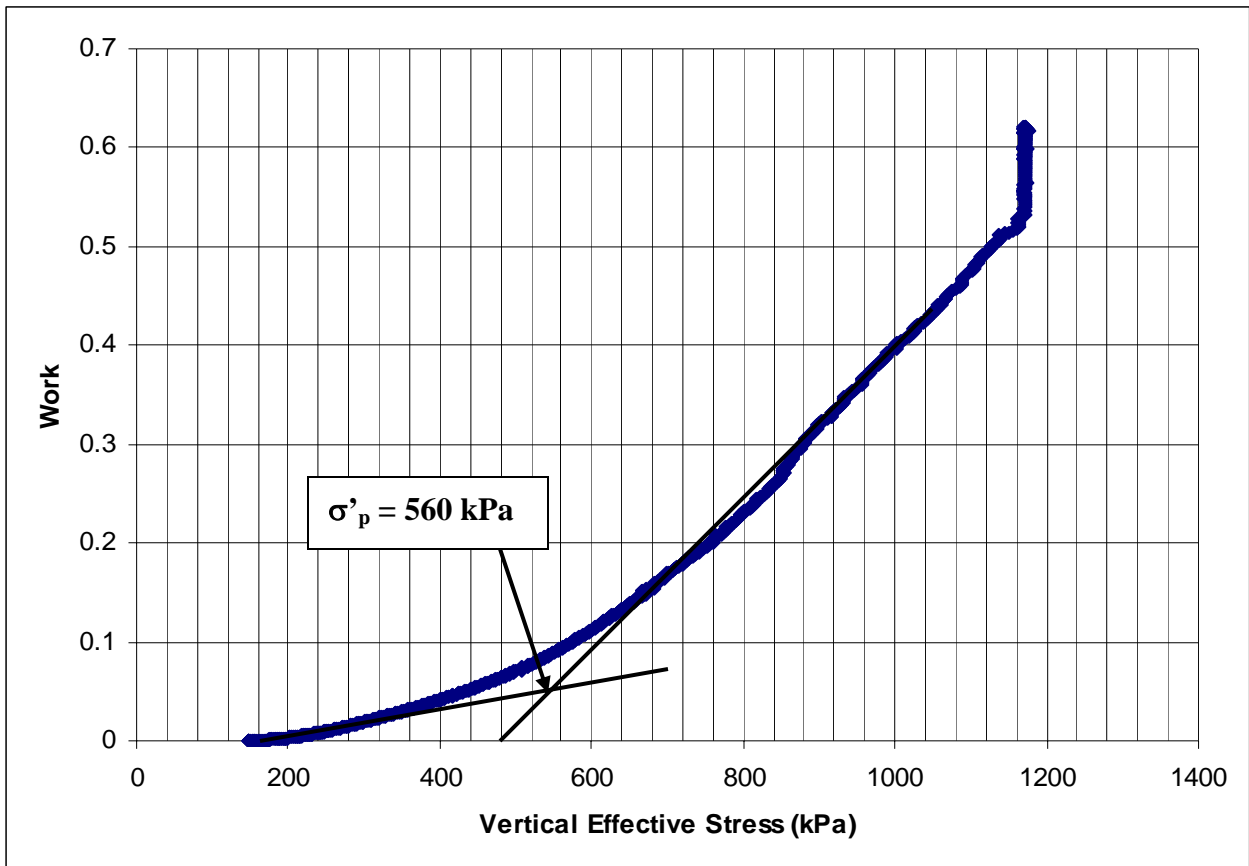
Figure 4.5: Work vs. Vertical Effective Stress – Triaxial Test # 815

Shear Plots

The following plots are based on data taken during the undrained shearing phase of Triaxial Test # 815. Stresses are normalized to the average value of the vertical stress computed during secondary compression and reported in Table 5.3.

Undrained Shear Strength (Shear Stress versus Axial Strain)

This plot describes the variation in shear stress as the axial strain increased under undrained condition. Maximum shear strength (the undrained shear strength, in this research) is achieved very shortly into the test, at only about 1.4% axial strain. Hence, there is very little strain to failure. Very little strain softening is experienced by the sediments as the strain increases. The behavior is very close to elasto-plastic behavior.
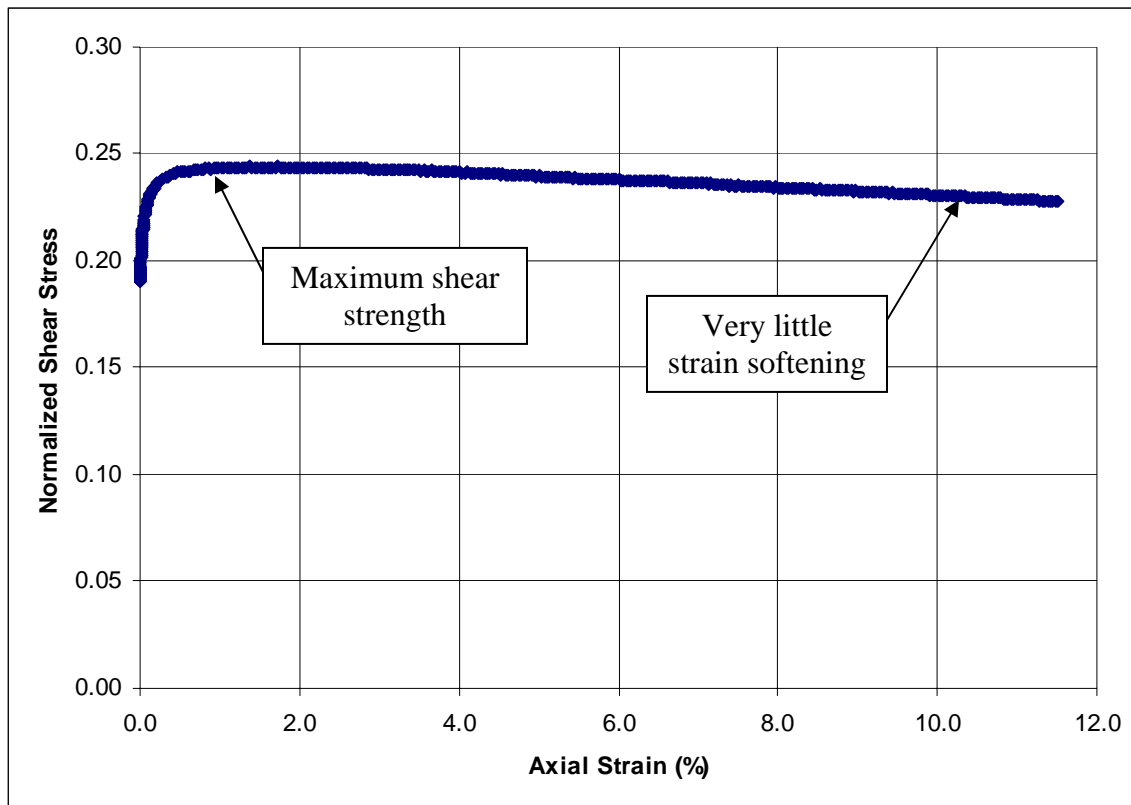
Figure 4. 6: Normalized Shear Strength vs. Axial Strain - Triaxial Test #815
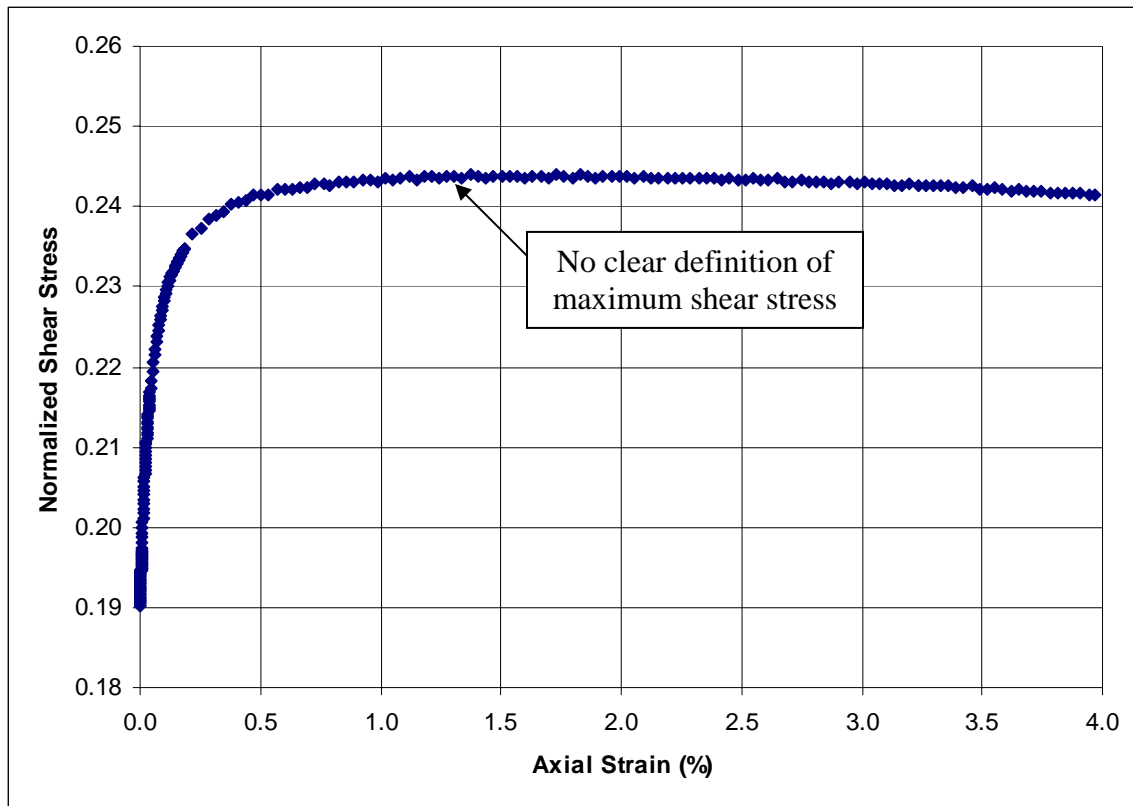
Figure 4.7: Close-up of Normalized Shear Stress vs. Axial Strain - Triaxial Test # 815

A close-up of the shear stress versus axial strain curve at the point of yielding shows that there is not much strain softening after the point of maximum shear, and shear stress decreases slowly with an increase in axial strain. Moreover, as the shearing begins, normalized shear stress begins at 0.19, which is the value of K_o shear stresses. An approximate increase of only 30% (normalized shear stress of 0.245) leads the soil to plastic deformations.

Undrained Stress Path

After consolidation is complete, the specimen is ready to be sheared. At this point, axial deformation is increased while holding cell pressure constant and the back pressure valves of the triaxial have been closed so that pore pressure is not controlled by the apparatus, but instead responds naturally to the increase in axial stress. As the specimen shears, the A value begins at approximately 1/3. All specimen reach maximum shear strength (S_u) within 1 – 2% axial strain. All tests take the general shape shown in Figure 4.8, with the exception of TX #810. This test has a larger increase in A at the point of maximum shear strength than the other six tests. This is believed to be caused by the longer amount of time that it experienced secondary compression after consolidation was complete. As secondary compression occurs, continued volumetric strain builds up within the specimen and could alter the strength and shape of the undrained stress path. Moreover, there is an increase in shear during this time period and thus there is a lower K_o value.
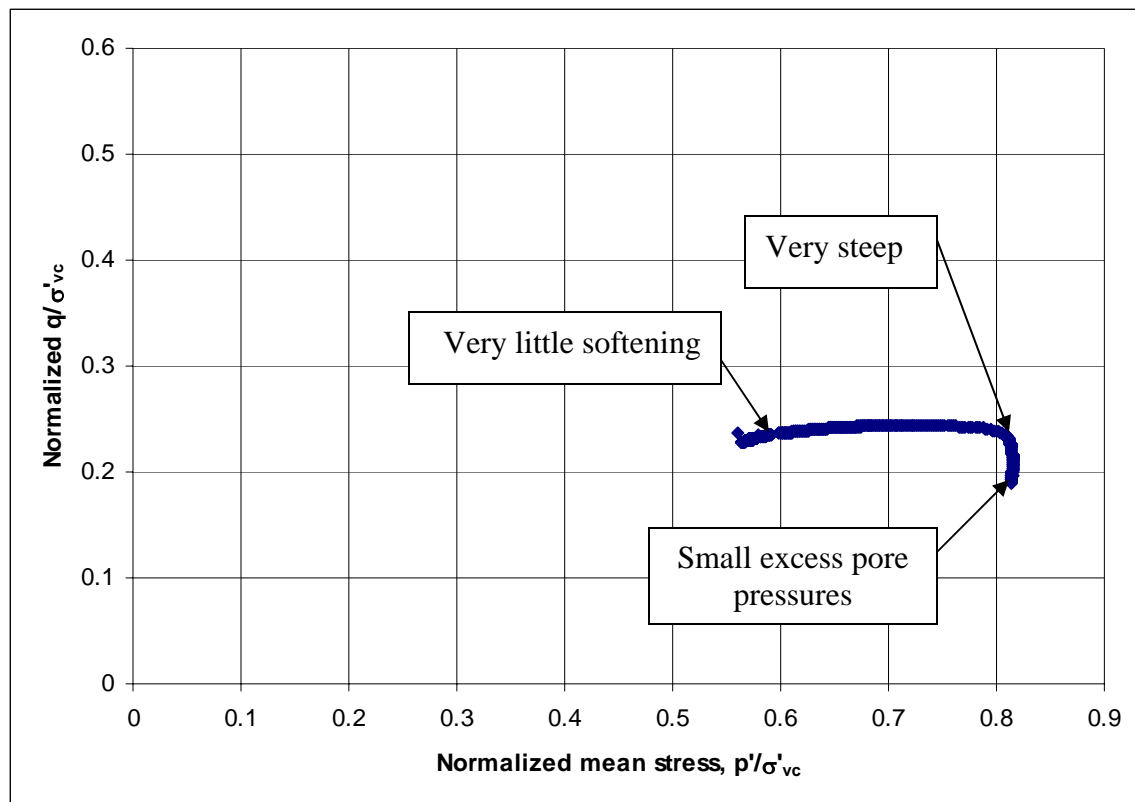
Figure 4.8: Undrained Stress Path – Triaxial Test # 815

Excess Pore Pressure

Excess pore pressure is induced within a specimen as it is loaded and in all cases shows contractive behavior. In this set of tests, as noted, undrained shearing occurs, which means that flow is not allowed out of or into the specimen during the shearing phase.

Pore pressure continues to build up as axial strain is increased and about half of the maximum value of excess pore pressure is induced by 2% axial strain. The pore pressure is still increasing in this case at the end of the test. This suggests that the steady state condition has not been reached.
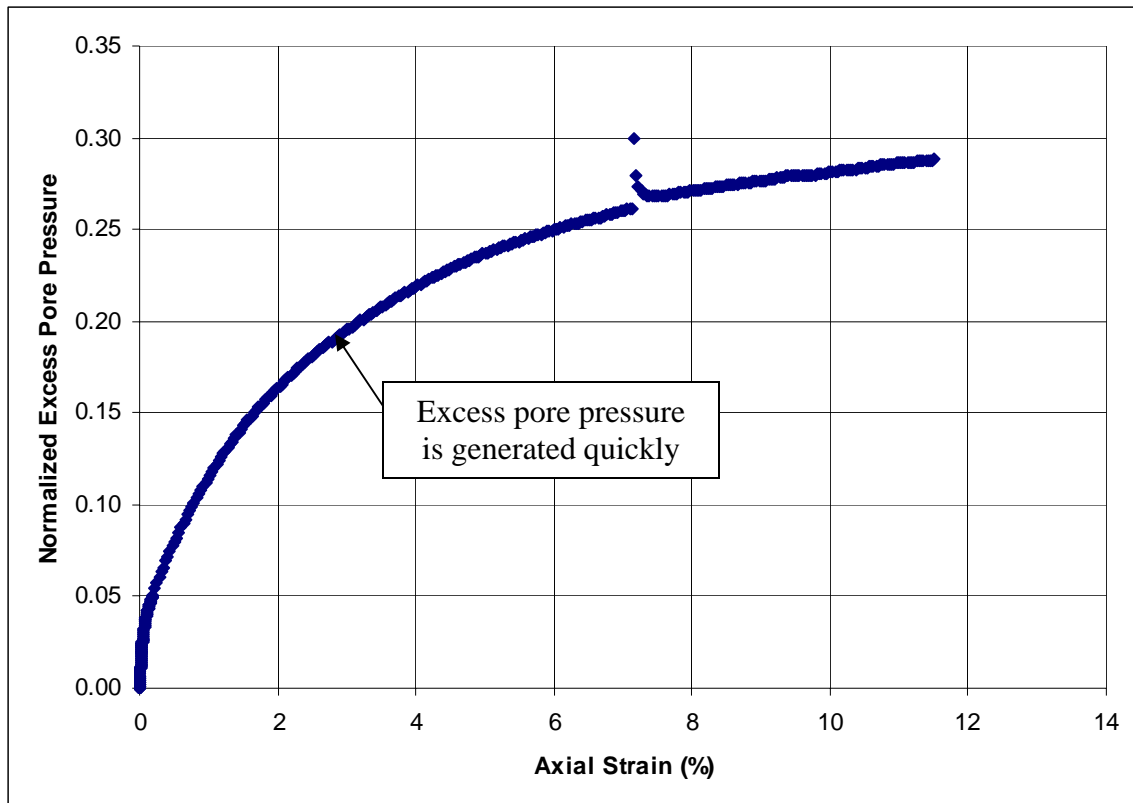
Figure 4.9: Excess Pore Pressure versus Axial Strain – Triaxial Test # 815

Shear-Induced Pore Pressure

As the specimen is sheared, there is an increase in pore pressure that is created as a result of shearing. The normalized value of shear induced pore pressure versus axial strain is shown below and noted in the summary sheet, located in the appendix. The shear-induced pore pressure and the excess pore pressure in triaxial test # 815 are approximately the same value.
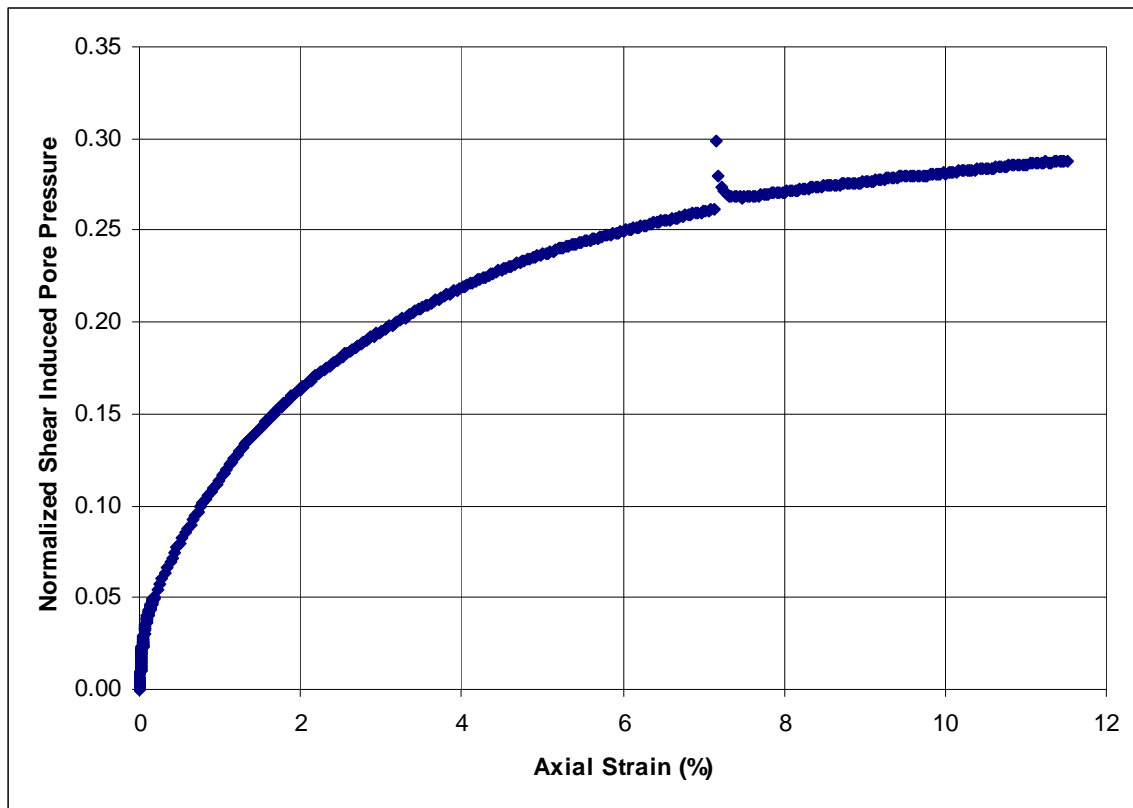
Figure 4.10: Shear-Induced Pore Pressures versus Axial Strain – Triaxial Test #815

The A Parameter Versus Axial Strain

The A parameter describes the slope of the undrained stress path with respect to the initial point (end of consolidation in the stress space) throughout the shearing portion of the test. The A parameter depends very much on the history of the soil. A soft, normally consolidated clay (assumed to be the case in-situ in this particular research) tends to have a parameter A not too far from unity. On the other hand, an overconsoidated clay has a lower value of A (Lambe and Whitman, 1969). Assuming a saturation of 100%, A_f (A at failure) for normally consolidated clay occurs from 0.7 to 1.3 (Bjerrum, 1957).

In this case, A begins at 0.33, which is the expected starting value. Within a couple percent of axial strain, the clay quickly reaches A = 1.5, and by this point, the specimen has experienced plastic deformations.
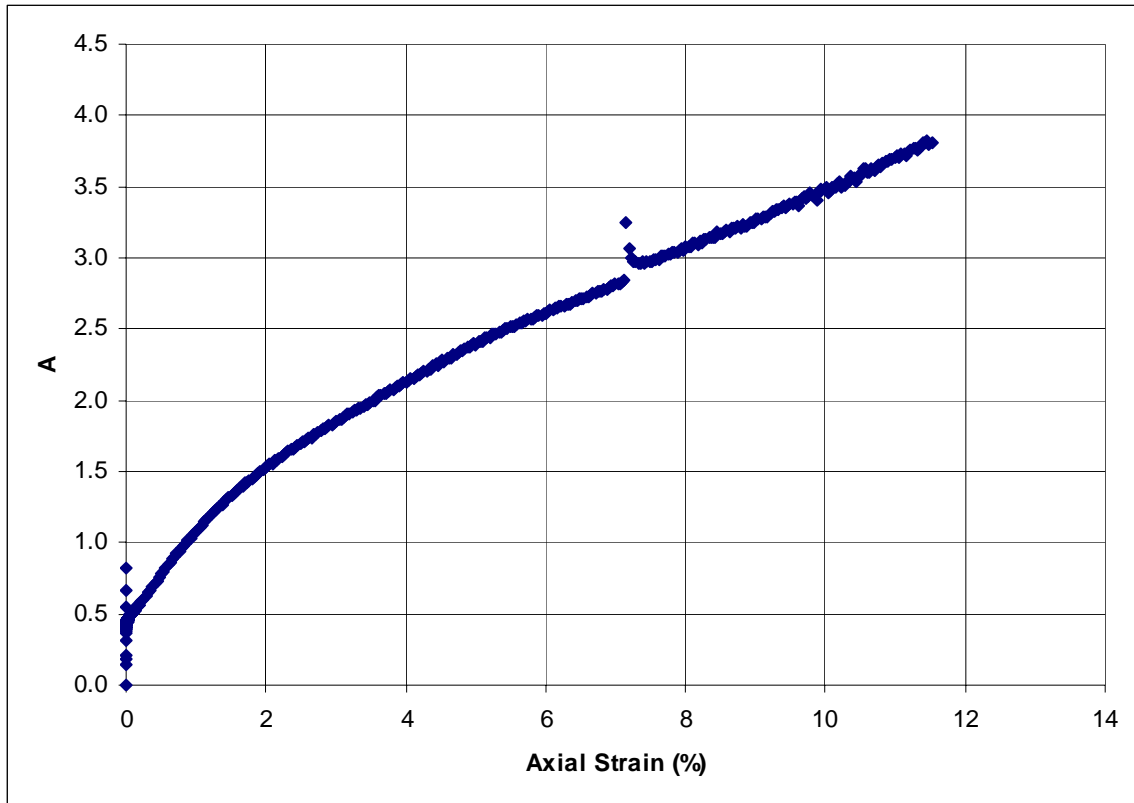
Figure 4.11: The A Parameter versus Axial Strain - Triaxial Test # 815

Secant Modulus as a Function of Axial Strain

Secant modulus is the slope of the stress-strain curve between the initial point and any other point (Lambe and Whitman, 1969). As the stress-strain relationship develops throughout a test, the modulus of the soil starts at E_{max} (the elastic value) is linear over some range of strain and then decreases. As the soil yields, the secant modulus begins to decrease as the soil experiences plastic deformation. The plot below of secant modulus shows that initial normalized modulus of the soil and as the soil begins to fail, the value of the secant modulus decreases.

All tests manifest almost identical results for the secant modulus versus increase in axial strain. It is fairly constant through 0.01% strain. However, after this point, the value of secant modulus begins to decrease quickly.
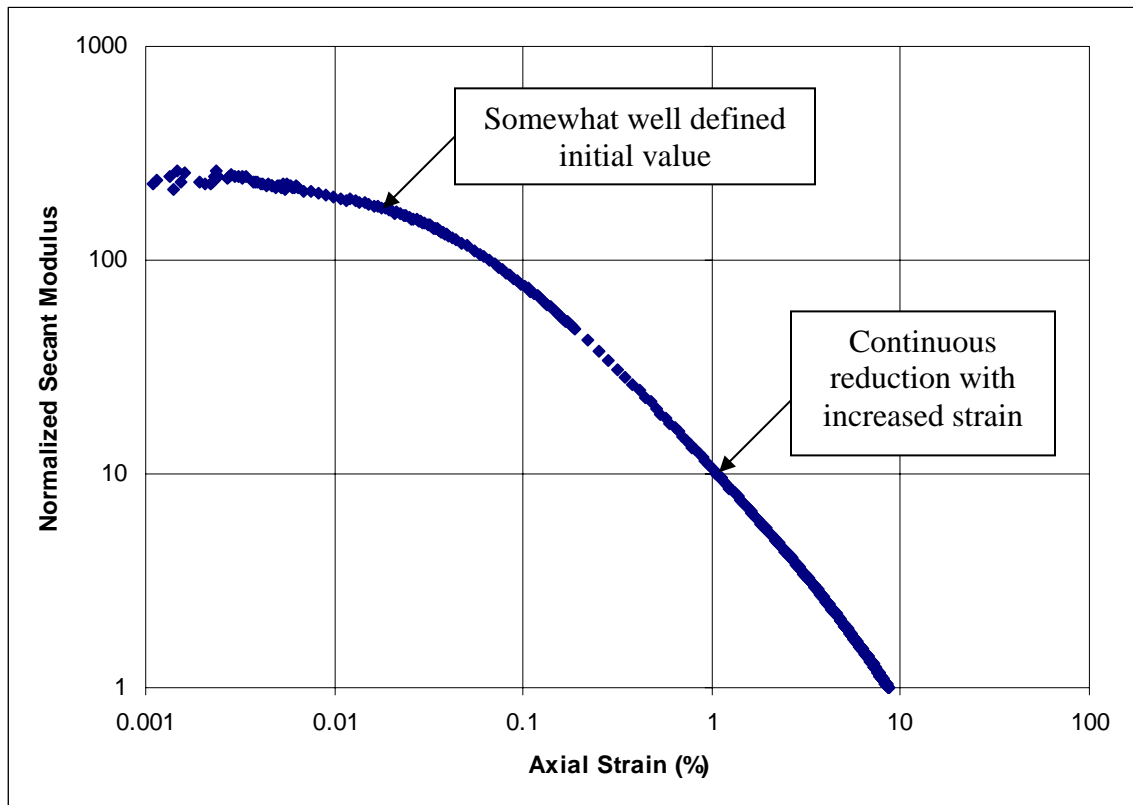
Figure 4.12: Secant Modulus vs. Axial Strain – Triaxial Test # 815

Friction Angle as a Function of Axial Strain

Friction angle increases as long as axial strain increases in all tests, with the exception of TX810. All tests yield a maximum friction angle of $24° \pm 2°$ by the end of the test. General behavior of this plot shows a sharp increase as the specimen is being sheared. As the specimen is sheared, the maximum shear stress occurs and the vertical effective stress decreases. As a result, the friction angle increases as the mean stress goes down.
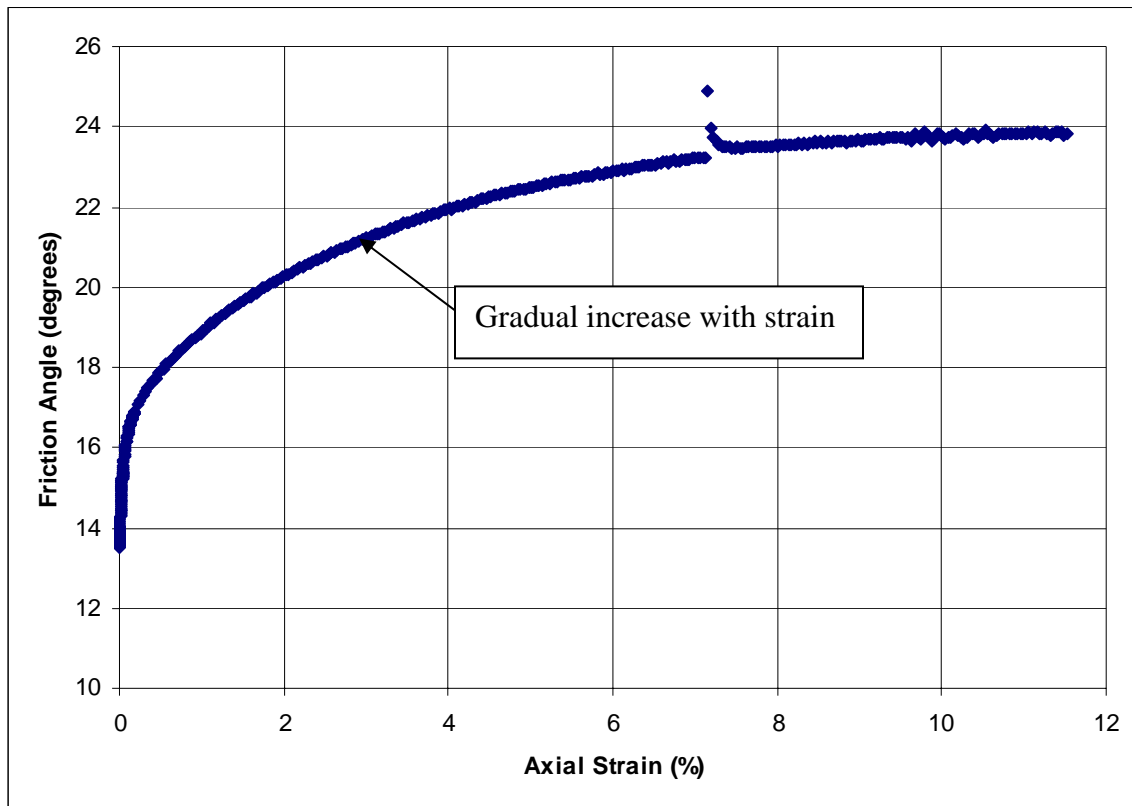
Figure 4.13: Friction Angle vs. Axial Strain – Triaxial Test # 815

4.2 Presentation of CRS Data
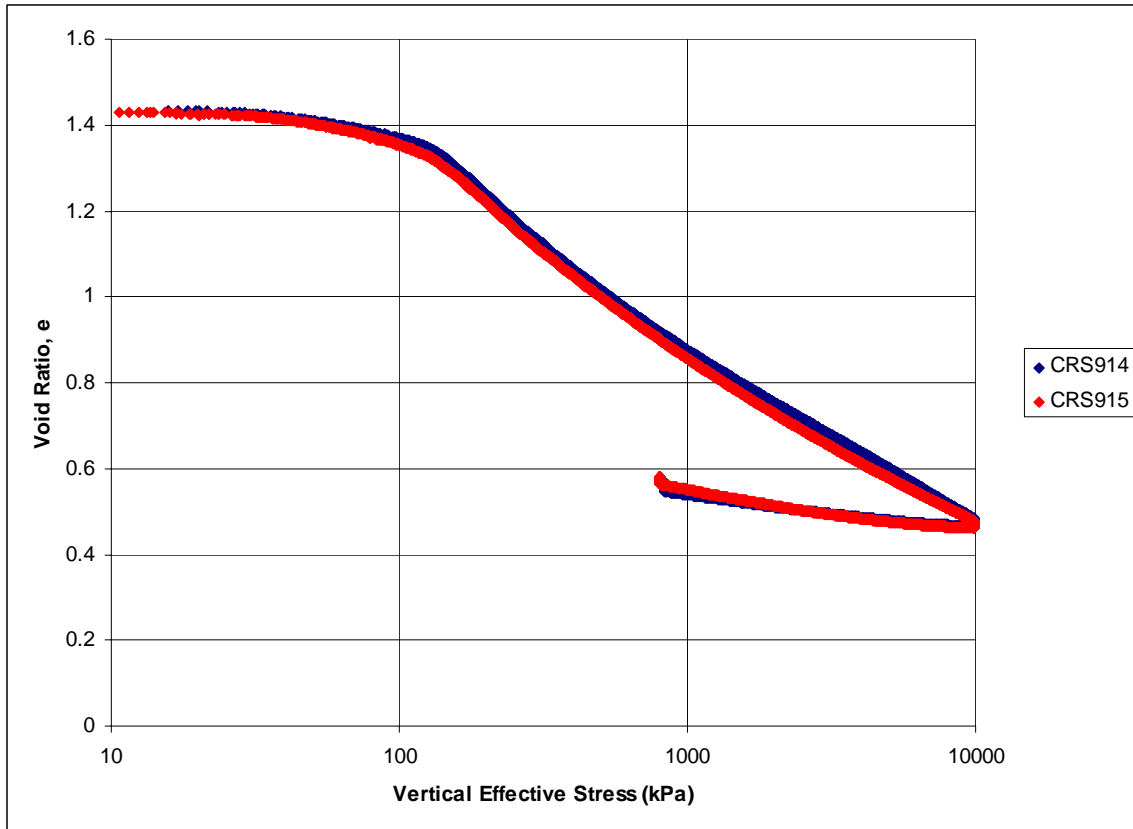
Figure 4.14: Axial Strain versus Vertical Effective Stress of CRS data of RGMC.
The blue line is CRS 914. The Red line is CRS915.

Two CRS tests were run on RGMC, prepared in the same manner as discussed in sections 3.5 and 3.6. The sample was consolidated in the laboratory to 100 kPa and did not experience unloading to OCR = 4. The CRS test was completed at a strain rate of 1% per hour, with 386 kPa back pressure, a maximum stress 10,000 kPa, 12 hours of secondary compression and unloaded at 1% per hour until OCR = 10.

The test results show that the permeability (k) of the material is approximately 3×10^{-9} cm/sec and the coefficient of consolidation (C_v) is approximately 4.5×10^{-4}.

At the end of the secondary compression phase, the pore pressure was still positive. All the results of the CRS tests are in Appendix A. CR is calculated at 0.45 for CRS914 and 0.46 for CRS915.

Chapter 5

Interpretation of Results

Theory is the language by means of which lessons of experience can be clearly expressed.

Karl von Terzaghi

5.1 Introduction

A discussion of issues of interest are presented in this chapter, including factors that may explain some of the behavior observed in this research and a brief comparison of RGMC to intact GMC material, and RGMC to RBBC and their similarity of strength with respect to K_o.

5.2 Comparison of CRS Data to Compression Curve

When comparing the results of the seven triaxial tests to the CRS data on the void ratio versus vertical effective stress space, it is easy to notice that some of the tests match up nicely with the CRS data and some do not. Tests #797, 801 and 804 agree very nicely with the CRS and seem to define the envelope. Test # 807 corroborates this, lying directly online with the CRS data. However, tests #810, #812 and #815 do not agree and appear not to have made the envelope defined by the other tests and the CRS test. The unloading curve and the reloading curve have, approximately, the same slope, as expected.

CRS results show that the preconsolidation stress is approximately 100 kPa. This corresponds to the load applied in the laboratory. However, preconsolidation stress calculated from the analysis of the triaxial data does not match stress applied to consolidate the material in the laboratory in order to prepare the specimen for triaxial tests.

C_v has been calculated at $4x10^{-4} cm^2/sec$ from the data collected by the LVDT placed on the specimen during laboratory consolidation.

These results match up nicely with C_v calculated from the data collected from the CRS testing program (CRS914: $C_v = 4.4 \times 10^{-4}$; CRS915: $C_v = 2.5 \times 10^{-4}$).
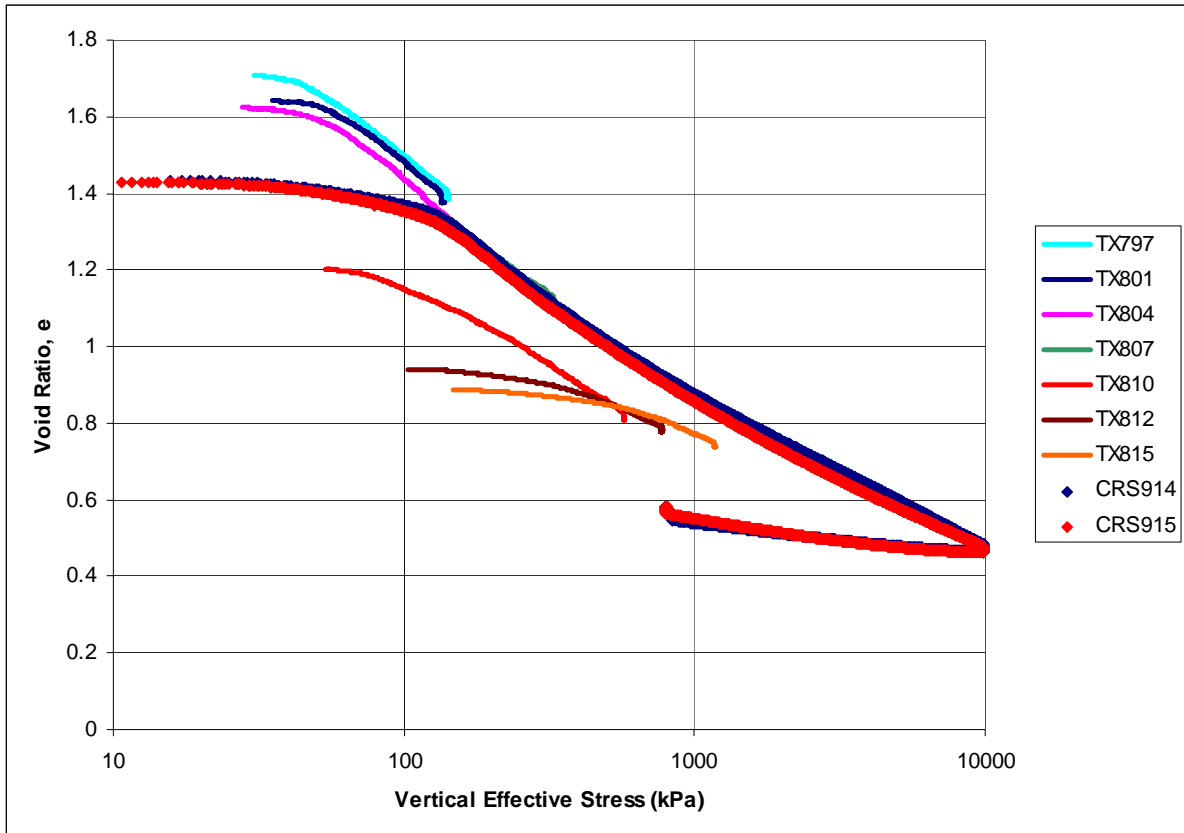
Figure 5.1: Void Ratio versus Vertical Effective Stress – Comparison of triaxial data to CRS data.

5.3 Comparison of Compression Curves From Triaxial and CRS
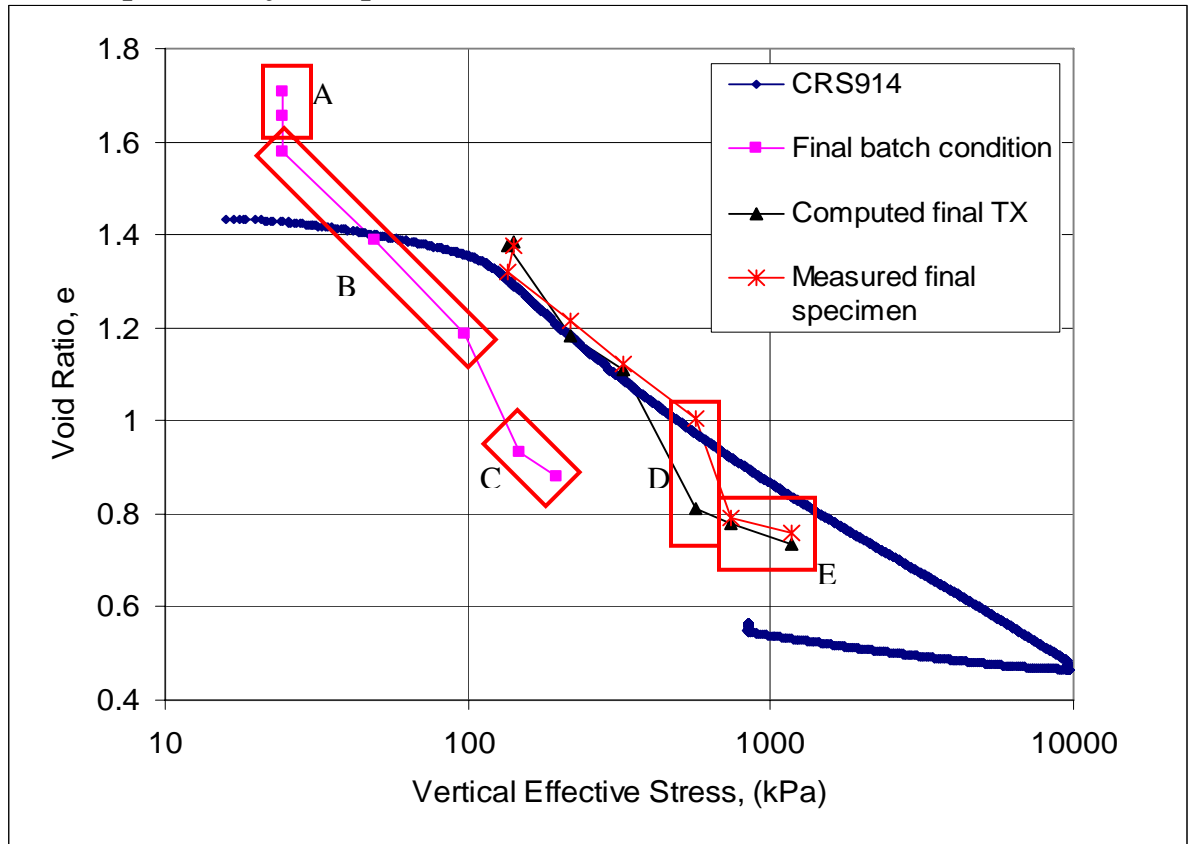
Figure 5.2: Comparison of Compression Curves from Triaxial Data and CRS Data

Figure 5.2 shows CRS914 data compared to void ratios from three different sections of the triaxial testing: from the trimmings of the specimen before testing; from the calculated triaxial data file; and from the moisture content of the specimen after the triaxial test. The data labeled "final batch consolidation" are from the initial triaxial specimen void ratio plotted at the final batch laboratory consolidation stress. This corresponds to an OCR = 4 condition. The data titled "computed final TX" are from the volume change measured during triaxial consolidation at the final triaxial stress. The data labeled "measured final specimen" are from the measured water content at the end of the triaxial test plotted at the final consolidation stress.

The box titled "A" in Figure 5.2 corresponds to TX #797 and #801, which are from the same batch and have not fully consolidated due to the short increment time. "B" refers to material which has the correct trend, namely they are parallel to the virgin consolidation line, as represented by CRS914. A and B include data points which are all inside the

virgin compression line because of the initial OCR = 4 condition prior to starting the triaxial test. The data within "C" shows much lower void ratio, with corresponding end void ratios shown in "E," from both the triaxial reduced data and specimen water content, which suggest material from a different location in the borehole (TX #812 and #815). "D" shows two points from TX #810 which do not agree. The end void ratio from the reduced data file shows 0.881 while the final water content taken from this specimen calculates to 1.004. There is an error which causes a discontinuity between the two data points which is believed to be derived from an internal leak of the triaxial apparatus, causing a low K_o, and thus, a high undrained shear strength. The data points not within a box agree with what is expected, namely void ratio decreases as stress increases and the calculated final void ratio and corresponding water content from the specimen agree.

As mentioned in section 3.6, silicone oil was used to coat the sides of the consolidation tubes as the soil was cast. However, this was not done in # 797. As a result, shear strains may have built up on the sides of the specimen during extrusion more than it would have had a coat of silicone oil been added before the slurry was placed. The other two tests, # 801 and #804, as well as all other tests, included silicone oil on the sides of the consolidation tube. Behavior of # 801 and # 804 are quite similar when compare to that of # 797. Shear stress of the two tests prepared the same way show very similar results, contrary to # 797.

5.4 K₀ versus Initial Strain
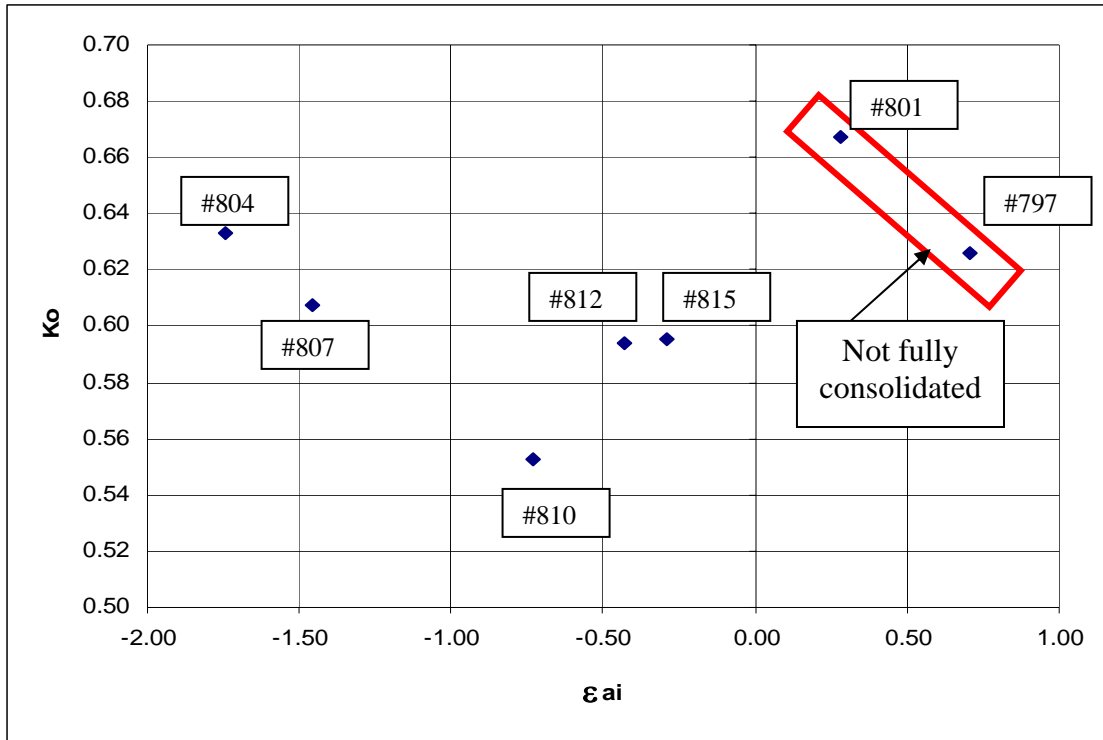
Figure 5.3: Ko versus Axial Strain Corresponding to Sampling Effective Stress

All but two specimens experienced swelling upon setup in the triaxial cell: triaxial test

#797 and #801. The swelling is indicated by a negative value of ε_{ai}, (axial strain corresponding to sampling effective stress Figure 5.3). Tests #797 and #801 do not experience negative values of ε_{ai}. An explanation for this is not letting the final load during sample consolidation (in these two tests, 98 kPa) rest on the specimen for enough time, which is consistent with observations in the previous Figure 5.2. All subsequent batches experienced the final load increment for at least five days, (two days). Test TX #810 continues to be suspected erroneous.

5.5 Shear Strength versus Stress Level

From Figure 5.4 there does not appear to be a trend between shear strength and consolidation stress. Again, TX #810 is clearly an outlier. The normalized strength values

have mean of 0.2484 and a standard deviation of 0.0064, which is a very weak value of strength with a narrow range. From this plot, it again appears that test #810 is erroneous.
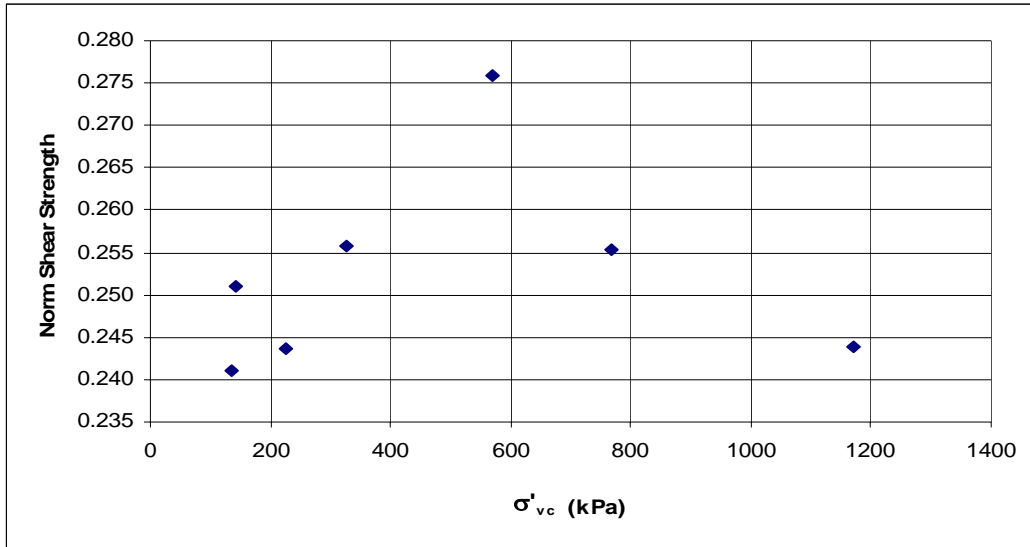
Figure 5.4: Normalized Shear Strength versus Consolidation Effective Stress

5.6 Friction Angle versus Stress Level

Presented in Figure 5.5 is the relationship between effective friction angle at maximum obliquity during the triaxial test versus the consolidation effective stress. There does not appear to be any distinct relationship between the two.
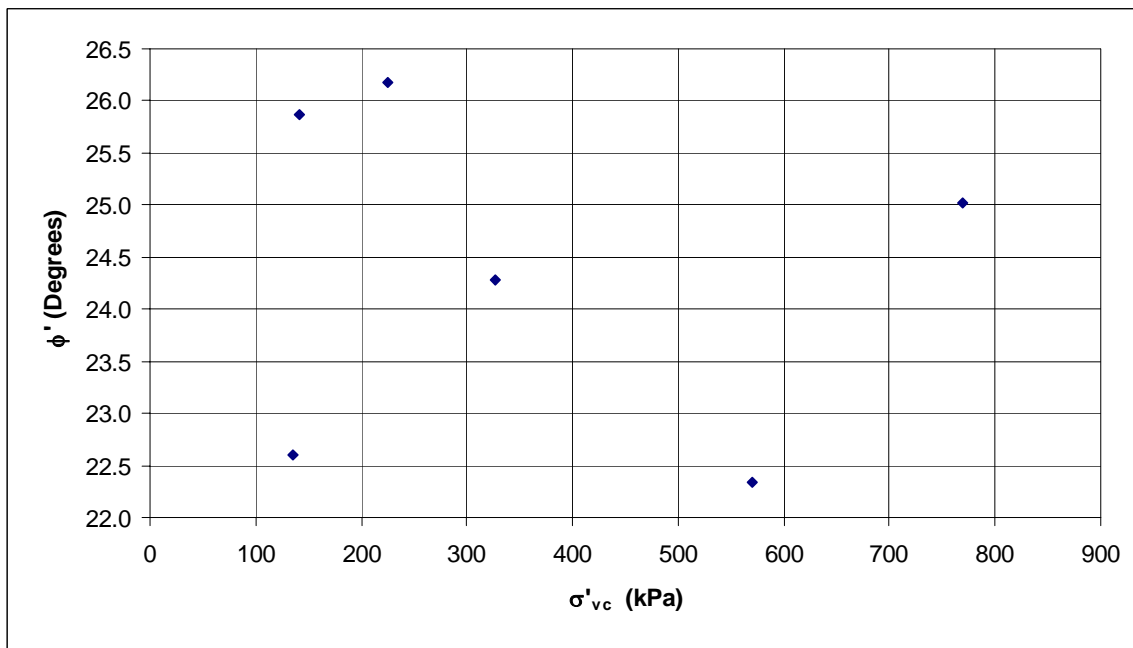
Figure 5.5: Friction Angle at Maximum Obliquity versus Consolidation Effective Stress

5.7 K_o versus Shear Strength

Figure 5.6 shows the relationship between Normalized Shear Strength and K_o. Overall, the trend appears that shear stress decreases with increasing K_o. Even TX # 810 agrees with these data. However, TX #810 appears to have the wrong K_o value, it is too low comparative to the rest of the data and thus explains this test's high strength, relative to other tests. However, there does not seem to be a trend between K_o and the following: consolidation stress; modulus and friction angle.
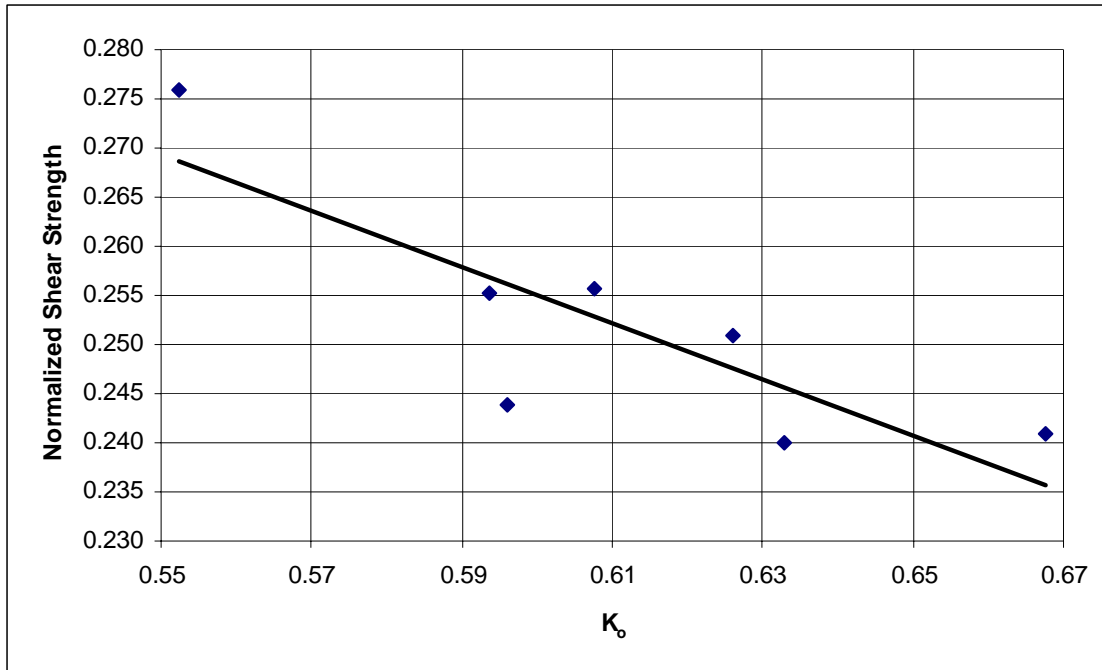
Figure 5.6: Normalized Shear Strength versus K_o

5.8 Comparison of RGMC to Intact Material from Leg 308

In 2006, a number of triaxial K_o consolidated, undrained compression loading tests (CK_oUC) were conducted on intact material taken from APC tubes collected during Expedition Leg 308. During that time, tests were administered to determine the effect and amount of disturbance within the samples. Moreover, information regarding the soil's strength, friction angle, modulus, etc. was also documented. Most importantly, these tests results allow a comparison between resedimented and intact Gulf of Mexico clay to be made. Figure 5.7 provides, a comparison of normalized shear strength versus K_o. The

pink squares represent data points in the data set of intact Gulf of Mexico Clay; the red triangles are from the data set collected in this research.
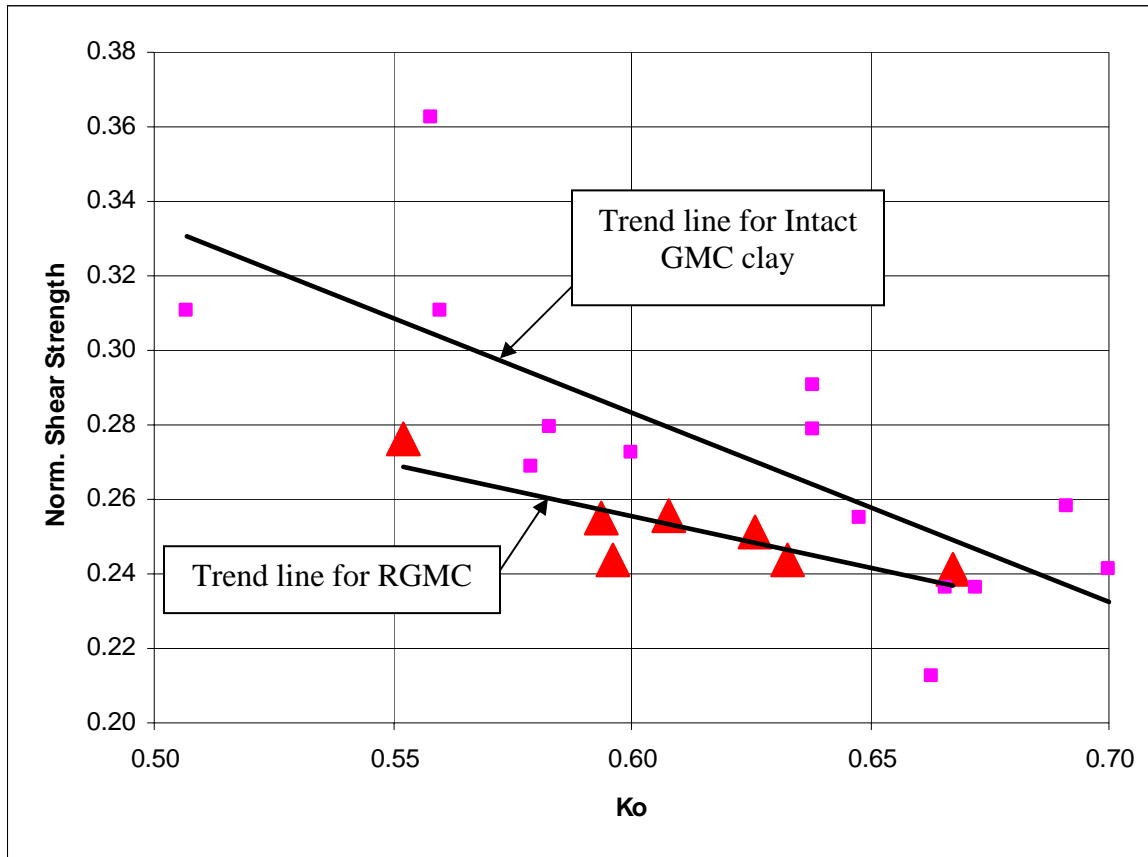
Figure 5.7: Comparison of RGMC and Intact GMC, K_o versus Shear Strength Values

From the plot, it is easily seen there are a wide range of data points collected from the intact data set. There is a downward trend of normalized shear strength with an increase in K_o value. This trend is recreated with the data from the RGMC, although there is less scatter with the RGMC than the intact GMC. One potential reason for the intact material data points being highly scattered from the trend line is that disturbance within the specimen may be altering the results and the material is different from sample to sample. It is assumed that disturbance of RGMC is avoided with the addition of silicone oil to reduce side friction, and handling specimens with extreme care during transportation between the laboratory where it was prepared and the triaxial cell. Below are the data points for both intact GMC and RGMC normalized shear strength and K_o values.

Table 5.1: Comparison of Normalized Shear Strength and Corresponding K_o Values for Intact GMC and RGMC

Intact Material Data			RGMC Data		
Triaxial Number	Normalized Undrained Shear Strength	K_o	Triaxial Number	Normalized Undrained Shear Strength	K_o
725	0.2125	0.663	797	0.2510	0.626
728	0.2552	0.648	801	0.2410	0.667
729	0.2728	0.600	804	0.2399	0.633
730	0.2905	0.638	807	0.2558	0.608
735	0.2790	0.638	810	0.2760	0.552
736	0.3628	0.558	812	0.2553	0.594
737	0.2583	0.691	815	0.2439	0.596
770	0.3104	0.507			
773	0.2413	0.700			
774	0.2688	0.579			
775	0.2795	0.583			
776	0.2362	0.672			
778	0.3104	0.560			
779	0.2365	0.666			

5.9 Comparison of RGMC to RBBC

A very extensively studied material at MIT is RBBC. This material has been the center of research studies currently ongoing at MIT and a comparison of the two materials is presented. The two clays exhibit quite different undrained shear strengths in the normally consolidated range. RBBC's strength ranges from 0.28 to 0.33 and RGMC between 0.24 and 0.27. RBBC has far less scatter in the plot than does RGMC. RBBC in the data shown was consolidated at a range from approximately 150 kPa up to 10,000 kPa where RGMC was consolidated from approximately 150 kPa up to 1,500 kPa. Both exhibit a decrease in shear strength as an increase in K_o occurs, similar to that of intact GMC. The range of undrained shear strength is a function of consolidation stress for RBBC, i.e. as consolidation stress increases, undrained shear strength decreases. There is not enough data to make the same conclusions about RGMC.
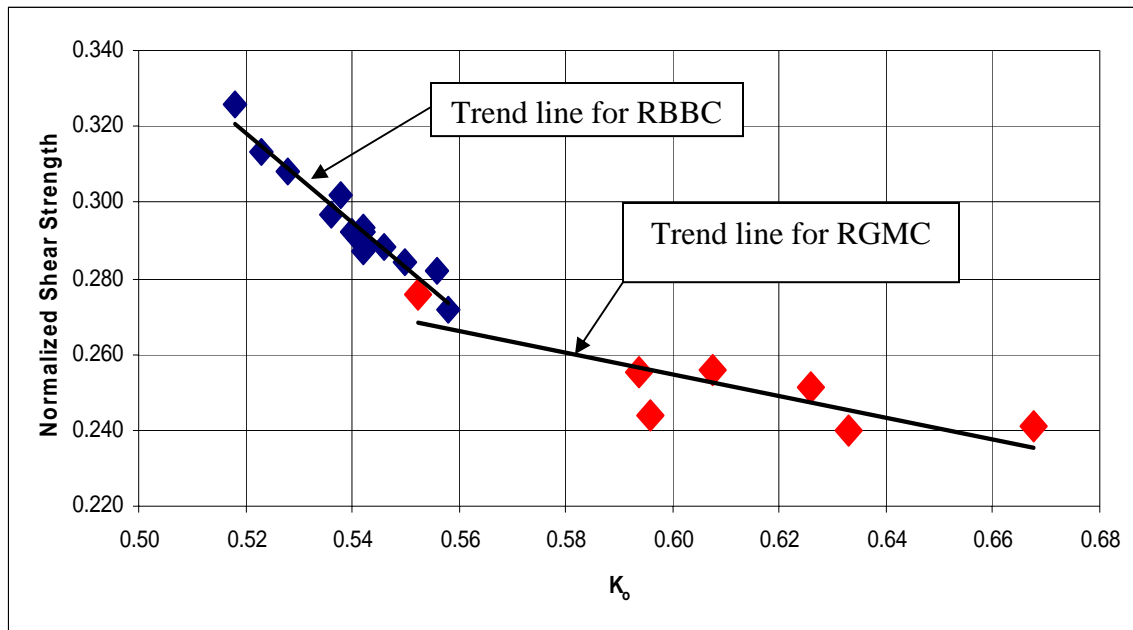
Figure 5.8: Undrained Shear Strength versus Ko value for Resedimented Boston Blue Clay and Resedimented Gulf of Mexico Clay

5.10 Normalized Shear Strength as a Function of Axial Strain

Figure 5.9 shows the relationship between Normalized Shear Strength and Axial Strain. Again, the range of normalized shear strength of a wide variety of soils (Boston Blue clay, Kaolinite, arctic soils, Taipei Clay, etc.) has been identified between 0.28 and 0.33. The range for this set of RGMC clay is 0.24 and 0.27, which is much weaker when compared to RBBC. Also, the data shows that there is no general trend in the relationship between consolidation stress and undrained shear strength. After the soil reaches its undrained shear strength, the soil experiences very little strain softening, but it is not a terribly dramatic decrease from the maximum stress. Test #810, which tested as the highest value of shear strength, had the biggest strain softening effect of all the tests.
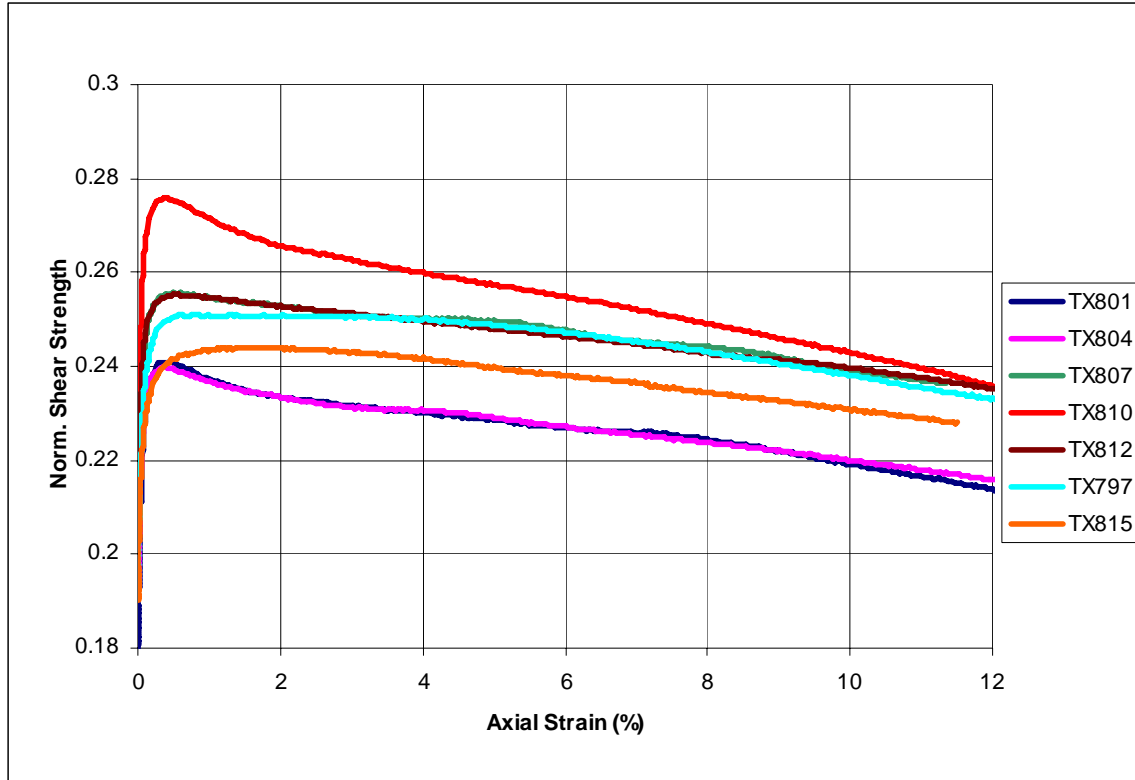
Figure 5.9: Normalized Shear Strength versus Axial Strain

5.11 Discussion of Results

It is not known why preconsolidation stress did not match with the laboratory consolidation stress; even in cases where it is proven that end of primary has been achieved.

At first glance at this resedimented Gulf of Mexico clay, it is clear that it is a very soft, and highly compressible material, having a strain of approximately 60% while consolidating in the laboratory in preparation for triaxial testing.

During the shearing phase of the test, triaxial test # 810 has an unusual undrained stress path, compared with the other tests. The path has a normal A value beginning at 0.33, and fails within a couple percent strain, but has a very sharp increase in the A value, causing a dramatic change in direction of the stress path. This behavior may be related to the consolidation path the specimen took during testing. The test results yield a relatively low

K_o value, which in turn have presented a higher strength than the other six test results. Again, the data for TX # 810 is erroneous and believed to be caused by an internal leak.

There is some anomalous data regarding the stiffness of the material manifested in the axial strain versus vertical effective stress and void ratio versus vertical effective stress plots. Both plots show a linear slope (strain versus stress the linear portion is in the NC region and void ratio versus stress occurs throughout) which is peculiar given that one is in a log scale and the other is not.

5.12 Summary Graphs and Tables

Presented in the end of this chapter are the summary graphs and tables of the results gathered in this testing program. The graphs for the triaxial presented are cumulative of all tests and are separated into two sections: consolidation and shear. The CRS graphs follow the triaxial graphs.

The following summary graphs for consolidation include:

- K_o versus Vertical Effective Stress (Figure 5.10)
- Void ratio versus Vertical effective Stress (Figure 5.11)

Shear summary graphs include:

- Normalized shear strength versus Axial Strain (Figure 5.12)
- Undrained stress path (Figure 5.13)
- Friction angle versus Axial Strain (Figure 5.14)
- The A parameter versus Axial Strain (Figure 5.15)
- Excess Pore Pressure versus Axial Strain (Figure 5.16)
- Shear-Induced Pore Pressure versus Axial Strain (Figure 5.17)
- Secant Modulus versus Axial Strain (Figure 5.18)

The CRS results are also presented within this section, including:

- Void Ratio versus Vertical Effective Stress (Figure 5.19)
- Permeability versus Void Ratio (Figure 5.20)
- C_v versus Vertical Effective Stress (Figure 5.21)
- Pore Pressure Ratio versus Vertical Effective Stress (Figure 5.22)

Finally, there are summary tables which include essential information collected from each triaxial test, both during the consolidation and shearing phases of the test. In addition, this table includes the information for the two CRS tests.

From the Consolidation Summary Sheet (Table 5.2)

- Index Tests:
    - ω_n, water content from specimen trimmings (%)
    - SD, standard deviation of values of water content
    - # obs, number of observations of water content
- Specimen data characterize the condition of the trimmed specimen:
    - ω_n, natural water content (%)
    - γ_t, total unit weight (g/cm^3)
    - e_i, initial void ratio
    - S_i, initial saturation
    - G_s, specific gravity (assumed)
- Conditions
    - σ'_i, initial sampling effective stress (kPa)
    - ε_{ai}, corresponding axial strain to sampling effective stress (%)
    - U_b, back pressure saturation, with $\sigma' = \sigma'_i$ (kPa)
    - ε_{ab}, resulting axial strain due to back pressure (%)
    - B, B-value
    - ε_{vol}, required inflow of water due to back pressure saturation (%)
- Consolidation Results
    - σ'_p, preconsolidation stress from analysis of triaxial compression curve (kPa)
    - ε_a/hr, strain rate at which specimen is consolidated (%/hour)
    - C_c, compression index
    - CR, compression ratio
    - ε_a, axial strain at end of secondary compression (%)

- ε_{vol}, volumetric strain at end of secondary compression (%)

- $\sigma'_{vc} = \sigma'_{vm}$, maximum/consolidation effective stress (kPa)

- K_c, average at rest pressure ratio during secondary compression

- t_s, time secondary compression is experienced (hours)

Shear results include (Table 5.3):

- Specimen Data

  - ω_n, natural water content (%)

  - γ_t, total unit weight (g/cm^3)

  - e_i, initial void ratio

  - S_i, initial saturation

  - G_s, specific gravity (assumed)

- Conditions (prior to shearing):

  - e_c, void ratio at end of consolidation and secondary compression

  - K_c, average at rest pressure ratio during secondary compression

  - σ'_{vc}, maximum/consolidation vertical effective stress (kPa)

  - ε_{ac}, axial strain at end of consolidation and secondary compression (%)

  - ε_a/hr, strain rate at which specimen is sheared (%/hour)

- At maximum shear and maximum obliquity:

  - ε_a, axial strain (%)

  - q_{corr}/σ'_{vc}, shear stress normalized with the corrected consolidation vertical effective stress

  - q/σ'_{vc}, normalized shear stress with the consolidation vertical effective stress

  - $\Delta u_e/\sigma'_{vc}$, normalized excess pore pressure

  - $\Delta u_s/\sigma'_{vc}$, normalized shear-induced pore pressure

  - p'/σ'_{vc}, normalized mean effective stress

  - q/p', stress ratio

  - ϕ', effective friction angle (degrees)

- o   A, Skempton's pore pressure parameter
- Normalized Secant Modulus attained at the following points during shear:
  - o ε_a (axial strain) at 0.001%
  - o ε_a (axial strain) at 0.01%
  - o ε_a (axial strain) at 0.1%
  - o $\Delta q / \Delta q_{max}$ equals 0.3
  - o $\Delta q / \Delta q_{max}$ equals 0.5
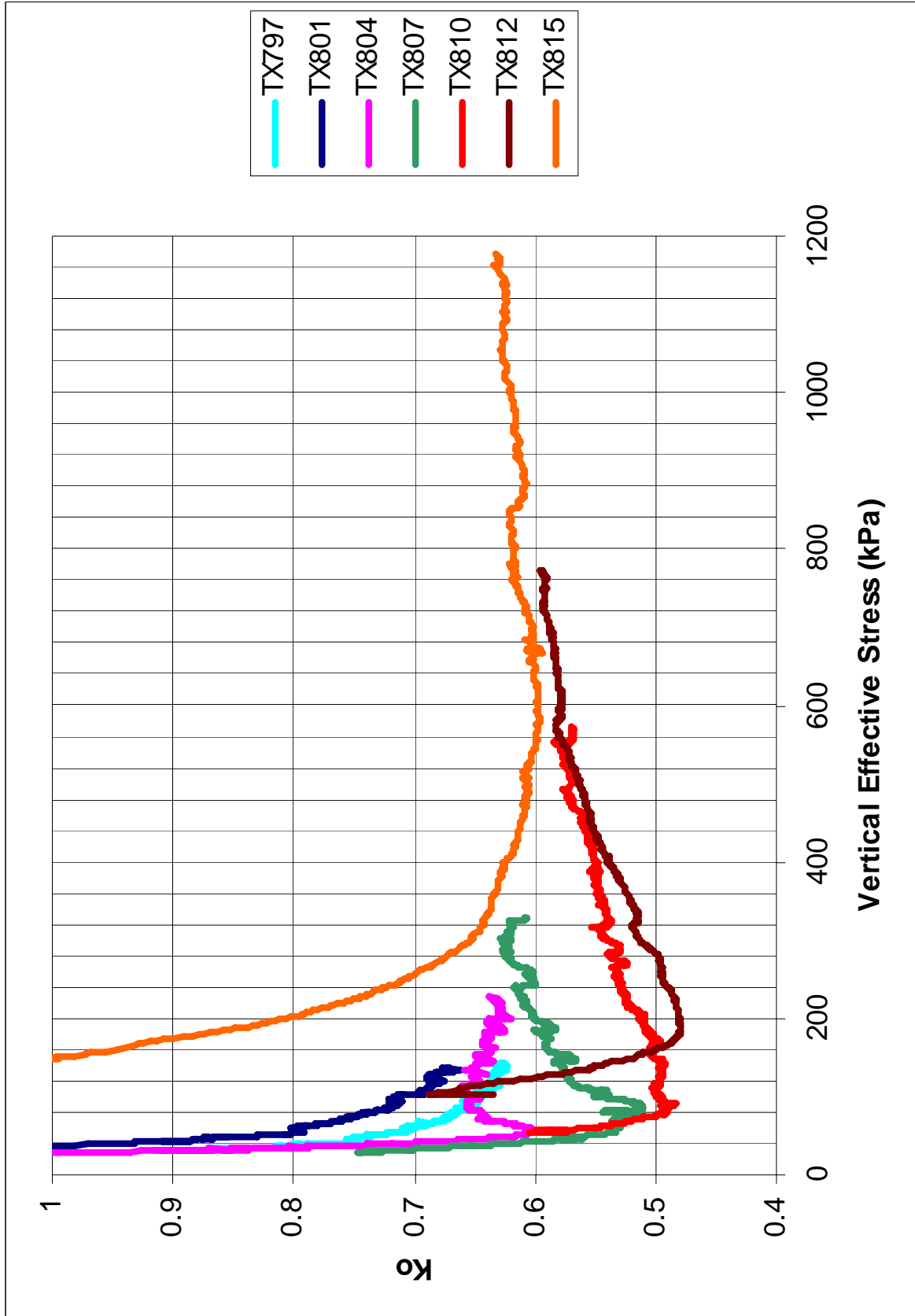
Figure 5.10: K_o Versus Vertical Effective Stress – Summary Table of Triaxial Testing of RGMC
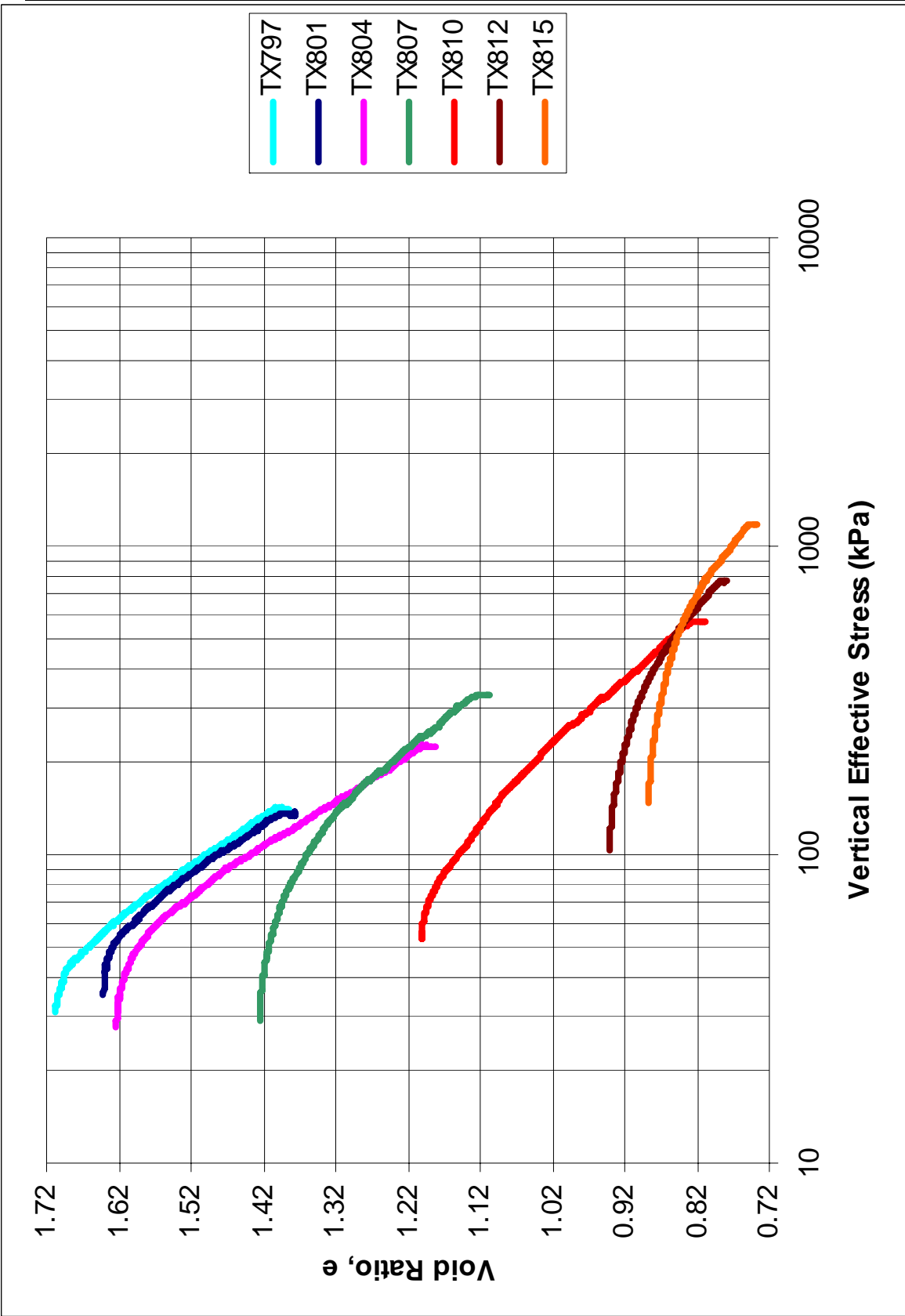
Figure 5.11: Void Ratio Versus Vertical Effective Stress – Summary Table of Triaxial Testing of RGMC
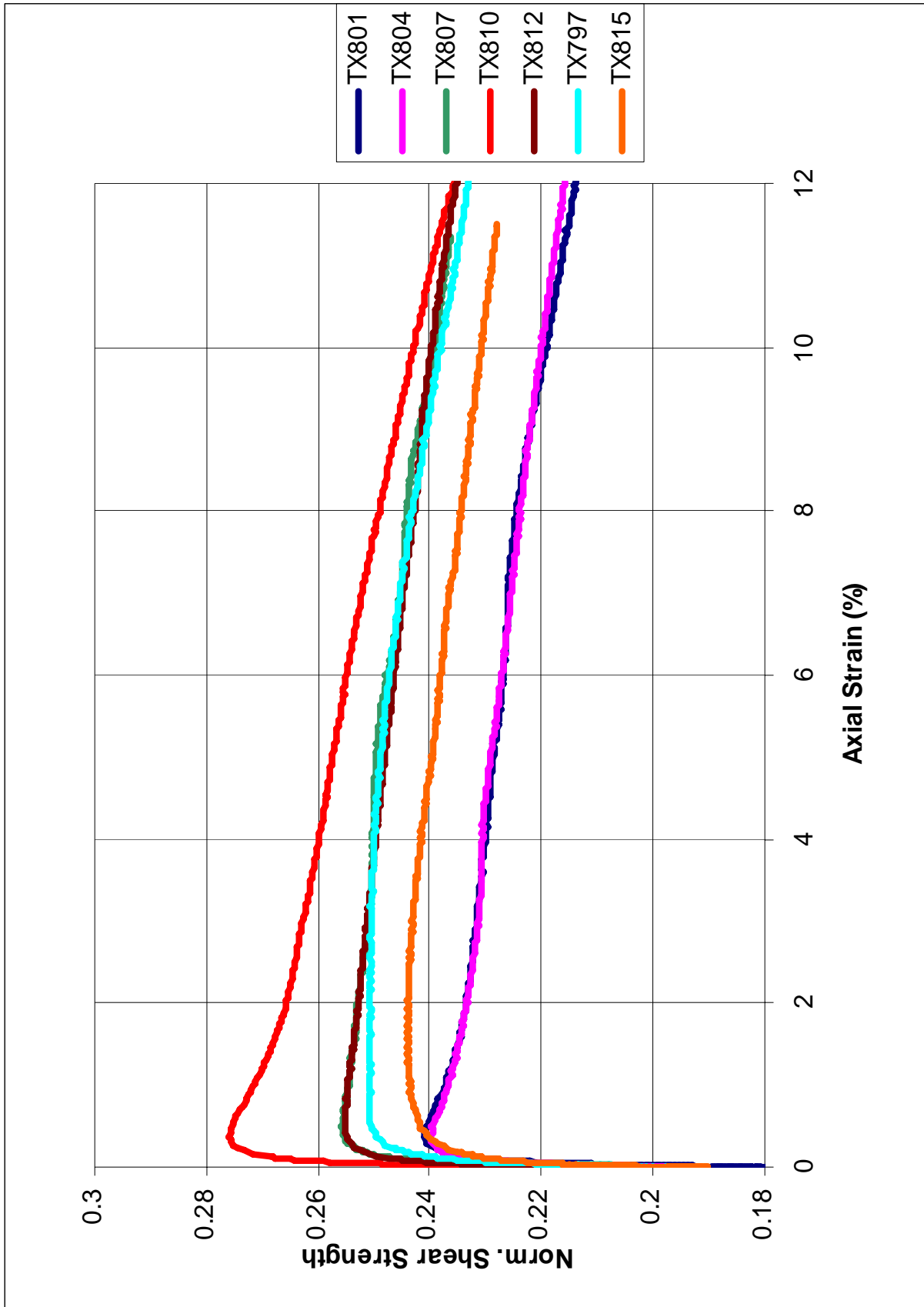
Figure 5.12: Normalized Shear Strength Versus Axial Strain – Summary Table of Triaxial Testing of RGMC
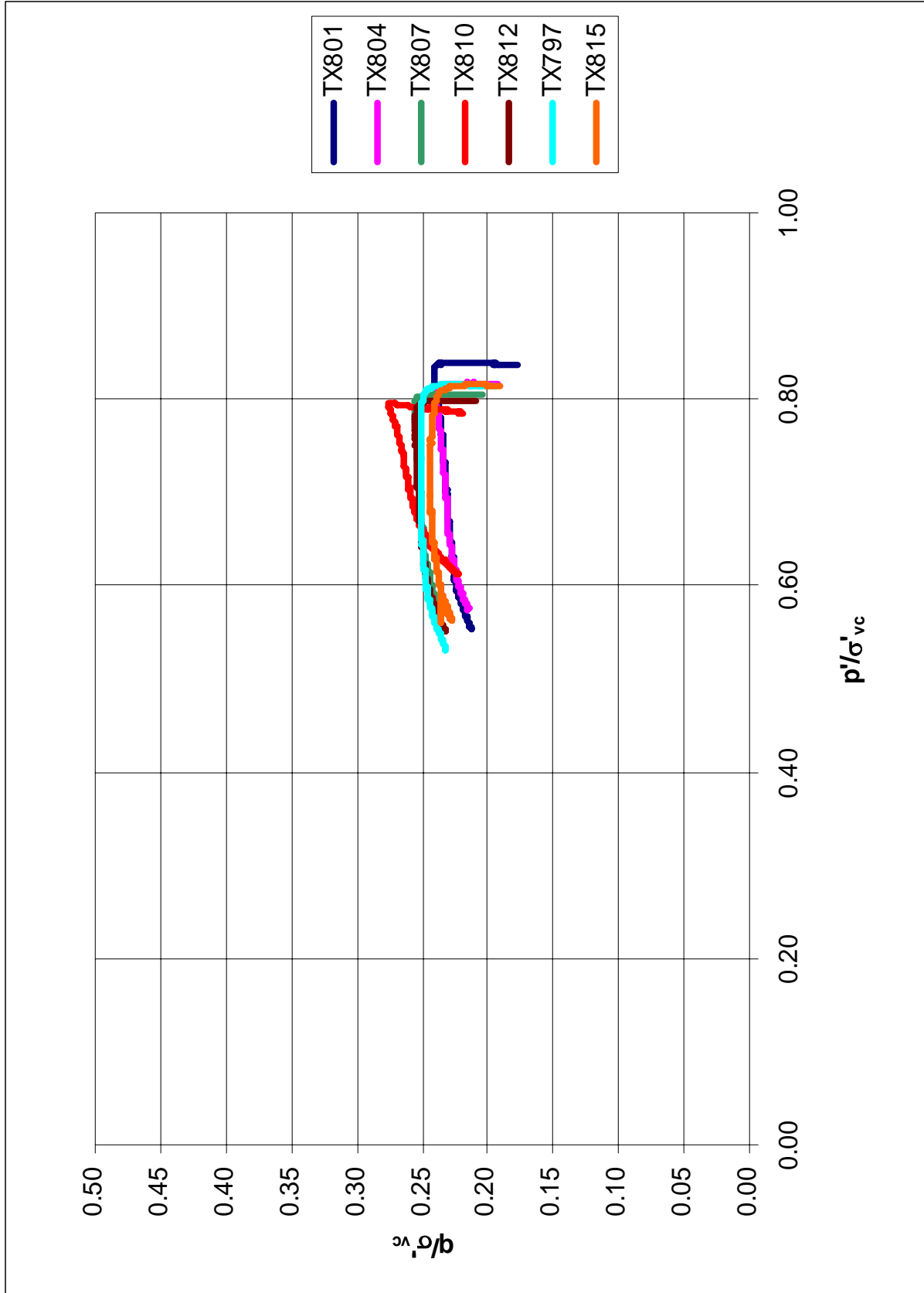
Figure 5.13 : Normalized Undrained Stress Path – Summary Table of Triaxial Testing of RGMC
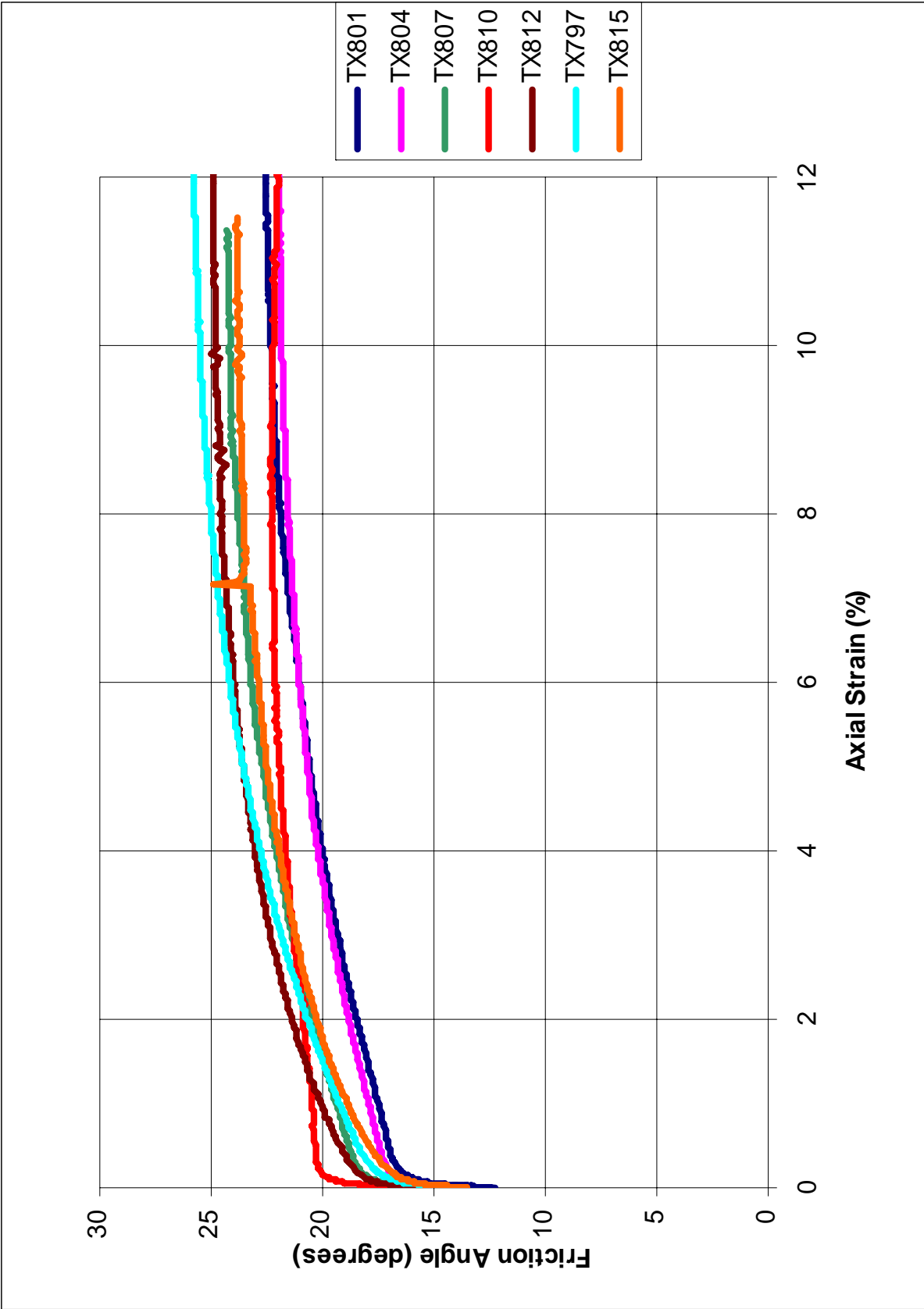
Figure 5.14: Friction Angle Versus Axial Strain – Summary Table of Triaxial Testing of RGMC
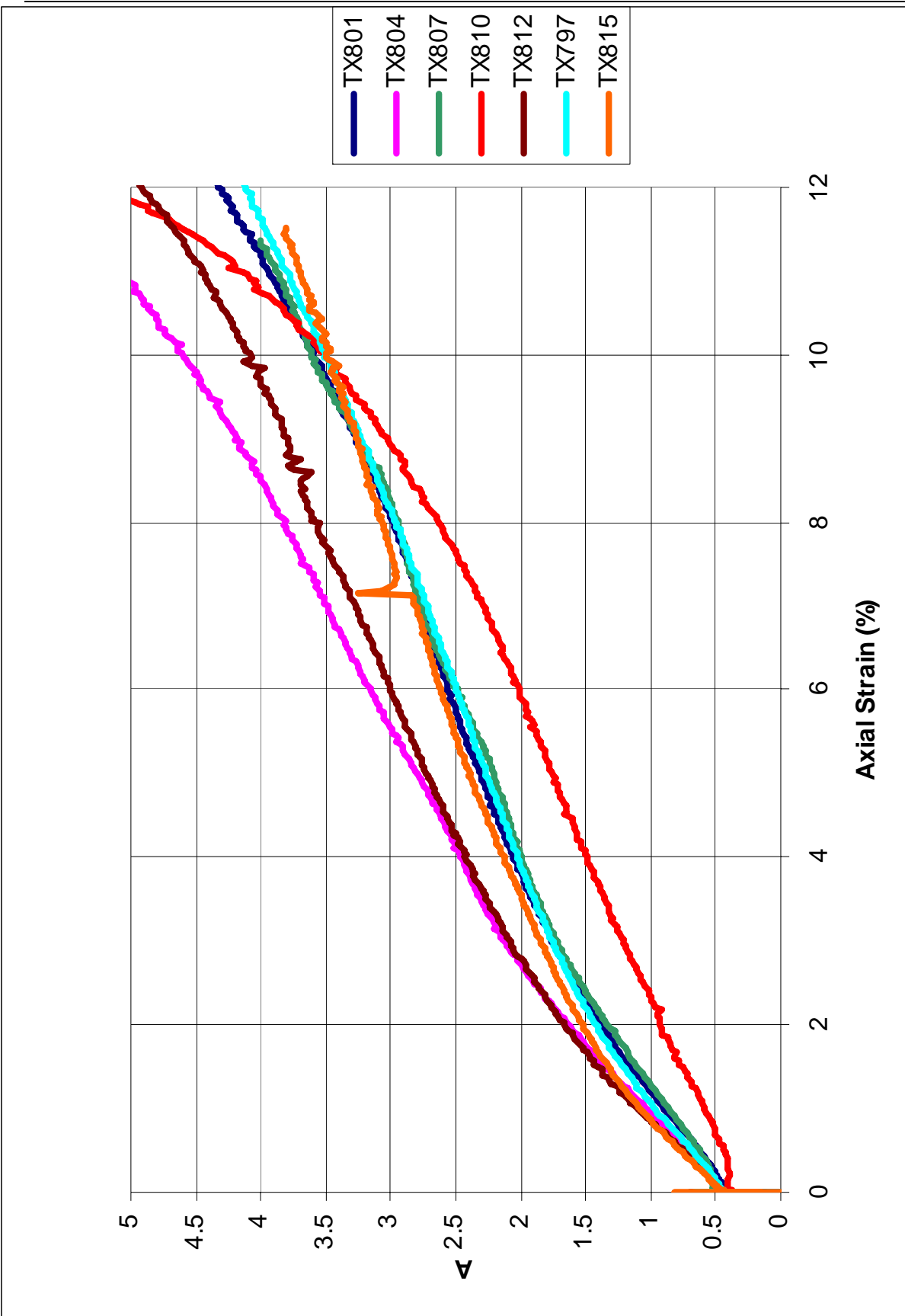
Figure 5.15: The A Parameter Versus Axial Strain – Summary Table of Triaxial Testing of RGMC
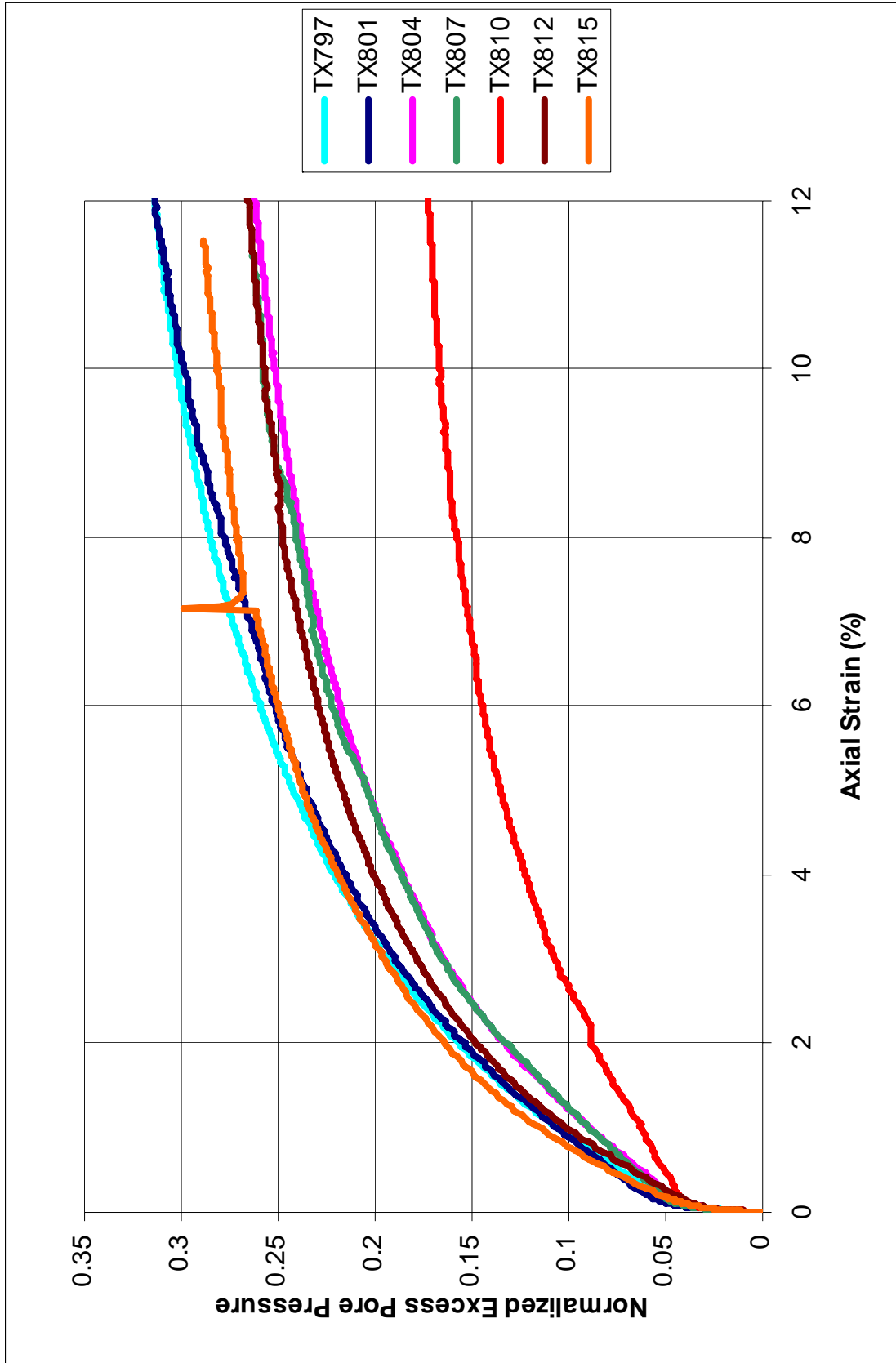
Figure 5.16: Normalized Excess Pore Pressure Versus Axial Strain – Summary Table of Triaxial Testing of RGMC
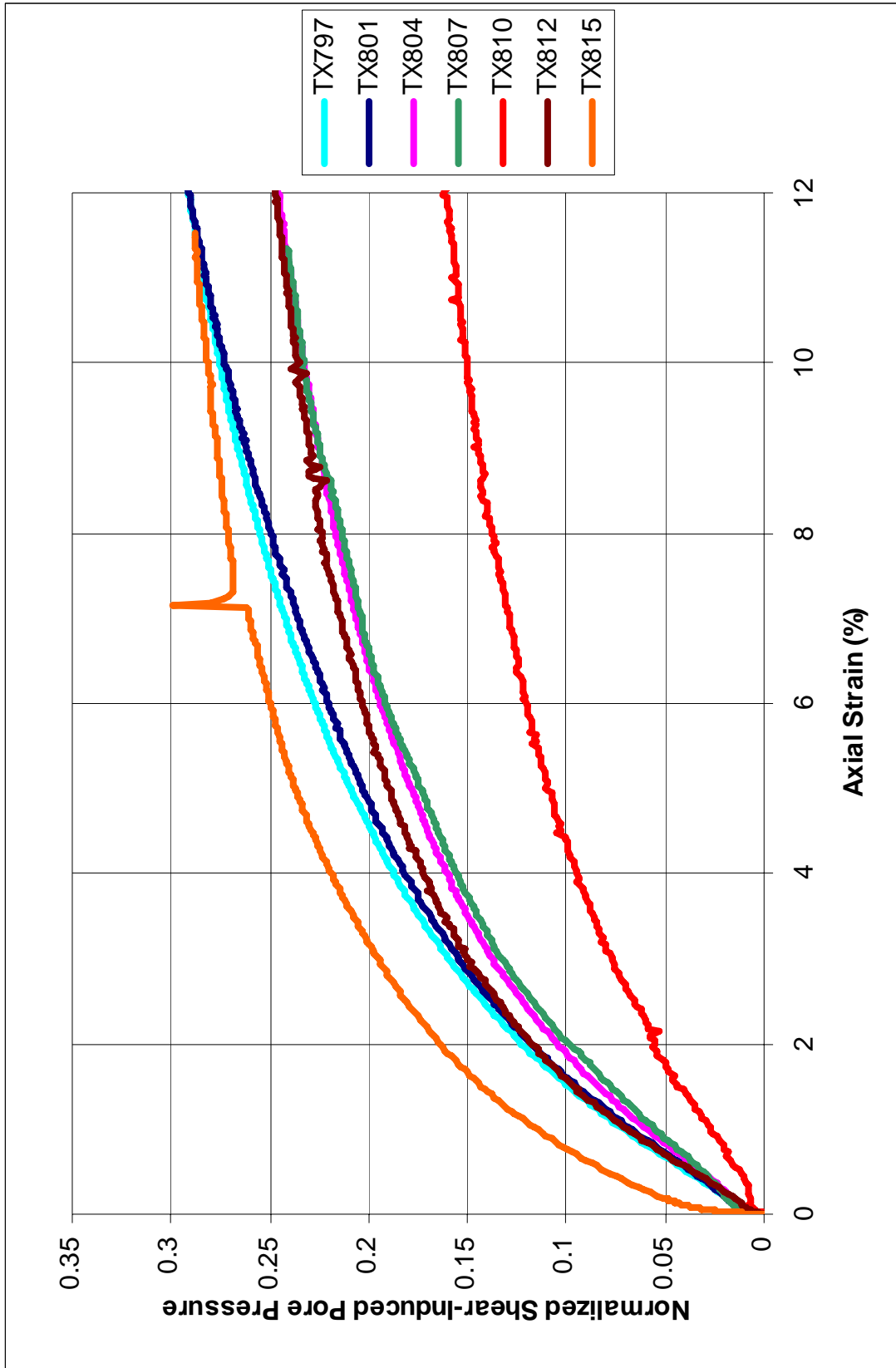
Figure 5.17: Normalized Shear-Induced Pore Pressure Versus Axial Strain – Summary Table of Triaxial Testing of RGMC
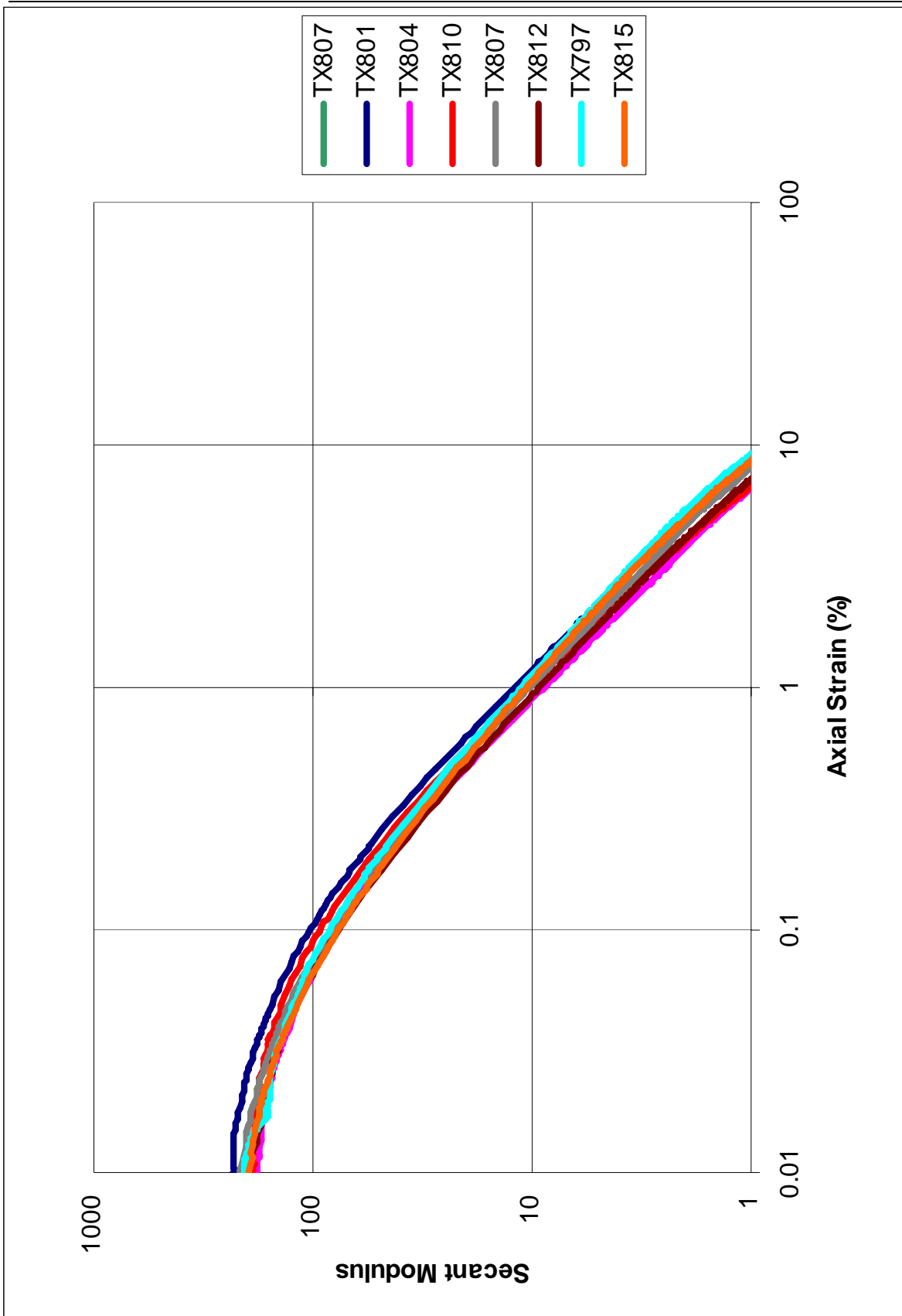
Figure 5.18: Secant Modulus Versus Axial Strain – Summary Table of Triaxial Testing of RGMC
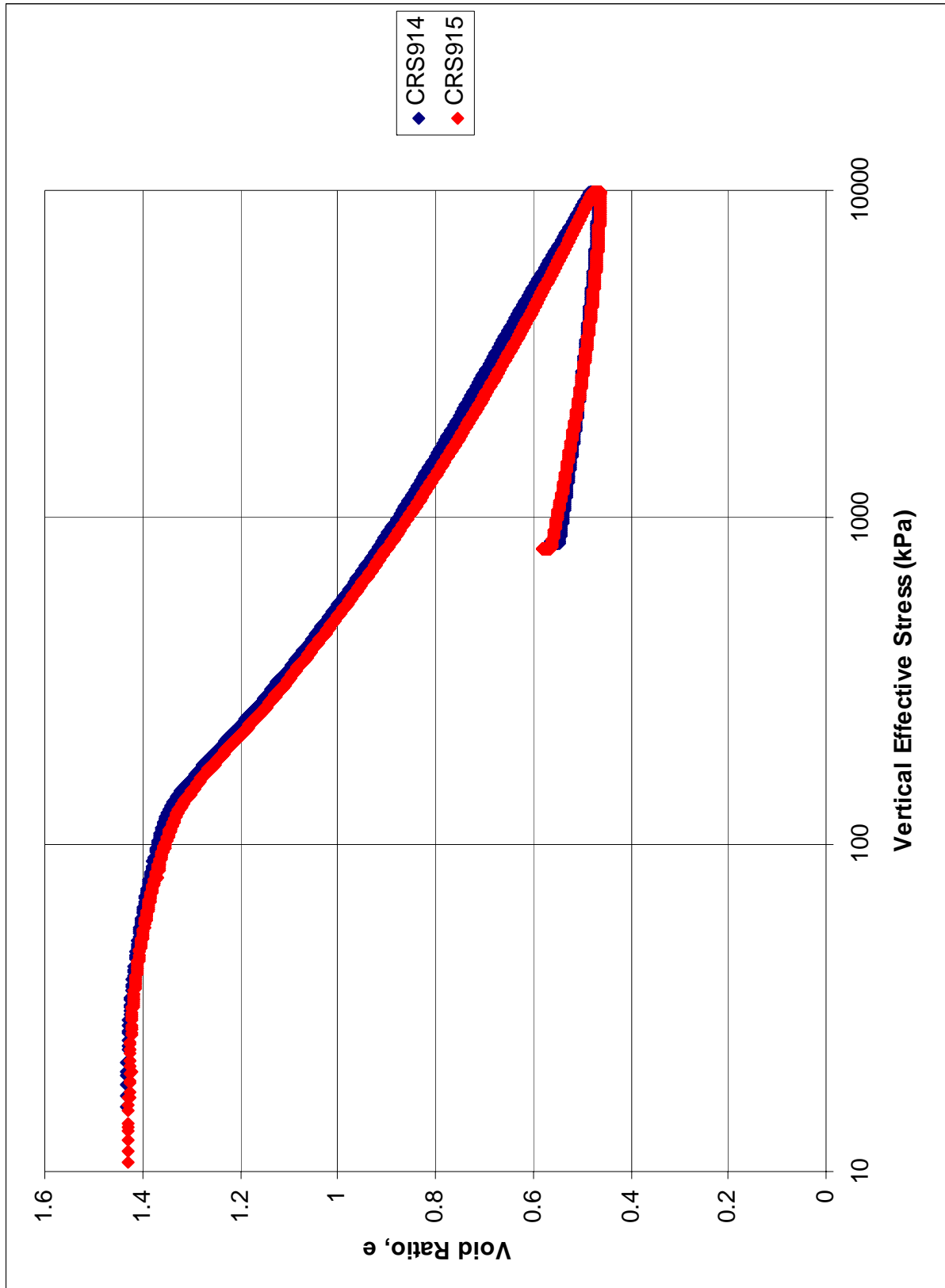
Figure 5.19: Void Ratio Versus Vertical Effective Stress - Constant Rate of Strain Test of RGMC
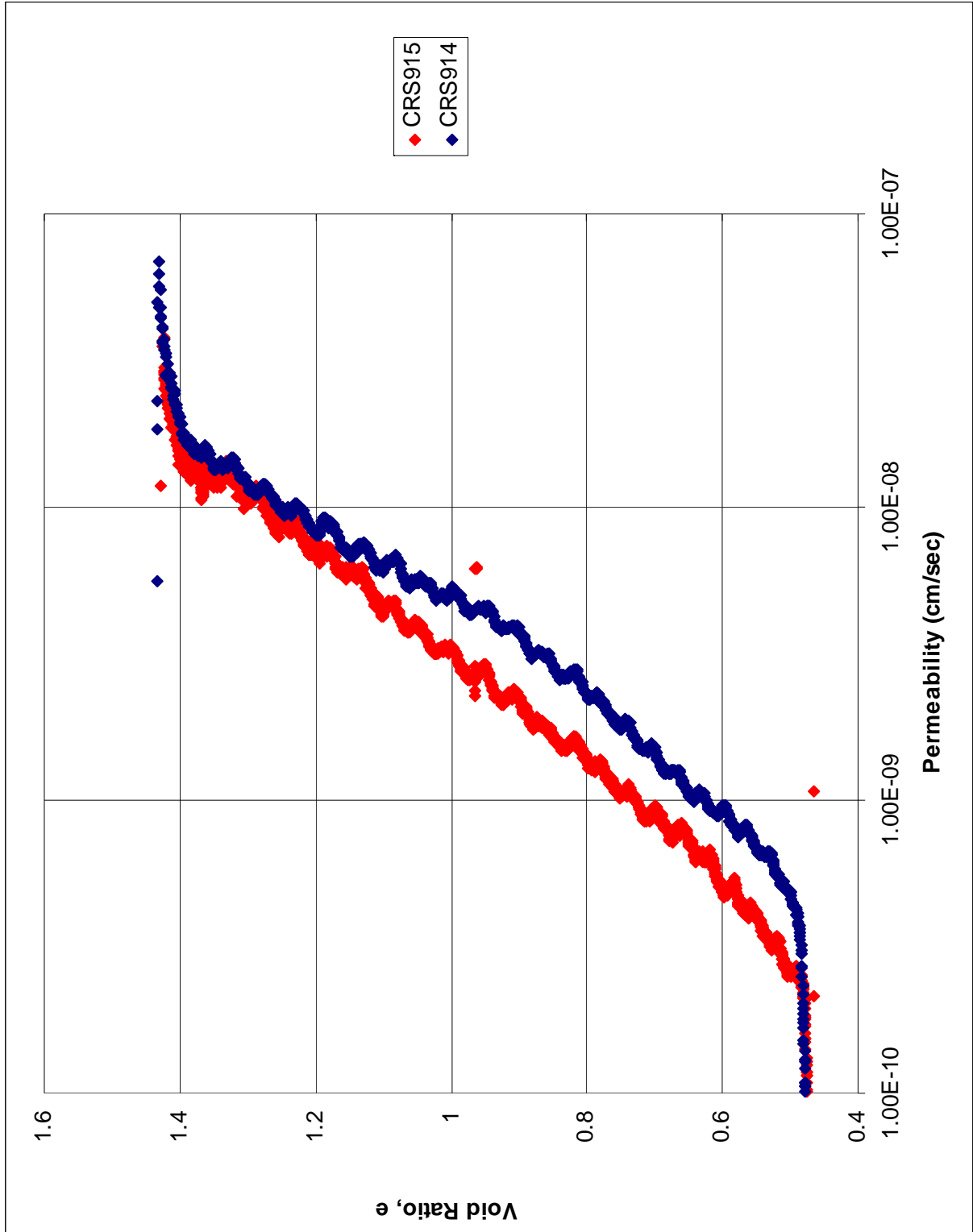
Figure 5.20: Void Ratio Versus Permeability - Constant Rate of Strain Test of RGMC
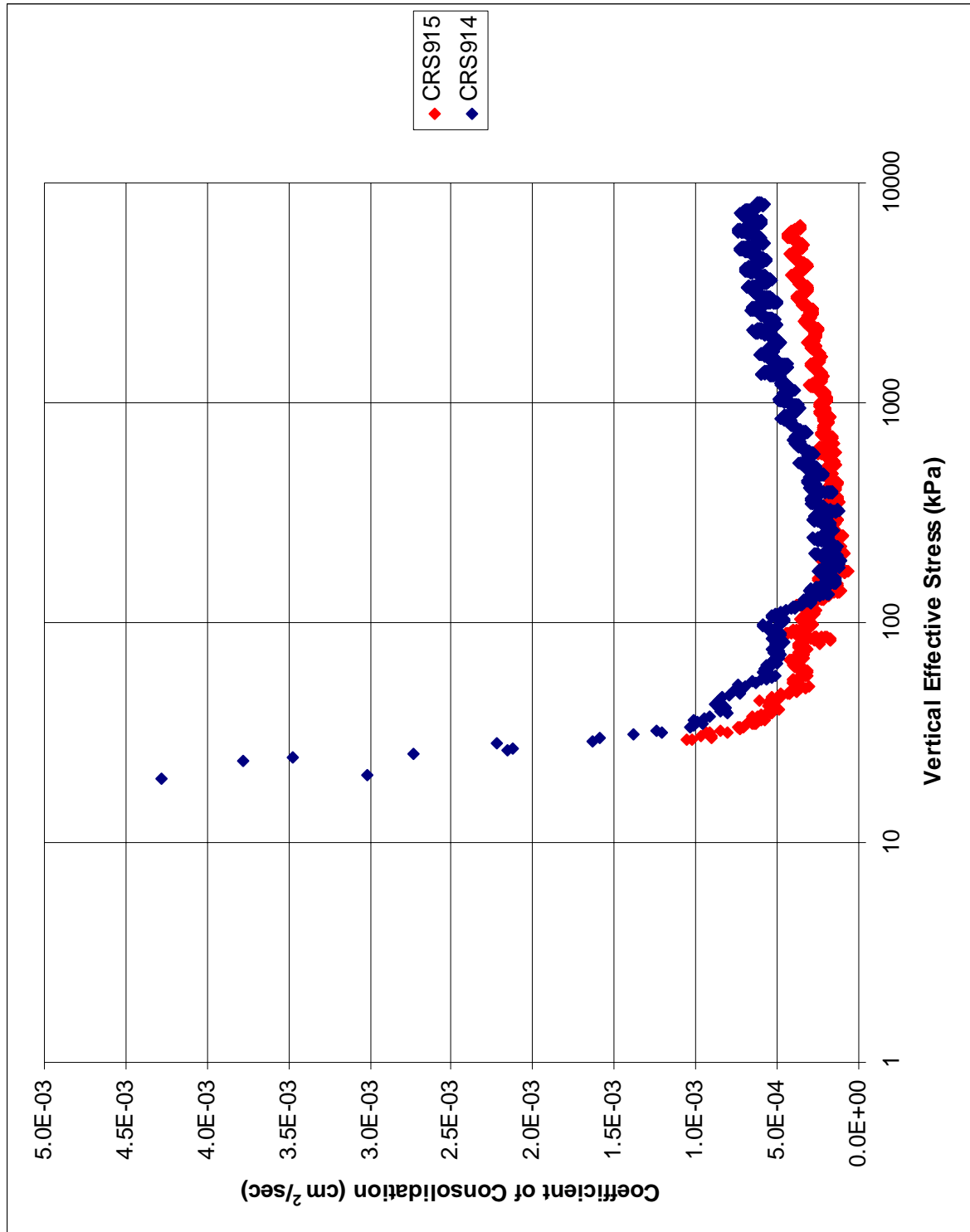
Figure 5.21: Coefficient of Consolidation Versus Vertical Effective Stress - Constant Rate of Strain Test of RGMC
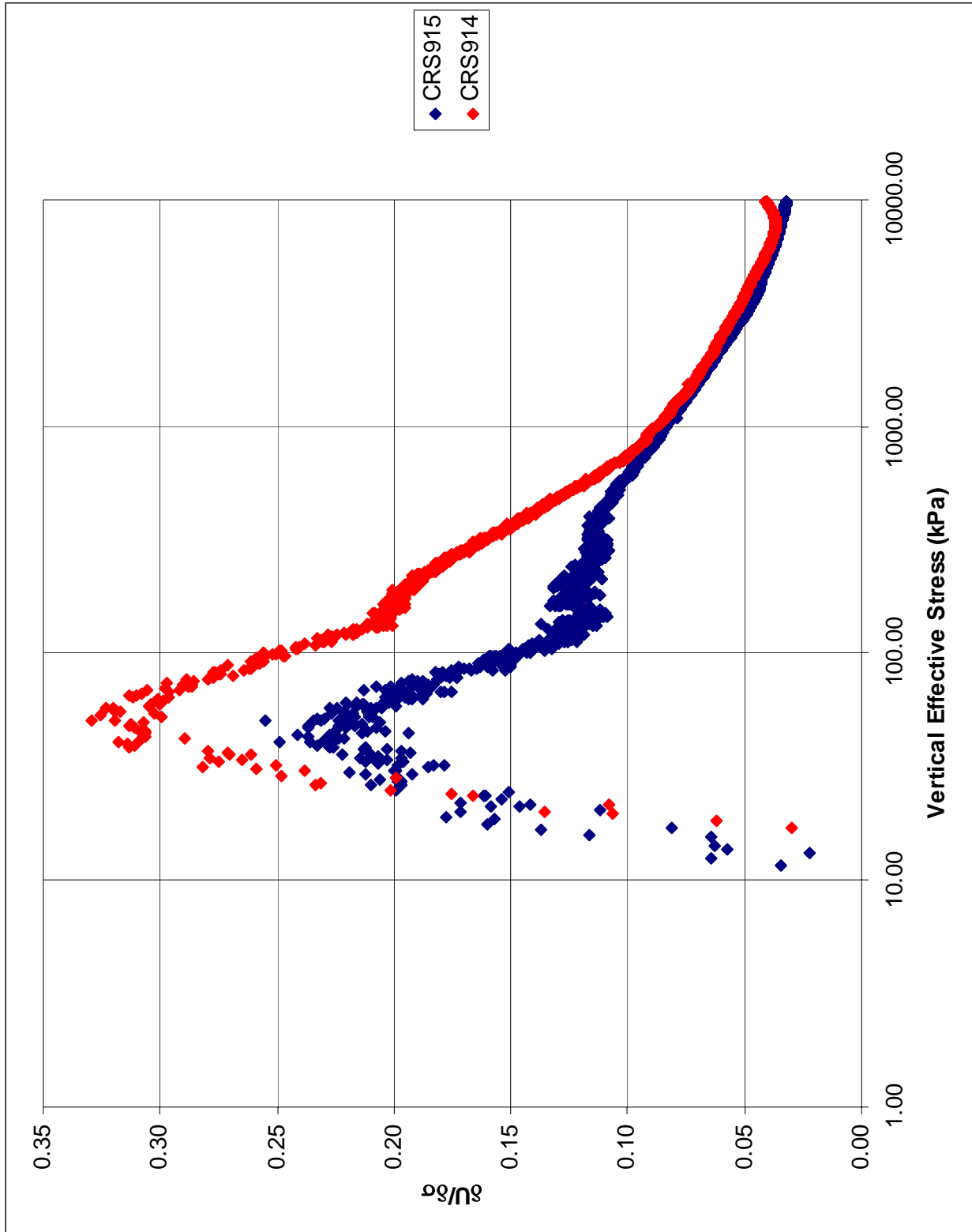
Figure 5.22: Pore Pressure Ratio Versus Vertical Effective Stress - Constant Rate of Strain Test of RGMC

Table 5.2: Summary of Triaxial Consolidation Results: **RESEDIMENTED GULF OF MEXICO CLAY**

Last Revised: 5/14/2008

Column groups: Index Tests (ωn, SD, # obs) | Specimen Data (ωn, Ip, γt / ei, Si, Gs) | Conditions (σ'i/εa, ub/εab, B/εvol) | General (σ'p, εa/hr / Cc, CR) | Consolidation Results @ Max Stress (εa, εvol / σ'vm, Kc, ts) and @ Preshear (εa, εvol, Kc / σ'vc, OCR, ts) | Remarks / Assumptions

Test #	ωn	SD	# obs	ωn	Ip	γt	ei	Si	Gs	σ'i	εa	ub	εab	B	εvol	σ'p	εa/hr	Cc	CR	εa (max)	εvol (max)	σ'vm	Kc (max)	ts (max)	εa (ps)	εvol (ps)	Kc (ps)	σ'vc	OCR	ts (ps)	Remarks / Assumptions
TX797	49.5	N/A	1	61.25		1.655	1.708	99.7	2.78	7.8	0.00	196.1	0.71	0.92	-2.20	43.2	0.11	0.61	0.22	11.90	11.87	140.7	0.626	24.0	11.90	11.87	0.626	140.7	1.00	24.0	BATCH 01 / σ'lc = 98 kPa
TX801	59.1	4.7	2	59.12		1.668	1.653	99.5	2.78	30.4	0.04	294.2	0.28	0.92	-2.70	59.8	0.11	0.36	0.13	10.08	9.94	134.8	0.667	39.7	10.08	10.02	0.667	134.8	1.00	39.7	BATCH 02 / σ'lc = 98 kPa
TX804	55.6	4.9	2	55.93		1.681	1.578	98.5	2.78	15.7	-0.03	392.3	-1.74	0.88	-6.36	68.7	0.11	0.70	0.27	17.07	17.05	224.8	0.633	22.2	17.07	17.05	0.633	224.8	1.00	22.2	BATCH 03 / σ'lc = 98 kPa
TX807	49.2	3.9	2	49.25		1.736	1.390	98.5	2.78	23.5	-0.20	294.2	-1.46	0.88	-6.66	122.6	0.11	0.48	0.20	13.43	13.25	327.4	0.608	31.4	13.43	13.25	0.608	327.4	1.00	31.4	BATCH 04 / σ'lc = 196 kPa
TX810	42.2	3.1	2	40.93		1.793	1.185	96.0	2.78	19.6	-0.04	196.1	-0.73	0.88	-8.32	176.5	0.11	0.48	0.22	17.13	17.87	570.2	0.552	59.5	17.13	17.87	0.552	570.2	1.00	59.5	BATCH 07 / σ'p = 392.3 kPa
TX812	27.8	4.5	2	32.22		1.902	0.933	96.0	2.78	30.4	-0.02	196.1	-0.43	0.92	-7.59	343.2	0.11	0.35	0.18	8.45	8.39	769.0	0.594	25.2	8.45	8.39	0.594	769.0	1.00	25.2	BATCH 06 / σ'lc = 588.4 kPa
TX815	31.6	1.8	2	31.16		1.938	0.881	98.3	2.78	137.3	-0.07	294.2	-0.29	0.88	-3.08	520.0	0.10	0.33	0.18	7.33	7.37	1170.8	0.596	26.0	7.33	7.37	0.596	1170.8	1.00	26.0	BATCH 05 / σ'lc = 784.5 kPa
CRS914	50.0	1.1	3	52.19		1.745	1.426	101.7	2.78	15.8	-0.34	402.0	-0.34	N/A	N/A	100.0	1.76	0.45	0.18	N/A	N/A	N/A	N/A	N/A	N/A	N/A	N/A	N/A	N/A	N/A	BATCH 05 / σ'lc = 784.5 kPa
CRS915	49.2	1.0	3	52.26		1.745	1.426	101.9	2.78	11.0	-0.09	400.5	-0.09	N/A	N/A	100.0	0.94	0.48	0.20	N/A	N/A	N/A	N/A	N/A	N/A	N/A	N/A	N/A	N/A	N/A	BATCH 08 / σ'lc = 98.0 kPa

a) Marker location in tube
b) Stresses in kPa
c) 98.06 kPa = 2048 psf
d) Depth in Feet
e) Time in hours
f) Water content, limits, saturation, strain, and B value in %
g) density in gm/cm³

Table 5.3: Summary of Triaxial Undrained Shear Results: **RESEDIMENTED GULF OF MEXICO CLAY**

Last Revised: 5/14/2008

Test # (Specimen Location)	Specimen Data ω_n / I_p / γ_t	e_i / S_i / G_s	ε_a/hr	e_c / K_c	σ'_{vc} / ε_{ac} / OCR	At Max Shear q/σ'_{vc} / ε_a	$\Delta u_e/\sigma'_{vc}$ / $\Delta u_s/\sigma'_{vc}$ / p'/σ'_{vc}	q/p' / ϕ' / A	At Max Obliquity q/σ'_{vc} / ε_a	$\Delta u_e/\sigma'_{vc}$ / $\Delta u_s/\sigma'_{vc}$ / p'/σ'_{vc}	q/p' / ϕ' / A	E_u/σ'_{vc} @ ε_a= 0.001% / 0.01% / 0.1%	$\Delta q/\Delta q_m$ 0.3 / 0.5	Comments
TX797	61.25 / / 1.655	1.708 / 99.7 / 2.78	0.510	1.386 / 0.626	140.7 / 11.90 / 1.00	0.2510 / 1.32	0.1244 / 0.0897 / 0.7428	0.3379 / 19.8 / 1.13	0.2318 / 12.53	0.3164 / 0.2947 / 0.5314	0.4362 / 25.9 / 4.2994	235 / 207 / 84	81 / 64	BATCH 01, σ'_{lc} = 98 kPa
TX801	59.12 / / 1.668	1.653 / 99.45 / 2.78	0.500	1.375 / 0.667	134.8 / 10.08 / 1.00	0.2410 / 0.46	0.0750 / 0.0335 / 0.8239	0.2925 / 17.0 / 0.60	0.2128 / 12.40	0.3167 / 0.2944 / 0.5535	0.3844 / 22.6 / 4.4925	316 / 227 / 105	221 / 179	BATCH 02, σ'_{lc} = 98 kPa
TX804	55.93 / / 1.681	1.578 / 98.5 / 2.78	0.527	1.184 / 0.633	224.8 / 17.07 / 1.00	0.2399 / 0.39	0.0590 / 0.0273 / 0.8042	0.2983 / 17.4 / 0.62	0.2149 / 12.42	0.2640 / 0.2486 / 0.5746	0.3740 / 22.0 / 5.9408	258 / 171 / 73	160 / 129	BATCH 03, σ'_{lc} = 98 kPa
TX807	49.25 / / 1.736	1.39 / 98.46 / 2.78	0.501	1.109 / 0.608	327.4 / 13.43 / 1.00	0.2558 / 0.50	0.0657 / 0.0306 / 0.7921	0.3229 / 18.8 / 0.63	0.2366 / 11.26	0.2630 / 0.2407 / 0.5755	0.4111 / 24.3 / 3.9568	285 / 216 / 66	194 / 168	BATCH 04, σ'_{lc} = 196 kPa
TX810	40.93 / / 1.793	1.185 / 96 / 2.78	0.524	0.810 / 0.552	570.2 / 17.13 / 1.00	0.2760 / 0.37	0.0464 / 0.0084 / 0.7955	0.3469 / 20.3 / 0.41	0.2477 / 8.47	0.1608 / 0.1428 / 0.6516	0.3802 / 22.3 / 2.8433	N/A / 201 / 86	178 / 156	BATCH 07, σ'_{lc} = 392.3 kPa, Failure Plane
TX812	32.22 / / 1.902	0.933 / 96.02 / 2.78	0.489	0.779 / 0.594	769.0 / 8.45 / 1.00	0.2553 / 0.50	0.0697 / 0.0390 / 0.7745	0.3296 / 19.2 / 0.7433	0.2331 / 12.74	0.2707 / 0.2545 / 0.5512	0.4230 / 25.0 / 5.4469	237 / 196 / 71	172 / 142	BATCH 06, σ'_{lc} = 588.4 kPa
TX815	27.3 / / 1.938	0.881 / 98.32 / 2.78	0.485	0.736 / 0.596	1170.8 / 7.33 / 1.00	0.2439 / 1.37	0.1364 / 0.1005 / 0.7310	0.3337 / 19.5 / 1.27	0.2361 / 7.16	0.2991 / 0.2682 / 0.5607	0.4212 / 24.9 / 3.2489	226 / 199 / 72	174 / 125	BATCH 05, σ'_{lc} = 784.5 kPa

a) Marker location in tube
b) Stresses in kPa
c) 98.06 kPa = 2048 psf
d) Depth in Feet
e) Time in hours
f) Water content, saturation, and strain in %
g) density in gm/cm³

Chapter 6

Summary, Conclusions, Recommendations

No man should escape our universities without knowing how little he knows.

J. Robert Oppenheimer

6.1 Introduction

This chapter summarizes the results obtained from the seven triaxial compression loading tests performed on RGMC. Moreover, it proposes additional research that would be beneficial to contributing to a collective data set that would corroborate and help to explain results presented from this research.

6.2 Results and Conclusions

Batch Consolidation

Batch consolidation was completed on a number of stress levels. Ultimately, what the specimen experienced in the laboratory during consolidation was not the value of preconsolidation achieved during K_o consolidation in the triaxial test. This fact is contradictory to the data collected by LVDTs on the specimen showing the end of primary had indeed been achieved. Since a great deal of care was taken not to disturb specimen upon extrusion and transport to the triaxial cell, it is not believed that disturbance caused this unexpected decrease in preconsolidation stress.

CRS Testing

The CRS data approximately confirms the value of C_v (0.00045 cm^2/sec with CRS data) calculated from LVDT readings on the specimen during laboratory consolidation, which is approximately 0.0004 cm^2/sec. The CRS data shows that the specimen has a preconsolidation stress of approximately 100 kPa, which was the applied stress during preparation of the specimen in the laboratory. However, loads applied to the specimens

used in the triaxial do not show that laboratory consolidation was achieved. When the CRS results are compared to the triaxial data, four tests (#797, #801, #804 and #807) agree together very nicely, i.e. the envelope is unique between the two data sets. This suggests that consolidation is complete in the triaxial apparatus. On the other hand, with the remaining tests (# 810, 812 and 815) the void ratio to vertical effective stress plots do not reach the compression envelope. Subsequent analysis of the results suggest that # 810 is a problematic test and should be discounted from the results. Futher, the material used to resediment # 812 and # 815 is from a different elevation and is believed to have different compression behavior.

Triaxial Testing

Sampling effective stress attained during initial setup of the test are too low. Typically, 25% of the preconsolidation stress is considered an agreeable amount of effective stress to experience during setup, whereas all the sampling effective stresses of the tests are lower than expected. K_o values range approximately 0.55 to 0.67. If test # 810 was not considered for the reasons described in section 5.10, NC K_o values would range approximately 0.60 to 0.67 with no discernable trends.

The data show a trend of increasing K_o values with decreasing shear stress on the specimen, which is in accord with current and past research of RBBC (Santagata, 1999).

There does not seem to be a relationship between K_o and the following: consolidation stress; modulus and effective friction angle. Average strength was 0.2484, average friction angle at maximum shear strength was 18.9 degrees and at maximum obliquity was 23.9 degrees. Average normalized modulus at 0.01% was 202.

6.3 Recommendations for Future Research

The data presented in this thesis is only a small sample of the data set that is needed in order to generate concrete trends and corroborate unique behavior manifested by this clay. There are important conclusions that one may take away from this thesis to help understand the behavior of in-situ Gulf of Mexico Clay from this region (Ursa Basin) such as a decrease in strength with an increase in the value of K_o.

It is recommended that a larger data set be acquired on this material so that trends and behavior that has been observed in this research can be corroborated and more in depth detail can be investigated. Also, testing to higher pressures than the amounts presented in this thesis (σ'_{vm} = 150 to 1,200 kPa) would be of interest in cases where preconsolidation stress and stress applications to the soil exceed that of the pressures tested in this thesis.

A thorough investigation of the permeability of the soil as a function of vertical effective stress is another aspect that would be important to understanding the behavior of Gulf of Mexico clays. A large data set of constant rate of strain tests covering a vast range of preconsolidation stresses would be needed in order to grasp the behavior of this clay. It is believed that larger preconsolidation stress would lead to smaller values of permeability which would help to explain the development of excess pore pressures within the clay during loading.

REFERENCES

Ahmed, I. (1990). "Investigation of Normalized Behavior of Boston Blue Clay Using Geonor Direct Simple Shear Apparatus," S.M. thesis, Dept. of Civil and Environmental Enigneering, MIT, Cambridge, MA. 392 pp.

Bishop, A.W., Henkel, D.J., (1957) "The Measurement of Soil Properties in the Triaxial Test." Edward Arnold Publishers, London, England, UK, 227 pp.

Expedition 308 Summary. (2006). Proceedings of the Integrated Ocean Drilling Program, Volume 308. Retrieved: April, 2008. http://publications.iodp.org/proceedings/308/EXP_REPT/CHAPTERS/308_101.PDF

Germaine, J.T. (2007). "1.37 Geotechnical Measurements and Exploration Class Notes." MIT, Cambridge, MA

Holtz, R.D., Kovacs, W.D., (1981). "An Introduction to Geotechnical Engineering." Prentice Hall, Upper Saddle River, New Jersey, 733 pp.

Ladd, C.C. (2007). "1.361 Soil Mechanics (MIT): Class Notes." MIT, Cambridge, MA

Ladd, C.C., (1964). " Stress-Strain Behavior of Saturated Clay and Basic Strength Principles." Dept. of Civil Engineering, MIT, Cambridge, MA, 105 pp.

Lambe, T.W., Whitman, R.V., (1969). "Soil Mechanics," John Wiley & Sons, New York City, NY, USA, 553 pp.

Santagata, M.C., (1999). "Factors Affecting the Initial Stiffness and Stiffness Degradation of Cohesive Soils," Ph.D. thesis, Dept. of Civil and Environmental Engineering, MIT, Cambridge, MA, 337 pp.

Sinfield, J.V., (1994). "An Experimental Investigation of Sampling Distrubance Effects in Resedimented Boston Blue Clay," S.M. thesis, Dept. of Civil and Environmental Engineering, MIT, Cambridge, MA. 413 pp.

Sheahan, T.C., (1991). "An Experimental Study of the Time-Dependent Undrained Shear Behavior of Resedimented Clay Using Automated Stress Path Triaxial Equipment," Sc.D. thesis, Dept. of Civil Engineering, MIT, Cambridge, MA, 952 pp.

APPENDIX A

PLOTS FROM CONSOLIDATION AND UNDRAINED SHEAR DATA COLLECTED FROM ALL TRIAXIAL TESTS OF RESEDIMENTED GULF OF MEXICO CLAY
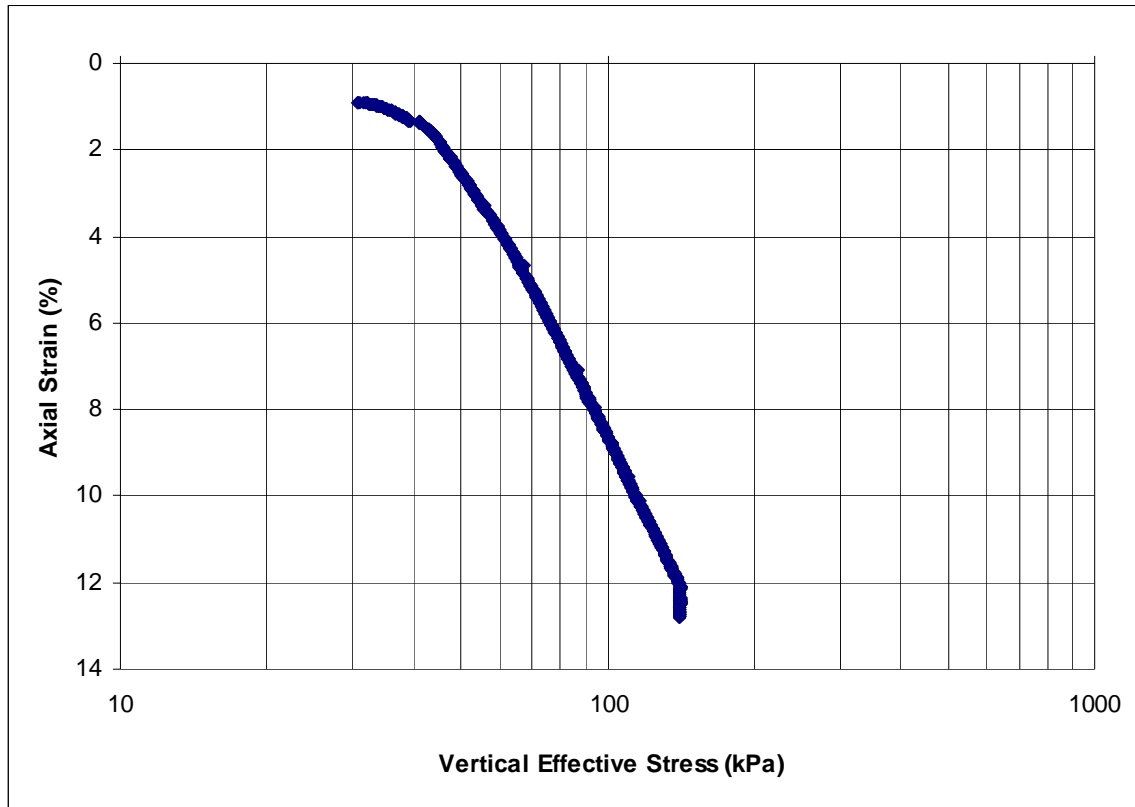
Figure A.1: Axial Strain Versus Vertical Effective Stress – Triaxial Test # 797
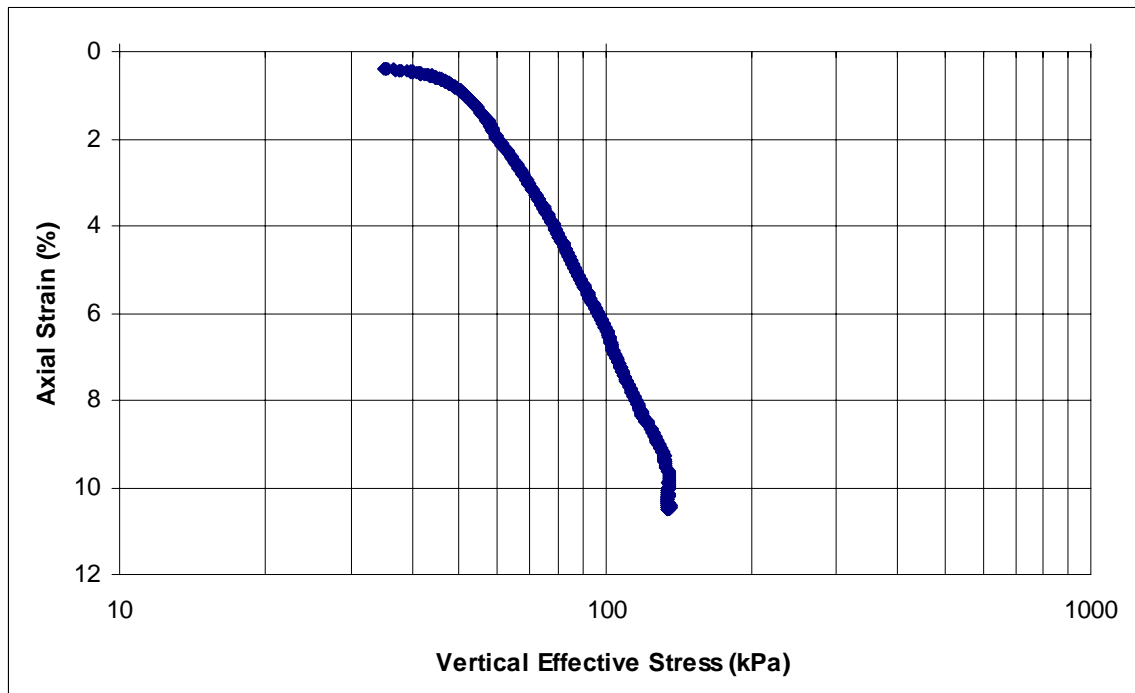
Figure A.2: Axial Strain Versus Vertical Effective Stress – Triaxial Test #801

Figure A.3: Axial Strain Versus Vertical Effective Stress – Triaxial Test #804
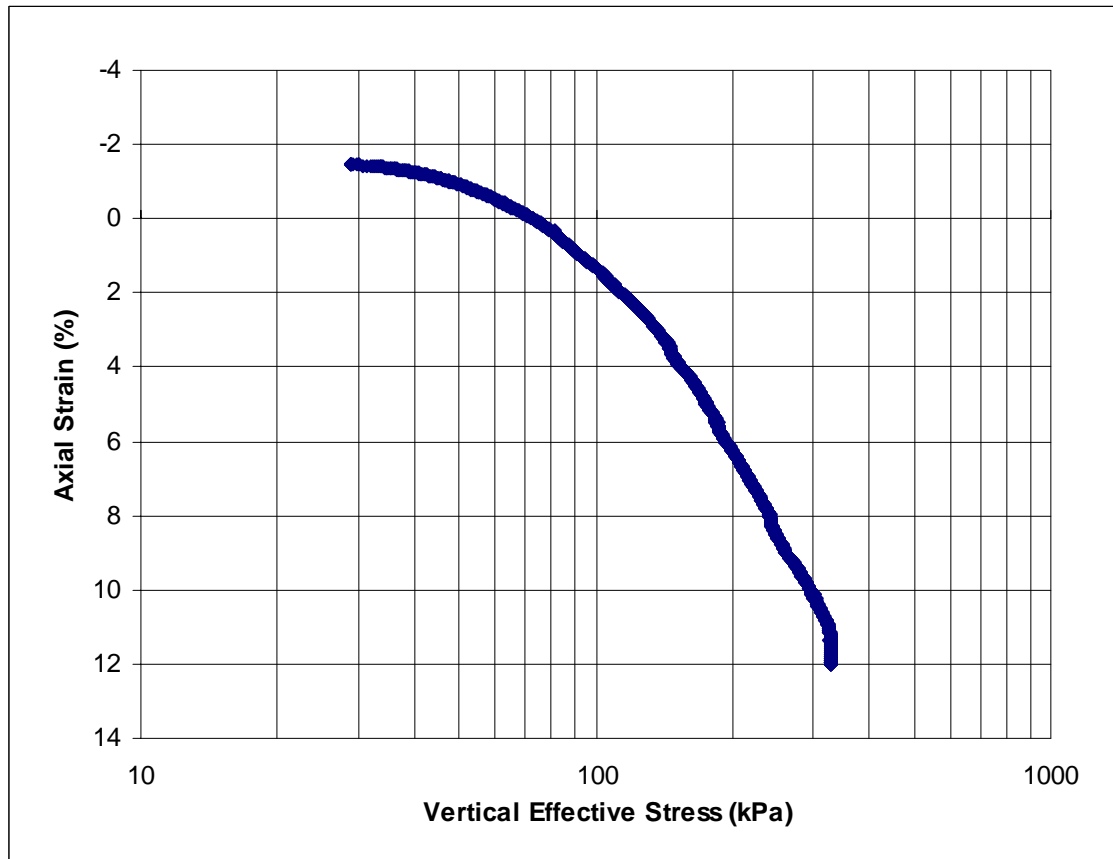
Figure A.4: Axial Strain Versus Vertical Effective Stress – Triaxial Test #807
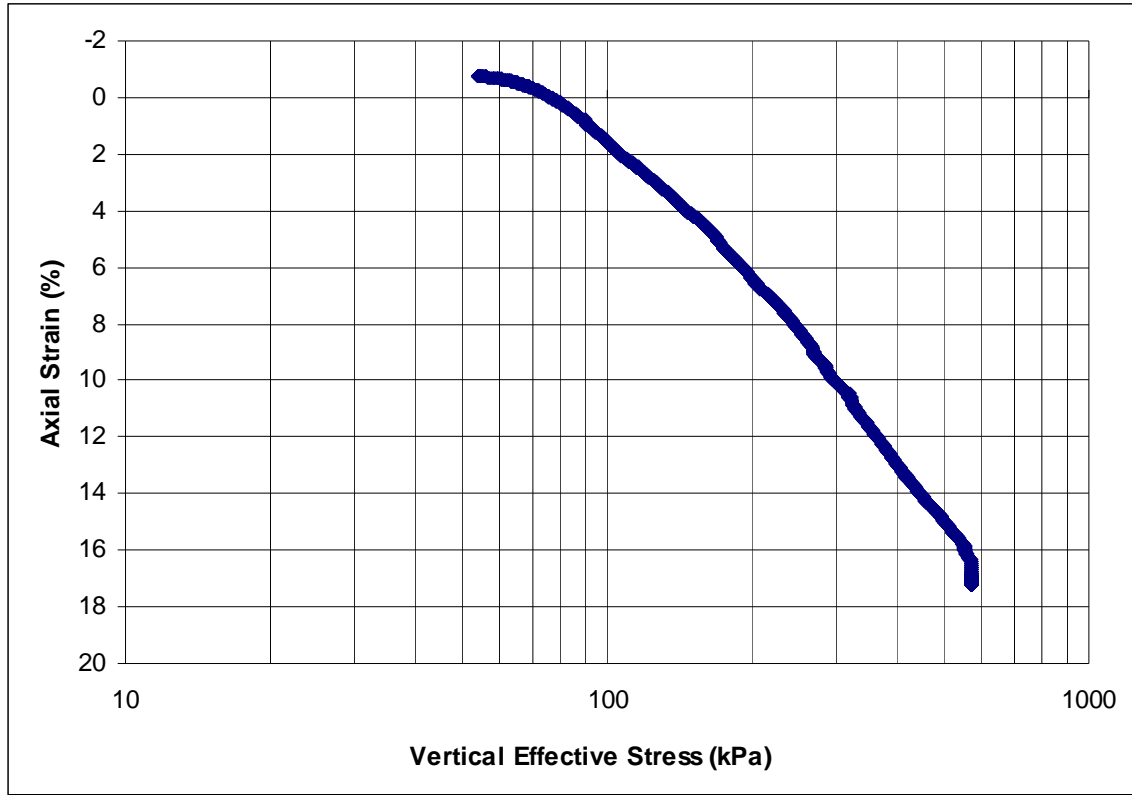
Figure A.5: Axial Strain Versus Vertical Effective Stress – Triaxial Test # 810
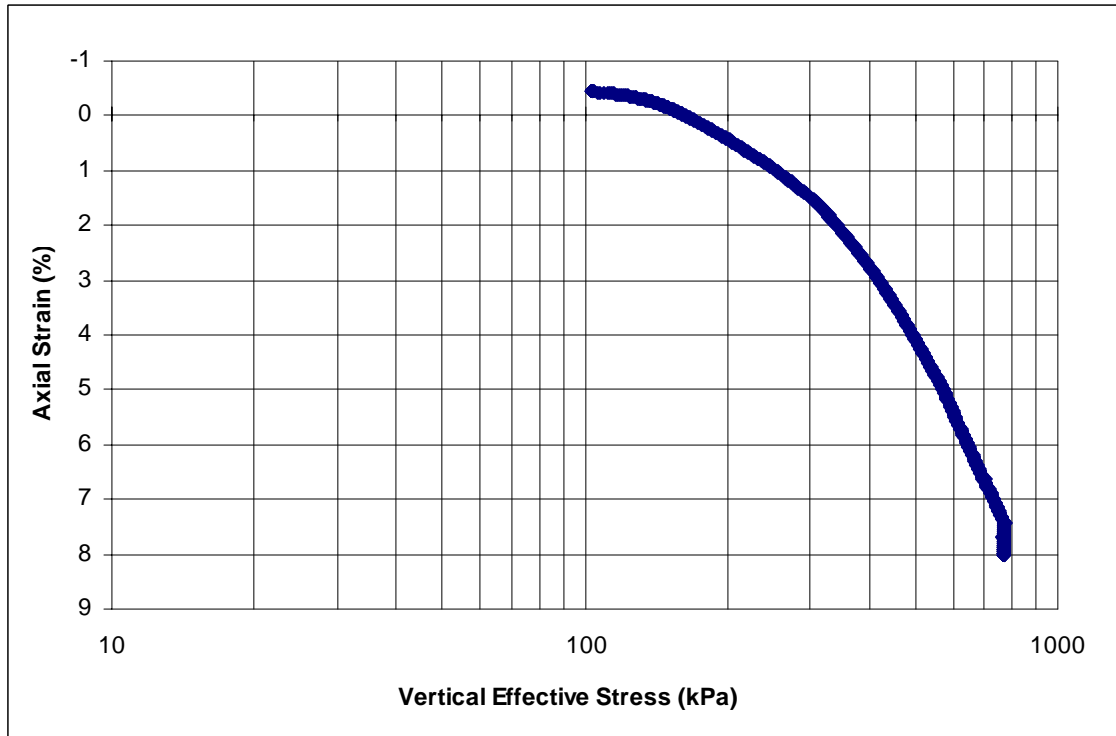
Figure A.6: Strain Versus Vertical Effective Stress – Triaxial Test # 812
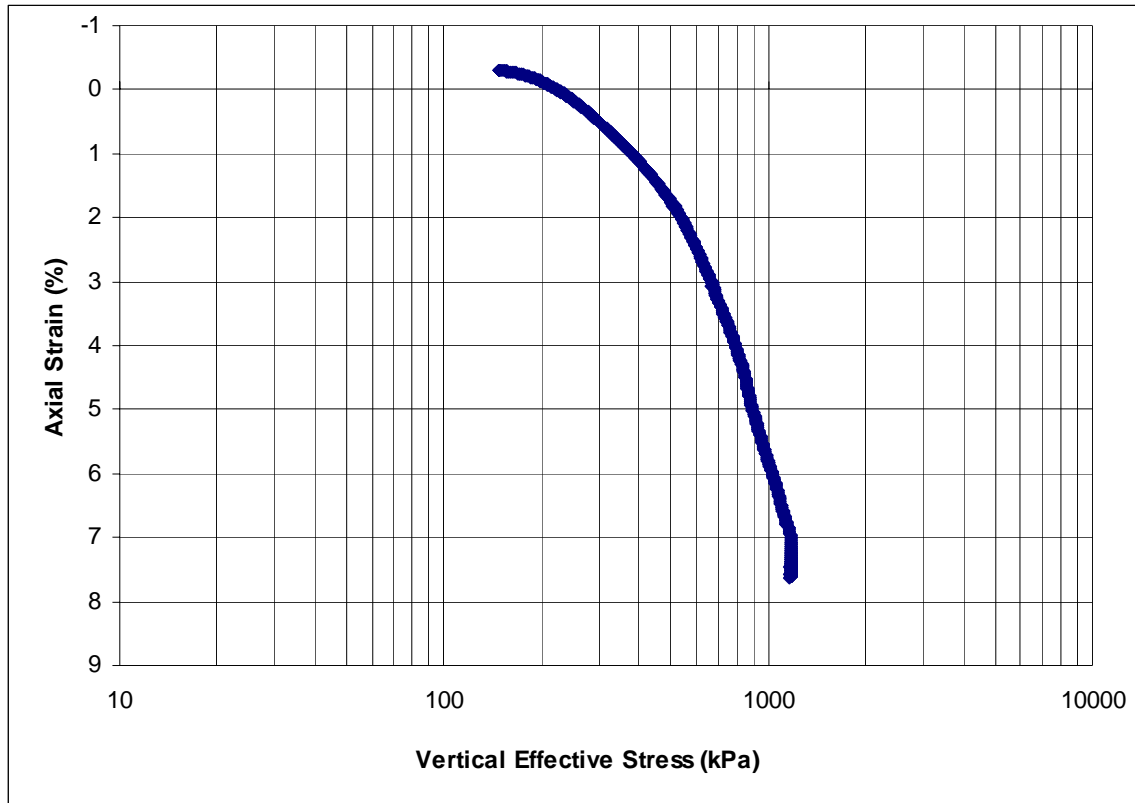
Figure A.7: Strain Versus Vertical Effective Stress – Triaxial Test # 815
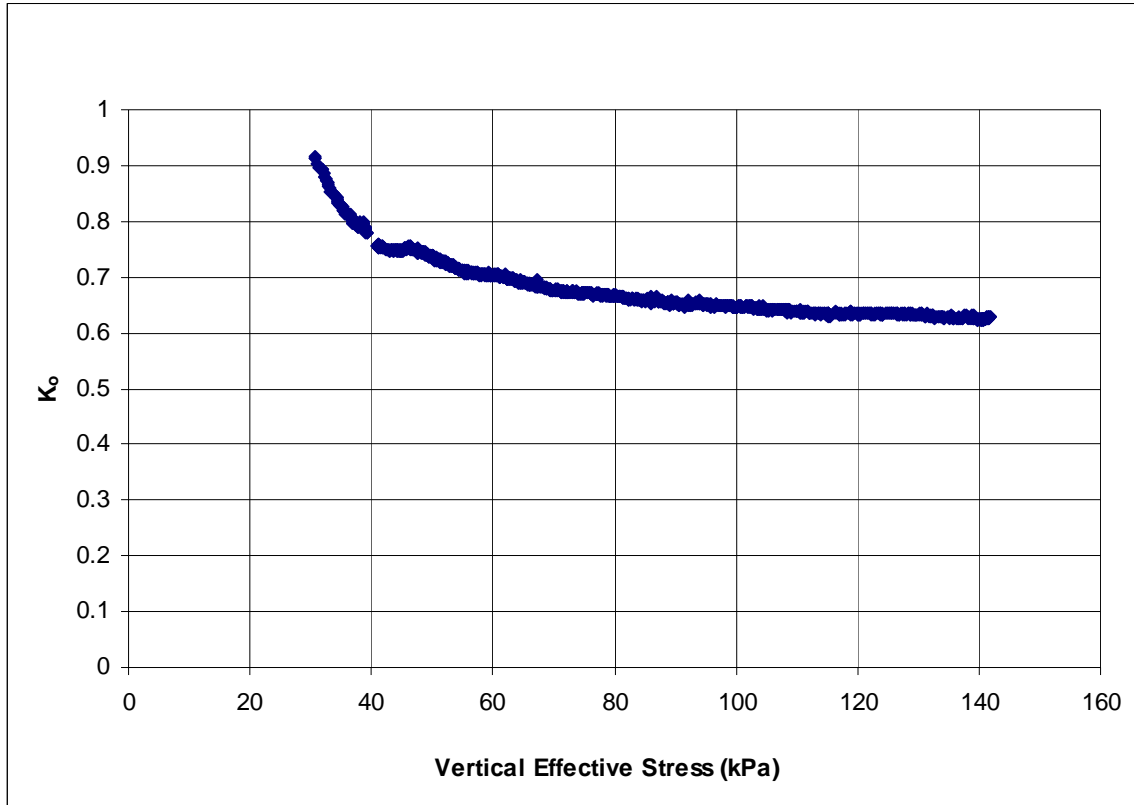
Figure A.8: K_o Versus Vertical Effective Stress – Triaxial Test # 797
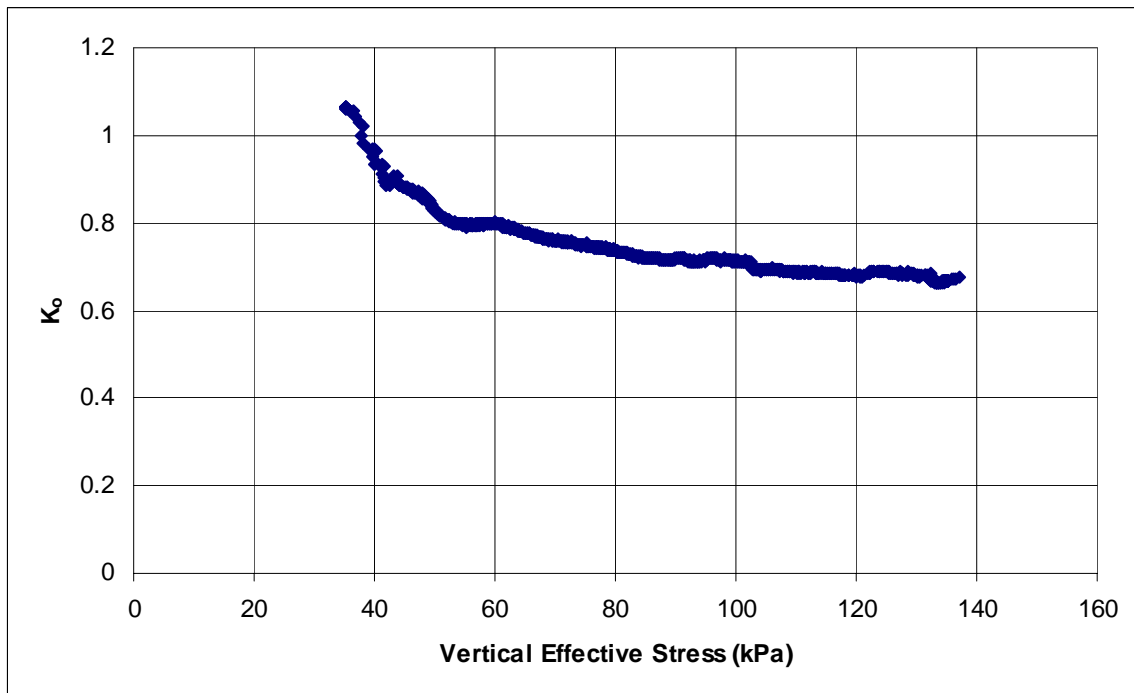
Figure A.9: K_o Versus Vertical Effective Stress – Triaxial Test # 801
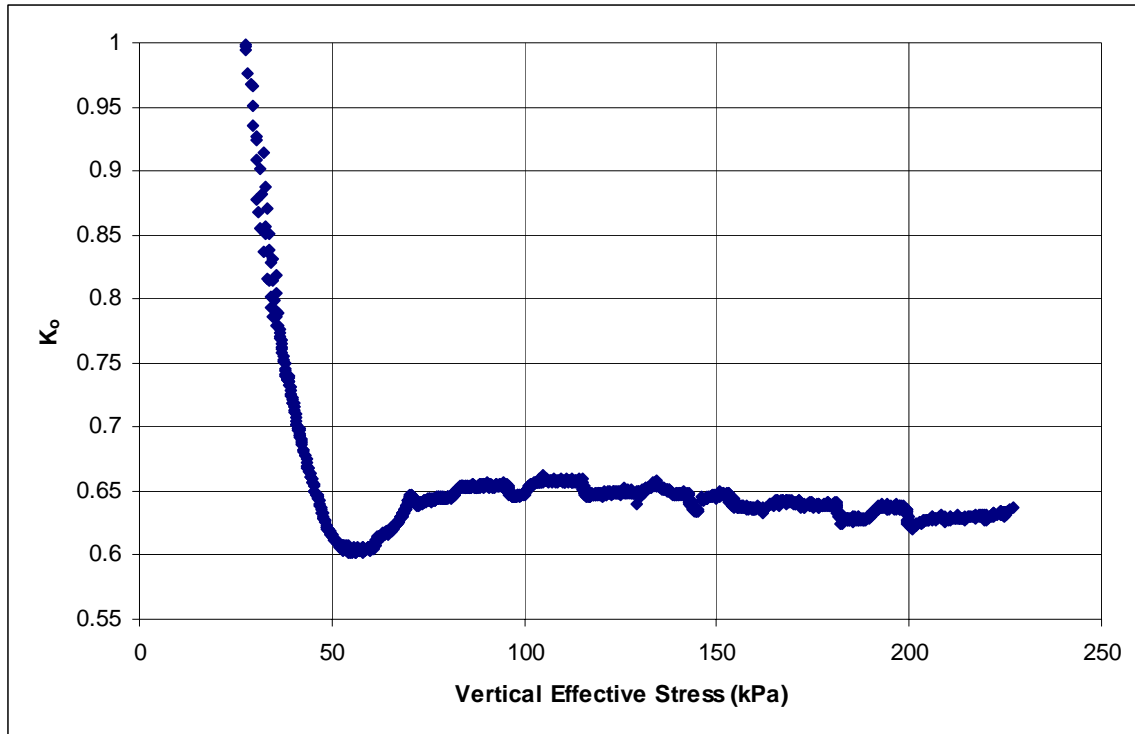
Figure A.10: K_o Versus Vertical Effective Stress – Triaxial Test # 804
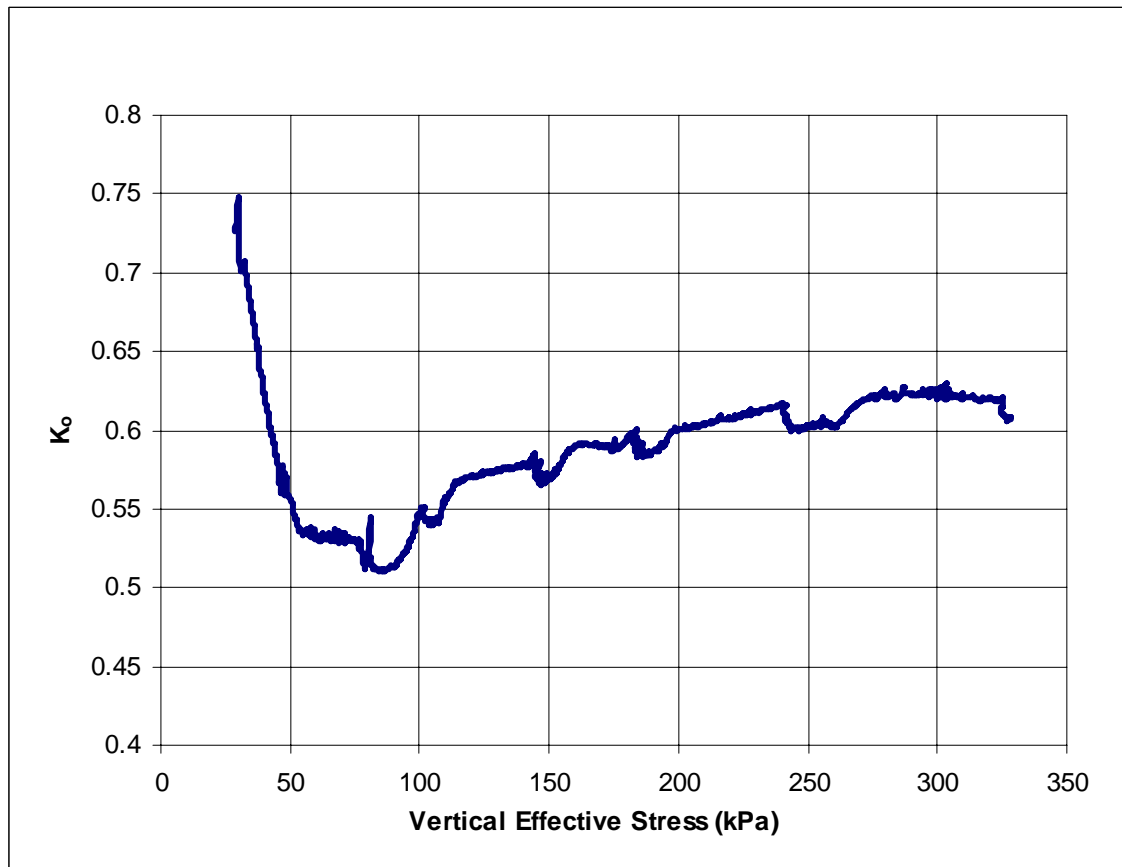
Figure A.11: K_o Versus Vertical Effective Stress – Triaxial Test # 807
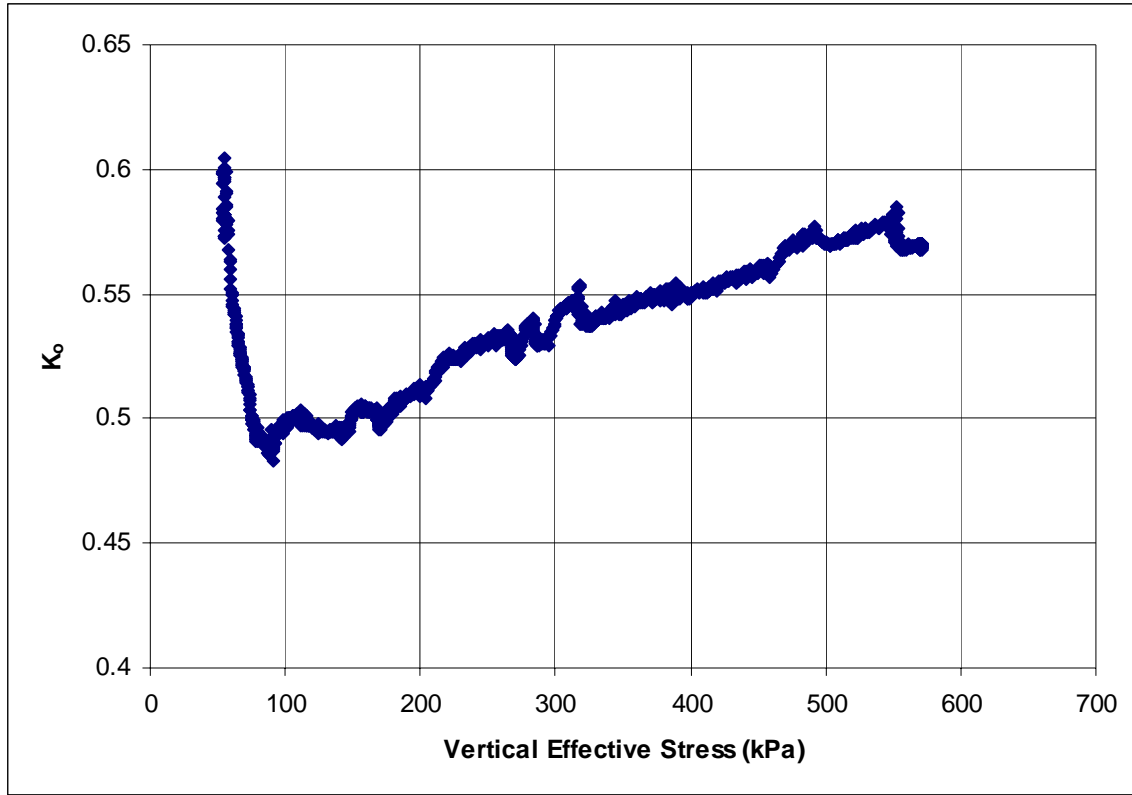
Figure A.12: K_o Versus Vertical Effective Stress – Triaxial Test # 810
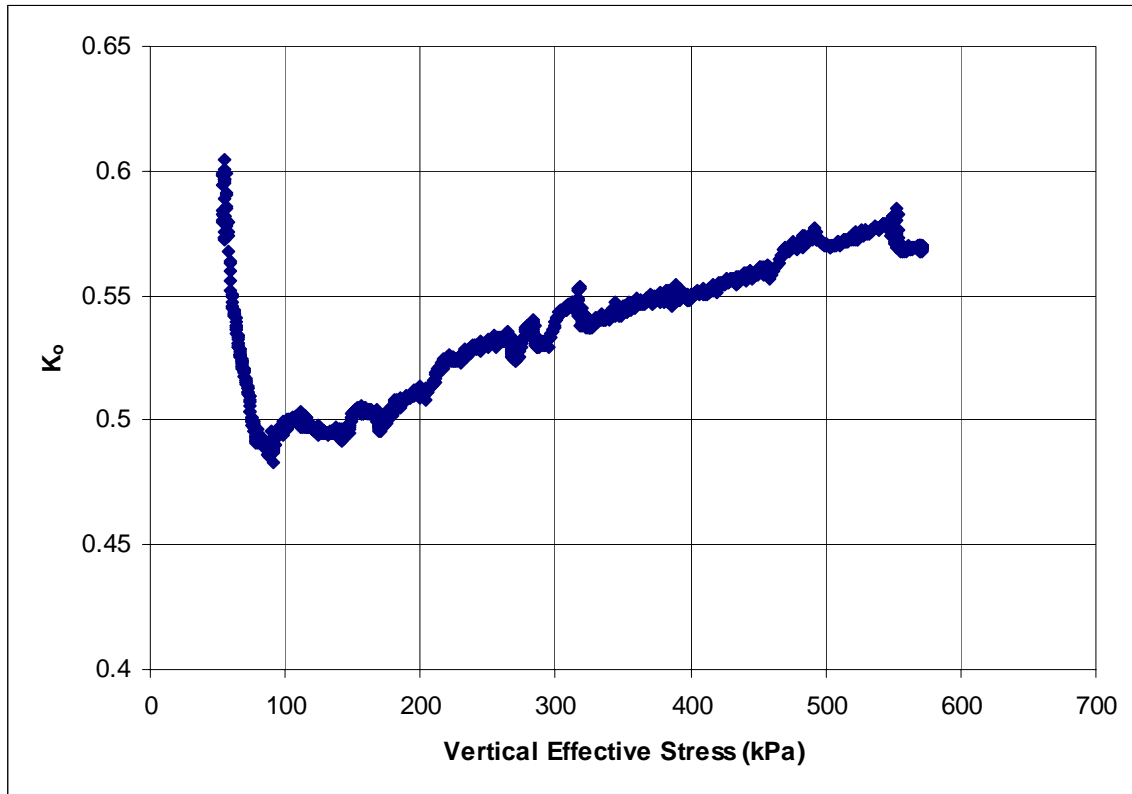
Figure A.13: K_o Versus Vertical Effective Stress – Triaxial Test # 812
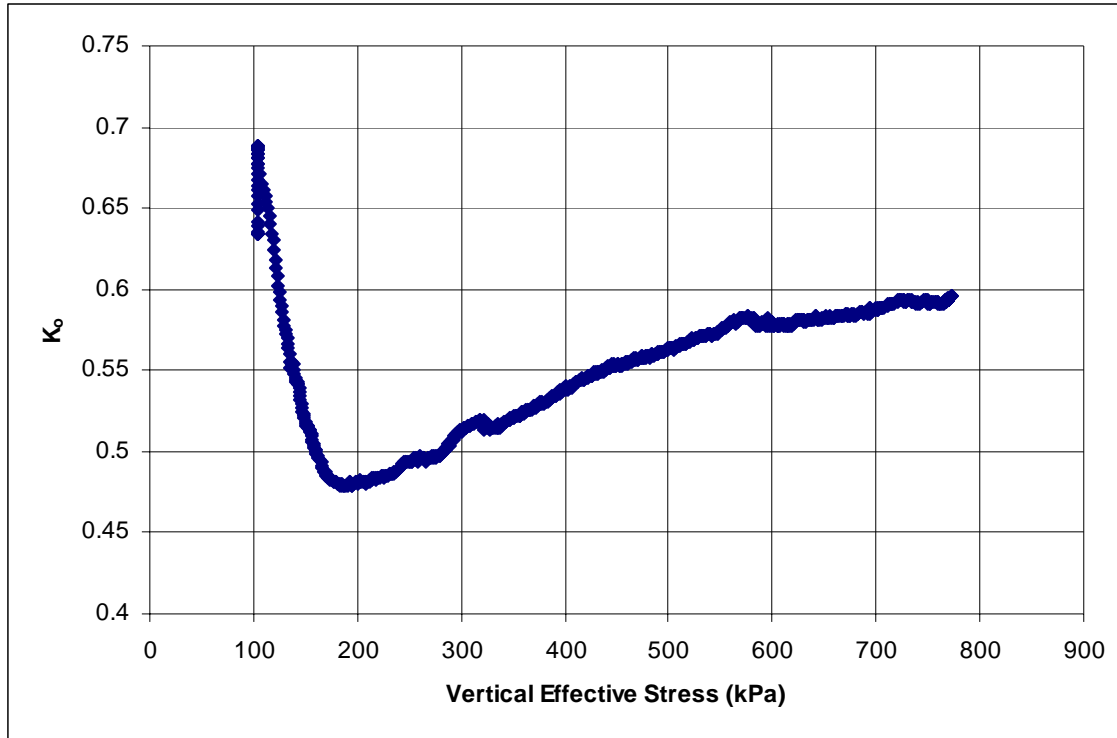
Figure A.14: K_o Versus Vertical Effective Stress – Triaxial Test # 815
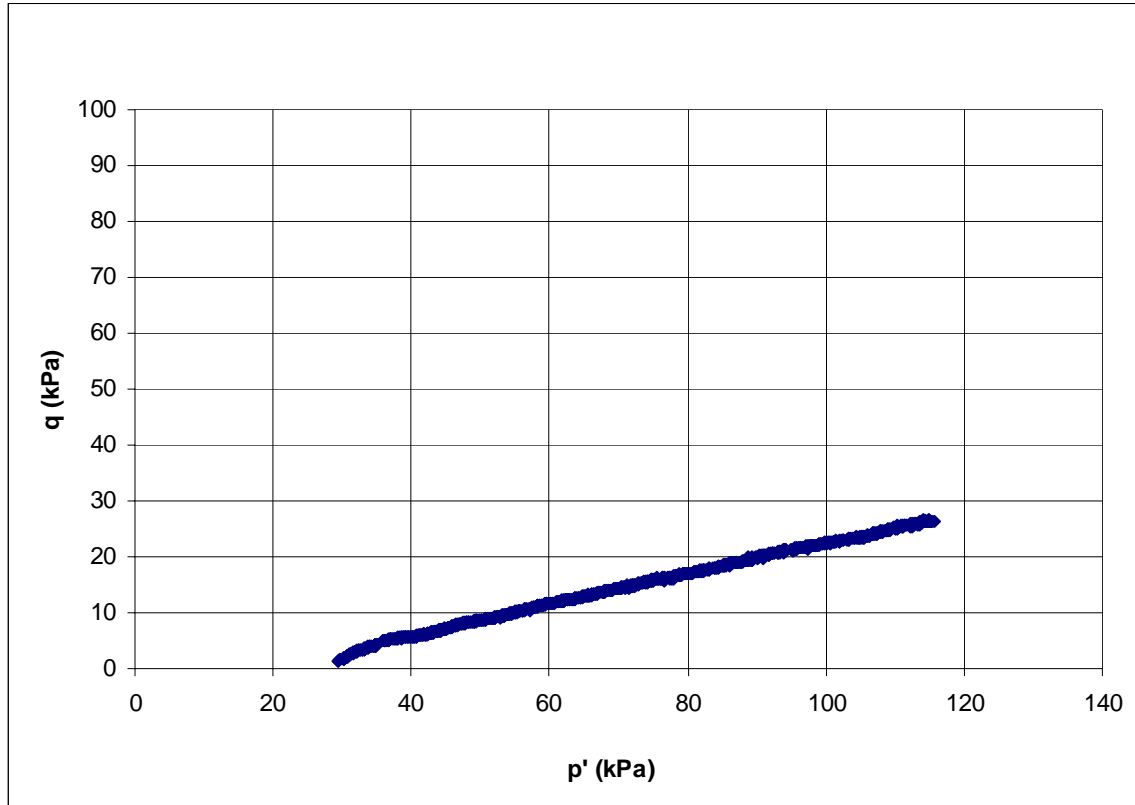
Figure A.15: K_o Consolidation Stress Path – Triaxial Test # 797
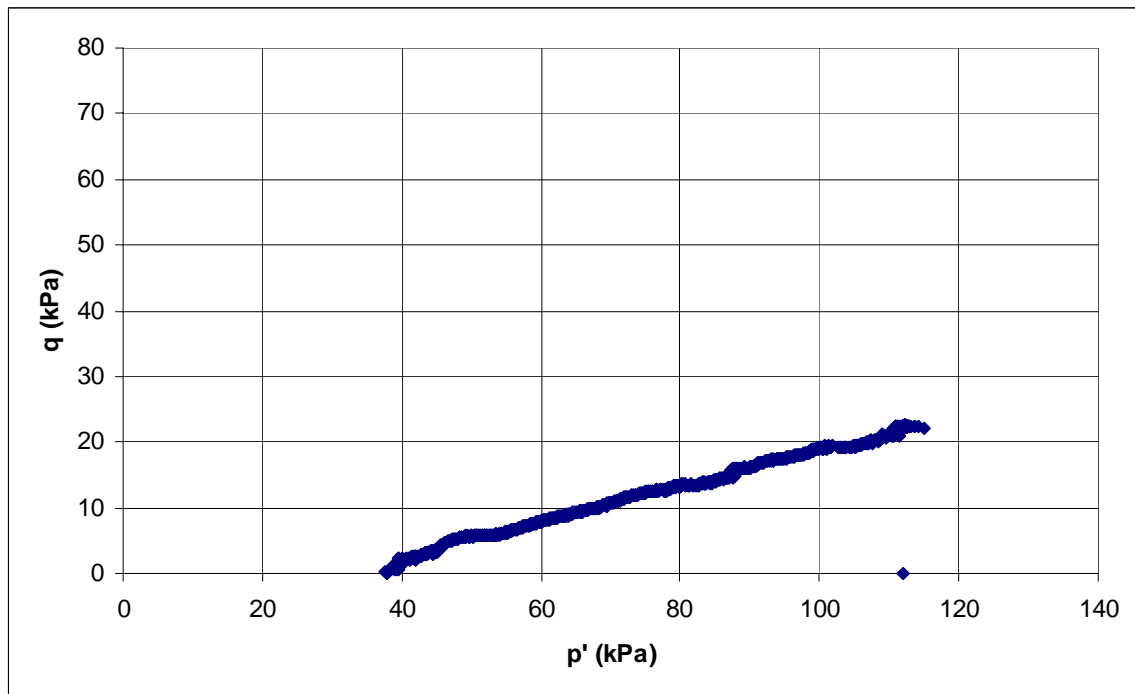
Figure A.16: K_o Consolidation Stress Path – Triaxial Test # 801
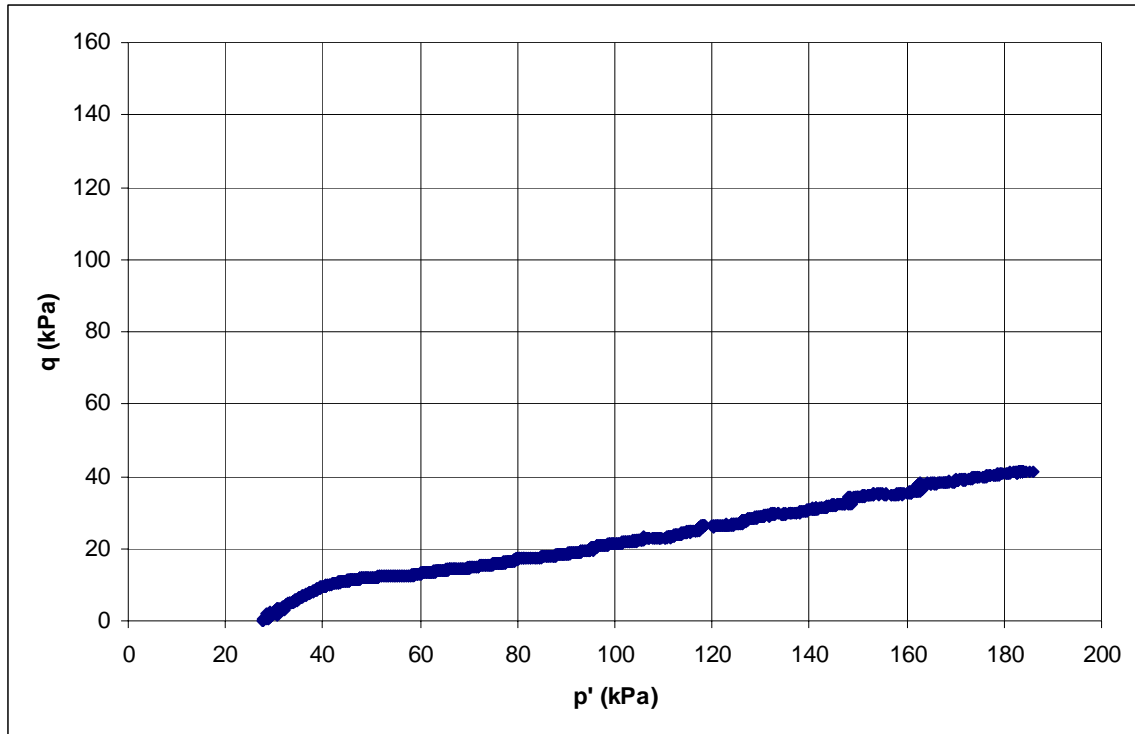
Figure A.17: K_o Consolidation Stress Path – Triaxial Test # 804
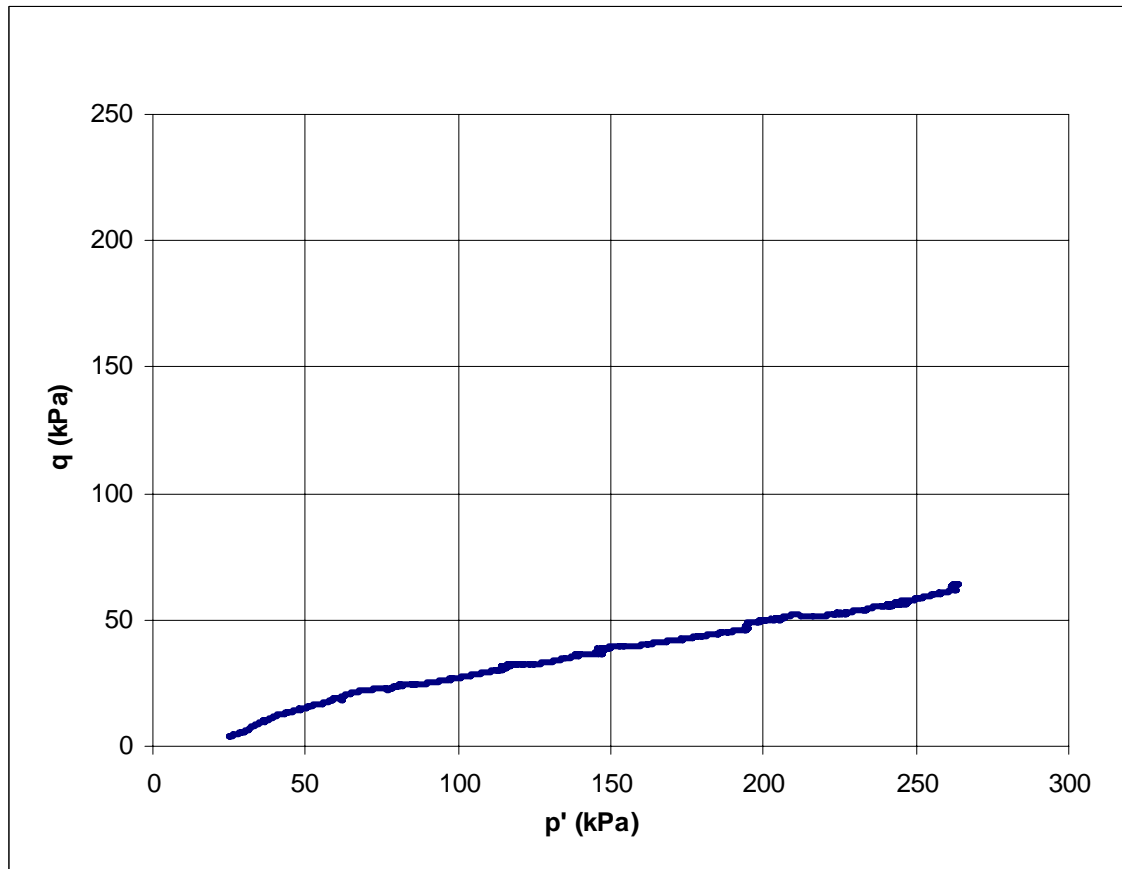
Figure A.18: K_o Consolidation Stress Path – Triaxial Test # 807
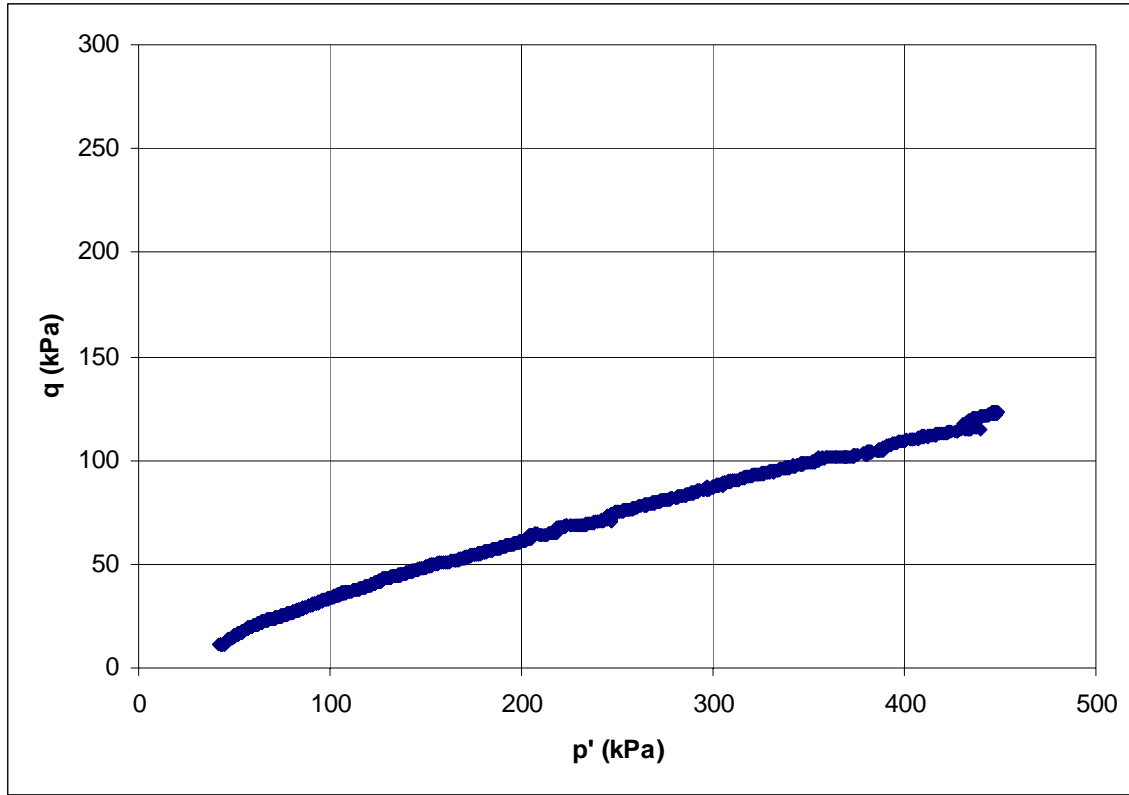
Figure A.19: K_o Consolidation Stress Path – Triaxial Test # 810
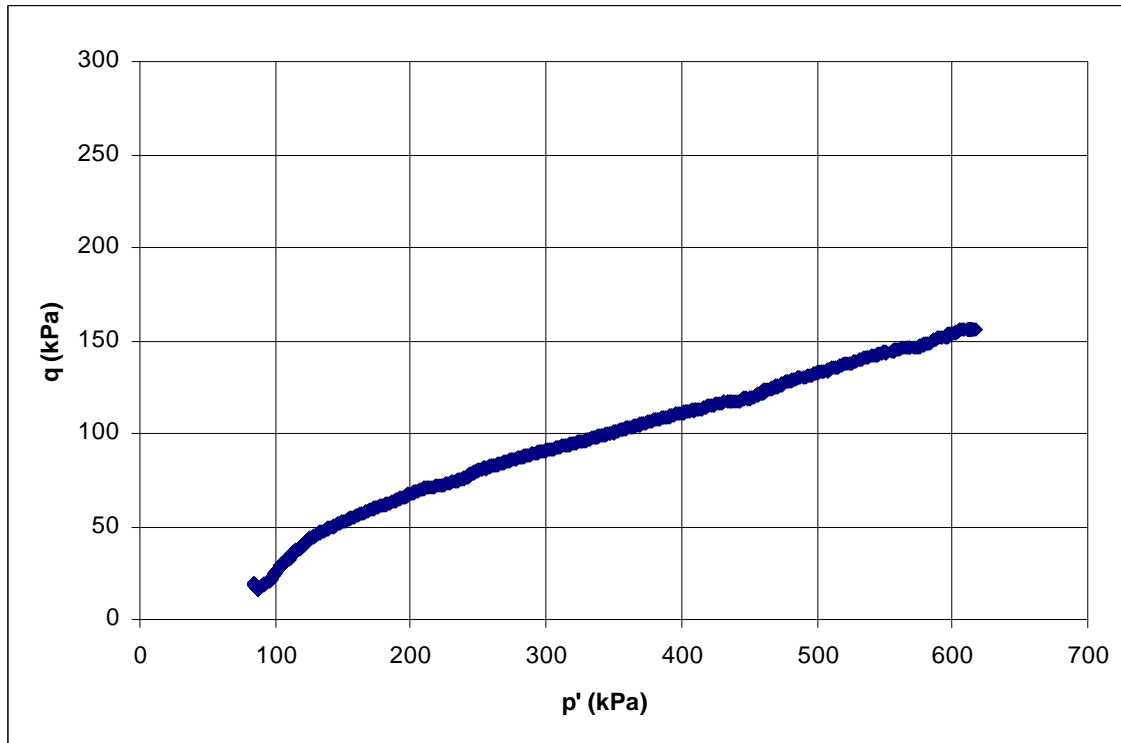
Figure A.20: K_o Consolidation Stress Path – Triaxial Test # 812
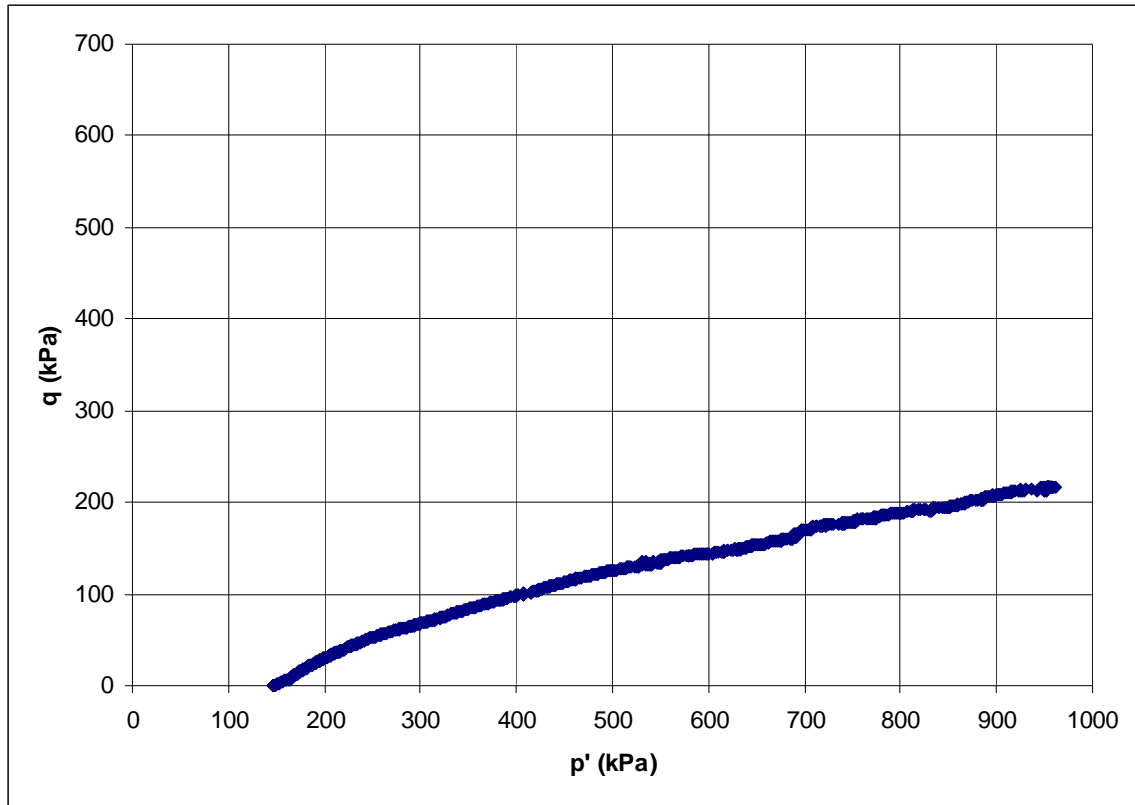
Figure A.21: K_o Consolidation Stress Path – Triaxial Test # 815
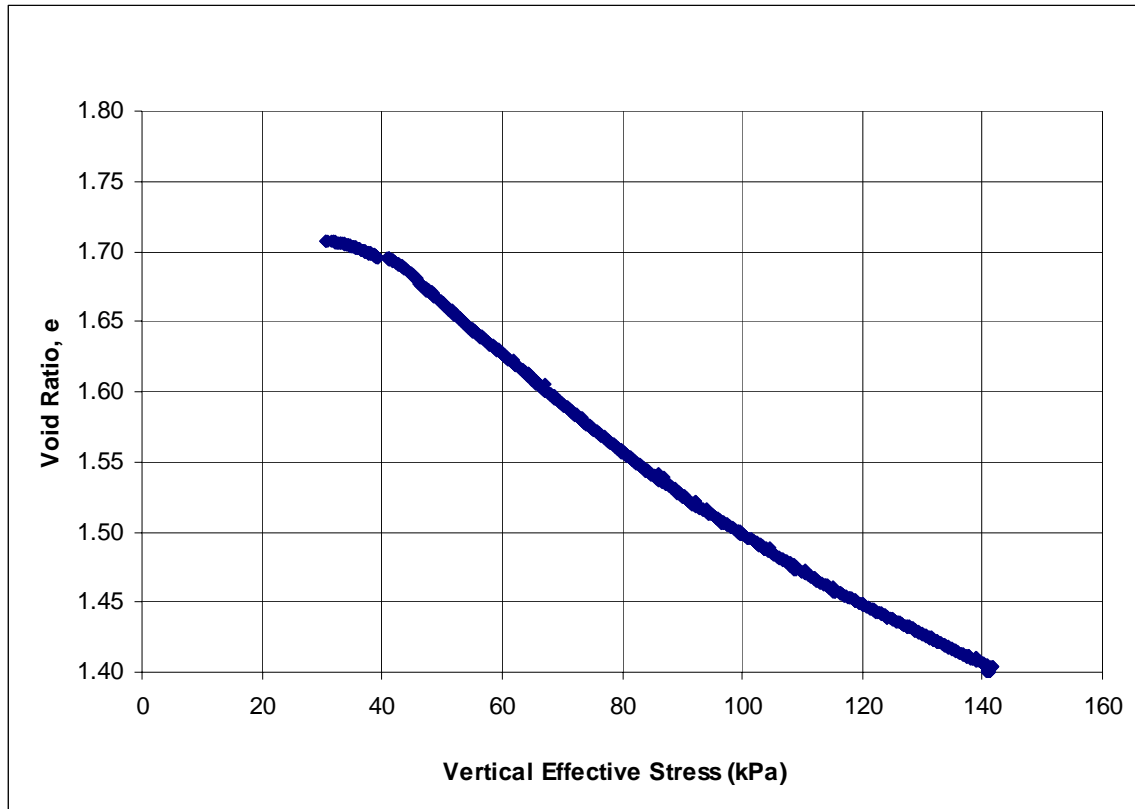
Figure A.22: Void Ratio Versus Vertical Effective Stress – Triaxial Test # 797

Figure A.23: Void Ratio Versus Vertical Effective Stress – Triaxial Test # 801
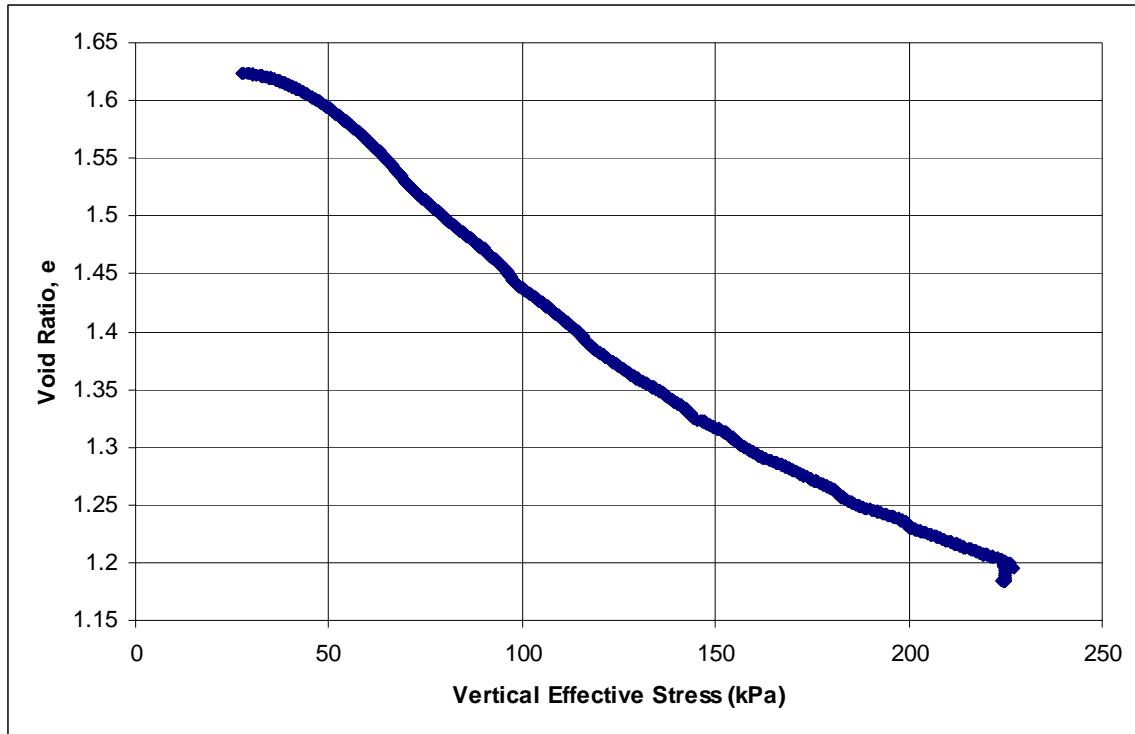
Figure A.24: Void Ratio Versus Vertical Effective Stress – Triaxial Test # 804
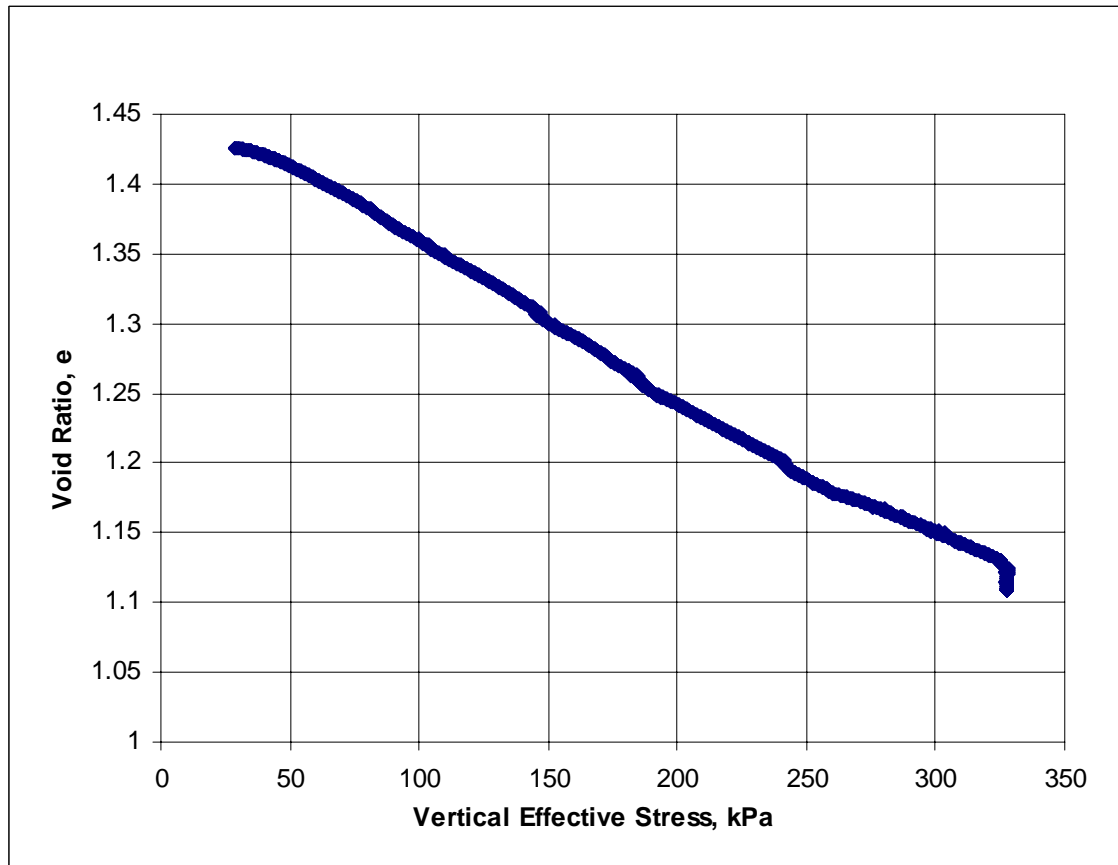
Figure A.25: Void Ratio Versus Vertical Effective Stress – Triaxial Test # 807
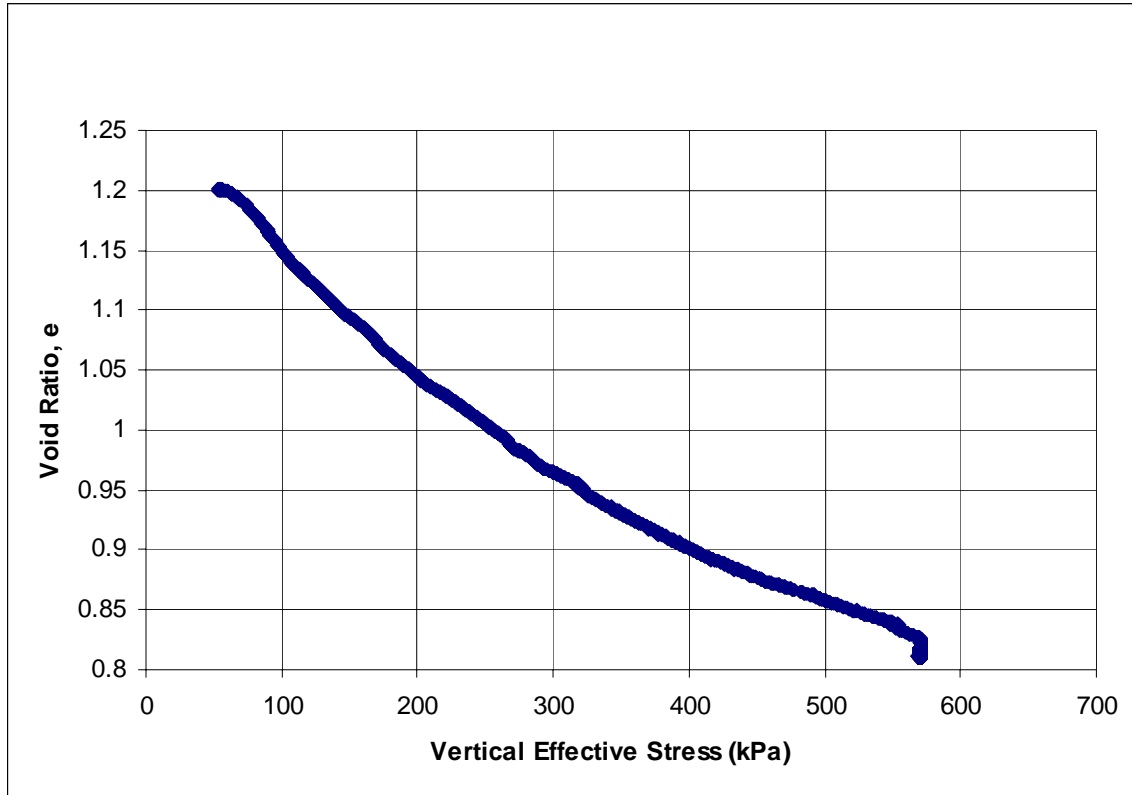
Figure A.26: Void Ratio Versus Vertical Effective Stress – Triaxial Test # 810
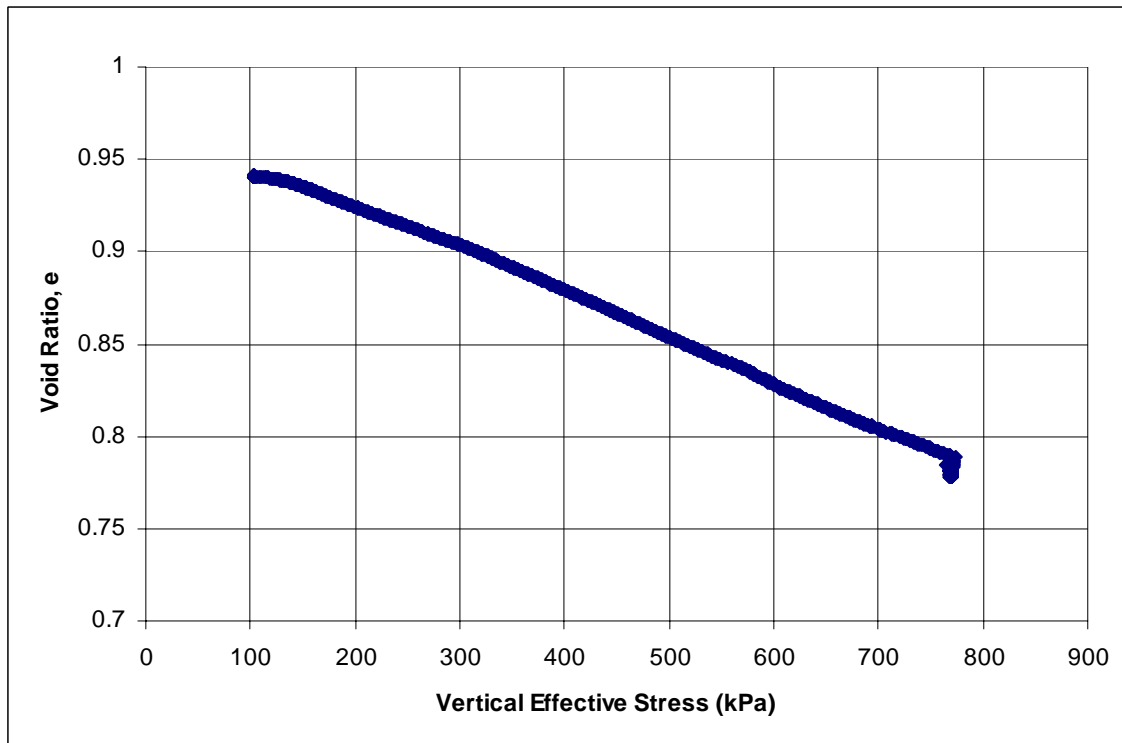
Figure A.27: Void Ratio Versus Vertical Effective Stress – Triaxial Test # 812
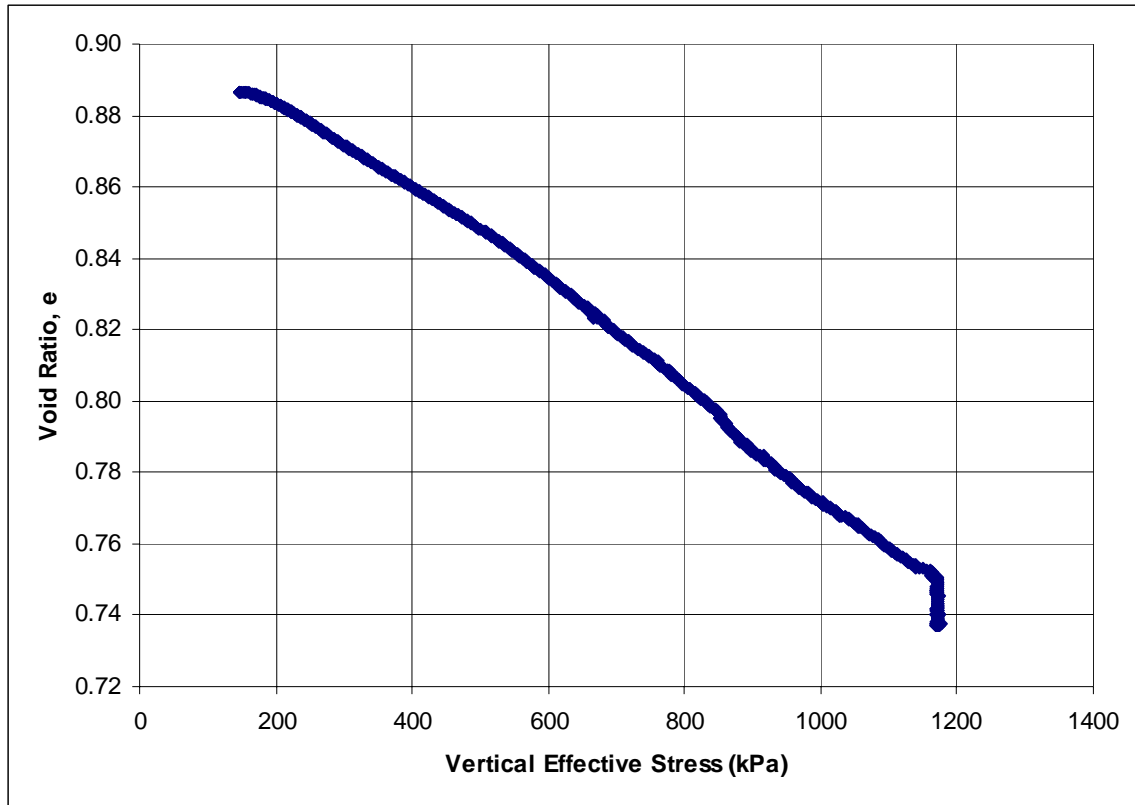
Figure A.28: Void Ratio Versus Vertical Effective Stress – Triaxial Test # 815
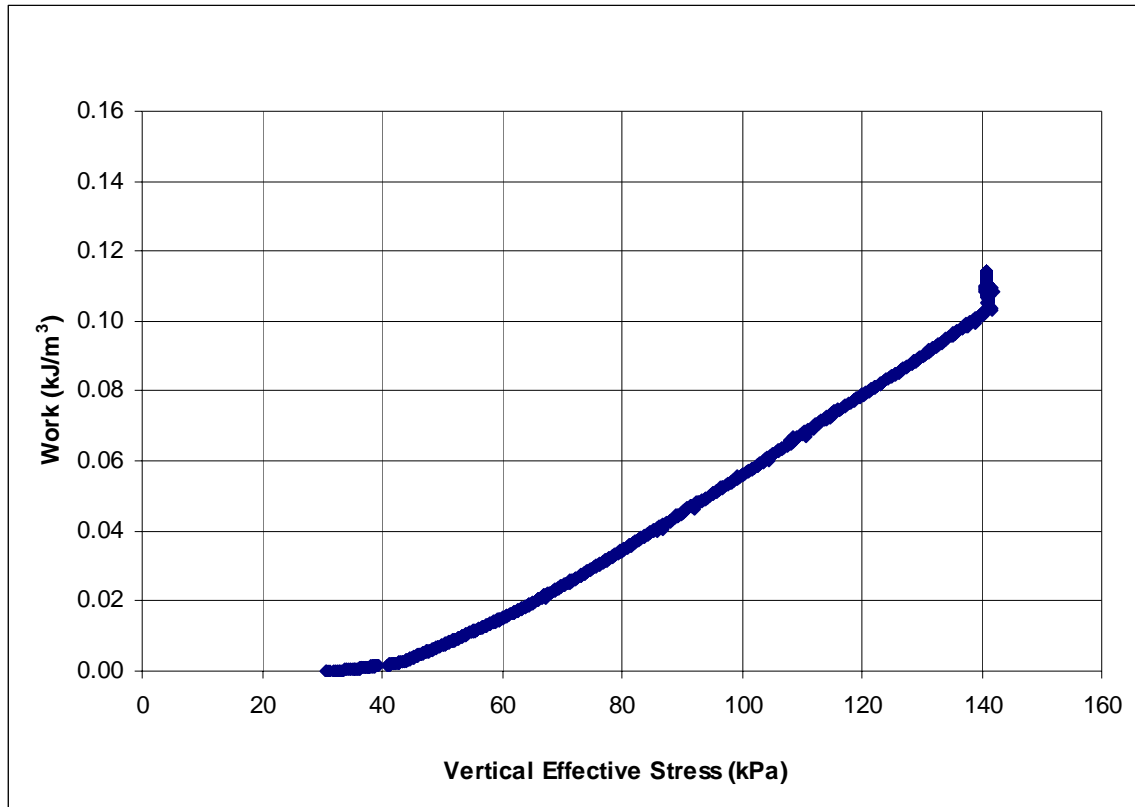
Figure A.29: Work Versus Vertical Effective Stress – Triaxial Test # 797
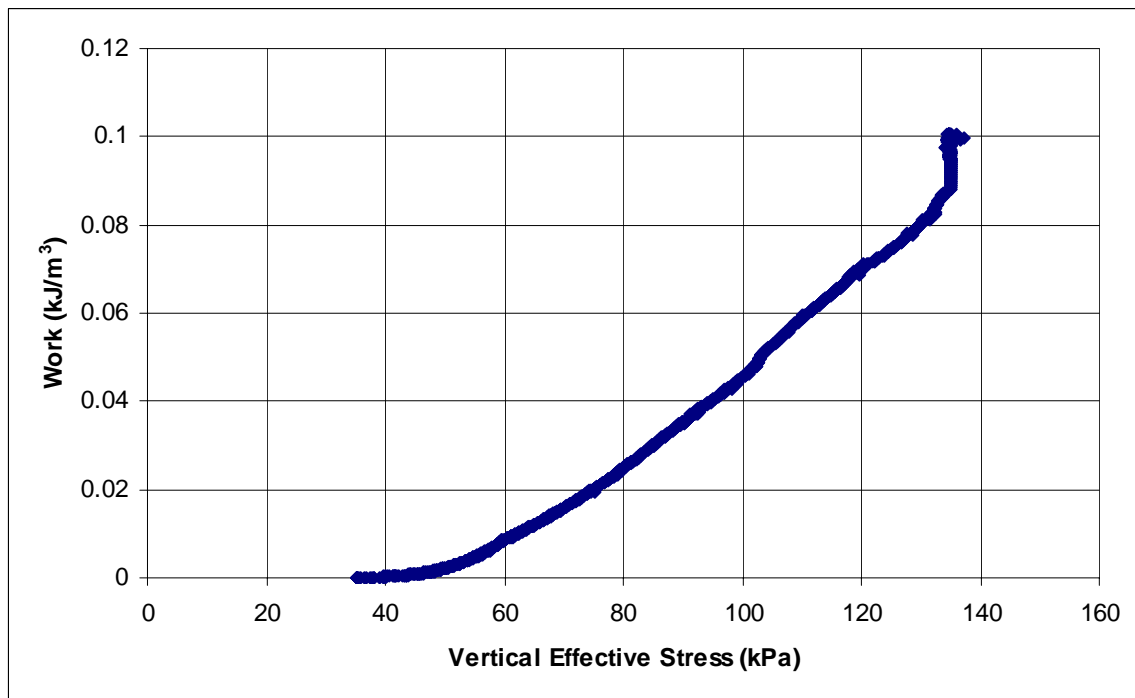
Figure A.30: Work Versus Vertical Effective Stress – Triaxial Test # 801
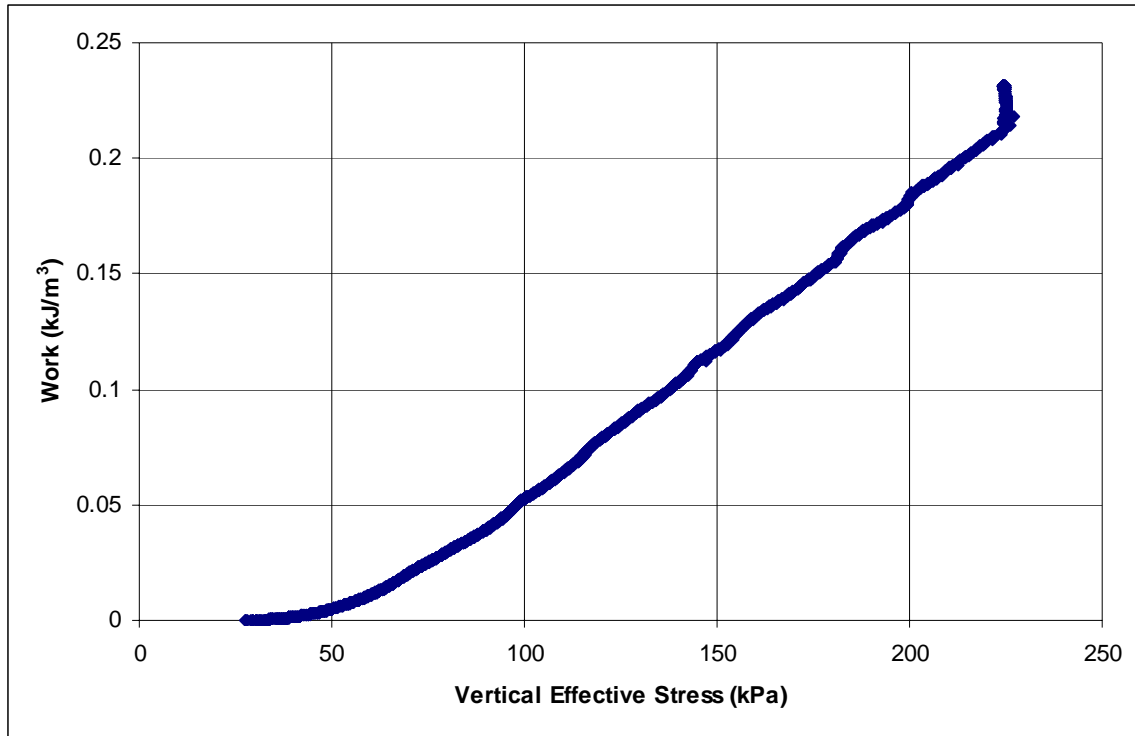
Figure A.31: Work Versus Vertical Effective Stress – Triaxial Test # 804
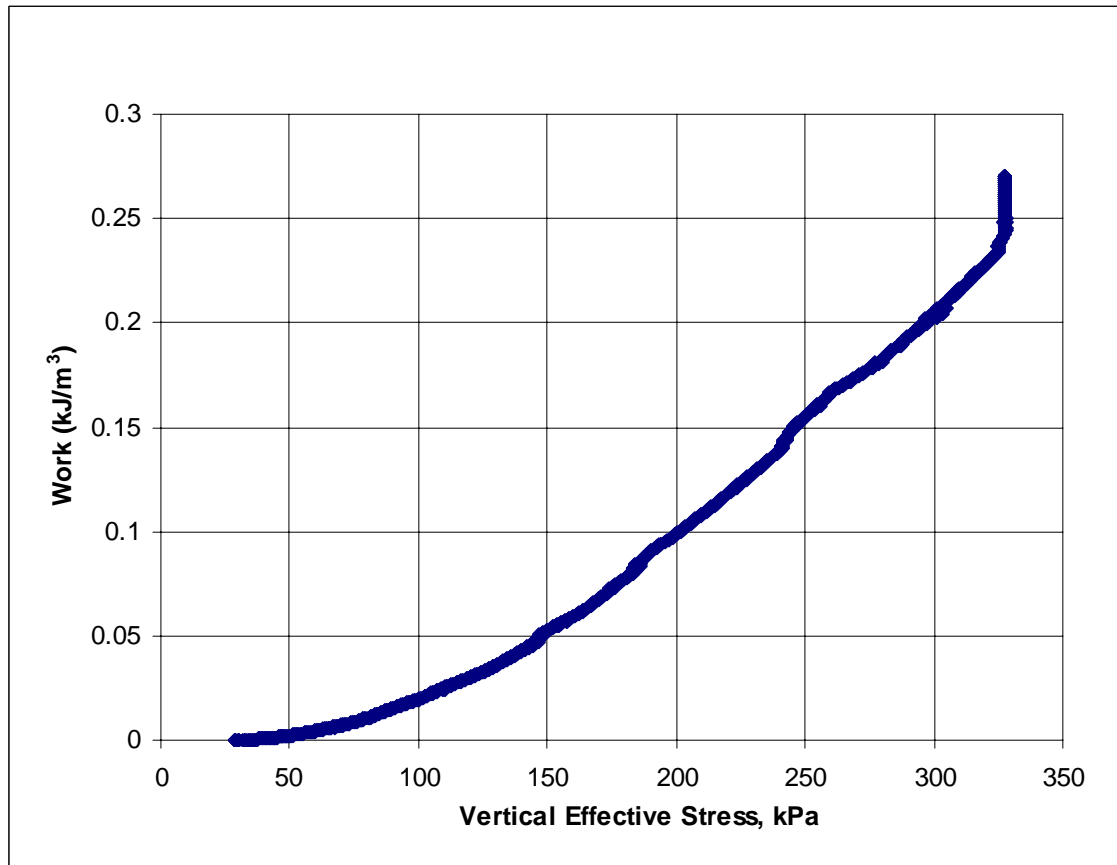
Figure A.32: Work Versus Vertical Effective Stress – Triaxial Test # 807
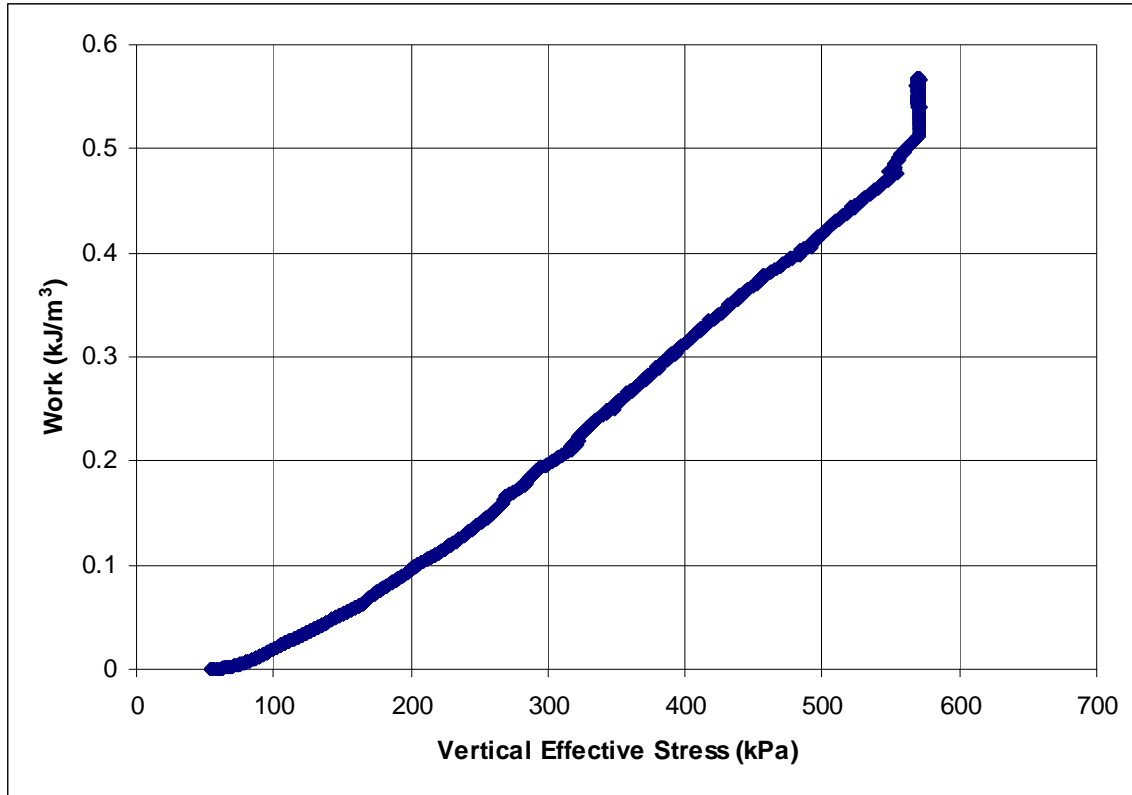
Figure A.33: Work Versus Vertical Effective Stress – Triaxial Test # 810
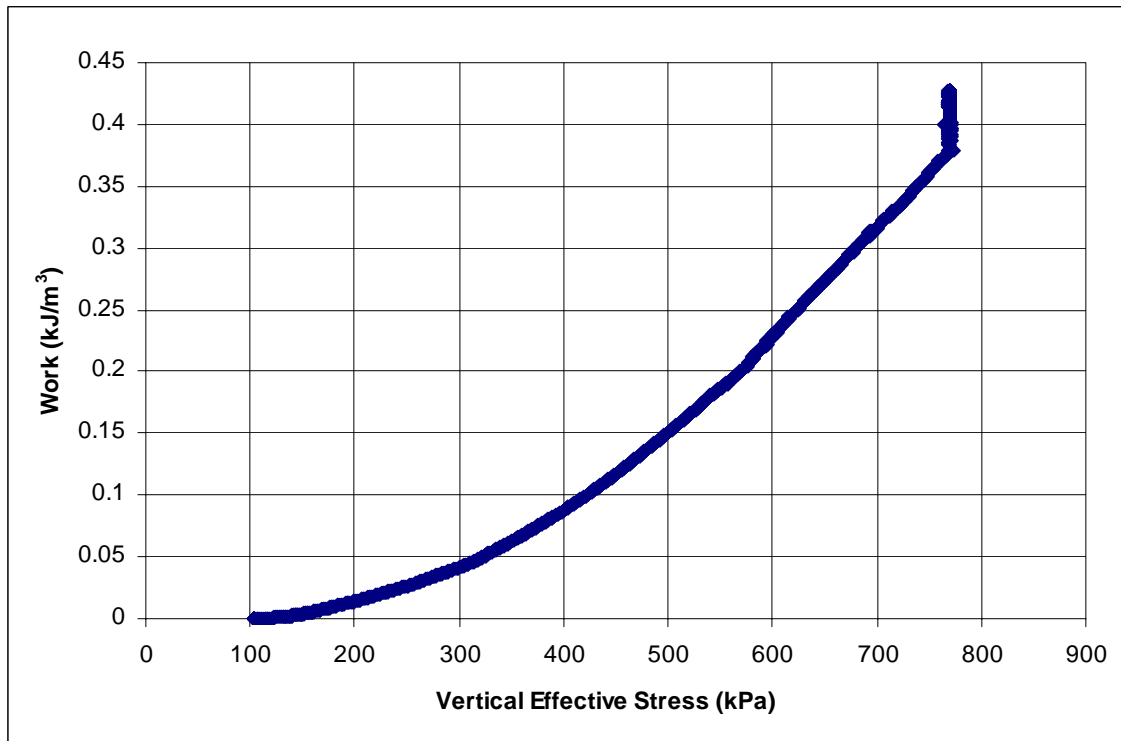
Figure A.34: Work Versus Vertical Effective Stress – Triaxial Test # 812
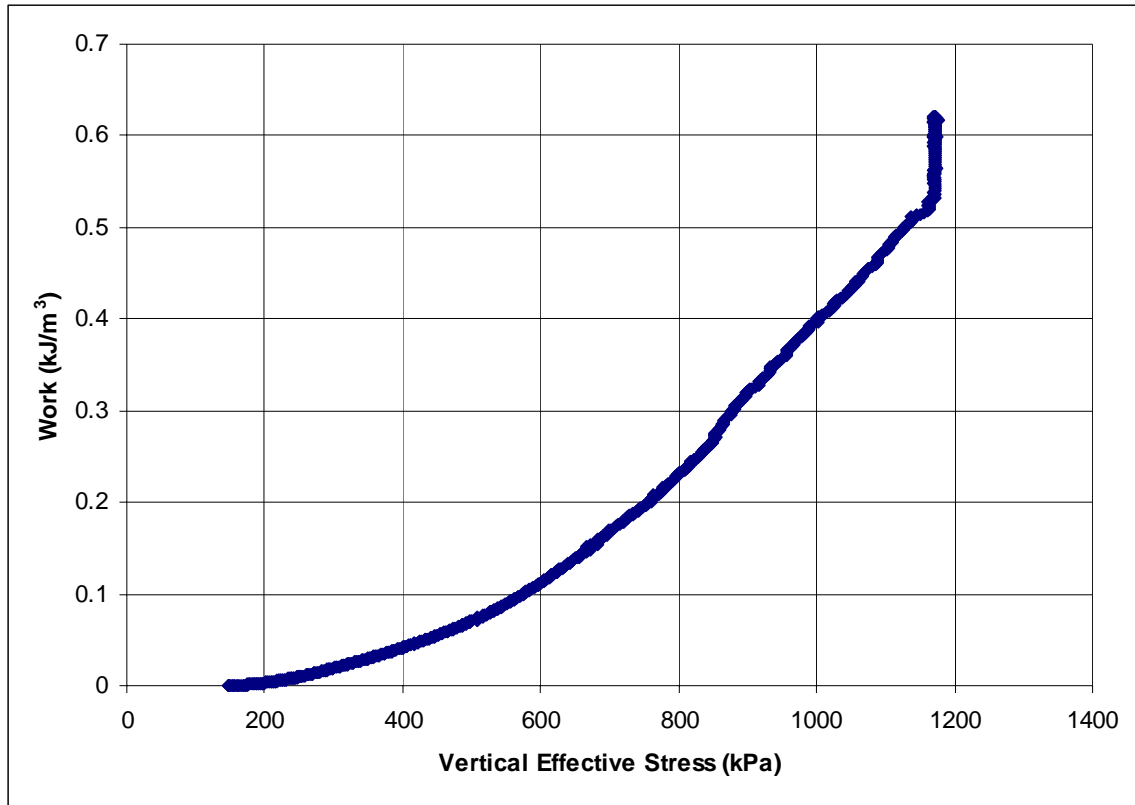
Figure A.35: Work Versus Vertical Effective Stress – Triaxial Test # 815
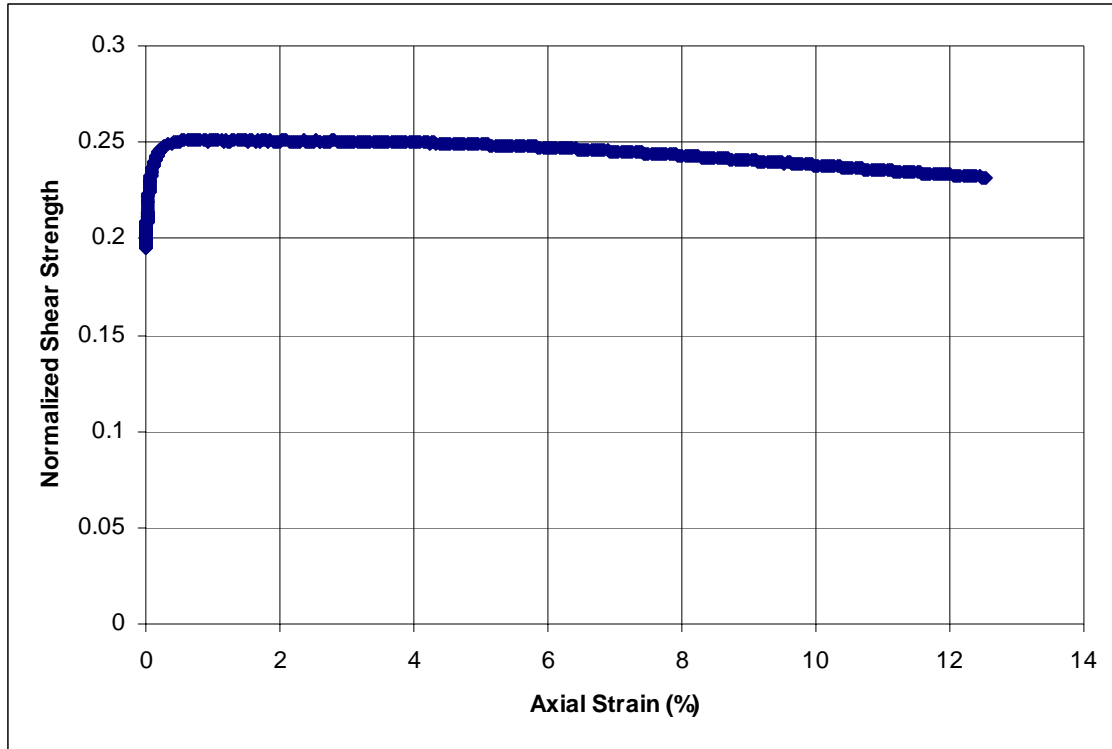
Figure A.36: Normalized Shear Strength Versus Axial Strain – Triaxial Test # 797
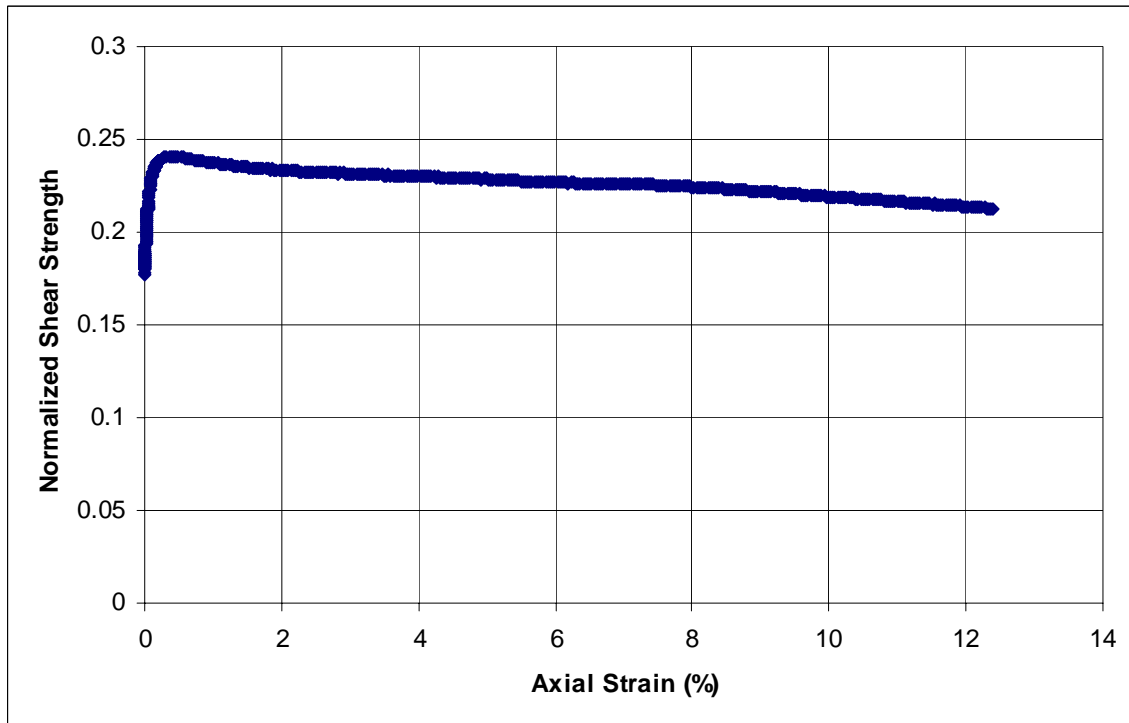
Figure A.37: Normalized Shear Strength Versus Axial Strain – Triaxial Test # 801
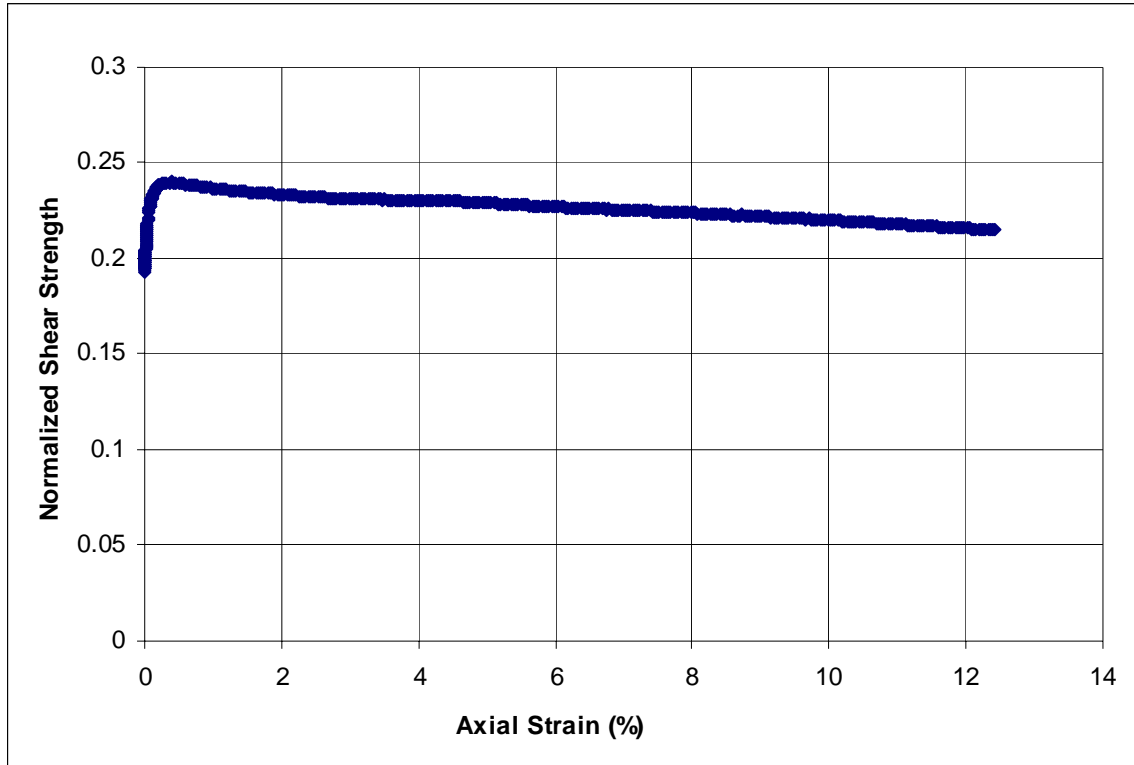
Figure A.38: Normalized Shear Strength Versus Axial Strain – Triaxial Test # 804
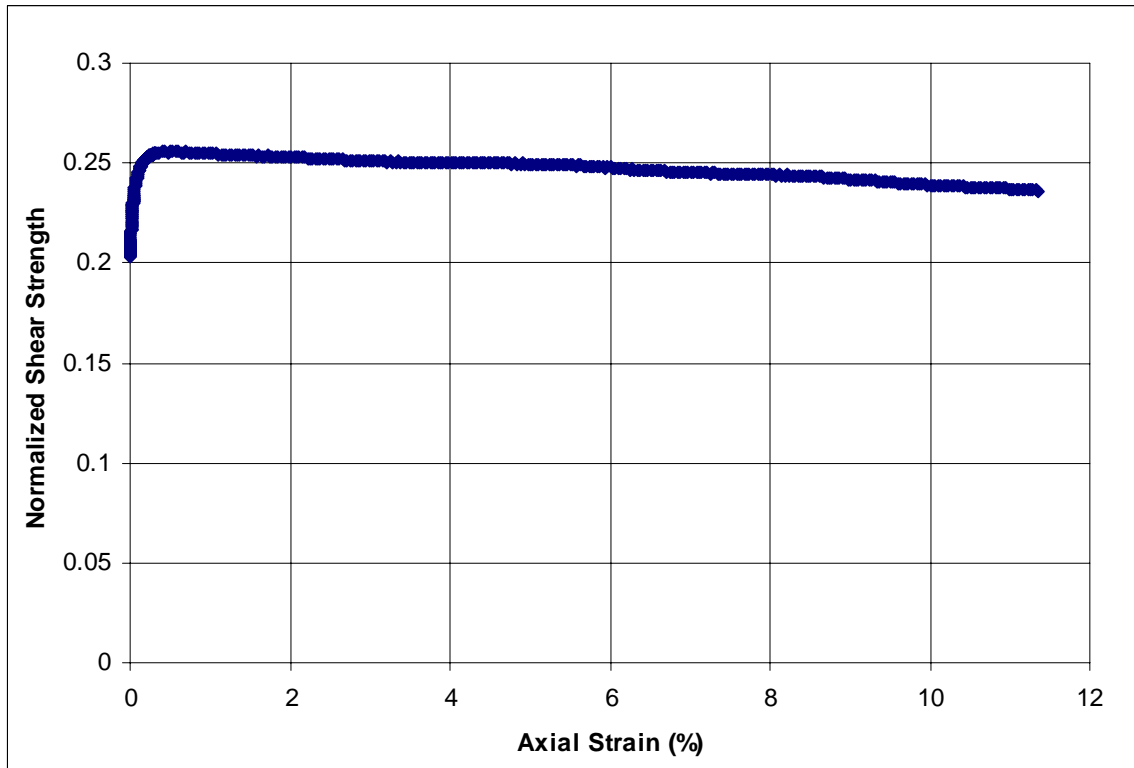
Figure A.39: Normalized Shear Strength Versus Axial Strain – Triaxial Test # 807
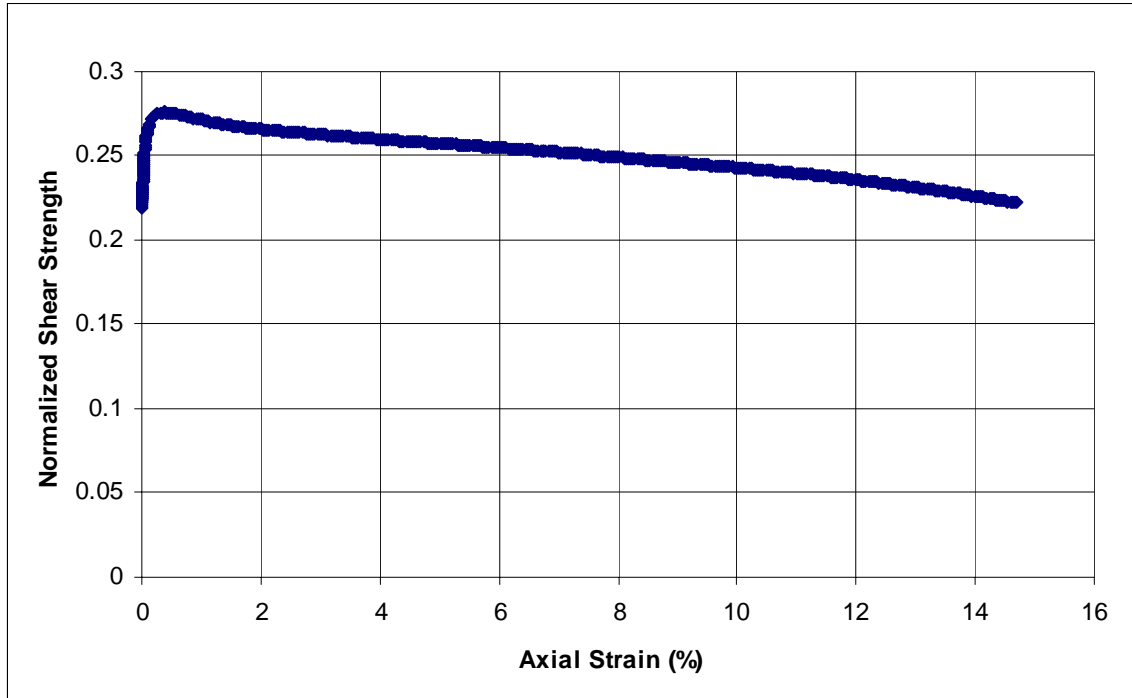
Figure A.40: Normalized Shear Strength Versus Axial Strain – Triaxial Test # 810
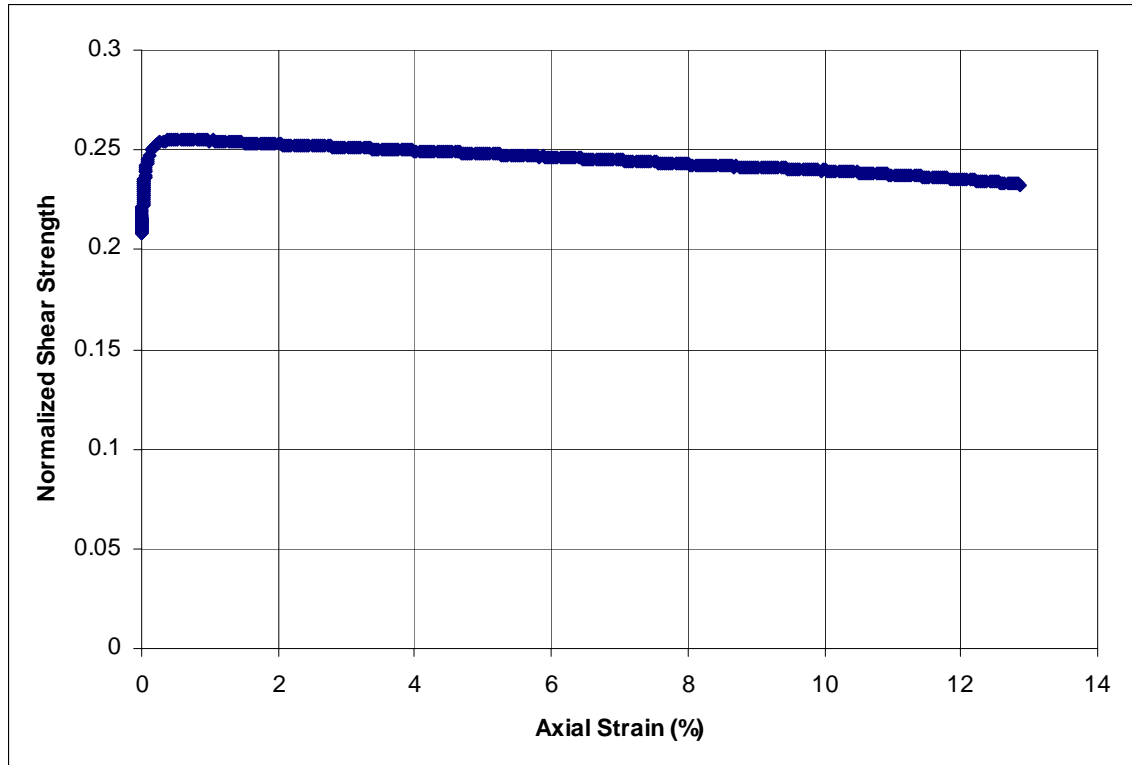
Figure A.41: Normalized Shear Strength Versus Axial Strain – Triaxial Test # 812
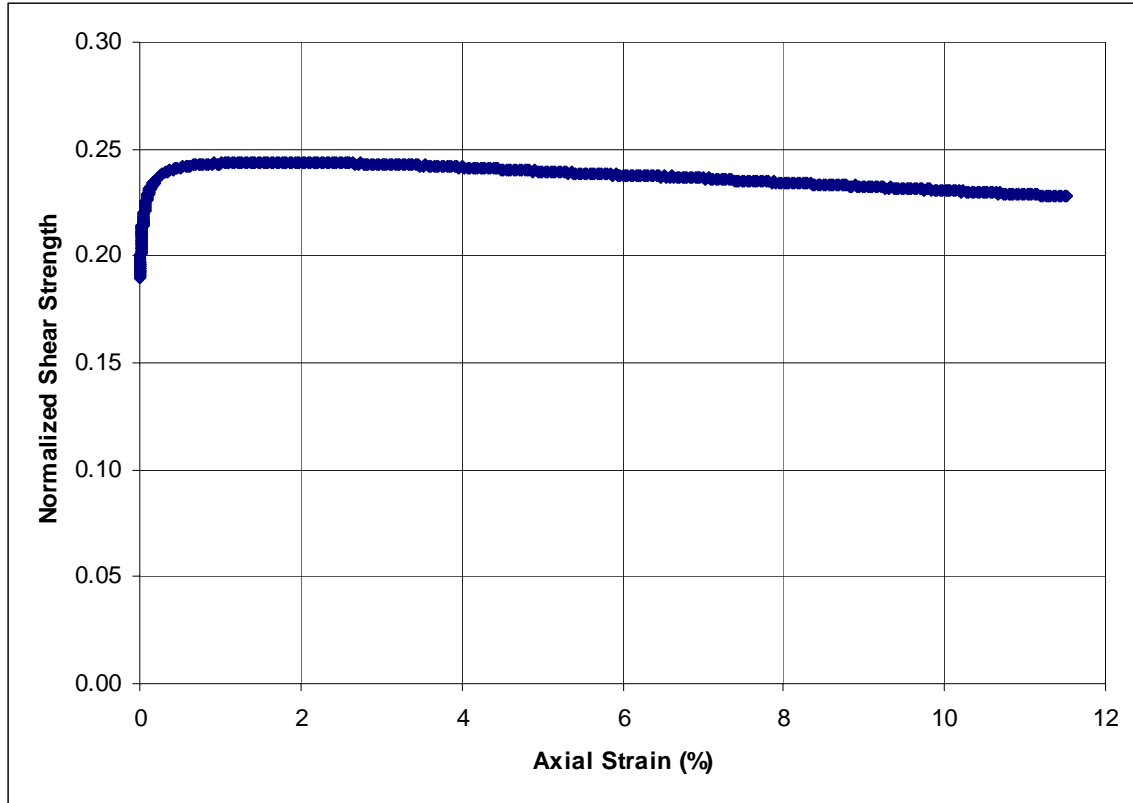
Figure A.42: Normalized Shear Strength Versus Axial Strain – Triaxial Test # 815
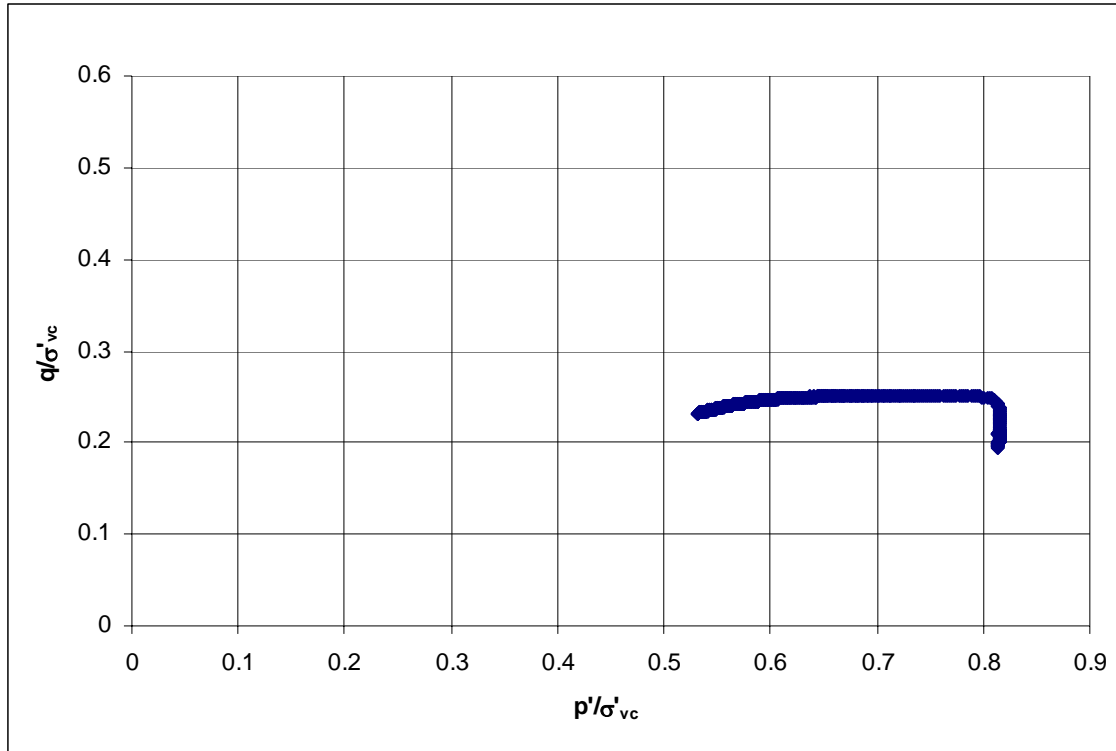
Figure A.43: Undrained Stress Path – Triaxial Test # 797
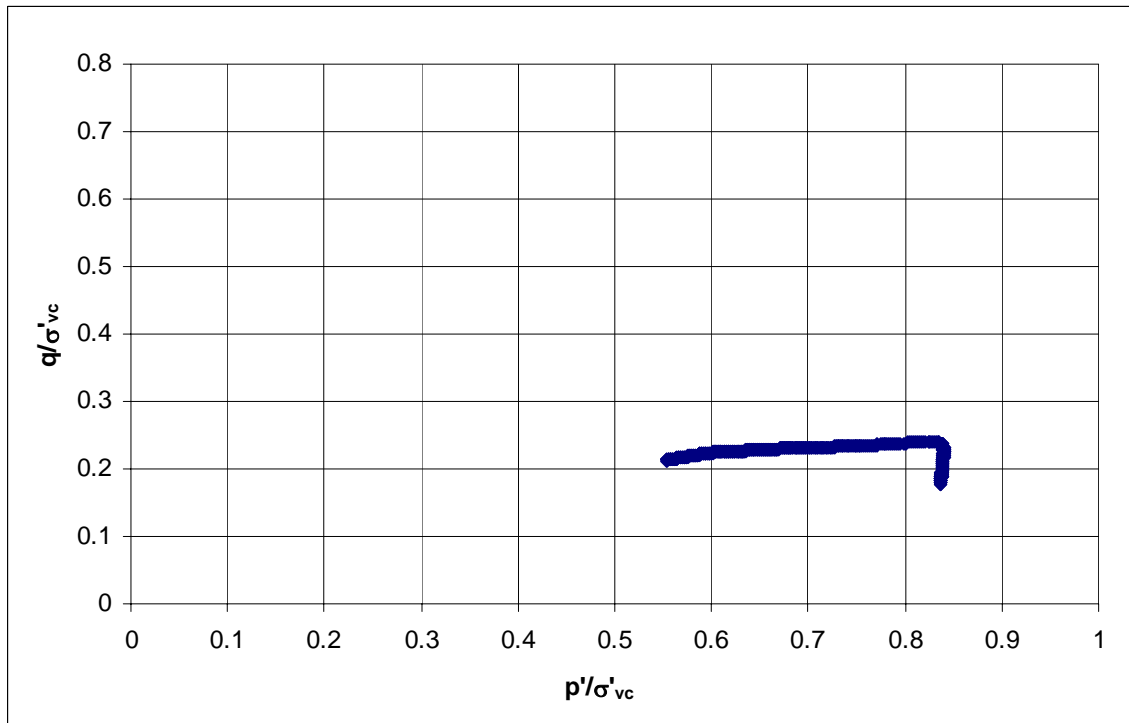
Figure A.44: Undrained Stress Path – Triaxial Test # 801
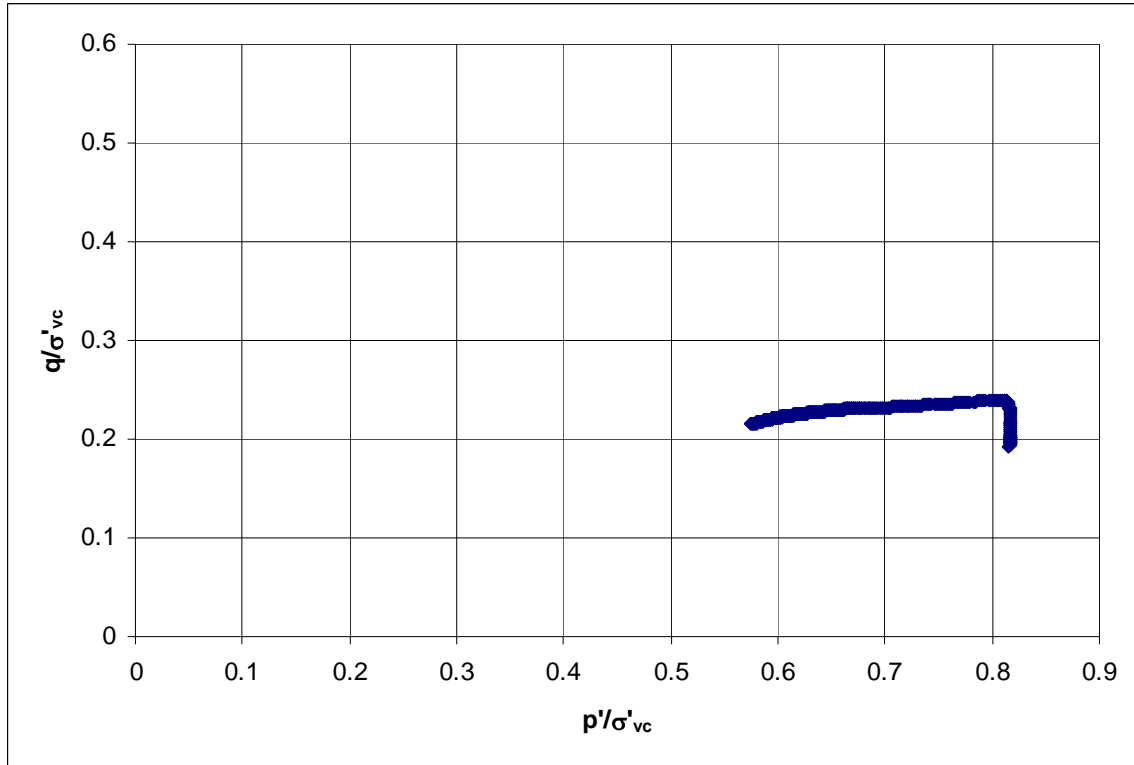
Figure A.45: Undrained Stress Path – Triaxial Test # 804
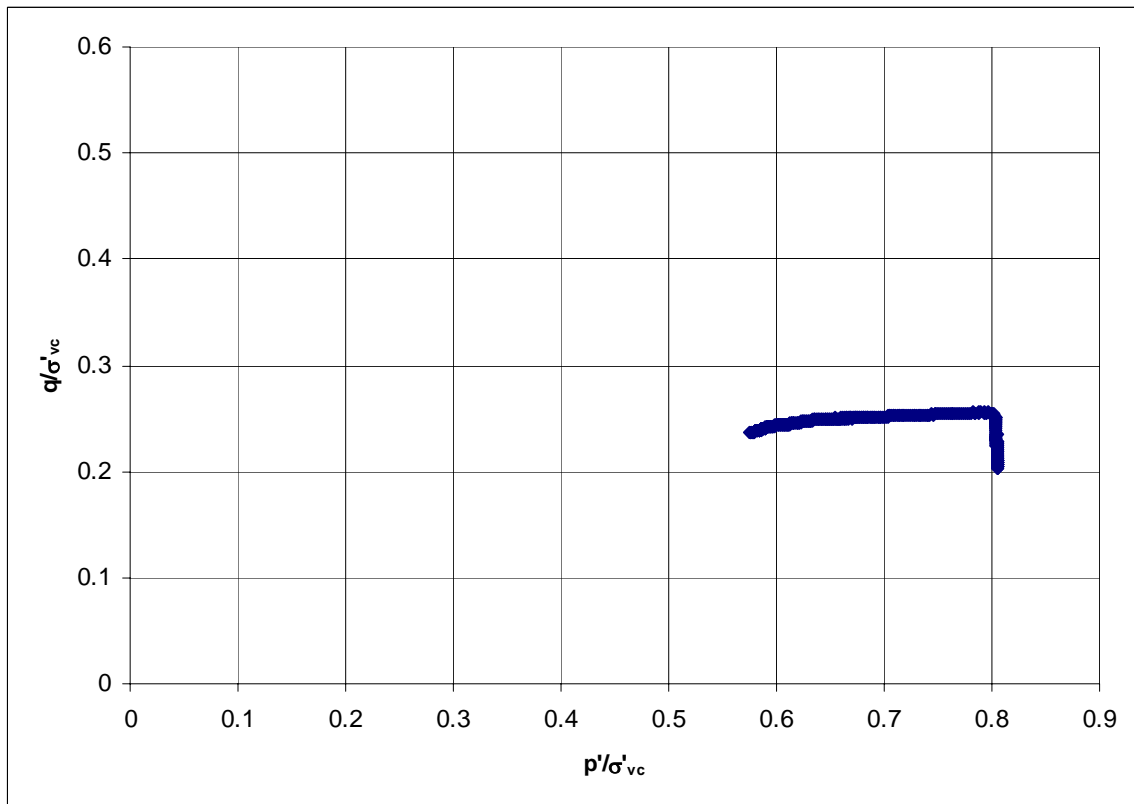
Figure A.46: Undrained Stress Path – Triaxial Test # 807
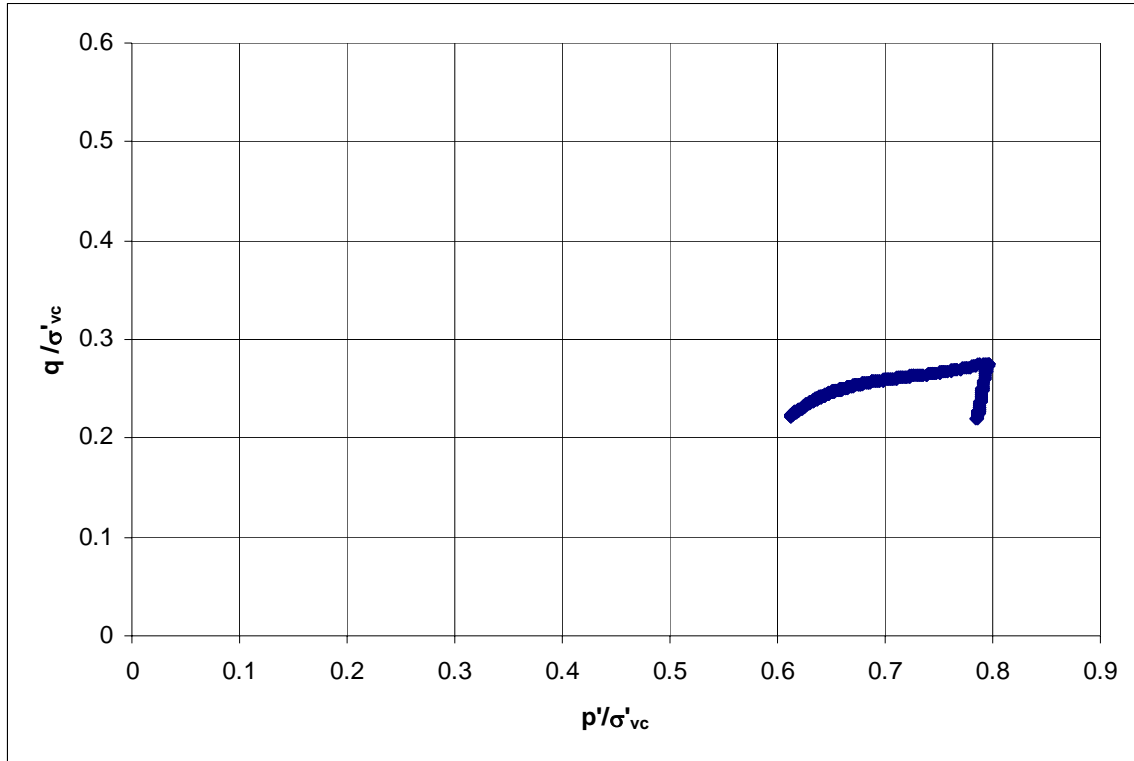
Figure A.47: Undrained Stress Path – Triaxial Test # 810
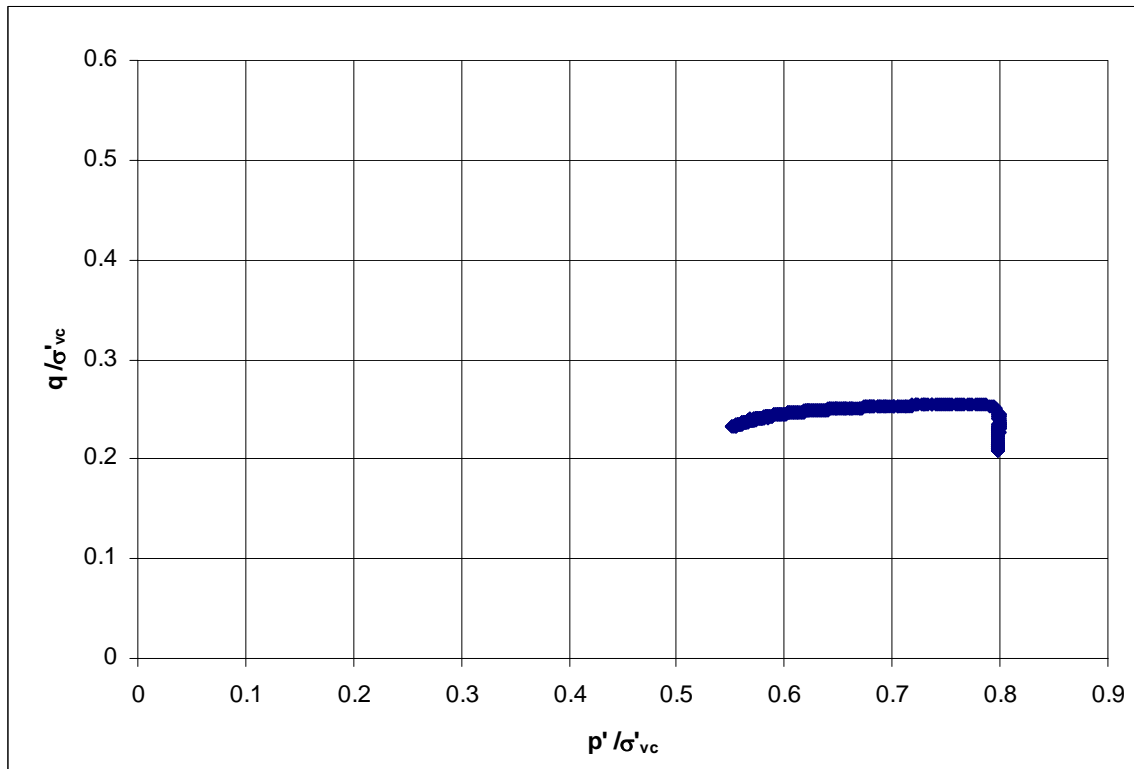
Figure A.48: Undrained Stress Path – Triaxial Test # 812
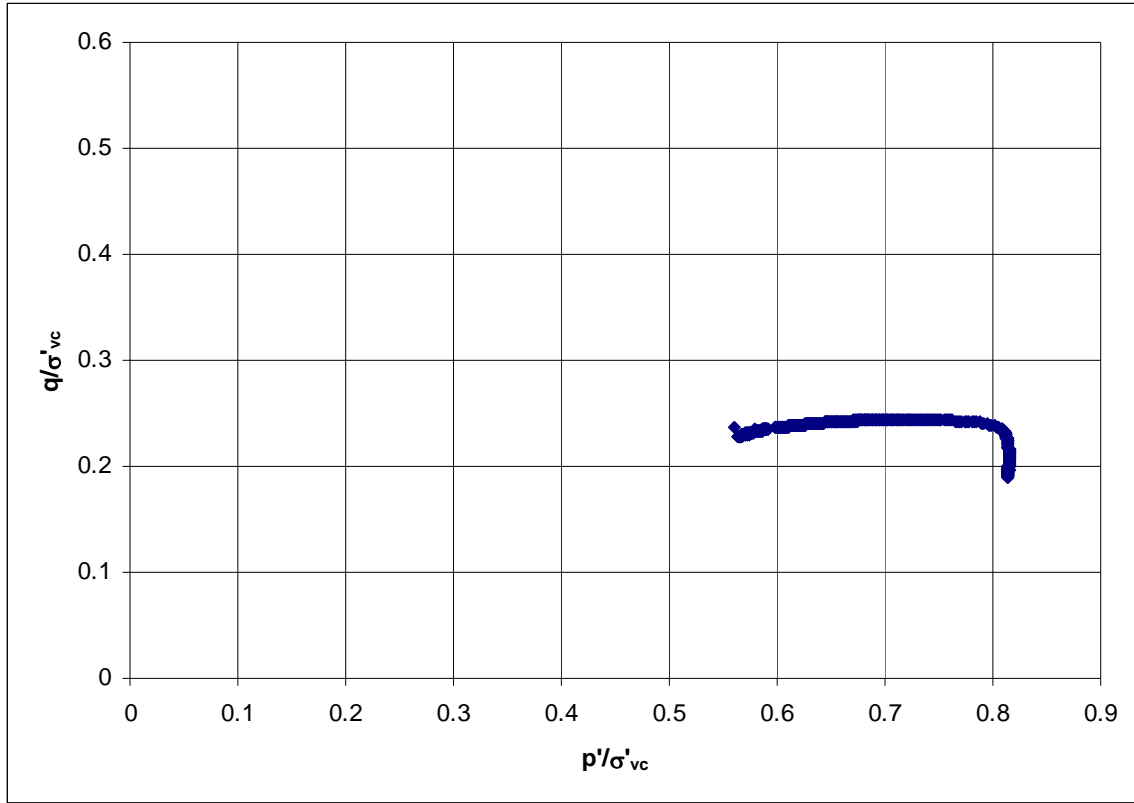
Figure A.49: Undrained Stress Path – Triaxial Test # 815
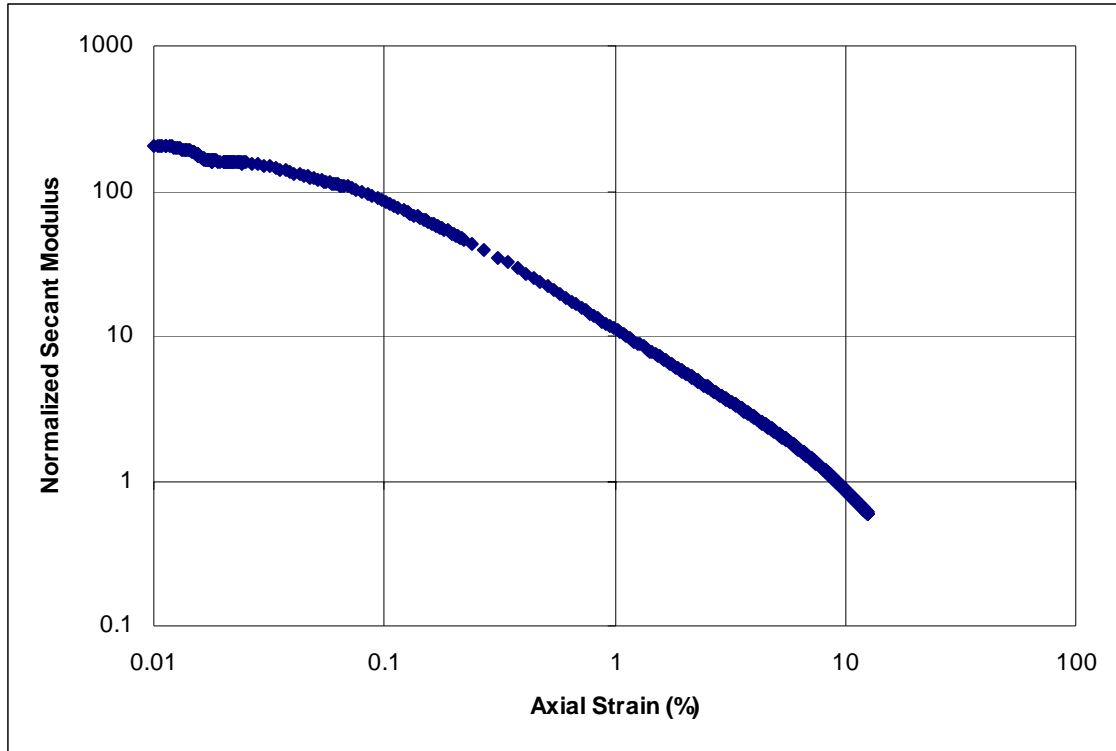
Figure A.50: Normalized Secant Modulus Versus Axial Strain – Triaxial Test # 797
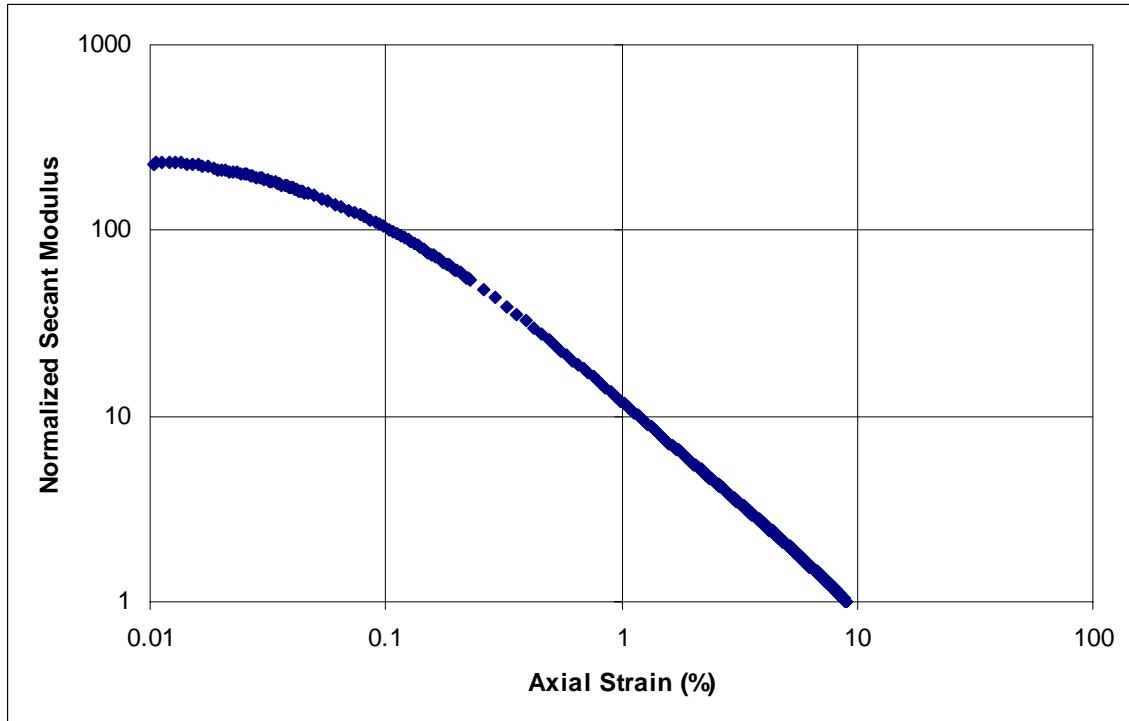
Figure A.51: Normalized Secant Modulus Versus Axial Strain – Triaxial Test # 801
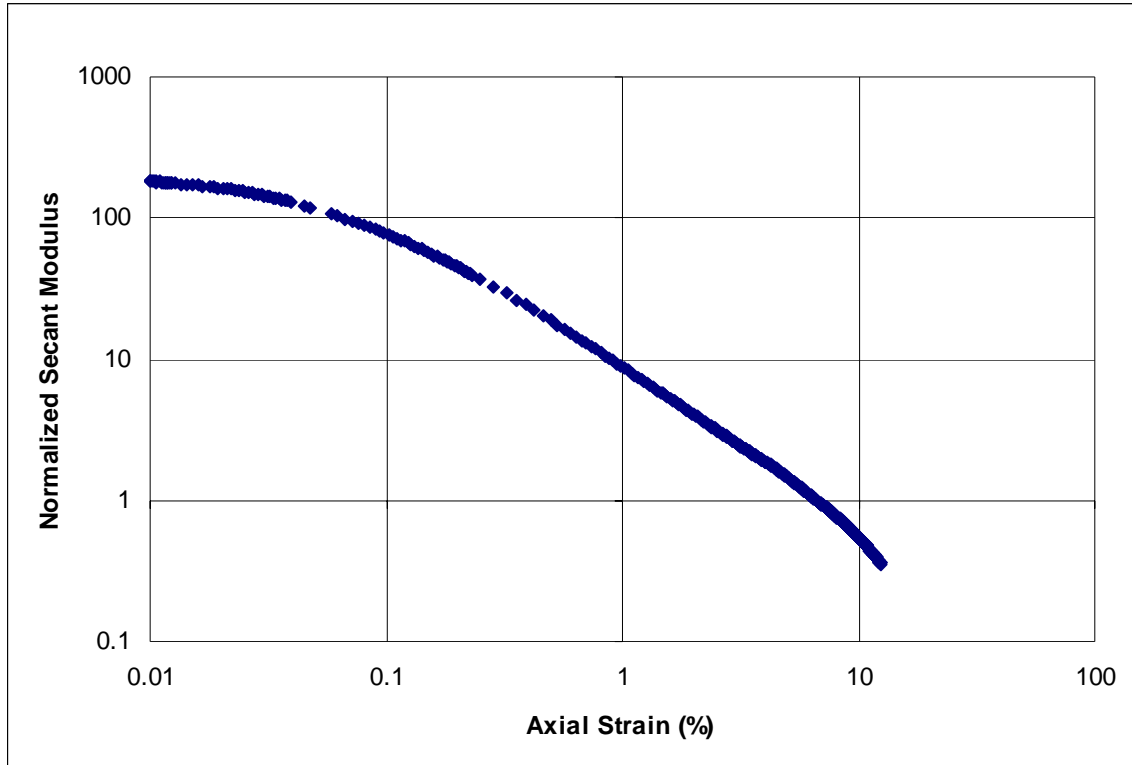
Figure A.52: Normalized Secant Modulus Versus Axial Strain – Triaxial Test # 804
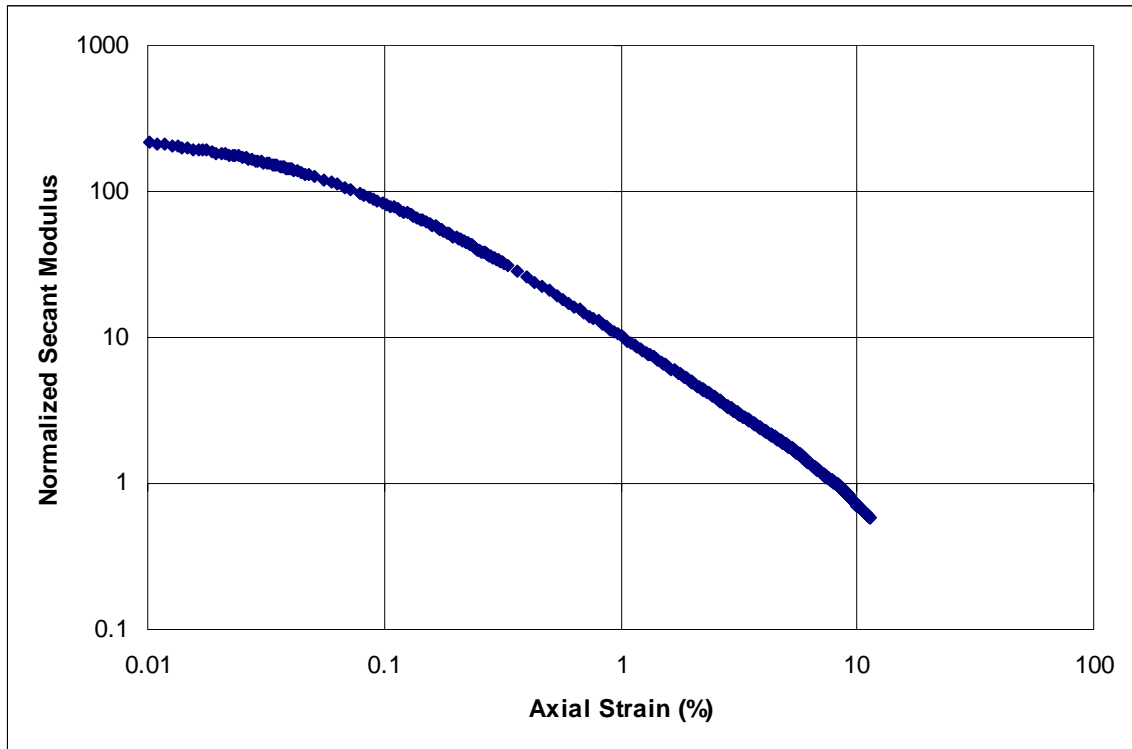
Figure A.53: Normalized Secant Modulus Versus Axial Strain – Triaxial Test # 807
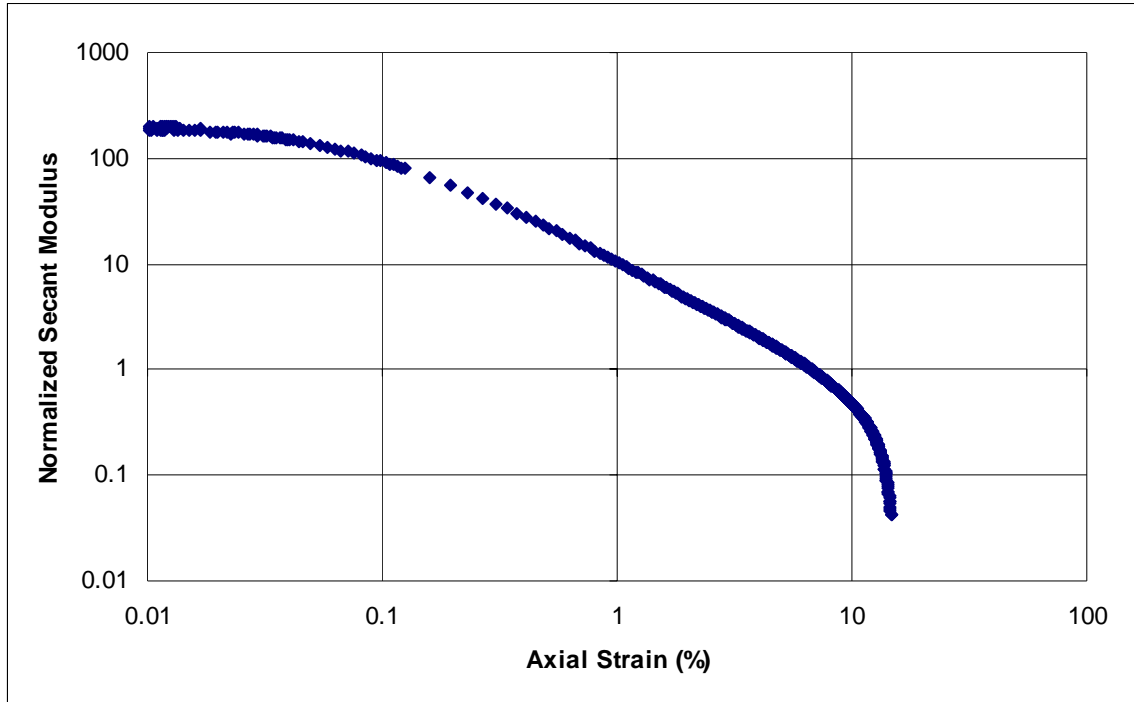
Figure A.54: Normalized Secant Modulus Versus Axial Strain – Triaxial Test # 810
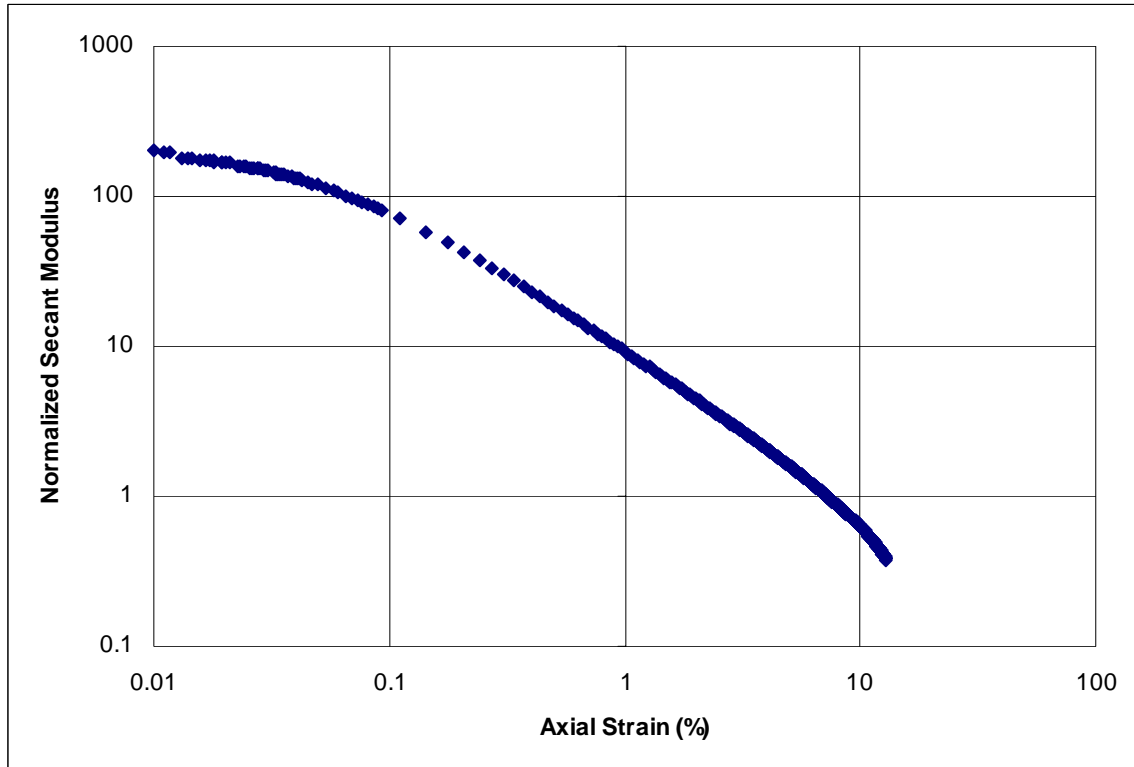
Figure A.55: Normalized Secant Modulus Versus Axial Strain – Triaxial Test # 812
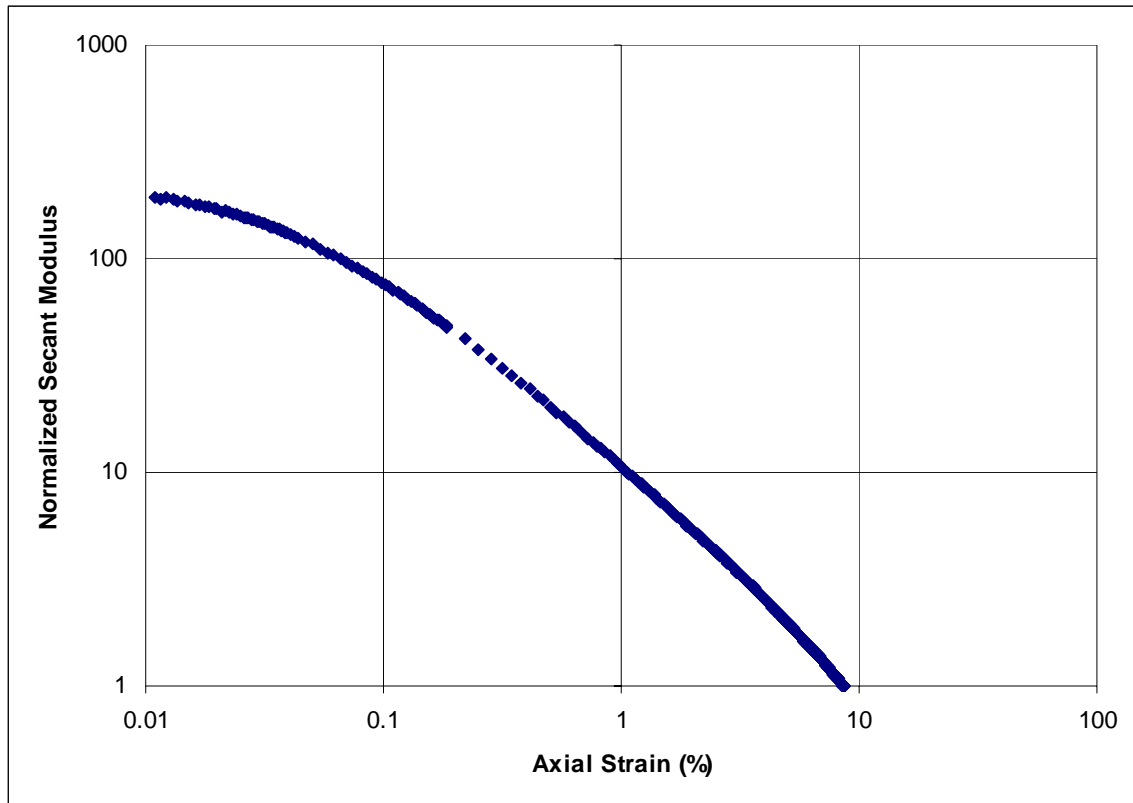
Figure A.56: Normalized Secant Modulus Versus Axial Strain – Triaxial Test # 815
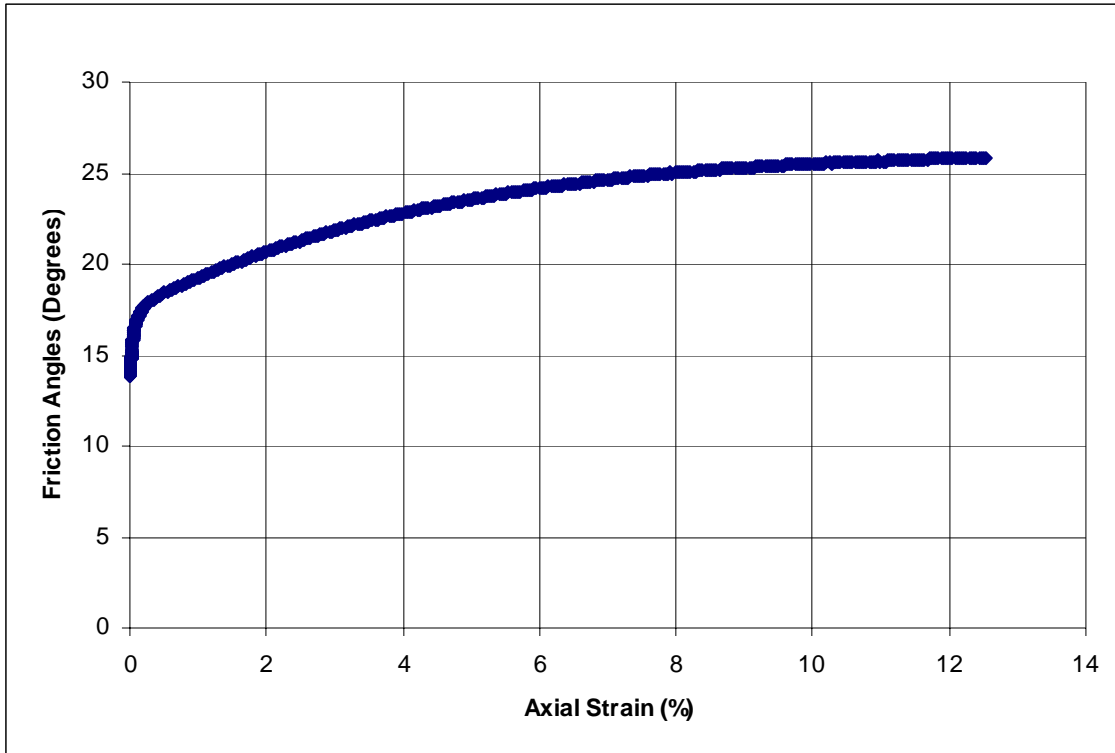
Figure A.57: Friction Angle Versus Axial Strain – Triaxial Test # 797
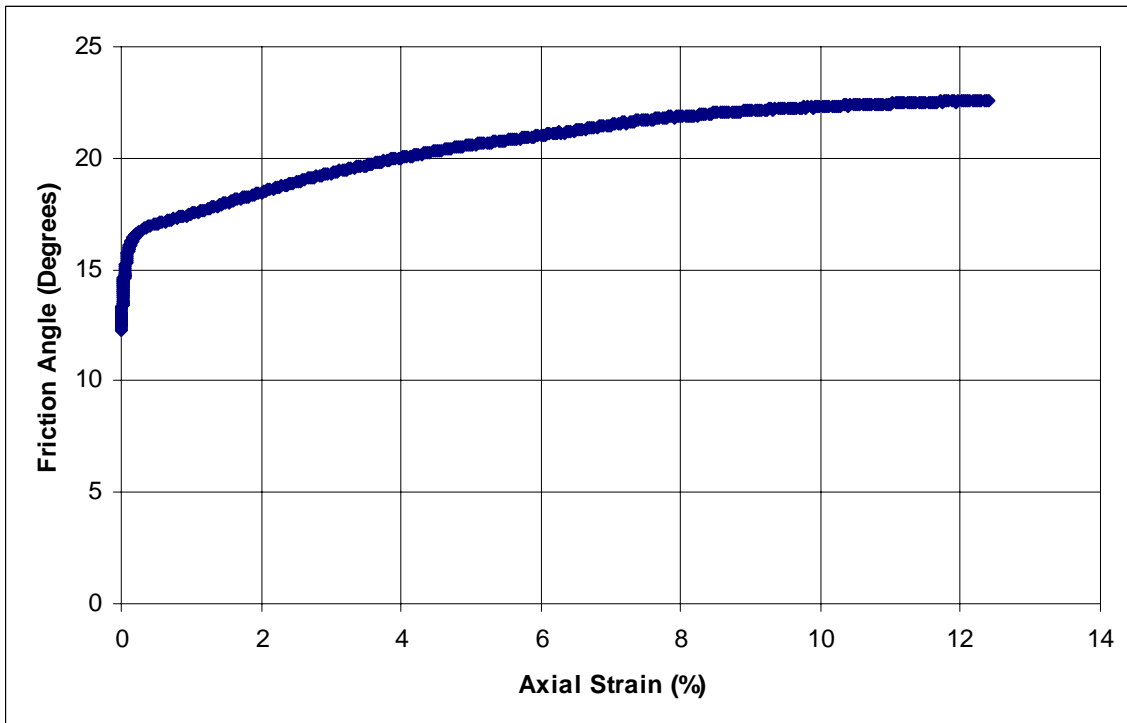
Figure A.58: Friction Angle Versus Axial Strain – Triaxial Test # 801
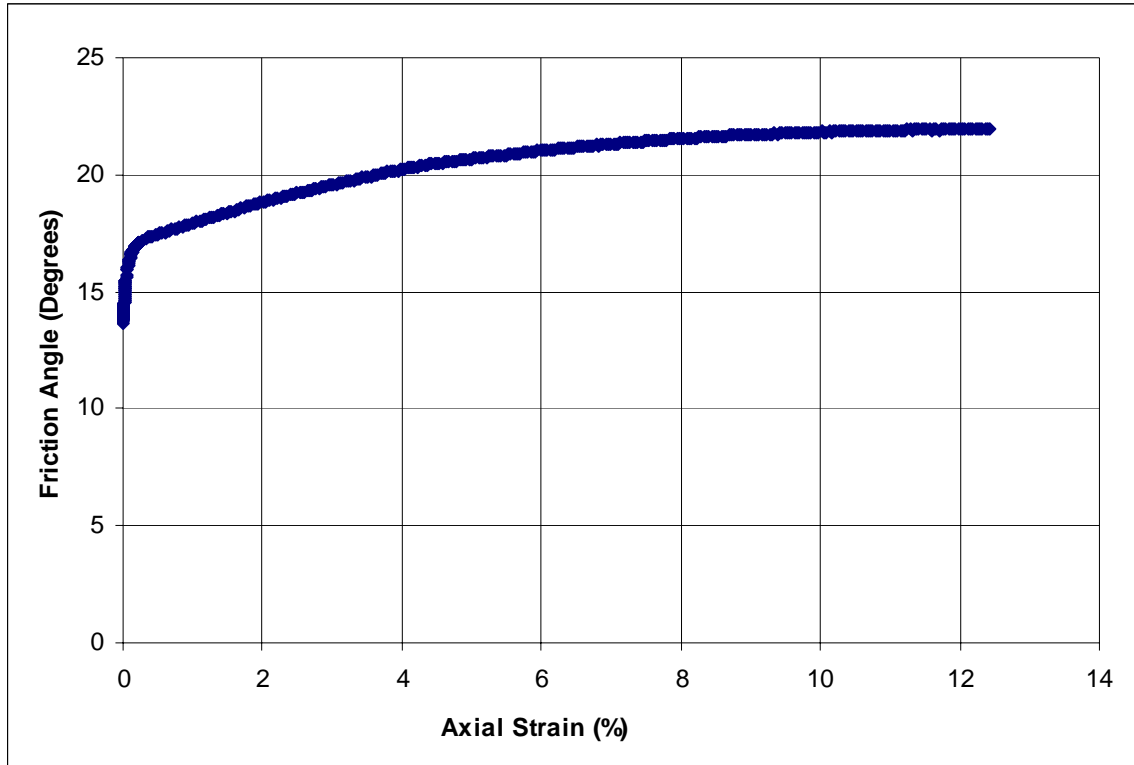
Figure A.59: Friction Angle Versus Axial Strain – Triaxial Test # 804
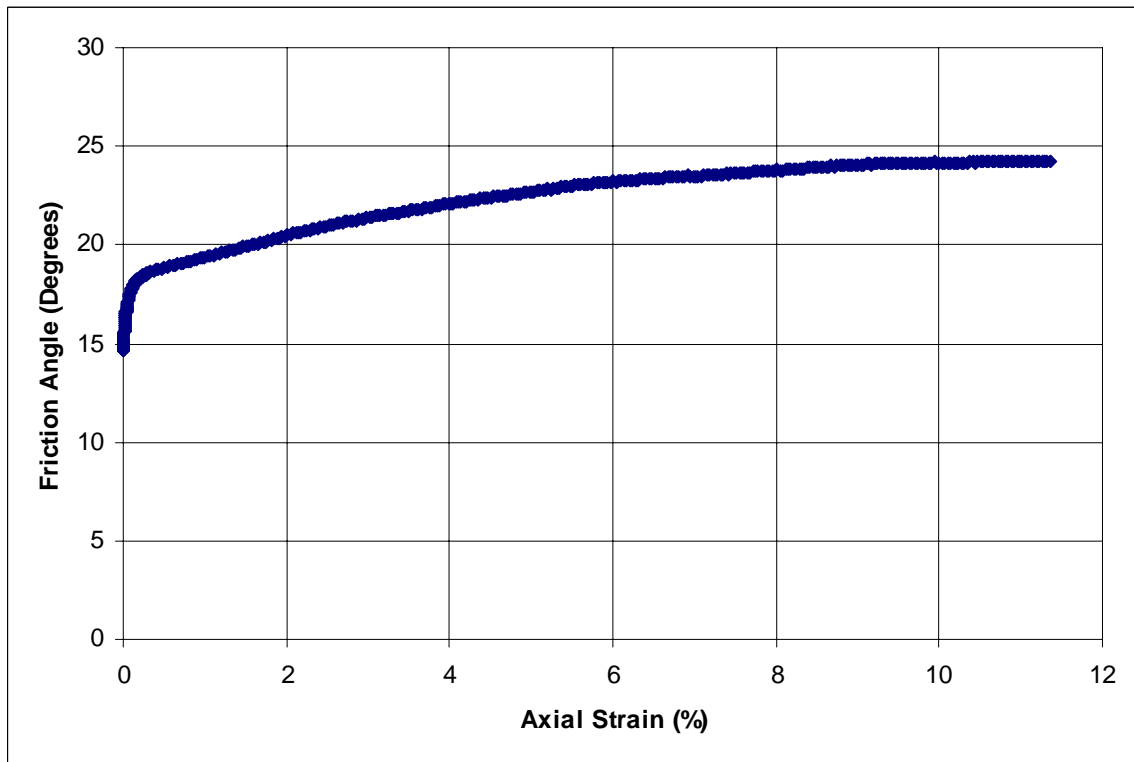
Figure A.60: Friction Angle Versus Axial Strain – Triaxial Test # 807
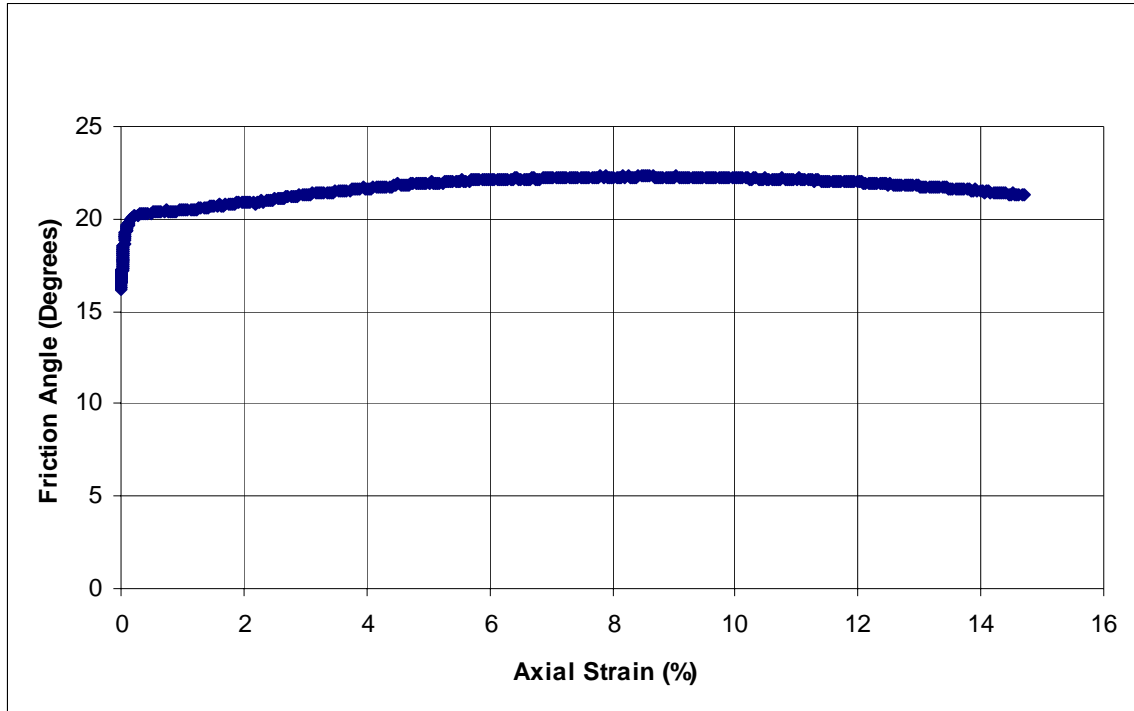
Figure A.61: Friction Angle Versus Axial Strain – Triaxial Test # 810
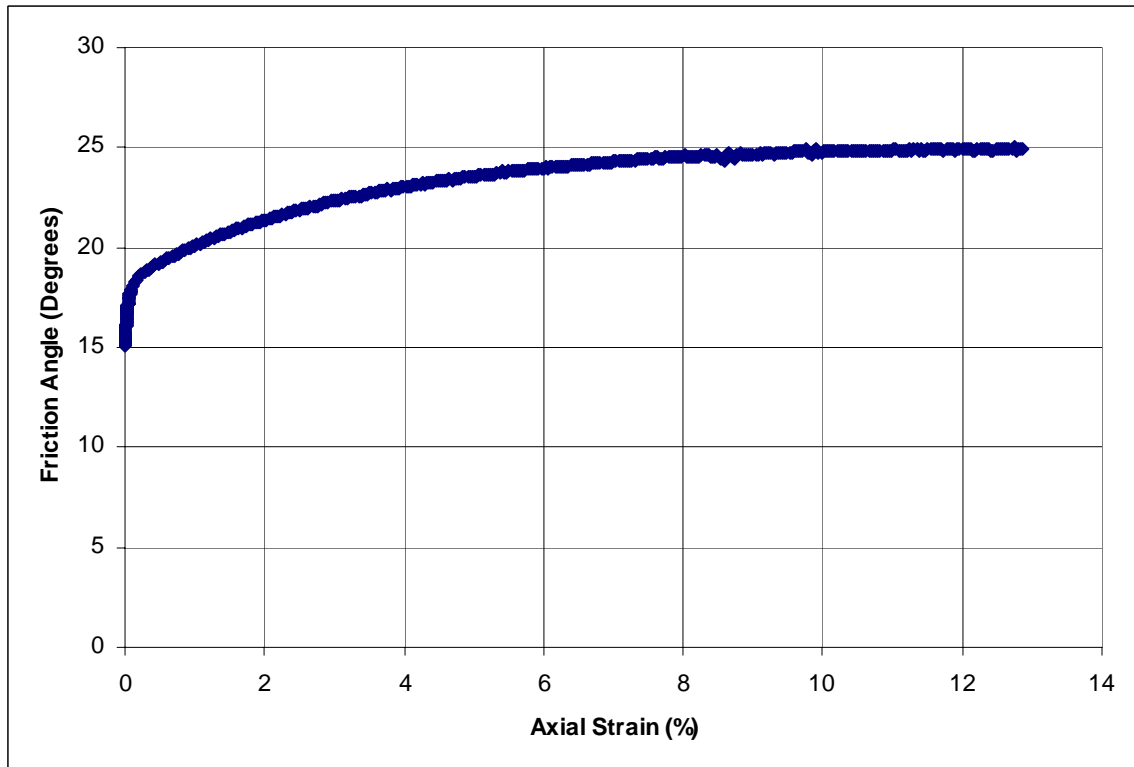
Figure A.62: Friction Angle Versus Axial Strain – Triaxial Test # 812
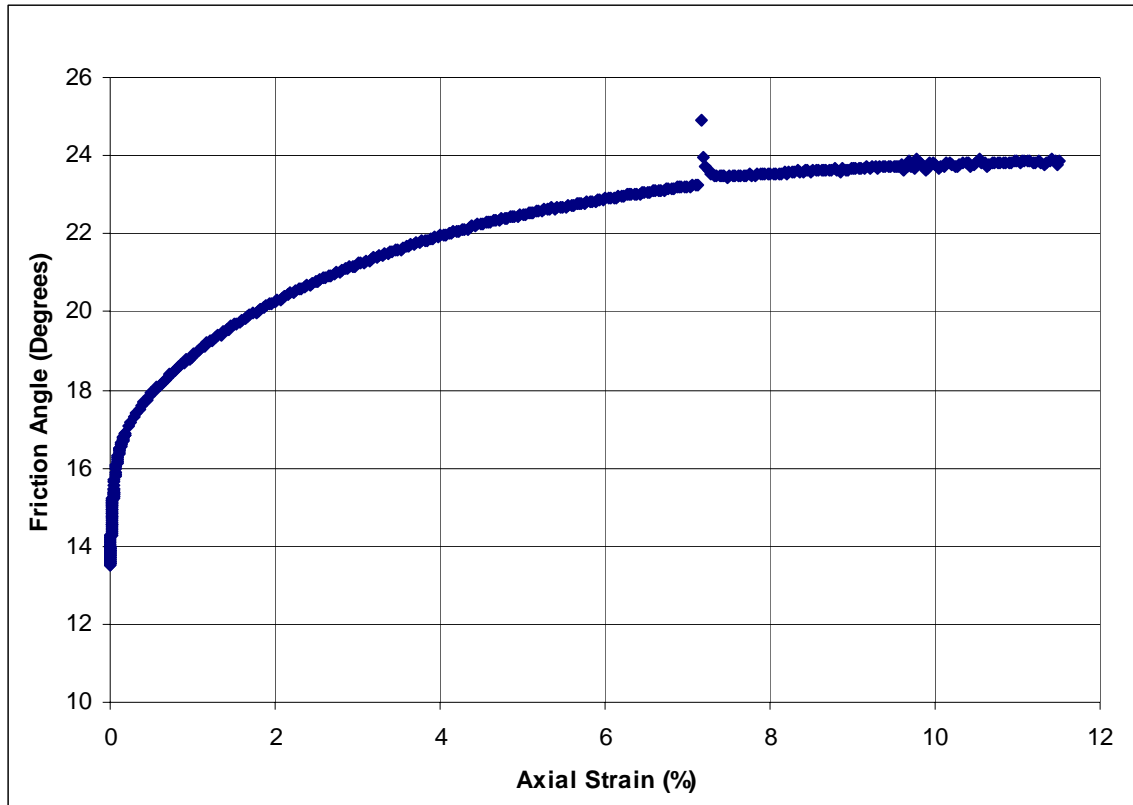
Figure A.63: Friction Angle Versus Axial Strain – Triaxial Test # 815
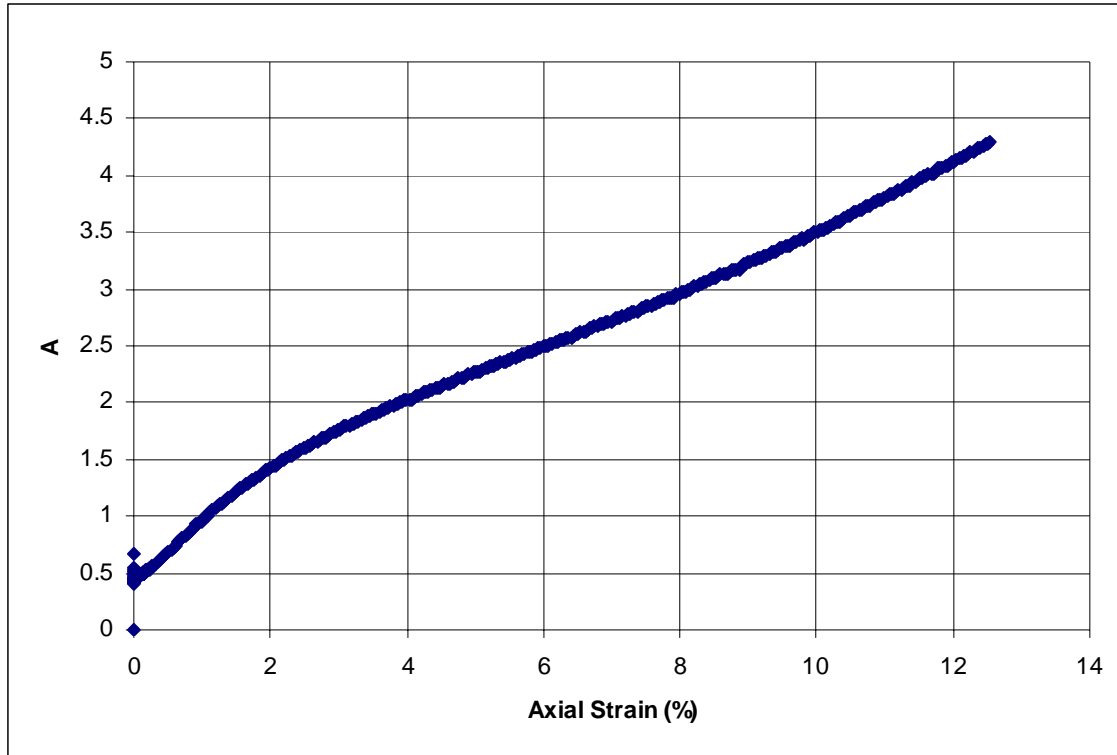
Figure A.64: The A Parameter Versus Axial Strain – Triaxial Test # 797
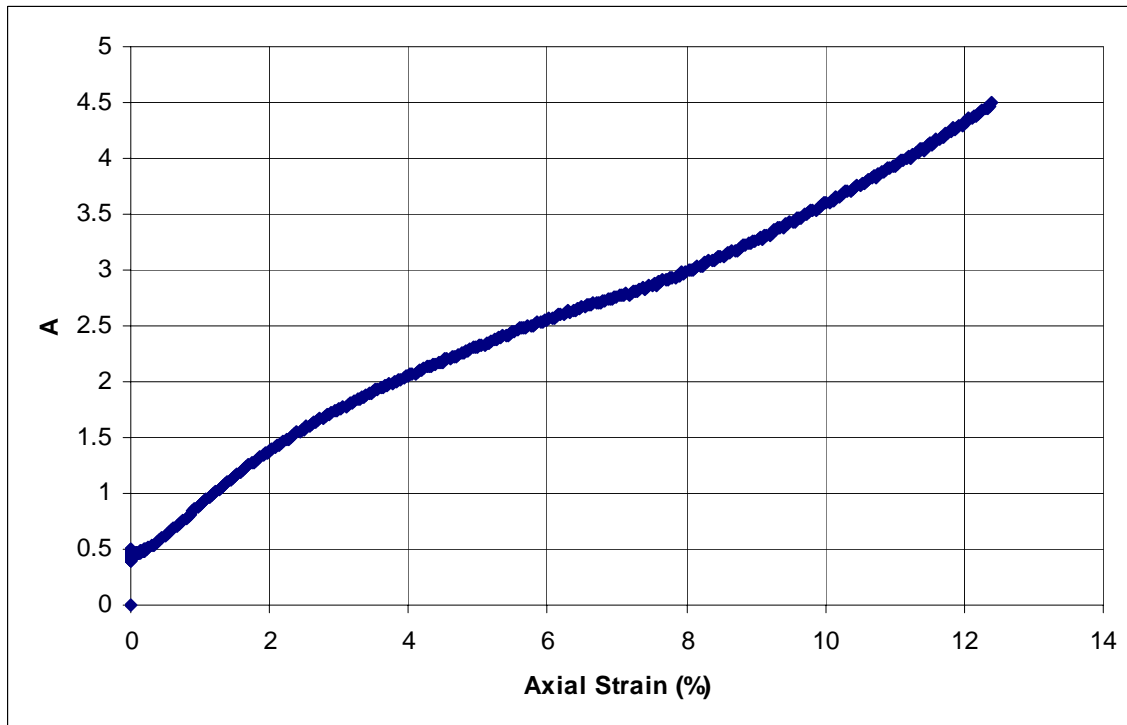
Figure A.65: The A Parameter Versus Axial Strain – Triaxial Test # 801
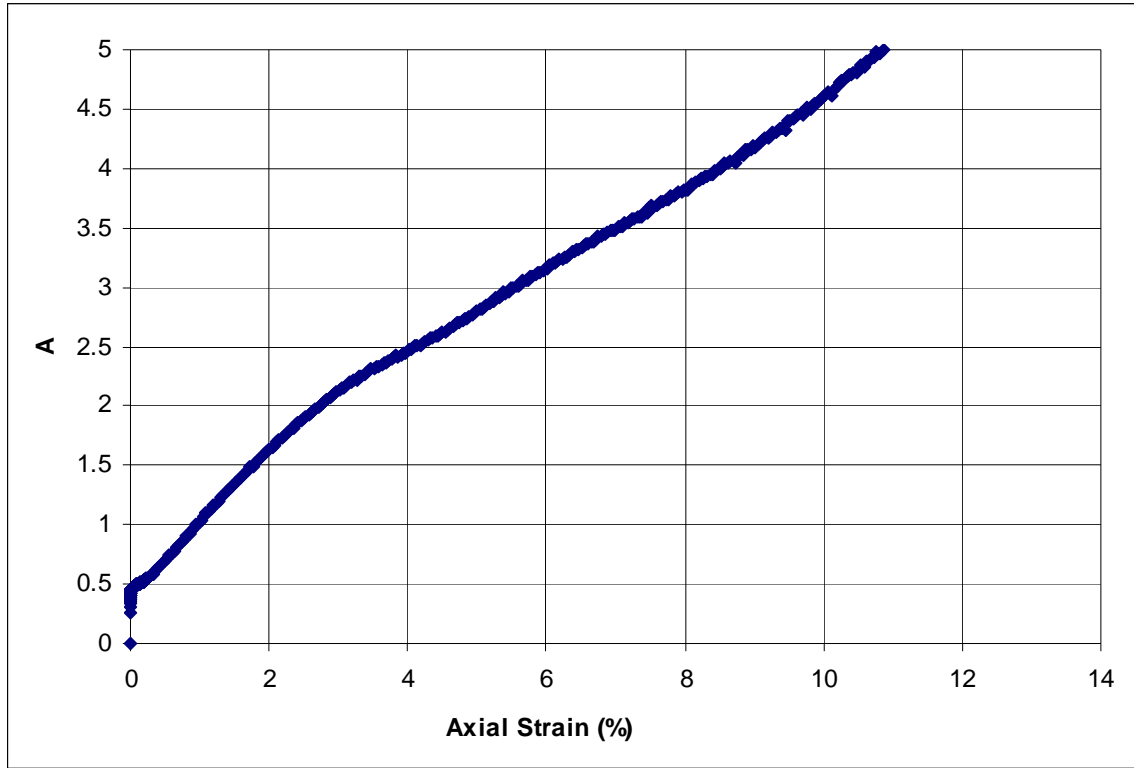
Figure A.66: The A Parameter Versus Axial Strain – Triaxial Test # 804
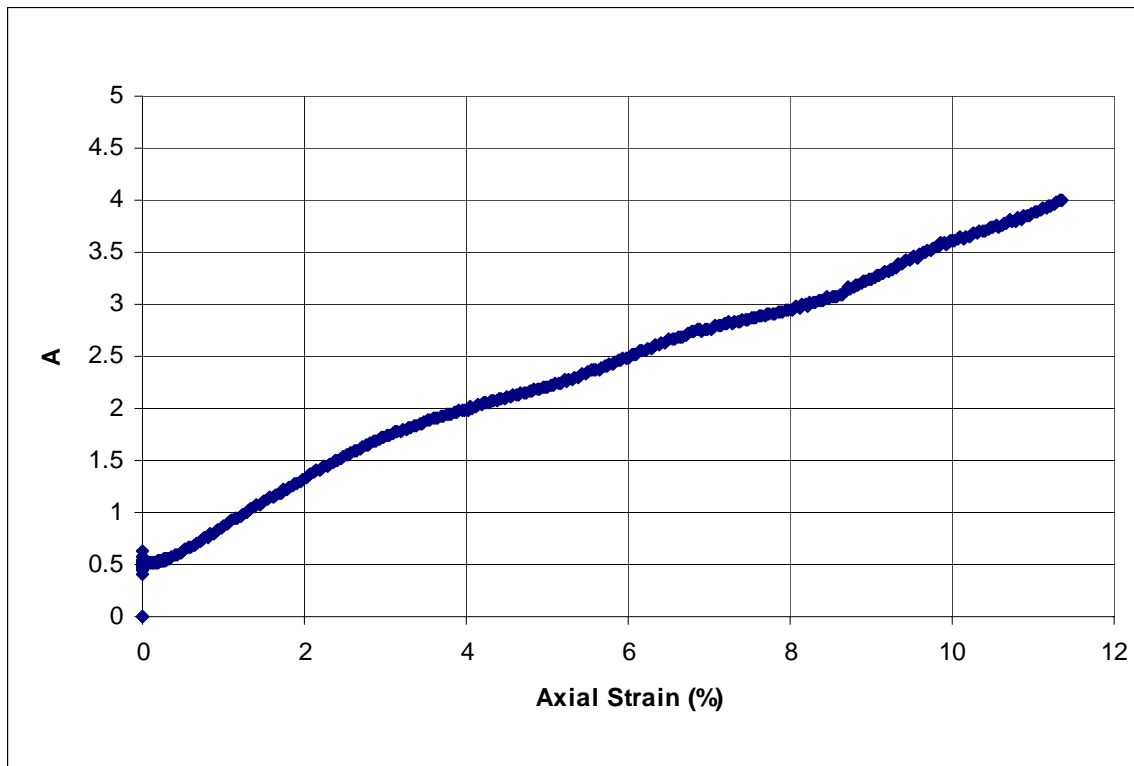
Figure A.67: The A Parameter Versus Axial Strain – Triaxial Test # 807
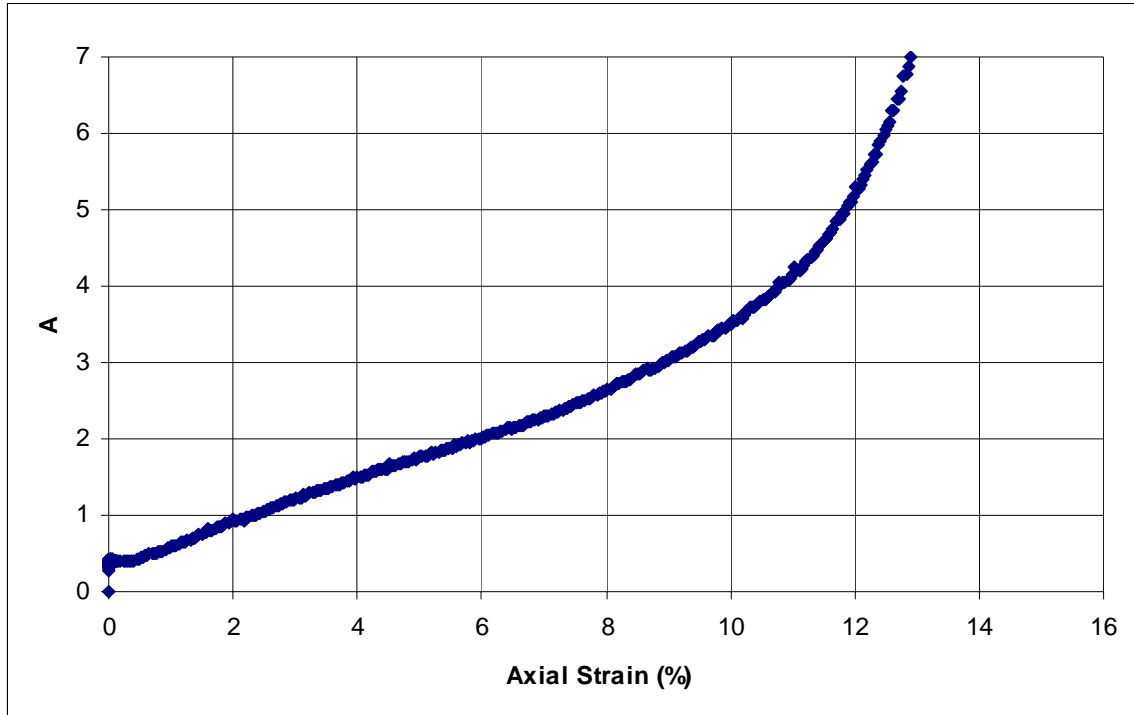
Figure A.68: The A Parameter Versus Axial Strain – Triaxial Test # 810
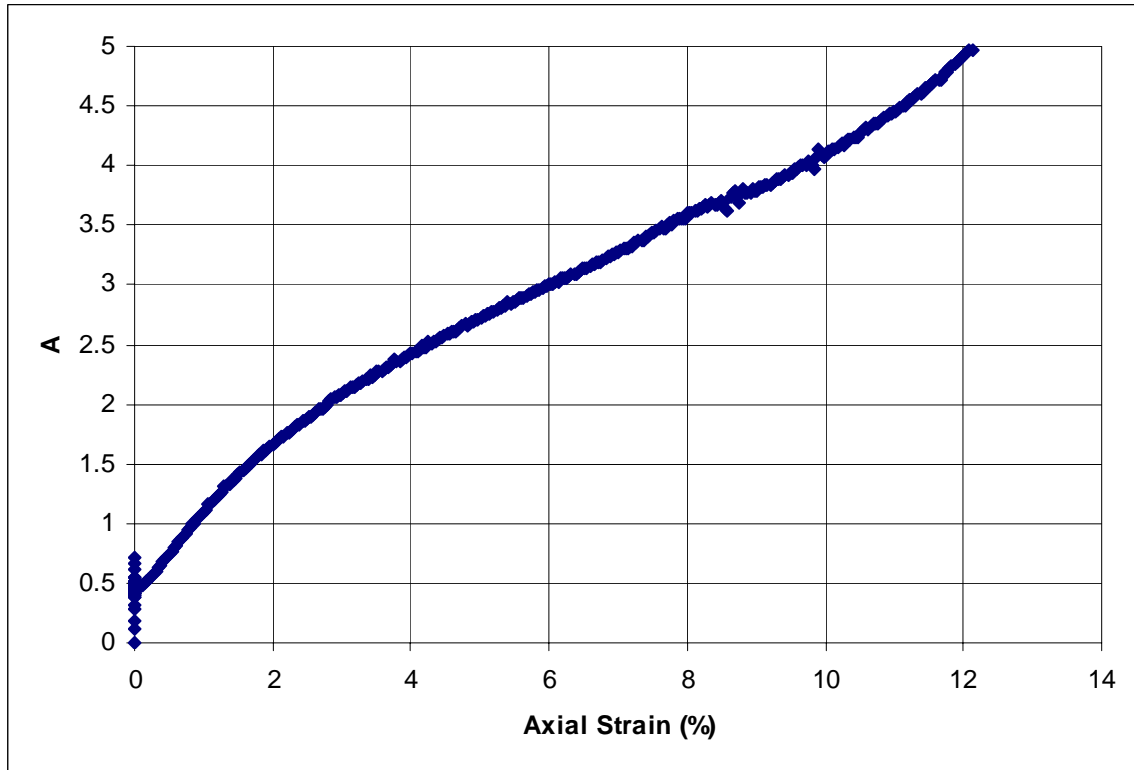
Figure A.69: The A Parameter Versus Axial Strain – Triaxial Test # 812
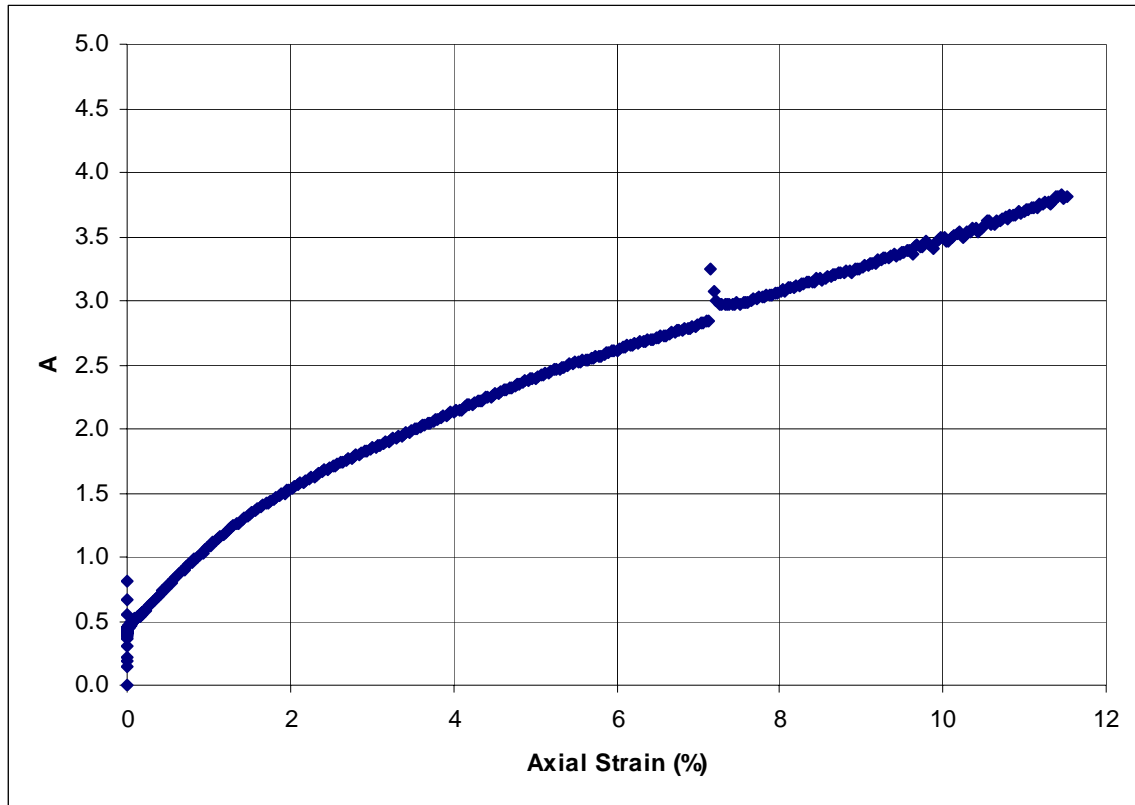
Figure A.70: The A Parameter Versus Axial Strain – Triaxial Test # 815
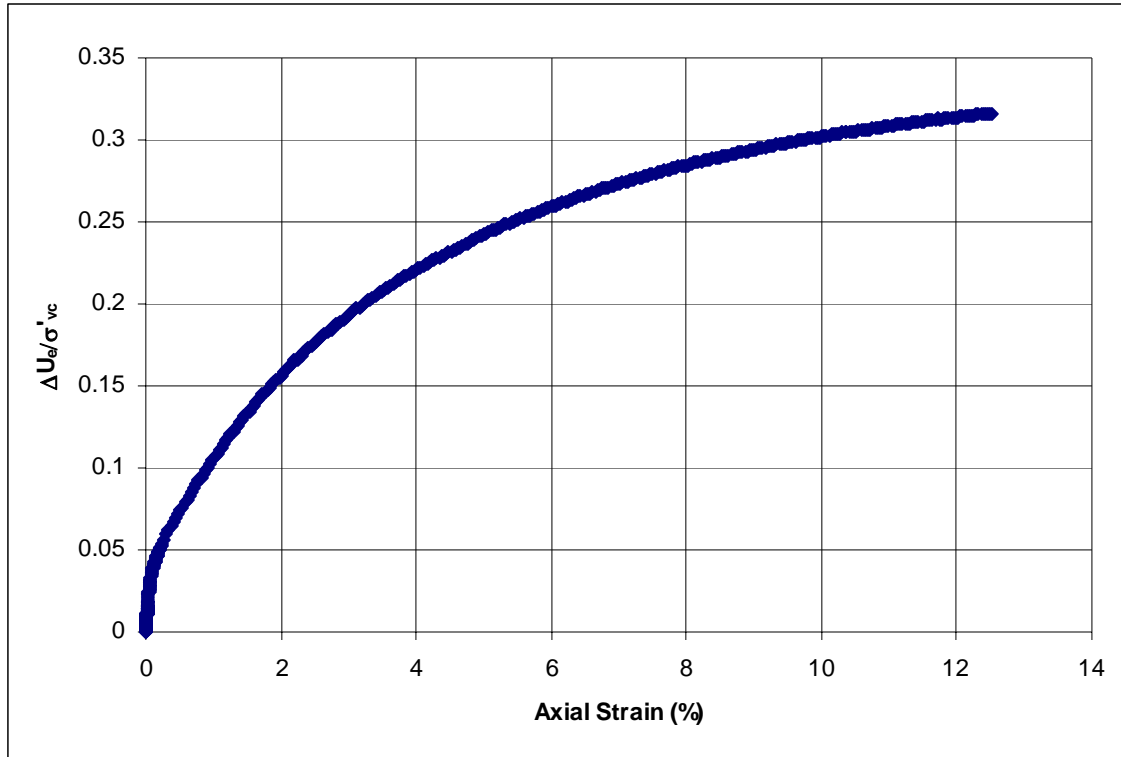
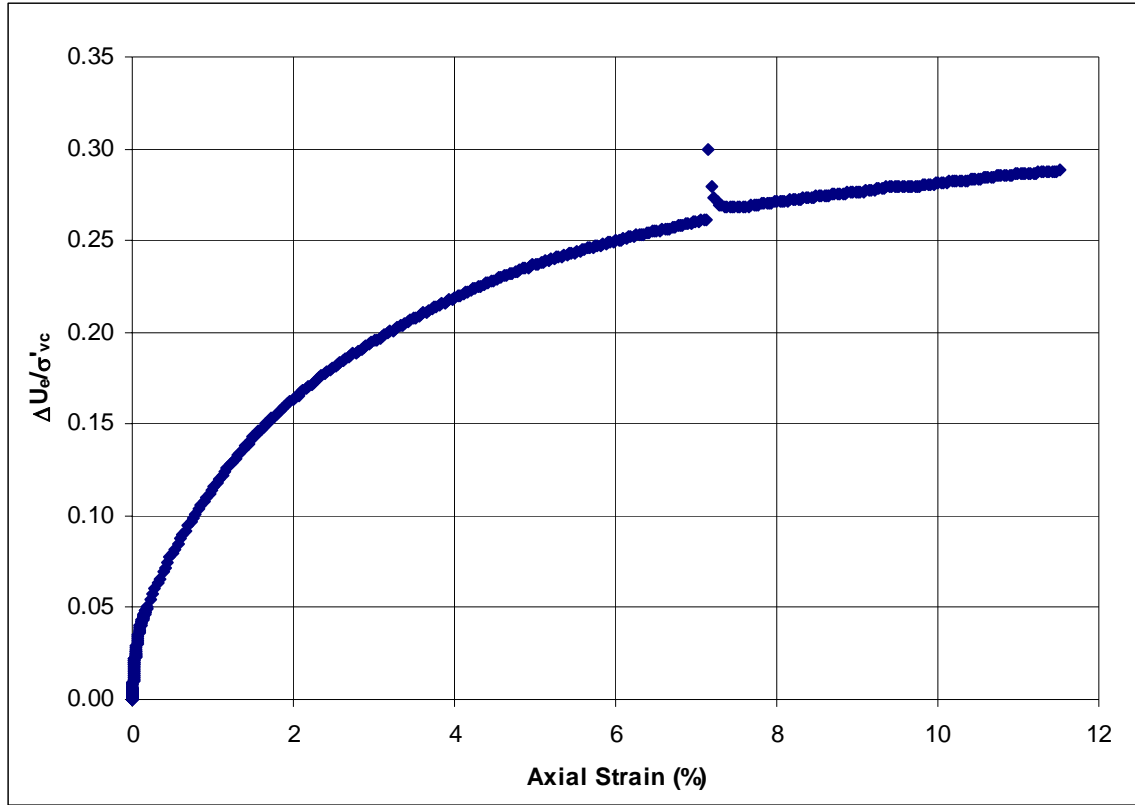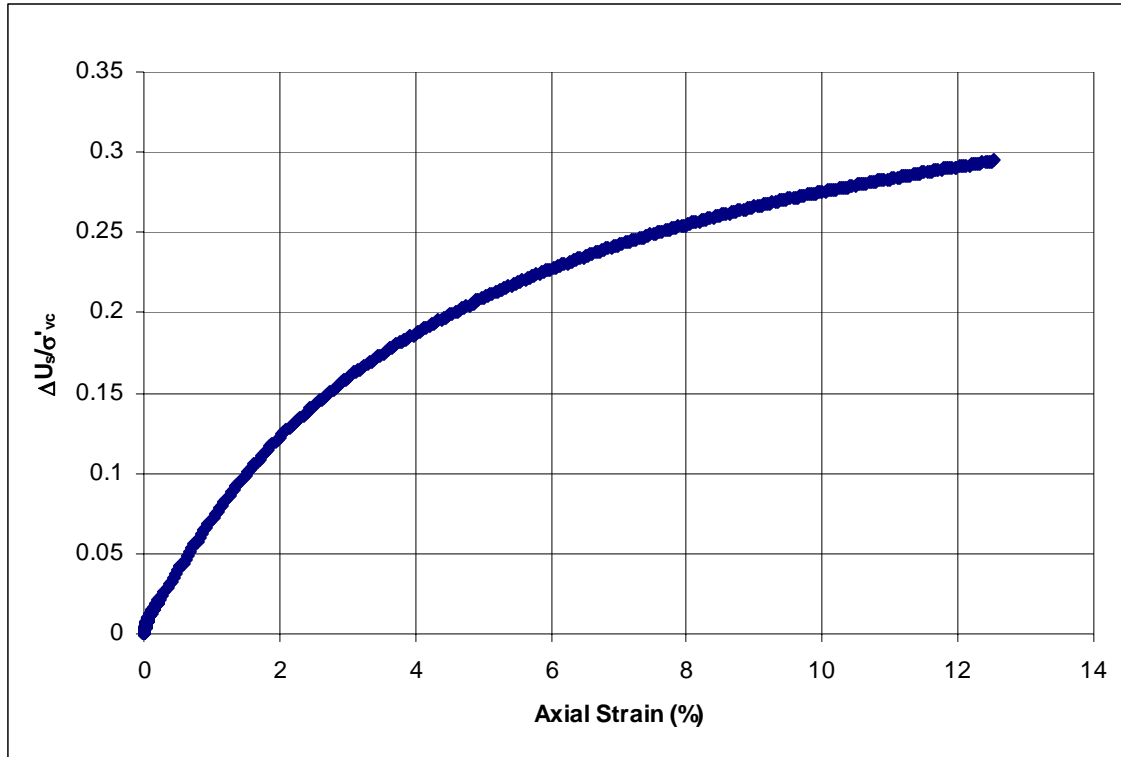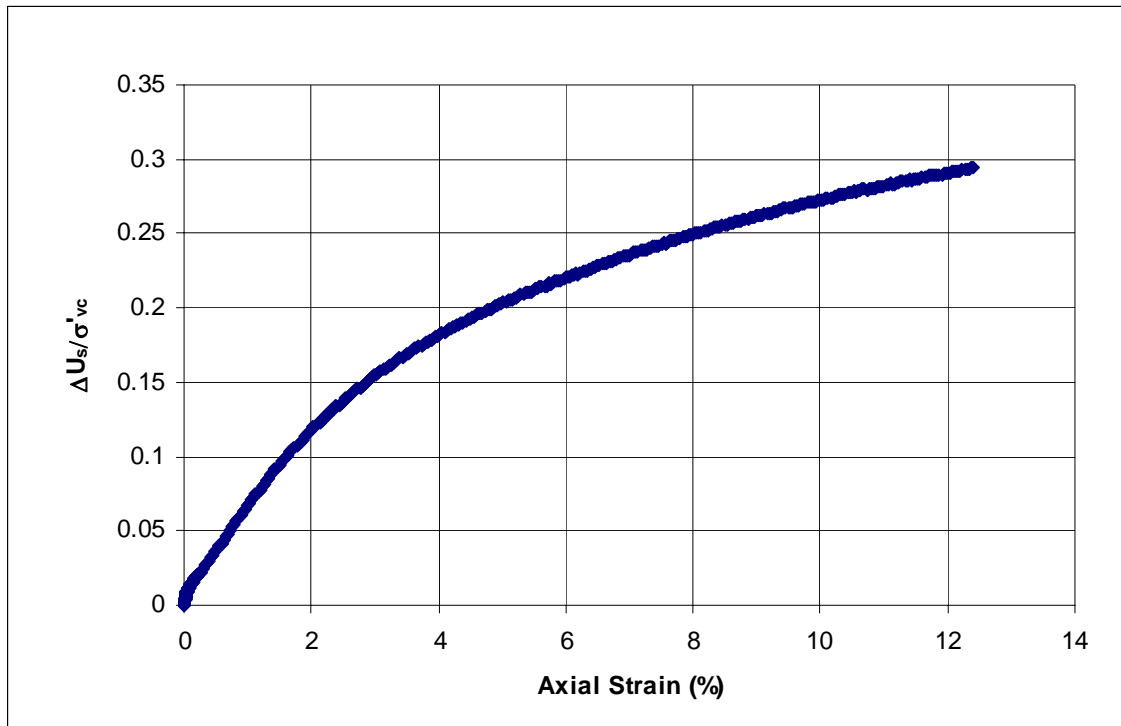**Figure A.71:** Excess Pore Pressure Versus Axial Strain – Triaxial Test # 797
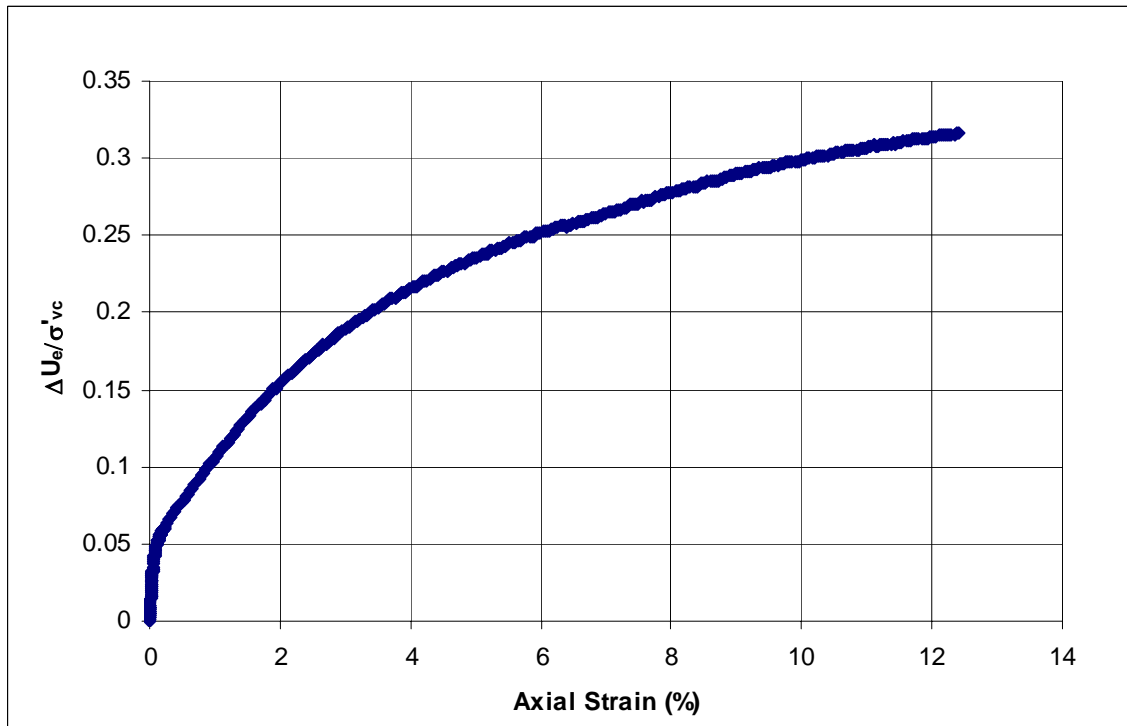
Figure A.72: Excess Pore Pressure Versus Axial Strain – Triaxial Test # 801
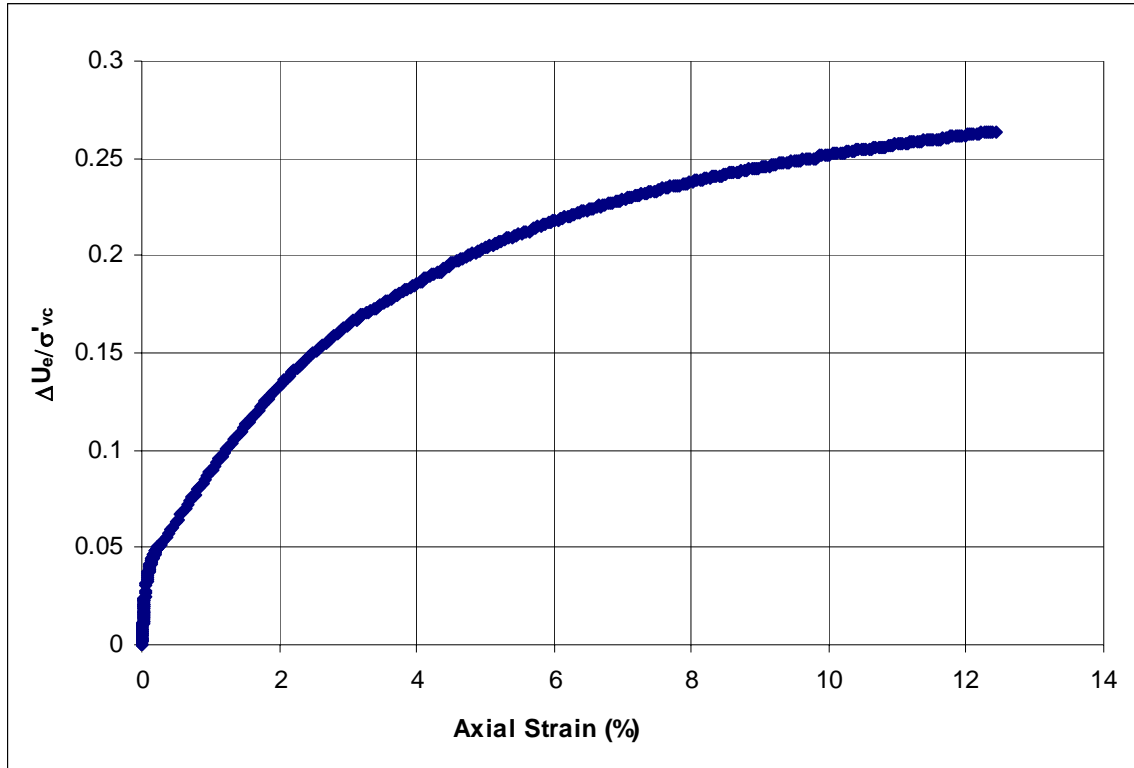
Figure A.73: Excess Pore Pressure Versus Axial Strain – Triaxial Test # 804
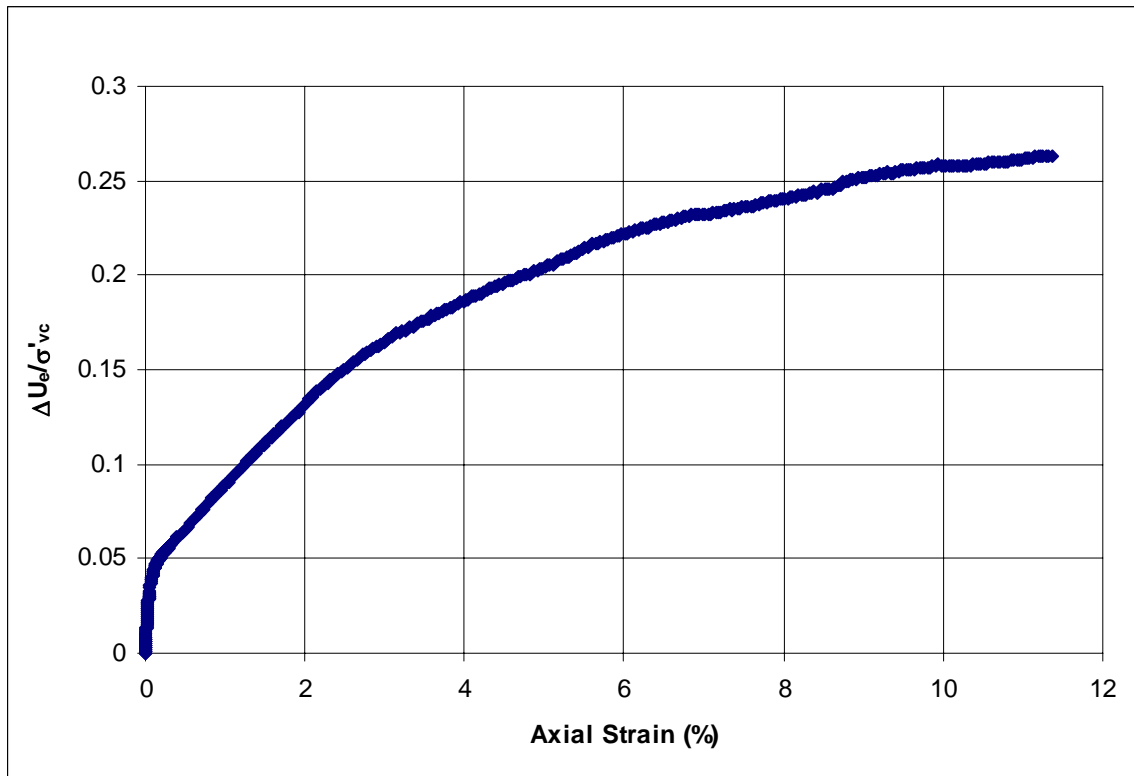
Figure A.74: Excess Pore Pressure Versus Axial Strain – Triaxial Test # 807
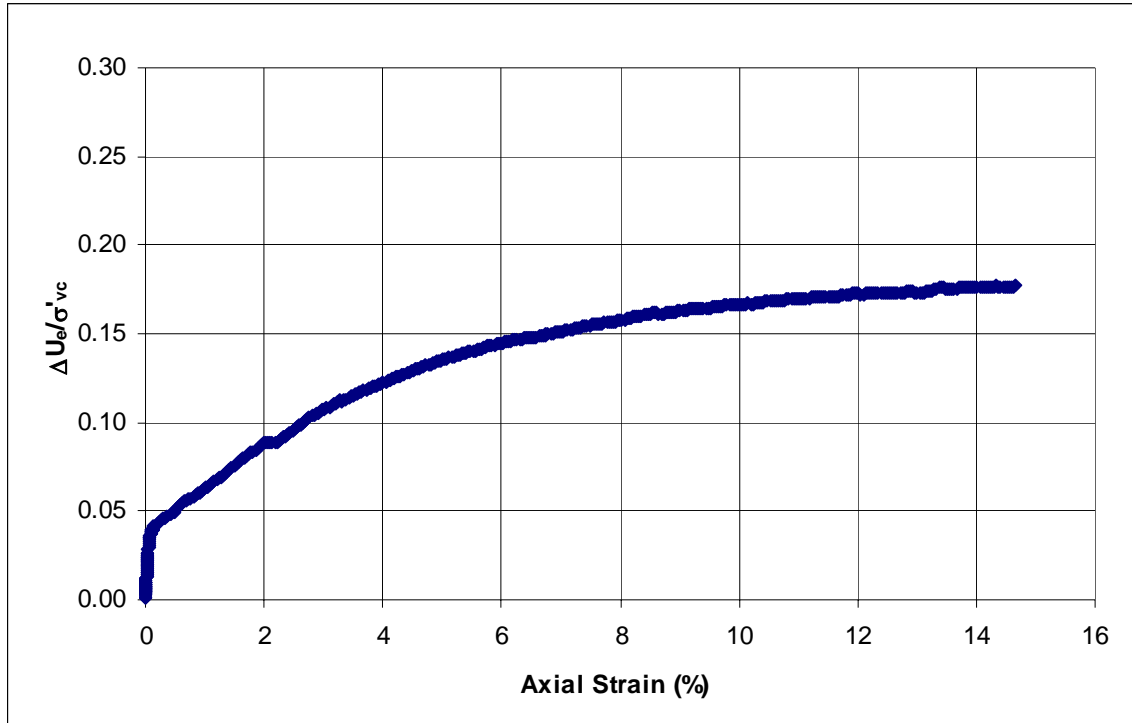
Figure A.75: Excess Pore Pressure Versus Axial Strain – Triaxial Test # 810
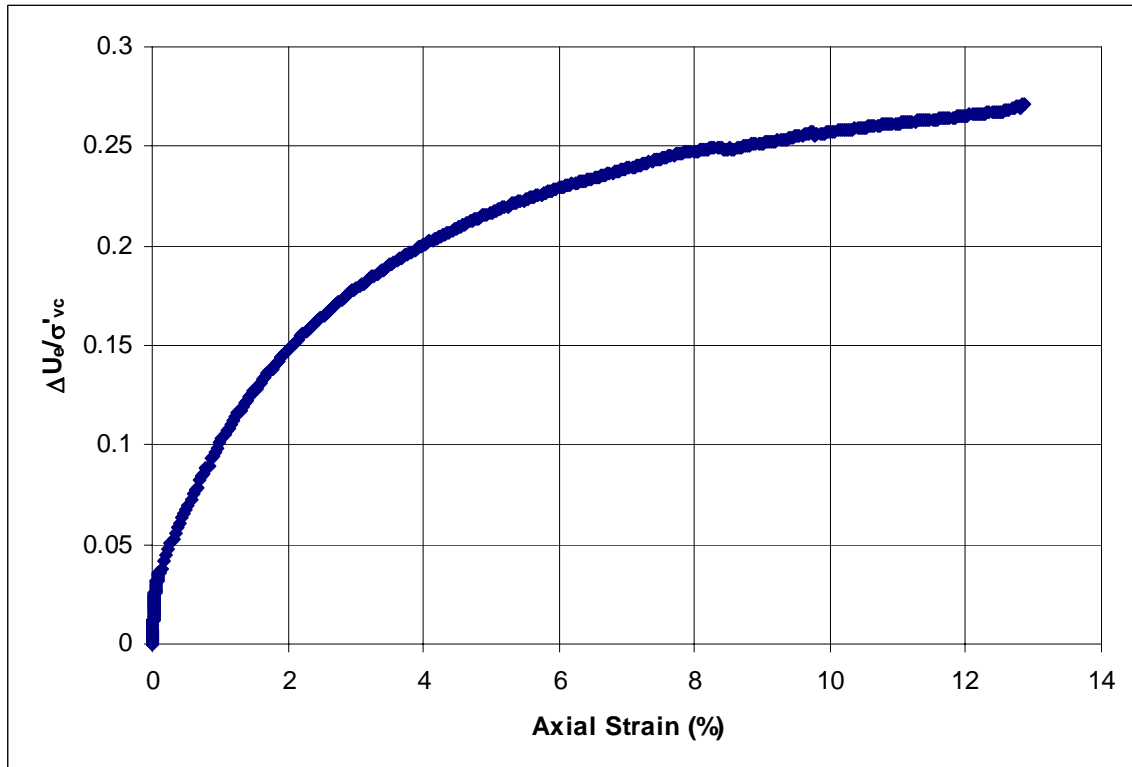
Figure A.76: Excess Pore Pressure Versus Axial Strain – Triaxial Test # 812

Figure A.77: Excess Pore Pressure Versus Axial Strain – Triaxial Test # 815

Figure A.78: Shear-Induced Pore Pressure Versus Axial Strain – Triaxial Test # 797

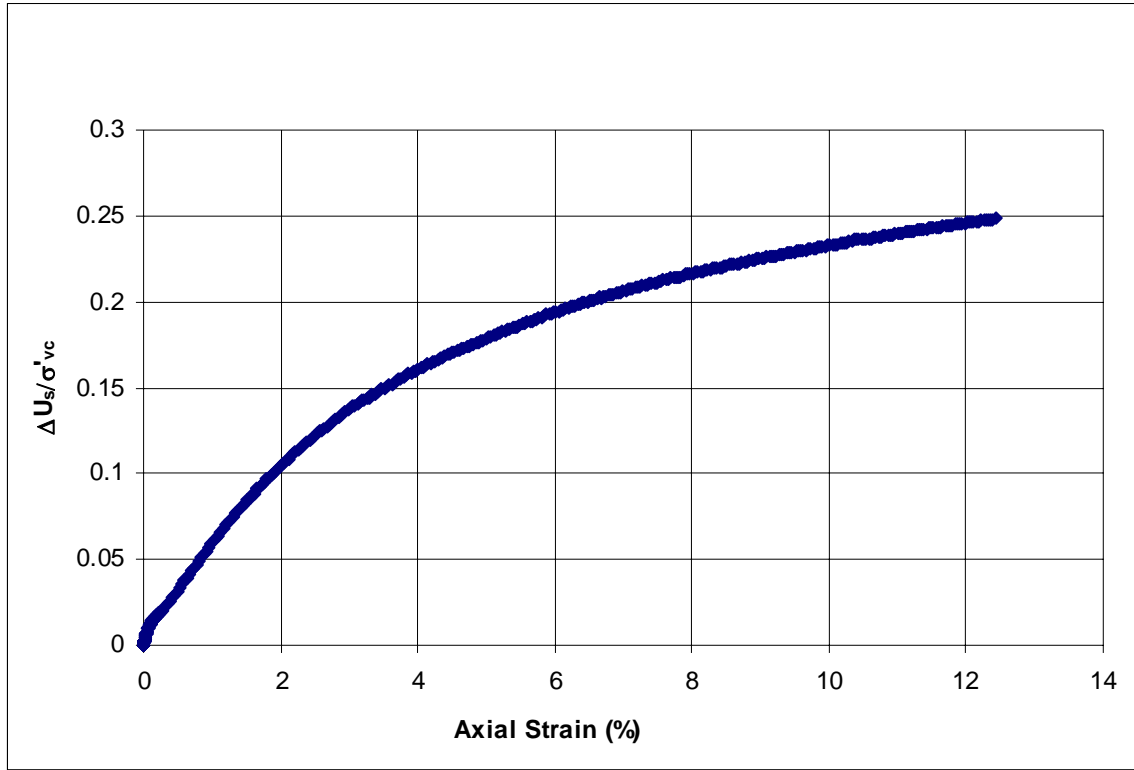**Figure A.79:** Shear-Induced Pore Pressure Versus Axial Strain – Triaxial Test # 801

Figure A.80: Shear-Induced Pore Pressure Versus Axial Strain – Triaxial Test # 804
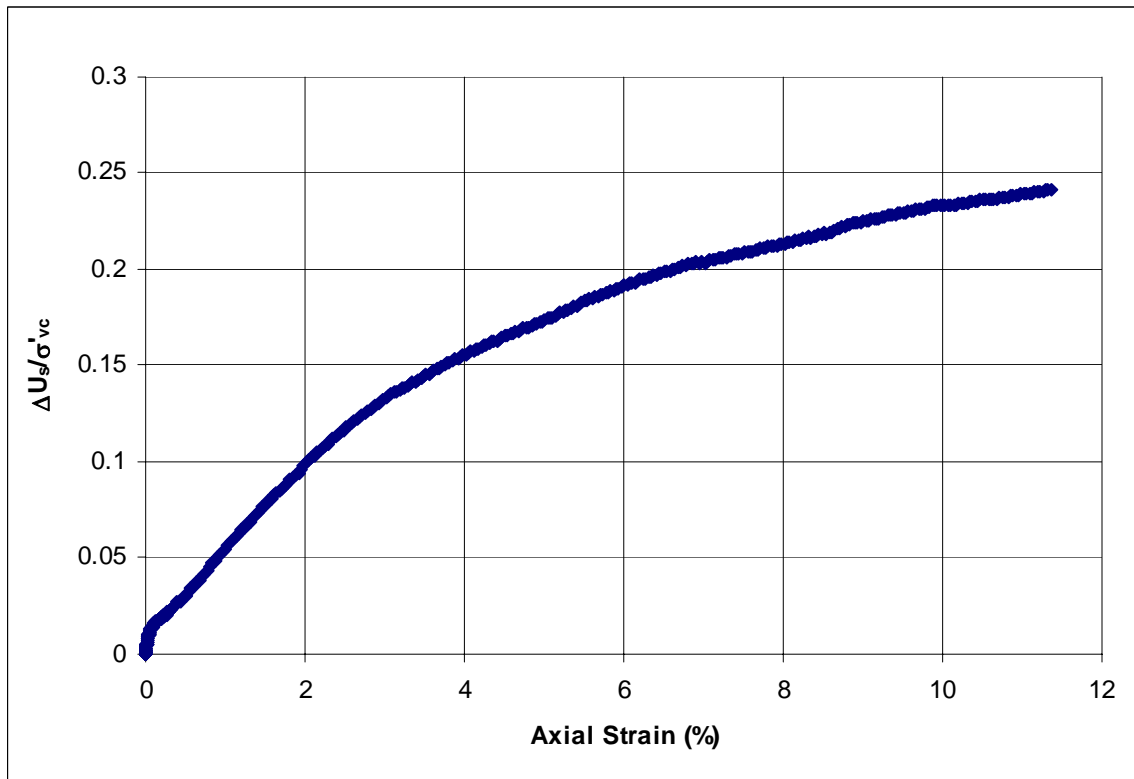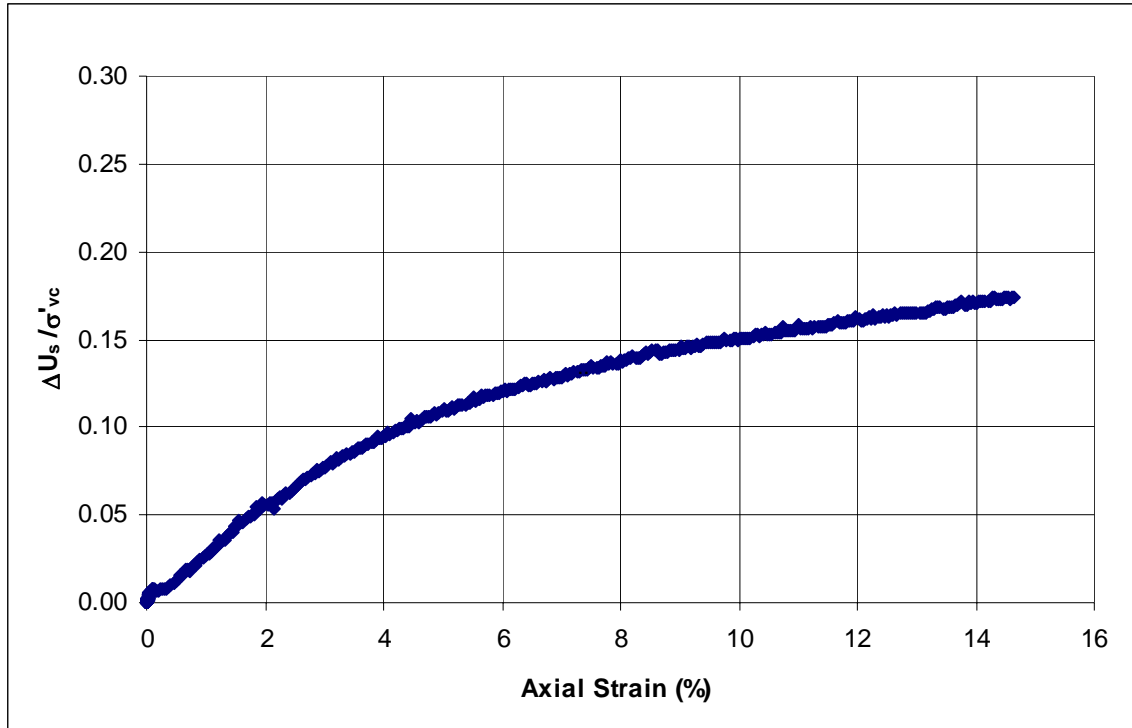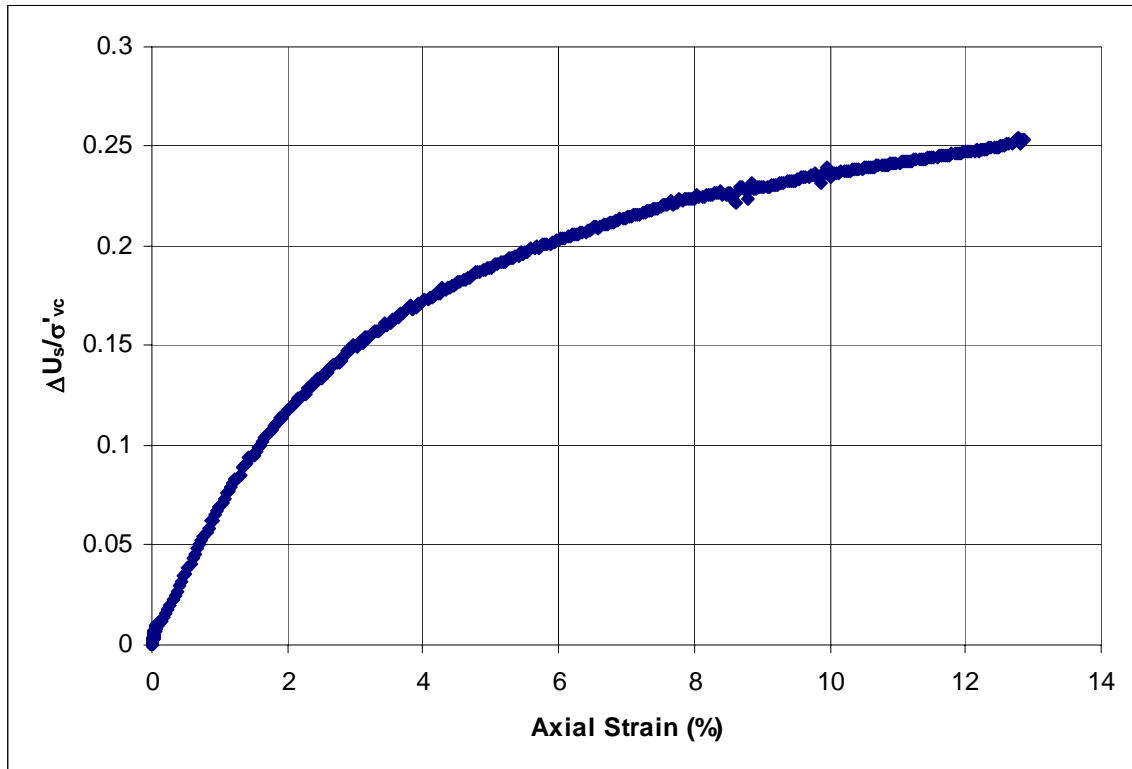

Figure A.81: Shear-Induced Pore Pressure Versus Axial Strain – Triaxial Test # 807
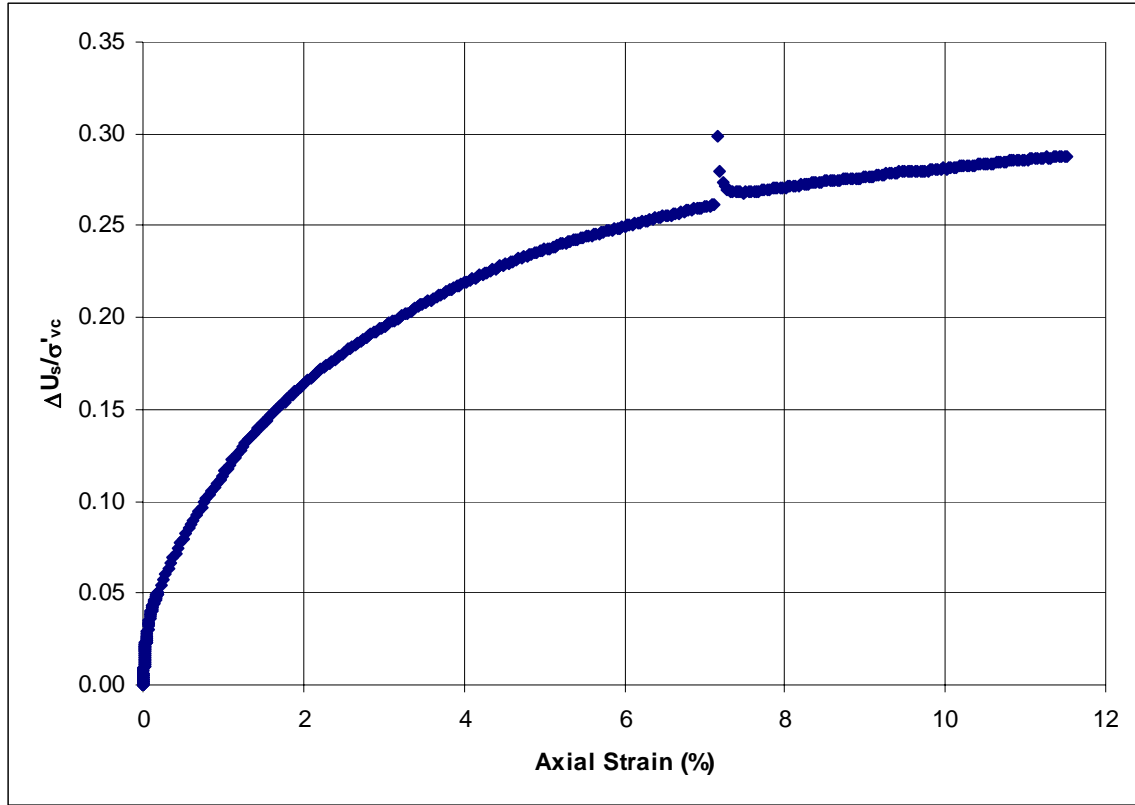
Figure A.82: Shear-Induced Pore Pressure Versus Axial Strain – Triaxial Test # 810

Figure A.83: Shear-Induced Pore Pressure Versus Axial Strain – Triaxial Test # 812

Figure A.84: Shear-Induced Pore Pressure Versus Axial Strain – Triaxial Test # 815